Higgs and flavour phenomenology at the LHC era

PhD dissertation by

María Luisa López Ibáñez

under the supervision of

Óscar M. Vives García

VNIVERSITAT DE VALÈNCIA

FACULTAT DE FÍSICA

DEPARTAMENT DE FÍSICA TEÒRICA

Doctorado en Física

Noviembre - 2016

Óscar M. Vives García, Profesor del Departamento de Física Teórica de la Universitat de València

Certifica:

Que la presente memoria "Higgs and flavour phenomenology at the LHC era" ha sido realizada bajo su dirección en la Universitat de València por *María Luisa López Ibáñez* y constituye su Tesis para optar al grado de Doctora en Ciencias Físicas.

Y para que así conste, en cumplimiento de la legislación vigente, presenta en la Universitat de València la referida Tesis Doctoral y firma el presente certificado en València a dos de noviembre de dos mil dieciséis.

Resumen

El pasado julio de 2012 la última pieza que restaba por comprobar del Modelo Estándar (SM) -el bosón de Higgs- fue detectada por los dos grandes experimentos multipropósito del CERN, ATLAS y CMS, a una energía de 125 GeV.
El Modelo Estándar es el marco teórico en el que se describen tres, de las cuatro interacciones fundamentales conocidas, que rigen la dinámica de todas las partículas subatómicas conocidas y que han sido observadas experimentalmente. En él se integran, pero no unifican, la teoría electrodébil -que a su vez conjuga electromagnetismo e interacción débil- y la cromodinámica cuántica, asociada a la interacción nuclear fuerte. Formalmente el grupo de simetría puede ser escrito como: $SU(3)_c \otimes SU(2)_L \otimes U(1)_Y$.
El contenido en partículas fundamentales se puede dividir en tres secciones: bosones de gauge, fermiones de materia y el bosón de Higgs. Los bosones de gauge están asociados a los grupos de simetría -y, por tanto, interacciones- del SM, uno por cada generador del grupo en cuestión. Los fermiones de materia se ordenan en multipletes y se les asignan ciertos números cuánticos que determinan sus cargas, según las cuales interaccionan con los bosones de gauge. Existen tres generaciones de fermiones, que se pueden dividir en quarks y leptones dependiendo de si tienen carga de color (asociada a $SU(3)_c$). El bosón de Higgs es, por su parte, un escalar sin color que aparece tras la rotura espontánea de la simetría electrodébil -para dar lugar al grupo electromagnético- que genera las masas de bosones de gauge y fermiones.
A día de hoy, el Modelo Estándar es la teoría física más exacta y más precisamente medida. Ha superado todos los test experimentales con resultados sobresalientes. A través de ella se predijo, antes de ser observados, la existencia de los bosones gauge W y Z, el gluón, el quark top y el mecanismo de Higgs con su bosón resultante. Además, ha sido confirmada en numerosos test de precisión. Sin embargo, deja numerosos aspectos de la física actual sin respuesta y es extensamente aceptado por la comunidad científica el hecho de que no puede ser una teoría final y, por tanto, debería ser tratada como una teoría efectiva asociada a una cierta escala de energía.

Algunas de estas cuestiones que quedan al margen son: la naturaleza de la materia y la energía oscura, la cuantización de la gravedad, la asimetría materia-antimateria o la naturaleza de los neutrinos. Aparte, son muchos los interrogantes que surgen a partir de ella, por ejemplo: ¿por qué tres generaciones de partículas?, ¿qué origen tienen o cómo se explican las estructuras de sabor en el sector quark y leptónico?, ¿hay una teoría que unifique las tres interacciones fundamentales del SM?, ¿de qué depende que μ -el parámetro del potencial de Higgs que origina la rotura espontánea de simetría- adquiera un valor negativo?, ¿existen escalas a energías mucho mayores donde nuevos efectos físicos se suceden?, ¿por qué la masa del Higgs es tan ligera?. La respuesta a estas cuestiones no es trivial en absoluto y, quizá, tengan que pasar décadas hasta que hallemos las respuestas correctas para algunas de ellas.

Supersimetría es un ejemplo de modelo teórico que amplía el SM y que podría dar respuesta a algunas de las preguntas formuladas anteriormente. De hecho, durante las últimas décadas, ha sido la opción más extendida y estudiada. En ella, las coordenadas (bosónicas) espaciotemporales se amplían para introducir cuatro coordenadas espinoriales adicionales. De esta forma, el álgebra supersimétrica queda definida en términos de conmutadores y anticonmutadores de operadores bosónicos y espinoriales. Además, gracias a esta nueva formulación del álgebra, las consecuencias del Teorema de Coleman-Mandula son eludidas y se consigue la combinación no trivial del grupo de Poincaré -asociado a las simetrías espaciotemporales del sistema- con grupos de Lie asociados a las simetrías internas de las partículas -que determinan las interacciones que conocemos-. Como consecuencia, particulas de naturaleza tan dispar como puedan ser bosones y fermiones, resultan estar relacionados y, de hecho, son agrupados en supermultipletes. Por ejemplo, cada fermión de Weyl conocido podría tener asociado un bosón escalar con el que conviviera en un mismo supermultiplete -*supermultiplete quiral*- o los bosones vectoriales podrían estar asociados a fermiones de Majorana y ser las componentes físicas de un *supermultiplete vectorial*.

Algunas de las virtudes más preciadas de esta teoría, estrechamente ligadas a los problemas que deja en pendientes el SM, son: en ella, nuevas fuentes de violación de CP aparecen y, con ello, la posibilidad de formular un proceso de bariogénesis que prediga adecuadamente la asimetría materia-antimatería observada hoy día; por otro lado, la imposición de una simetría adicional, R-parity que podría estar estrechamente relacionada con la conservación del número B-L característica fundamental del SM, proporciona de forma natural un candidato a materia oscura; además, esta teoría predice la rotura espontánea de las interacciones electrodébiles de forma radiativa debido al *running* de los parámetros al pasar de altas energías a bajas; por último, una de

las propiedades más importantes es que, bajo supersimetría, la masa del Higgs como escalar fundamental quedaría protegida frente a correcciones radiativas y, por tanto, el valor que conocemos para su masa sería completamente compatible con teorías a escalas de energía mucho mayores.

En modelos mínimos de supersimetría, como el MSSM (*Minimal Supersymmetric Standard Model*), el grupo de gauge del SM se mantiene y sólo el espectro de partículas se ve ampliado por motivos tanto teóricos, que hacen que la teoría sea internamente coherente, como experimentales, adecuando las predicciones a resultados ya conocidos y validados. Sin embargo, supersimetría, si efectivamente se da en la naturaleza, ha de ser una simetría rota, ya que, ninguna partícula supersimétrica ha sido detectada aún y, bajo una supersimetría exacta, las partículas pertenecientes a un mismo supermultiplete deberían tener masas iguales. Puesto que no sabemos como se produce esta rotura de simetría, lo que se suele hacer es parametrizar nuestra ignoracia con operadores no renormalizables que la rompen explícitamente, pero de una manera suave (*soft*). Una vez especificadas este tipo de interacciones, junto a los Yukawas heredados del SM, análisis fenomenológicos y predicciones teóricas pueden ser calculadas y enfrentadas a los resultados experimentales actuales.

Los análisis fenomenológicos que componen esta tesis pueden dividirse en dos partes: en primer lugar, estudios sobre el sector del Higgs en el MSSM generalizándolo al caso en el que haya violación explícita de CP y, en segundo lugar, un estudio sobre el origen de las estructuras de sabor que, en modelos como éste, pueden encontrarse en los acoplamientos Yukawa, en los términos de masa que aparecen en el lagrangiano *soft* y en los acoplamientos trilineales a través de los cuales dos sfermiones interaccionan con bosones de Higgs.

El sector del Higgs en el MSSM, a diferencia del Modelo Estándar en el que un único doblete de Higgs da masa a todos los fermiones y bosones de gauge, está constituido por dos superdobletes de isospín que se acoplan o bien a quarks tipo *up* o bien a quarks tipo *down* y leptones. La introducción de estos dos dobletes es necesaria debido a las propiedades del superpotencial y por aspectos tales como como la existencia de anomalías que, en caso contrario, no cancelarían. Esto hace también que, a primer orden, las corrientes neutras con cambio de sabor queden suprimidas. En este tipo de modelos, tras la rotura espontánea de la simetría electrodébil, se obtienen cinco partículas de Higgs -tres neutras y dos cargadas- y tres bosones de Goldstone que son absorbidos por los modos longitudinales de los bosones de gauge débiles. Por otro lado, se puede estudiar la invariancia de CP del potencial de Higgs y se demuestra, efectivamente, que existen una conservación de CP a primer orden; pues las fases que

aparecen en el potencial pueden ser reabsorbidas por los campos mediante las rotaciones adecuadas, quedando un potencial exclusivamente real. Sin embargo, cuando uno considera correcciones a órdenes superiores de los parámetros, se encuentra que esta invariancia bajo transformaciones de CP desaparece y, por tanto, la posibilidad de tener autoestados de CP que se correspondan con los autoestados de masa. Es entonces cuando interesantes efectos fenomenológicos pueden aparecer y en los que nosotros centramos nuestro estudio.

En el primer análisis, modelos MSSM en los que la violación de CP se da a través de la presencia de fases complejas en los acoplamientos trilineares asociados a la tercera generación de sfermiones. En este marco de trabajo, nuestra intención es analizar si, con la implementación de todos los límites experimentales existentes, la posibilidad de identificar el escalar descubierto con el segundo Higgs más ligero del espectro de estos modelos está aún abierta. Es importante señalar aquí que nosotros no imponemos ningún tipo de relación a escalas superiores ni obtenemos los parámetros a la escala electrodébil a través del *running* de las ecuaciones, sino que tratamos todos los parámetros como libres e independientes; en particular las masas de los bosones de Higgs y su matriz de mezcla. Lo que examinamos, en primer lugar, es la señal experimental obtenida en el canal $\gamma\gamma$ que H_2 ha de reproducir. Para ello, un patrón muy concreto de mezcla entre los bosones ha de darse: el Higgs medido ha de ser predominantemente tipo ϕ_u^0 mientras que los dos restantes han de repartirse la parte pseudoescalar y ϕ_d^0. Esto implica que los acoplamientos de H_1 y H_3 con quarks tipo *up* quedan prácticamente suprimidos, a la vez que, los acomplamientos con quarks tipo *down* y leptones se potencian mucho más e, incluso, pueden llegar a ser mucho más intensos que los que se obtendrían normalmente entre un Higgs SM y este tipo de fermiones. Esto es debido a que existe, en los acoplamientos asociados, una proporcionalidad con $\tan\beta$ que hace que estos aumenten significativamente para la región de valores altos y medios de este parámetro. Es en este momento cuando entran en juego algunas de las búsquedas llevadas a cabo por CMS y ATLAS, en relación a Higgses desintegrándose a dos leptones τ.

Para el rango de masas establecido, $m_{H_1}, m_{H_3} \leq 200$ GeV, y para valores medios-altos de $\tan\beta$, lo que nosotros observamos es que los límites experimentales actuales son suficientes como para poder descartar la posibilidad de tener un Higgs neutro adicional a H_2 en este rango de energías. Es decir, las búsquedas llevadas a cabo por CMS y ATLAS imponen tales límites en el canal $\tau\tau$ que la presencia de un Higgs neutro que genere una señal como la medida en el canal $\gamma\gamma$ -en nuestro modelo H_2- se hace incompatible con la existencia de otro Higgs en este rango de masas dado

que, heredando los *couplings* anteriormente mencionados, no hubiera sido ya observado. Sin embargo, aún tenemos la posibilidad de que $\tan\beta$ sea pequeña y estos dos análisis experimentales resulten ser compatibles. Analizamos esta región del espacio de parámetros y encontramos que, efectivamente, se pueden encontrar puntos compatibles que satisfagan los límites en el canal $\tau\tau$ y que reproduzcan la señal en $\gamma\gamma$. Pero nosotros queremos utilizar todos los resultados experimentales disponibles actualmente, y eso incluye medidas y límites procedentes de la física del sabor. En particular, encontramos que el proceso inclusivo $B \to X_s\gamma$ resulta ser muy restrictivo. Específicamente lo que observamos es que ninguno de los puntos surpervivientes comentados anteriormente es compatible con $b \to s\gamma$ a un nivel menor o igual a 2σ. El motivo es sencillo de averiguar una vez que se estudian todas las contribuciones que participan en este proceso: en un modelo MSSM con estructuras mínimas de sabor MFV (*Minimal Flavour Violating*) dos contribuciones se suman a las del SM, una debido al Higgs cargado y otra debido al chargino. La primera resulta ser inversamente proporcional a $\tan\beta$ y a la masa del Higgs cargado, mientras que, la segunda es proporcional a $\tan\beta$. Para valores bajos de este parámetro, la primera contribución crece mucho más de lo que la segunda es capaz de compensar -tienen signos opuestos- de forma que el *branching ratio* (BR) total toma valores que van más allá de los límites experimentales.

De esta forma, haciendo uso de tres observables cuidadosamente escogidos, somo capaces de demostrar que este interesante escenario queda completamente descartado. El siguiente paso podría ser estudiar el caso en el que el Higgs a 125 GeV se correspondiera con el Higgs más pesado -H_3-, pero en tal caso, las consecuencias serían similares: los valores posibles de masa de H_1 y H_2 quedarían limitados a m_{H_1}, $m_{H_2} \leq 125$ GeV y heredarían los acoplamientos de ϕ_d^0 y A^0 con los quarks tipo *down* y leptones. De esta forma, los acoplamientos con leptones τ serían lo suficientemente intesos en la región $\tan\beta \geq 7$ como para que hubieran sido detectados por CMS y ATLAS. Nos tendríamos que restringir, por tanto, a la región de valores pequeños de $\tan\beta$ en la que, para las masas dadas del Higgs cargado $m_{H^\pm} \lesssim 200$ GeV, el BR para el proceso $B \to X_s\gamma$ estaría en conflicto con el resultado experimental a 2σ. En conclusión, con los datos experimentales usados para el análisis, somos capaces de afirmar que el reciente bosón de Higgs descubierto y medido en el LHC ha de corresponderse, en un modelo supersimétrico como el MSSM -con o sin violación de CP-, con el Higgs neutro más ligero del espectro.

En nuestro segundo análisis, tomando como hipótesis el resultado del estudio anterior, testeamos el espacio de parámetros para conocer hasta que punto los resultados exper-

imentales actuales pueden restringir la presencia de bosones de Higgs adicionales para diferentes valores de $\tan\beta$. De nuevo, imponemos que H_1 reproduzca la señal medida por CMS y ATLAS en el canal $\gamma\gamma$, mientras que, los dos bosones neutros restantes, H_2 y H_3, deben tener una composición compatible con las búsquedas de Higgses adicionales a través del canal $\tau\tau$ en estos dos detectores. Además, los resultados de las búsquedas indirectas debidas a procesos como $B \to X_s\gamma$ y $B_s \to \mu^+\mu^-$ se tienen en cuenta para el análisis. Nuestros resultados para este escenario son los siguientes: para cualquier valor de $\tan\beta$ el límite inferior de masa para cualquier Higgs neutro está en los 300 GeV; este límite aumenta rápidamente para valores mayores de $\tan\beta$, ya que, los límites en el canal $\tau\tau$ se vuelven mucho más restrictivos. Por ejemplo, para $\tan\beta \sim 30$, Higgses neutros por debajo de 600 GeV quedan completamente excluídos. Como conclusión de este análisis merece la pena destacar el papel fundamental que tiene el canal $H_i \to \tau\tau$ en la búsqueda de Higgses extra, así como, el hecho de incluir límites experimentales debido a procesos a bajas energías como los mencionados anteriormente. Combinar en los análisis el máximo número posible de resultados experimentales ayuda a tener una imagen más completa del estado del espacio de parámetros y a obtener resultados más coherentes y acertados.

Nuestro tercer trabajo continúa en el sector del Higgs en un MSSM con violación de CP pero, ahora, estudiamos procesos con violación de sabor. Las corrientes neutras cargadas no se dan en el SM, de forma que, la posible medida de alguno de estos procesos indicaría inevitablemente la presencia de nueva física. En particular, escogemos la desintegración $H_i \to b\bar{s}+\bar{b}s$ como objeto de estudio. La razón para seleccionar éste, y no otro proceso, es el hecho de que el Higgs interacciona más intensamente con la tercera generación de fermiones -puesto que estos son más pesados y los acoplamientos con el Higgs son proporcionales a la masa- a la vez que, en comparación con leptones, las interacciones de color son un factor α_3^2/α_2^3 mayores. Además, para este análisis, se consideran dos escenarios: uno al que llamamos *full MSSM*, en el que las condiciones usuales de minimización del potencial se verifican y se tienen tres Higgses neutros mezclados entre sí, y el *generic supersymmetric SM* en el que la posible presencia de más bosones neutros escalares se parametriza y, de una forma efectiva, los elementos de la matriz de mezcla se pueden estudiar como parámetros libres únicamente delimitados por datos experimentales que han de satisfacerse. Los resultados en cada uno de los casos son: para el primer modelo encontramos que $\mathrm{BR}(H_1 \to b\bar{s} + s\bar{b})$ queda brutalmente suprimido a un valor $\mathcal{O}(10^{-6})$ debido a límites experimentales procedentes del proceso de sabor $B_s \to \mu^+\mu^-$ mientras que, para los Higgses más pesados, la imposición de todas las condiciones experimentales no limita demasiado

los BR asociados que se mantienen en $\mathcal{O}(10^{-3})$. El por qué de una respuesta tan discrepante por parte de uno y otros Higgses a la inclusión de límites de sabor, en particular del proceso $B_s \to \mu\mu$, es analizado en el texto y lo resumimos aquí: mientras que el BR para el proceso de desintegración del Higgs más ligero a los quarks b y s resulta inversamente proporcional a la masa de los Higgses pesados -que a todos los efectos pueden ser considerados como degenerados- el BR asociado a los otros Higgses no contiene esta dependencia; a su vez, las contribuciones más importantes al BR asociado al proceso de sabor resultan proceder de los Higgses pesados, de forma que, en total, el BR es proporcional a $\tan\beta$ e inversamente proporcional a la masa de estos Higgses. De esta forma, en el caso del Higgs ligero, valores grandes de BR se corresponden con valores bajos de las masas de los Higgses pesados para los que el BR de sabor se vuelve mucho más restrictivo, si nos movemos en el régimes de valores altos y medios de $\tan\beta$. En cambio, en el caso de los Higgses pesados, para cualquier valor de $\tan\beta$ puedo encontrar un valor de masa tal que el proceso de sabor no me limite y, puesto que el BR del proceso de desintegración de estos Higgses a los quarks b y s es independiente de sus masas, esto no me influye en los ratios posibles de desintegración. Para el segundo modelo, los resultados cualitativos se mantienen, aunque cambian significativamente los valores cuantitativos del BR del Higgs ligero. En este caso, para el Higgs más ligero, el BR aumenta hasta los $\mathcal{O}(10^{-4})$ mientras que, para los Higgses pesados, el valor del BR se mantiene igual al del caso anterior. En conclusión, aunque incluso en este último caso el BR para el Higgs descubierto queda fuera del alcance del LHC, es posible que el estudio de este tipo de procesos sea aún interesante en el contexto de colisionadores lineales.

Por último, en el capítulo final de esta tesis, se hace un análisis acerca del posible origen de las estructuras de sabor que se dan en algunos de los parámetros asociados a modelos supersimétricos, como el MSSM. En particular, tanto los acoplamientos Yukawa entre fermiones y Higgses, como los acoplamientos trilineales entre sfermiones y Higgses y las masas soft de los sfermiones pueden presentar estructuras no triviales de sabor. Nosotros, en este trabajo, nos centramos en el estudio de simetrías à la Froggatt-Nielsen (FN), como posible mecanismo a través del cual los acoplamientos Yukawa con las adecuadas jerarquías pueden obtenerse, así como, los trilinares y las matrices *soft*. El mecanismo de FN supone que existe una simetría de sabor y una escala a la que ésta se rompe de forma espontánea, debido a la adquisión de un *vev* por parte de uno o varios campos. De esta forma, términos que anteriormente eran de interacción entre *flavones* -campos que rompen la simetría de sabor- y los campos del MSSM pasan a ser vértices efectivos con acoplamientos Yukawa, trilineales o términos

de masa.
Sin embargo, para que esto se dé, uno ha de suponer que supersimetría está ya rota en el momento en el que los flavones adquieren su *vev*, puesto que de otra manera los términos *soft* no estarían presentes y, por lo tanto, no heredarían estas jerarquías de sabor. El mecanismo a través del cual supersimetría se rompe no está bien establecido, aunque sí hay consenso respecto al hecho de que la rotura de supersimetría ha de darse en un sector *oculto*, es decir, a través de unos campos que no interaccionan directamente con los campos del MSSM o, si lo hacen, se produce a través de unos acoplamientos muy suprimidos. Después de la ruptura de la simetría, ésta se comunicaría al sector *visible* del MSSM a través de los mensajeros. Diversas opciones se han propuesto respecto a esto, siendo una de ellas la gravedad. Es decir, sería a través de interacciones de origen gravitatorio como se propagaría la ruptura de supersimetría de un sector a otro. Por tanto, las interacciones entre el sector visible y los mensajeros vendrían suprimidas por la escala de Planck. De hecho, en este modelo tendríamos: $\Lambda_{\rm EW} \ll \Lambda_f \lesssim \Lambda_{\rm SUSY} = M_{\rm Planck}$. En particular, nosotros suponemos, para simplificar la discusión, la existencia de un sólo campo X cuyo F-term adquiere un *vev* que produciría la rotura espontánea de supersimetría.
Definimos, por tanto nuestro modelo, a partir de unas ciertas expresiones que determinan el superpotential y el potencial de Kähler. El primero dará origen a los acoplamientos Yukawa y, tras el *vev* del F-term de X, a los acoplamientos trilineares. Todos ellos tras las rotura de la simetría de sabor. El segundo, en cambio, da lugar a los términos de masas *soft*. Para nuestro análisis, proponemos dos ejemplos bastante significativos como grupos de sabor: el grupo abeliando $U(1)_f$ y el grupo no-abeliano $SU(3)_f$. En ambos casos, el superpotencial se especifica en términos de las interacciones entre los supermultipletes quirales y los flavones, así como, el potencial de Kähler, que es una función de supercampos quirales y antiquirales. Una vez que la simetría de sabor se rompe y los flavones adquieren su *vev*, cada elemento de matriz de los Yukawas viene dado como una cierta potencia de $\langle\phi\rangle/M \equiv \epsilon \ll 1$, donde $\langle\phi\rangle$ es el *vev* y M representa la escala de los mensajeros -mucho más pesados- que se integran con el fin de obtener un vértice efectivo. La potencia que corresponde a cada elemento tiene su origen en diagramas concretos -que se determina a través de las cargas asignadas a los campos- que acoplan los supermultipletes quirales correspondientes con los supermultipletes asociados al Higgs a través de flavones y campos mensajeros. De esta forma, la jerarquía presente en las matrices Yukawa aparece de forma natural a partir de la rotura de un grupo de simetría de sabor. Puesto que los acoplamientos trilineares surgen del superpotencial cuando SUSY se rompe como: $V = m_{3/2}\mathsf{W}$, con

$m_{3/2} = \langle F_{\mathsf{X}} \rangle / M_{\mathrm{P}}$; los trilineares se obtendían de una forma similar a los Yukawas, a partir de los diagramas obtenidos anteriormente para ellos, analizando todas las formas posibles en las que el F-term puede acoplarse. Cada una de estas formas, daría una contribución a ese elemento de matrix. De modo que: $a_{ij} = N\, m_{3/2}\, Y_{ij}$, donde N representa esta multiplicidad asociada a cada diagrama. Para obtener los términos de masas *soft* el proceso es completamente equivalente. Analizamos, en primer lugar, los acoplamientos efectivos que, tras la rotura de sabor, nos generarían el elemento $\Phi^{*i}\Phi_j$ del potencial de Kähler. Los términos de masa vienen dados a partir del Kähler como: $m^2_{3/2}\, \Phi^{*i}\Phi_j$. Por tanto, cada elemento se obtendría considerando todas las posibilidades en las que los F-terms de X y X^* pueden entrar en el diagrama que acopla Φ^{i*} con Φ_j a través de flavones y mensajeros.
Una vez obtenidas todas las estructuras de sabor a través de este mecanismo, los campos ha de ser redefinidos para llevarlos a la base canónica y, en caso de querer estudiar su fenomenología como nosotros hacemos, a la base SCKM en la que las matrices de masa de los quarks son diagonales. Los observables de sabor que nosotros utilizamos son Δm_K, ϵ_K y ϵ'/ϵ. De esta forma, somos capaces de obtener límites complementarios a los de los grandes colisionadores para masas de gluinos y squarks. Los resultados que obtenemos para los dos grupos considerados son: para el primer caso encontramos que, efectivamente, en este modelo simplificado, los límites que se deducen de esta fenomenología de sabor podrían mejorar aquellos obtenidos en el LHC para la producción directa de gluinos; en el segundo caso, no obstante, los límites que se generan son demasiado débiles en comparación con los obtenidos por CMS y ATLAS en sus búsquedas directas de supersimetría. Nuestras conclusiones, para este trabajo, son las siguientes: la física del sabor y el origen de las jerarquías en los acoplamientos Yukawa son una de las cuestiones a las que el SM no da respuesta y que podrían dirigirnos hacia el encuentro de nueva física. Estudios que complementen las búsquedas de los grandes colisionadores son cada vez más urgentes, ya que, pueden pasar décadas hasta que se consiga la energía necesaria como para poder producir estas partículas de forma directa. Sin embargo, estudios a bajas energías con alta precisión pueden ser la clave para encontrar, de forma indirecta, los efectos de estas masivas partículas como perturbaciones a los procesos ya conocidos que se dan, o no, en el SM. Nosotros, por nuestra parte, consideramos que este es el camino a seguir y por tanto una ampliación de este trabajo está en marcha en la que nuestra intención es estudiar con detalle uno o dos casos concretos en el que se implemente tanto la fenomenología del sector sector quark como el leptónico, lo cual no se ha sido realizado con detalle anteriormente.

Contents

Overview

During the last decades, supersymmetry (SUSY) has been a fascinating way to figure out phenomena that lie beyond the well-established Standard Model (SM). One of the most interesting reasons why theoretical physicists have been lead to believe that supersymmetry should play a fundamental role in particle physics is the fact that the supersymmetry algebra is the only graded Lie algebra capable to relate the spacetime symmetries with the internal symmetries of the fundamental particles giving a framework where gravitation might be quantized.

Apparently, the first known mention of a supersymmetry algebra was by Hironari Miyazawa [1–3] in a work where a novel algebra in which baryons and mesons could be arranged together in the same (super)multiplet was proposed. However, it was not until the 1970s when supersymmetry was rediscovered and largely explored. In 1971, Neveu-Schwarz [4] and Ramond [5] working on supersymmetries regarding them as a new anticommuting gauge symmetries in the context of two-dimensional dual theories whereas, independently, Gol'fand and Likhtman [6] found it as an extension of the Poincaré algebra where two bispinor generators were added. Later on, in 1974, Wess and Zumino presented for the first time a four-dimensional point particle supersymmetric theory identifying the characteristic renormalization features of the model [7–9] and, in 1975, another important result arrived due to Hagg, Lopuszanski and Sohnius [10] who presented the full collection of possible generators for supersymmetries on the grounds of the Coleman-Mandula theorem. Finally, in 1977, the basis of the first realistic supersymmetric version of the Standard Model were set up by Pierre Fayet [11–14].

Since then, an spectacular progress has been made in the construction of sophisticated models able to explain diverse phenomenae that the SM cannot encompass. Among them, *naturalness* and a solution to the *hierarchy problem* (if SUSY particles show up around the TeV scale), gauge couplings unification, a dark matter candidate, new sources of CP-violation for baryogenesis in inflation, a more natural origin of sponta-

neous symmetry breaking and a straightforward generalization embracing quantum gravity.

One of the most controversial questions is the hierarchy problem, which in fact is a difficulty that in the SM, by itself, does not arise [15]. In general, fine tunning issues are either related to explicit nonperturbative aspects of the theory or embeddings of the SM into a more complete dynamics visible at high energies, such as could be supergravity at the Planck scale. The Higgs boson, as a fundamental scalar particle, suffers from the fact that its mass is not protected for any symmetry and it receives enormous loop corrections from every particle that couples, directly or indirectly, to it. The supersymmetric solution to this problem consists of a miraculous cancellation that occurs due to the different sign of the corrections belongin to SM particles and its supersymmetric partners. However, if this symmetry is badly broken and the masses of the supersymmetric particles are much larger than the standard ones, the hierarchy and naturalness problems would be reintroduced again. For a Higgs mass $\mathcal{O}(100$ GeV) GeV, the new particles should not be heavier than $\mathcal{O}(1$ TeV).

Another good feature of supersymmetry is that even in minimal models, unlike the SM, the unification of the gauge couplings is achieved due to the inclusion of the right particle content. Similarly, the introduction of an additional symmetry *R-parity* provides a good cold dark matter candidate. Also, the presence of numerous new CP-violating phases in the theory may help in the mechanism of baryogenesis for the matter-antimatter asymmetry.

Regarding the electroweak symmetry breaking, one should recall that in the SM the spontaneous breaking of the symmetry takes places owed to the negative value of one parameter. In principle, this is not theoretically justified in the SM but in supersymmetry it can be obtained naturally from the RG running of one of the parameters in the Higgs potential. Finally, the natural promotion of supersymmetry as a local symmetry, directly leads to the formulation of a theory of quamtum gravity.

However, the High Energy Physics of the beginning of the 21st century have been strongly imprinted by the impressive success of the SM as the correct description of fundamental interactions up to energies of $\mathcal{O}(14$ TeV). In fact, thanks to the enormous efforts of experimentalists and theorists all over the world, the last piece of the puzzle -the Higgs particle confirming the Brout–Englert–Higgs mechanism to endow the SM particles with mass- have been found and the picture is now completed. In addition to that, much better sensitivities have been achieved with an astonishing agreement with the SM predictions. However, this enormous accomplishment, instead of being felt as a big success, has turn out to be quite a bitter victory since the particle physics

assigment of finding a road towards new physics has been not fulfilled. If we are all convinced that the SM cannot be the ultimate theory, we are in the dark about when, where and how physics beyond the SM should manifest itself.
As a matter of fact, one may argue [16] that the LHC has provided three indirect pieces of evidence favouring SUSY: the need to stabilize the electroweak vacuum and a successful prediction of the Higgs boson mass and its SM-like couplings by simple SUSY models [17–20]. The problem of the electroweak stability arises with the measured values for the top and Higgs masses, if no physics beyond the SM is considered. In SUSY, taking into account the effects of the supersymmetric particles, this question is solved. Regarding the SUSY predictions about the Higgs, SUSY establishes an upper bound for the lightest Higgs of 130 GeV in perfectly agreement with the discovered boson. Similarly, many models account for a lightest scalar SM-like where the discrepancies between its couplings and the couplings of a real SM scalar would be found with higher precision. The prospects for discovering SUSY effects in the near future include dedicated searches of jets plus missing energy, sleptons and light stops squarks in the LHC together with precision observables which may shed some light on the indirect presence of SUSY particles.

1

Introduction to Supersymmetry

The Coleman-Mandula theorem [23, 24] states that the symmetry group of any consistent quantum field theory cannot be any other but the trivial combination (direct product) of spacetime (Poincaré group) and internal symmetries. The supersymmetry algebra, by means of considering both commuting and anticommuting generators, relaxes the Coleman-Mandula assumptions and allows for a nontrivial extension of the Poincaré algebras providing a connection between spacetime symetries and the internal symmetries of the fundamental particles. As a consequence, particles with such a different nature as fermions and bosons turn out to be related.

1.1 Superspace and superfields

Supersymmetry is considerably simplified and conveniently formulated through the important geometric concept of superspace. Superspace is the extension of the usual spacetime, represented by the bosonic coordinates x^μ, by introducing four additional fermionic coordinates [25, 26]

$$\left\{ x^\mu,\ \theta^\alpha,\ \theta^\dagger_{\dot{\alpha}} \right\} \tag{1.1}$$

$\alpha = 1, 2$. These new fermionic coordinates are called Grassmann numbers (c-numbers) and because of their anti-commuting character they satisfy $\theta^{\alpha^2} = 0 = \theta^{\dagger^2}_{\dot{\alpha}}$. In the context of supersymmetry, they are complex constant two-component spinors with dimension $[\text{mass}]^{-1/2}$. In fact, they can be interpreted as the two components associated with a Majorana spinor $\theta^{\alpha^T} = \left(\theta^\alpha\ \theta^\dagger_{\dot{\alpha}}\right)$.

In this formulation, $N = 1$ global supersymmetry transformations can be thought of as infinitesimal translations in superspace, with ϵ and $\epsilon^\dagger$ the parameters of the transformation

$$\begin{aligned} x^\mu &\longrightarrow x^\mu + i\,\epsilon\sigma^\mu\theta^\dagger + i\,\epsilon^\dagger\bar{\sigma}^\mu\theta \\ \theta^\alpha &\longrightarrow \theta^\alpha + \epsilon^\alpha \qquad (1.2) \\ \theta^\dagger_{\dot{\alpha}} &\longrightarrow \theta^\dagger_{\dot{\alpha}} + \epsilon^\dagger_{\dot{\alpha}} \qquad (1.3) \end{aligned}$$

The generators of the group represent the infinitesimal action of the group on the parameter space. They can be written as differential operators which will act on superfields

$$Q_\alpha = i\frac{\partial}{\partial\theta^\alpha} - \left(\sigma^\mu\theta^\dagger\right)_\alpha \partial_\mu \qquad (1.4)$$

$$Q^{\dagger\dot{\alpha}} = i\frac{\partial}{\partial\theta^\dagger_{\dot{\alpha}}} - \left(\bar{\sigma}^\mu\theta\right)^{\dot{\alpha}} \partial_\mu \qquad (1.5)$$

where superfields are functions depending on the supercoordinates. It can be shown that the generators given above satisfy the following set of commutation and anti-commutation rules

$$\left\{Q_\alpha,\, Q^\dagger_{\dot{\alpha}}\right\} = -2\,\sigma^\mu_{\alpha\dot{\alpha}}\,P_\mu \qquad (1.6)$$

$$\{Q_\alpha,\, Q_\beta\} = 0 = \left\{Q^\dagger_{\dot{\alpha}},\, Q^\dagger_{\dot{\beta}}\right\} \qquad (1.7)$$

$$[\,Q_\alpha,\, P_\mu\,] = 0 = \left[\,Q^\dagger_{\dot{\alpha}},\, P_\mu\,\right] \qquad (1.8)$$

$$[\,Q_\alpha,\, M_{\mu\nu}\,] = -\frac{1}{2}\,(\sigma_{\mu\nu}\,Q)_\alpha \qquad (1.9)$$

$$\left[\,Q^\dagger_{\dot{\alpha}},\, M_{\mu\nu}\,\right] = \frac{1}{2}\left(Q^\dagger\,\bar{\sigma}_{\mu\nu}\right)_{\dot{\alpha}} \qquad (1.10)$$

where $\sigma^{\mu\nu} = \frac{i}{2}\,[\sigma^\mu, \bar{\sigma}^\nu]$, $P^\mu = -i\partial_\mu$ is the four-momentum generator of spacetime translations and $M^{\mu\nu}$ is the generator of Lorentz transformations. Eq.(1.8) tells us that P^2 will be a Casimir operator of the algegra and therefore the fields belonging to the same irreducible representation must have equal masses, at least if the symmetry is exact. On the contrary, eqs.(1.9) and (1.10) imply the non-conservation of spin wherein a supermultiplet. As a matter of fact, one may prove that every representation of the algebra must contain an equal number of fermionic and bosonic states [27]. This algebra may be entirely rewritten in terms of commutators making use of ϵ and $\epsilon^\dagger$.

As pointed out before, superfields are functions of superspace. Actually, they should be understood in terms of their power series expansions in θ and $\theta^\dagger$ [25]. As we are considering two components for θ^α and two for $\theta^\dagger_{\dot\alpha}$, the highest order term allowed in the expansion will contain $\theta\theta$ and $\theta^\dagger\theta^\dagger$. Hence, the most general superfield can be written as

$$\mathsf{S}(x,\theta,\theta^\dagger) = \phi + \theta\,\xi + \theta^\dagger\,\chi^\dagger + \theta\theta\,F + \theta^\dagger\theta^\dagger\,c + \theta^\dagger\bar\sigma^\mu\theta\,A_\mu + \theta^\dagger\theta^\dagger\theta\,\eta + \theta\theta\theta^\dagger\zeta^\dagger + \theta\theta\theta^\dagger\theta^\dagger\,d$$

where ϕ, F, c, A_μ and d are eight complex bosonics fields (or sixteen real) and ξ, $\chi^\dagger$, η and $\zeta^\dagger$ are four two-component Weyl fermion fields.
The effect in a general scalar superfield of an infinitesimal SUSY transformation on the superspace can be computed through the differential operators obtained in eqs.(1.4) and (1.5)

$$\begin{aligned}\sqrt{2}\,\delta_\epsilon\mathsf{S} &= -i\,\left(\epsilon Q + \epsilon^\dagger Q^\dagger\right)\,\mathsf{S} \\ &= \mathsf{S}(x^\mu + i\epsilon\sigma^\mu\theta^\dagger + i\epsilon^\dagger\bar\sigma^\mu\theta,\,\theta+\epsilon,\,\theta^\dagger+\epsilon^\dagger) \;-\; \mathsf{S}(x^\mu,\,\theta,\,\theta^\dagger)\end{aligned} \tag{1.11}$$

In particular, the component field transformations will be given by

$$\sqrt{2}\,\delta_\epsilon\phi = \epsilon\xi + \epsilon^\dagger\chi^\dagger \tag{1.12}$$

$$\sqrt{2}\,\delta_\epsilon\xi_\alpha = 2\epsilon_\alpha F - \left(\sigma^\mu\epsilon^\dagger\right)_\alpha\,(A_\mu + i\partial_\mu\phi) \tag{1.13}$$

$$\sqrt{2}\,\delta_\epsilon\chi^{\dagger\dot\alpha} = 2\epsilon^{\dagger\dot\alpha}c + (\bar\sigma^\mu\epsilon)^{\dot\alpha}\,(A_\mu - i\partial_\mu\phi) \tag{1.14}$$

$$\sqrt{2}\,\delta_\epsilon F = \epsilon^\dagger\zeta^\dagger - \frac{i}{2}\epsilon^\dagger\bar\sigma^\mu\partial_\mu\xi \tag{1.15}$$

$$\sqrt{2}\,\delta_\epsilon c = \epsilon\eta - \frac{i}{2}\epsilon\sigma^\mu\partial_\mu\chi^\dagger \tag{1.16}$$

$$\sqrt{2}\,\delta_\epsilon A^\mu = \epsilon\sigma^\mu\zeta^\dagger - \epsilon^\dagger\bar\sigma\eta - \frac{i}{2}\epsilon\sigma^\nu\bar\sigma^\mu\partial_\nu\xi + \frac{i}{2}\epsilon^\dagger\bar\sigma^\nu\sigma^\mu\partial_\nu\chi^\dagger \tag{1.17}$$

$$\sqrt{2}\,\delta_\epsilon\eta_\alpha = 2\epsilon_\alpha d - i(\sigma^\mu\epsilon^\dagger)_\alpha\partial_\mu c - \frac{i}{2}(\sigma^\nu\bar\sigma^\mu\epsilon)_\alpha\partial_\mu A_\nu \tag{1.18}$$

$$\sqrt{2}\,\delta_\epsilon\zeta^{\dagger\dot\alpha} = 2\epsilon^{\dagger\dot\alpha}d - i(\bar\sigma^\mu\epsilon)^{\dot\alpha}\partial_\mu F + \frac{i}{2}(\bar\sigma^\nu\sigma^\mu\epsilon^\dagger)^{\dot\alpha}\partial_\mu A_\nu \tag{1.19}$$

$$\sqrt{2}\,\delta_\epsilon d = -\frac{i}{2}\epsilon^\dagger\bar\sigma^\mu\partial_\mu\eta - \frac{i}{2}\epsilon\sigma^\mu\partial_\mu\zeta^\dagger \tag{1.20}$$

However, it can be shown that this general supermultiplet is a reducible representation of the supersymmetry algebra. Irreducible representations may be always found by imposing covariant constraints [26], that is constraints involving only superfields

and their covariant derivatives. Thus, a new derivation compatible with SUSY transformations is required: $\delta_\epsilon(D_\alpha \mathsf{S}) = D_\alpha(\delta_\epsilon \mathsf{S})$. It is evident that $\partial/\partial\theta^\alpha$ and $\partial/\partial\theta^\dagger_{\dot\alpha}$ are not valid for this purpose. In $N = 1$ supersymmetry, chiral covariant derivatives are defined as

$$D_\alpha = \frac{\partial}{\partial\theta^\alpha} - i\left(\sigma^\mu\theta^\dagger\right)_\alpha \partial_\mu \tag{1.21}$$

$$\overline{D}^{\dot\alpha} = \frac{\partial}{\partial\theta^\dagger_{\dot\alpha}} - i\left(\bar\sigma^\mu\theta\right)^{\dot\alpha} \partial_\mu \tag{1.22}$$

so that, with this definition, chiral covariant derivatives acting on superfields return superfields. Moreover, an irreducible representation of the algebra may be obtained through the condition

$$\overline{D}_{\dot\alpha}\Phi = 0 \tag{1.23}$$

This superfield is called a chiral (left-chiral) superfield. Its complex conjugated would be an anti-chiral (right-chiral) superfield and would be defined by $D_\alpha\Phi^* = 0$. In terms of $y^\mu = x^\mu + i\theta^\dagger\bar\sigma^\mu\theta$ and θ, Eq.(1.23) has a very simple solution

$$\Phi = \phi(y) + \sqrt{2}\theta\,\psi(y) + \theta\theta\,F(y) \tag{1.24}$$

Hence a chiral supermultiplet contains as component fields a complex scalar, ϕ, a two-component Weyl fermion, ψ, and the auxiliary bosonic field F. In the case where it represents a fundamental chiral supermultiplet, its dimension is [mass][1]. It is also straightforward to see that holomorphic functions of chiral superfields are also chiral superfields and that from any general superfield S a chiral superfield may be obtained as

$$\Phi = \overline{DD}\,\mathsf{S} \qquad\qquad \Phi^* = DD\,\mathsf{S} \tag{1.25}$$

since $\overline{D}_{\dot\alpha}\overline{D}_{\dot\beta}\overline{D}_{\dot\gamma} = 0 = D^\alpha D^\beta D^\gamma$. Similarly, one may define vector or real supermultiplets as $\mathsf{V} = \mathsf{V}^*$. In the Wess-Zumino (WZ) gauge[1], the solution can be simply written as

[1] The most general expression for a vector supermultiplet is:

$$\begin{aligned}\mathsf{V} &= \phi + \theta\xi + \theta^\dagger\xi^\dagger + \theta\theta b + \theta^\dagger\theta^\dagger b^* + \theta^\dagger\bar\sigma^\mu\theta A_\mu + \theta^\dagger\theta^\dagger\theta(\lambda - \frac{i}{2}\sigma^\mu\partial_\mu\xi^\dagger) + \theta\theta\theta^\dagger(\lambda^\dagger - \frac{i}{2}\bar\sigma^\mu\partial_\mu\xi)\\ &+ \theta\theta\theta^\dagger\theta^\dagger(\frac{1}{2}D + \frac{1}{4}\partial_\mu\partial^\mu\phi)\end{aligned}$$

where a redefinition of the original fields in S -η, ζ and d- in terms of λ, D, ξ and ϕ has been introduced (the explicit expressions are given below). However, through a supergauge transformation some of

$$V_{\rm WZ} \;=\; \theta^\dagger\bar\sigma^\mu\theta\, A_\mu \;+\; \theta^\dagger\theta^\dagger\theta\lambda \;+\; \theta\theta\theta^\dagger\lambda^\dagger \;+\; \frac{1}{2}\theta\theta\theta^\dagger\theta^\dagger\, D \tag{1.26}$$

where some redefinitions have been introduced: $\zeta_\alpha = \eta_\alpha = \lambda_\alpha - i/2\,(\sigma^\mu\partial_\mu\xi^\dagger)$ and $d = 1/2\,D + 1/4\,\partial_\mu\partial^\mu\phi$. The presence of a vector field, A^μ, in Eq.(1.26) suggest that this supermultiplet will be exploited to construct supersymmetric gauge theories.

1.2 Lagrangians in superspace

Chiral and vector supermultiplets are the elemental blocks from which all supersymmetric renormalizable Lagrangians can be built. In particular, recalling eqs.(1.15) and (1.20) we may observe that both the F-term of a chiral superfield and the D-term of a vector supermultiplet tranform under supersymmetry as total derivatives. Therefore, supersymmetric-invariant actions can be formulated from them as

$$\delta_\epsilon\, A = 0 \quad \text{with} \quad A = \int dx^\mu \mathcal{L} \tag{1.27}$$

with the Lagrangian density $\mathcal{L}$ given by

$$[\mathsf{V}]_D \equiv\; \mathsf{V}(x,\,\theta,\,\theta^\dagger)|_{\theta\theta\theta^\dagger\theta^\dagger} \;=\; \int d^2\theta\, d^2\theta^\dagger\, \mathsf{V}(x,\,\theta,\,\theta^\dagger)|_{\theta=0}$$

or

$$[\Phi]_F + \text{ c.c. } \equiv\; \Phi|_{\theta\theta} \;+\; \Phi^*|_{\theta^\dagger\theta^\dagger} \;=\; \int d^2\theta\, \Phi(x,\,\theta)|_{\theta^\dagger=0} \;+\; \int d^2\theta^\dagger\, \Phi^*(x,\,\theta^\dagger)|_{\theta=0}$$

For chiral superfields, the complex conjugated should be introduced since the superfield is complex but the action must be real. Of course, it can be also shown that any F-term contribution in the Lagrangian can be written as a D-term, and vice versa, using that $\overline{DD}(\theta^\dagger\theta^\dagger) = DD(\theta\theta) = -4$ [17].

1.2.1 Chiral interactions

The most general supersymmetric renormalizable Lagrangian involving only chiral superfields is given by

these fields can be eliminated. Thus, a vector supermultiplet is said to be in the **Wess-Zumino gauge** when it is written just in terms of the vector field, the D-term and the Majorana fermion as in Eq.(1.26)

$$\mathcal{L}_{\rm chiral} \;=\; \big[\,\Phi^{*i}\Phi_i\,\big]_D \;+\; \Big(\big[\,\mathsf{W}(\Phi_i)\,\big]_F \;+\; \text{c.c.}\Big) \tag{1.28}$$

The first term corresponds with the D-term of a real vectorfield resulting from the product $\Phi^{*i}\Phi_i$, which can be computed in terms of the component fields as

$$\big[\,\Phi^{*i}\Phi_i\,\big]_D \;=\; \int d^2\theta\, d^2\theta^\dagger\; \Phi^{*i}\Phi_i = -\partial^\mu\phi^{*i}\partial_\mu\phi_i + i\psi^{\dagger i}\bar\sigma^\mu\partial_\mu\psi_i + F^{*i}F_i + \ldots \tag{1.29}$$

where the ellipses represent a total derivative which vanish upon integration. The remaining terms are the kinetic contributions for the component fields. The second term in Eq.(1.28) is the F-term of $\mathsf{W}(\Phi_i)$, which refers to an holomorphic function of chiral supermultiplets. Considering the particular form $\mathsf{W}(\Phi_i) = \frac{1}{2}M^{ij}\Phi_i\Phi_j + \frac{1}{6}y^{ijk}\Phi_i\Phi_j\Phi_k$, its F-term will be

$$\begin{aligned}\big[\,\mathsf{W}(\Phi_i)\,\big]_F \;&=\; \frac{1}{2}M^{ij}\,(\phi_iF_j \,+\, \phi_jF_i \,-\, \psi_i\psi_j\,) \\ &+\; \frac{1}{6}y^{ijk}\,(\phi_i\phi_jF_k \,+\, \phi_k\phi_iF_j \,+\, \phi_j\phi_kF_i \,-\, \psi_i\psi_j\phi_k \,+\, \psi_i\psi_k\phi_j \,+\, \psi_j\psi_k\phi_i\,)\end{aligned} \tag{1.30}$$

The auxiliary fields F_i can be integrated out from Eq.(1.29) and Eq.(1.30) using their Euler-Lagrange equations of motion

$$\begin{aligned}\frac{\partial\mathcal{L}}{\partial F^{*k}} \;&=\; F_k \,+\, W_k^* \;=\; 0 \quad\Longrightarrow\quad F_k \;=\; -\,W_k^* \\ \frac{\partial\mathcal{L}}{\partial F_k} \;&=\; F^{*k} \,+\, W^k \;=\; 0 \quad\Longrightarrow\quad F^{*k} \;=\; -\,W^k\end{aligned} \tag{1.31}$$

$$\begin{aligned}\text{with}\qquad W_k^* \;&=\; \frac{\partial\,[\mathsf{W}(\Phi)]_F^*}{\partial F^{*k}} \;=\; M_{ki}^*\,\phi^{*i} \,+\, \frac{1}{2}\,y_{kij}^*\,\phi^{*i}\phi^{*j} \\ W^k \;&=\; \frac{\partial\,[\mathsf{W}(\Phi)]_F}{\partial F_k} \;=\; M^{ki}\,\phi_i \,+\, \frac{1}{2}\,y^{kij}\,\phi_i\phi_j\end{aligned}$$

Once F_i have been removed, the complete Lagrangian for interactive chiral superfields in terms of the (physical) component fields will be given by

$$\begin{aligned}\mathcal{L}_{\rm chiral} \;&=\; -\partial^\mu\phi^{*i}\partial_\mu\phi_i \,+\, i\psi^{\dagger i}\bar\sigma^\mu\partial_\mu\psi_i \,-\, \frac{1}{2}M^{ij}\psi_i\psi_j \,-\, \frac{1}{2}M_{ij}^*\psi^{\dagger i}\psi^{\dagger j} \\ &-\; \frac{1}{2}y^{ijk}\phi_i\psi_j\psi_k \,-\, \frac{1}{2}y_{ijk}^*\phi^{*i}\psi^{\dagger j}\psi^{\dagger k} \,-\, V(\phi,\phi^*)\end{aligned} \tag{1.32}$$

In addition to the kinetic terms, mass-like contributions for the fermionic components appear in the first line and Yukawa interactions together with the scalar potential in the second line. The scalar potential consists of the purely scalar interactions

$$\begin{aligned} V(\phi,\phi^*) &= F^{*i}F_i = M^*_{ik}M^{kj}\,\phi^{*i}\phi_j + \frac{1}{2}\,M^{in}y^*_{jkn}\phi_i\phi^{*j}\phi^{*k} \\ &+ M^*_{in}y^{jkn}\phi^{*i}\phi_j\phi_k + \frac{1}{4}\,y^{ijn}y^*_{kln}\phi_i\phi_j\phi^{*k}\phi^{*l} \end{aligned} \tag{1.33}$$

1.2.2 Gauge interactions

Let us consider a general supergauge transformation associated with a symmetry whose generators are T^a in the representation $\mathcal{R}$. For each generator of the Lie algebra, we will have a vector boson field A^a_μ which will be contained in the associated vector supermultiplet $\mathsf{V^a}$. Then, if Ω^a represent the (chiral superfield) parameters of the gauge transformation, the transformation law for a vector supermultiplets will be

$$e^{\mathsf{V}} \longrightarrow e^{i\Omega^\dagger}\,e^{\mathsf{V}}\,e^{-i\Omega} \tag{1.34}$$

where $\Omega = 2g_a\Omega^a T^a$ and $\mathsf{V} = ig_aT^a\mathsf{V}^a$. The correspondent field strength superfield will be given by

$$\mathcal{W}_\alpha = -\frac{1}{4}\,\overline{DD}(e^{-V}D_\alpha e^V) \tag{1.35}$$

where again $\mathcal{W}_\alpha = 2g_a\mathcal{W}^a_\alpha T^a$. Observe that $\mathcal{W}_\alpha$ is a chiral superfield, since $\overline{D}_{\dot\alpha}\mathcal{W}^\beta = 0$. It can be useful to take into account that we can always choose the gauge in which we prefer to work. In particular, one may set the Wess-Zumino gauge and compute the F-term associated with $\mathcal{W}^{a\,\alpha}\mathcal{W}^a_\alpha$ as

$$\begin{aligned} [\,\mathcal{W}^{a\,\alpha}\mathcal{W}^a_\alpha\,]_F &= \frac{1}{4k_ag_a^2}\,\mathrm{Tr}\,[\,\mathcal{W}^\alpha\mathcal{W}_\alpha\,]_F = D^aD^a + 2i\lambda^a\sigma^\mu\nabla_\mu\lambda^{\dagger a} - \frac{1}{2}F^{a\mu\nu}F^a_{\mu\nu} \\ &+ \frac{i}{4}\epsilon^{\mu\nu\rho\kappa}\,F^a_{\mu\nu}F^a_{\rho\kappa} \end{aligned} \tag{1.36}$$

In this case, the result can be generalized since it correspond to a gauge-invariant term. Eq.(1.36) reproduces the kinetic terms and self-interactions for the vector supermultiplet component fields. Notice that as every chiral superfield, the complex conjugated term must be introduced in the theory too.

On the other hand, if chiral supermultiplets couple with the gauge fields, they will transform under gauge transformations as

$$\Phi_i \longrightarrow \left[e^{i\Omega}\, \Phi \right]_i \tag{1.37}$$

Therefore, Eq.(1.29) is not gauge-invariant any more and it needs to be reformulated in a suitable way. For instance,

$$\Phi^{*i}\, (e^{\mathsf{V}})_i{}^j\, \Phi_j \tag{1.38}$$

From eqs.(1.34) and (1.37), one may see that Eq.(1.38) is clearly gauge-invariant now. The correspondent D-term will be

$$\begin{aligned} \left[\Phi^{*i}\, (e^{\mathsf{V}})_i{}^j\, \Phi_j \right]_D &= -\nabla_\mu \phi^{*i} \nabla^\mu \phi_i \,+\, i\psi^{\dagger i} \bar{\sigma}^\mu \nabla_\mu \psi_i \,+\, F^{*i} F_i \\ &- \sqrt{2} g_a (\phi^* T^a \psi) \lambda^a \,-\, \sqrt{2} g_a \lambda^{\dagger a} (\psi^\dagger T^a \phi) \,+\, g_a (\phi^* T^a \phi) D^a \end{aligned} \tag{1.39}$$

Comparing with Eq.(1.29), the plain derivatives have been replaced by covariant derivatives (in the gauge sense) and additional vertices have been introduced. Regarding the gauge-covariant derivatives, they will be defined as usual

$$\nabla_\mu \;\equiv\; \partial_\mu \,-\, i\, g_a A^a_\mu T^a \tag{1.40}$$

About the vertices, a new triple vertex arises coupling gauginos, the fermionic fields within the vector supermultiplet, with scalars and fermions belonging to the chiral supermultiplet. Finally, considering Eq.(1.36) and Eq.(1.39), the auxiliary fields D^a can be removed from the total Lagrangian following the same procedure carried on before for F^i. Thus,

$$D^a \;=\; -\, g_a\, \phi^{*i}\, (T^a)_i{}^j\, \phi_j \tag{1.41}$$

Then, an additional term should be introduced in the scalar potential which will become

$$
\begin{aligned}
V(\phi,\phi^*) &= F^{*i}F_i + \frac{1}{2}\sum_a D^a D^a = \\
&= M^*_{ik}M^{kj}\,\phi^{*i}\phi_j + \frac{1}{2}\,M^{in}y^*_{jkn}\phi_i\phi^{*j}\phi^{*k} + M^*_{in}y^{jkn}\phi^{*i}\phi_j\phi_k \\
&+ \frac{1}{4}\,y^{ijn}y^*_{kln}\phi_i\phi_j\phi^{*k}\phi^{*l} + \frac{g_a^2}{2}\left(\sum_a \phi^* T^a \phi\right)^2
\end{aligned}
\tag{1.42}
$$

Summing up, the most general renormalizable Lagrangian for a interactive gauge theory may be compactly written as

$$
\begin{aligned}
\mathcal{L} &= \left(\frac{1}{4} - i\frac{g_a^2\Theta}{32\pi^2}\right)\,[\,\mathcal{W}^{a\alpha}\mathcal{W}^a_\alpha\,]_F + c.c. + \left[\,\Phi\left(e^{2g_a T^a \mathsf{V}^a}\right)\Phi\,\right]_D \\
&+ \left(\,[\mathsf{W}(\Phi_\mathsf{i})] + c.c\,\right)
\end{aligned}
\tag{1.43}
$$

1.3 The Minimal Supersymmetric Standard Model

The minimal supersymmetric version of the Standard Model (MSSM) [12,13] is defined by the following assumptions:

- Minimal SM gauge group: $SU(3)_C \times SU(2)_L \times U(1)_Y$.
- Minimal particle content.
- Yukawa interactions and R-parity conservation.
- Minimal soft SUSY-breaking terms.

In the MSSM no additional symmetries are added to the SM gauge group, apart from R-parity. R-parity correspond to a discrete $\mathbb{Z}_2$ symmetry which assigns a new quantum number to every particle [28]

$$
R_p = (-1)^{2s}\,(-1)^{3(B-L)} \tag{1.44}
$$

where s, B and L are the spin, baryon number and lepton number. Among other things, R-parity allows us to distinguish between two separate sectors: R_p-even particles, consisting of the SM particles, and R_p-odd particles, which includes their supersymmetric partners. In fact, imposing R-parity as an exact symmetry of the

Superfield	Components		Quantum Numbers		
	Scalar	Weyl fermion	$\mathbf{SU(3)_C}$	$\mathbf{SU(2)_L}$	$\mathbf{U(1)_Y}$
Φ_u	$\Phi_u \equiv (\Phi_u^+, \Phi_u^0)^T$	$(\widetilde{H}_u^+, \widetilde{H}_u^0)$	**1**	2	1/2
Φ_d	$\Phi_d \equiv (\Phi_d^0, \Phi_d^-)^T$	$(\widetilde{H}_d^0, \widetilde{H}_d^-)$	**1**	**2**	-1/2
L^i	$(\widetilde{\nu}^i, \widetilde{e}_L^i)$	(ν^i, e_L^i)	**1**	**2**	-1/2
E^i	$\widetilde{e}_R^{*i}$	$e_R^{i\dagger}$	**1**	**1**	1
Q^i	$(\widetilde{u}_L^i, \widetilde{d}_L^i)$	(u_L^i, d_L^i)	**3**	**2**	1/6
D^i	$\widetilde{d}_R^{*i}$	$d_R^{i\dagger}$	$\bar{\mathbf{3}}$	**1**	1/3
U^i	$\widetilde{u}_R^{*i}$	$u_R^{i\dagger}$	$\bar{\mathbf{3}}$	**1**	-2/3

Table 1.1: Chiral supermultiplets

theory forbids unwanted exchanges of sfermions between ordinary quarks and leptons that may be in conflict with experimental data, for instance the proton could decay with a short lifetime in the presence of terms violating both, L and B. Although R-parity might seem poorly justified from a theoretical point of view, one may argue that it is sensible to postulate it as a remnant discrete symmetry of a continuous B-L gauge symmetry spontaneously broken at some very high energy scale [29]. Some phenomenological consequences may be inferred from this conservation: first, supersymmetric particles will always be produced in pairs or, conversely, any supersymmetric particle must decay into states containing an odd number of superpartners; second, the lightest supersymmetric particle (LSP) must be absolutely stable, providing a natural candidate for dark matter.

1.3.1 Particle content

In a realistic supersymmetric version of the SM all quarks, leptons, gauge bosons and the Higgs ought to be associated with different supermultiplets and, therefore, their superpartners cannot be identified with any known particle. Fermions will be-

Superfield	Components		Quantum Numbers		
	Vector boson	Major. fermion	$\mathbf{SU(3)_C}$	$\mathbf{SU(2)_L}$	$\mathbf{U(1)_Y}$
G^a	g^a_μ	$\widetilde{g}^a$	**8**	**1**	0
W^a	W^a_μ	$\widetilde{W}^a$	**1**	**2**	0
B	B_μ	$\widetilde{B}$	**1**	**1**	0

Table 1.2: Vector supermultiplets

long to chiral supermultiplets[2] together with new spin-0 bosons called *sfermions* (for scalar fermions). Vector bosons will be contained in vector supermultiplets and their spin-1/2 companions will be Majorana fermions called *gauginos* (for gauge neutrino). Finally, in contrast to the SM, the Higgs sector will be made up by two chiral supermultiplets correspondent to two different isodoublets. The reason is twofold: on the one hand, the superpotential holomorphicity does not allow the presence of conjugated fields like $\bar{\Phi}$ and, on the other hand, a second isodoublet is needed to cancel the Adler-Bardeen-Jackiw anomalies [30–32] which otherwise would spoil the renormalizability of the theory. The fermionic superpartners of the Higgs bosons will be Weyl fermions and they will be named *Higgsinos* (for Higgs neutrinos). Tables 1.1 and 1.2 show the particle content of the MSSM just described before. In principle, the MSSM does not consider right-handed neutrinos.
Finally, after electroweak symmetry breaking (EWSB) W-bosons will mix with the B-boson generating $W^\pm$, Z^0 and γ^0 but also their superpartners will mix among them and with the Higgsinos so that the mass eigenstates will be given by two *charginos*, $\chi^\pm_{1,2}$, and four *neutralinos*, $\chi^0_{1,2,3,4}$.

1.3.2 Supersymmetric interactions

The whole collection of interactions respecting supersymmetry can be obtained from Eq.(1.30), Eq.(1.36) and Eq.(1.39) once the superpotential has been specified. In the MSSM, the superpotential is a function depending on chiral supermultiplets, totally compatible with gauge symmetries and invariant under R-parity transformations.

[2]See comment in Appendix B.1 concerning the standard convention to express chiral supermultiplets

Thus, the most general expression for it can be written as

$$\mathsf{W}_{\rm MSSM} \;=\; \mathsf{U}\,\mathbf{Y_u}\,\mathsf{Q}\,\Phi_{\mathsf{u}} \;-\; \mathsf{D}\,\mathbf{Y_d}\,\mathsf{Q}\,\Phi_{\mathsf{d}} \;-\; \mathsf{E}\,\mathbf{Y_e}\,\mathsf{L}\,\Phi_{\mathsf{d}} \;+\; \mu\,\Phi_{\mathsf{u}}\Phi_{\mathsf{d}} \tag{1.45}$$

where indices have been suppressed. Expanding the product between superfields

$$\begin{aligned}\mathsf{W}_{\rm MSSM} \;&=\; \mathsf{U}\,\mathbf{Y_u}\,\mathsf{U}_L\,\Phi_u^0 \;-\; \mathsf{U}\,\mathbf{Y_u}\,\mathsf{D}_L\,\Phi_u^+ \;+\; \mathsf{D}\,\mathbf{Y_d}\,\mathsf{D}_L\,\Phi_d^0 \;-\; \mathsf{D}\,\mathbf{Y_d}\,\mathsf{U}_L\,\Phi_d^- \\ &+\; \mathsf{E}\,\mathbf{Y_e}\,\mathsf{E}_L\,\Phi_d^0 \;-\; \mathsf{E}\,\mathbf{Y_e}\,\nu_L\,\Phi_d^- \;+\; \mu\,\left(\Phi_u^+\Phi_d^- \;-\; \Phi_u^0\Phi_d^0\right)\end{aligned} \tag{1.46}$$

Appart from the typical gauge interactions proceeding from the gauge-covariant derivatives in Eq.(1.36) and Eq.(1.39), numerous new vertices arise in the MSSM. For instance, once the auxiliary F-fields are replaced by their equations of motion, mass-like terms for Higgsinos and Yukawa interactions for Higgs-fermion-fermion and sfermion-Higgsino-fermion emerge, Eq.(1.32). We group them in $\mathcal{L}_Y$,

$$\begin{aligned}-\,\mathcal{L}_Y \;&=(\mathbf{Y_u})_{ij} \quad \Big(u_R^{i\,\dagger}\,u_L^j\,\Phi_u^0 \;+\; \widetilde{u}_R^{i^*}\,u_L^j\,\widetilde{H}_u^0 \;+\; u_R^{i\,\dagger}\,\widetilde{u}_L^j\,\widetilde{H}_u^0 \\ &\qquad\qquad - u_R^{i\,\dagger}\,d_L^j\,\Phi_u^+ \;-\; \widetilde{u}_R^{i^*}\,d_L^j\,\widetilde{H}_u^+ \;-\; u_R^{i\,\dagger}\,\widetilde{d}_L^j\,\widetilde{H}_u^+\Big) \\ &+\,(\mathbf{Y_d})_{ij} \quad \Big(d_R^{i\,\dagger}\,d_L^j\,\Phi_d^0 \;+\; \widetilde{d}_R^{i^*}\,d_L^j\,\widetilde{H}_d^0 \;+\; d_R^{i\,\dagger}\,\widetilde{d}_L^j\,\widetilde{H}_d^0 \\ &\qquad\qquad - d_R^{i\,\dagger}\,u_L^j\,\Phi_d^- \;-\; \widetilde{d}_R^{i^*}\,u_L^j\,\widetilde{H}_d^- \;-\; d_R^{i\,\dagger}\,\widetilde{u}_L^j\,\widetilde{H}_d^-\Big) \\ &+\,(\mathbf{Y_e})_{ij} \quad \Big(e_R^{i\,\dagger}\,e_L^j\,\Phi_d^0 \;+\; \widetilde{e}_R^{i^*}\,e_L^j\,\widetilde{H}_d^0 \;+\; e_R^{i\,\dagger}\,\widetilde{e}_L^j\,\widetilde{H}_d^0 \\ &\qquad\qquad - e_R^{i\,\dagger}\,\nu^j\,\Phi_d^- \;-\; \widetilde{e}_R^{i^*}\,\nu^j\,\widetilde{H}_d^- \;-\; e_R^{i\,\dagger}\,\widetilde{\nu}^j\,\widetilde{H}_d^-\Big) \\ &+\quad \mu \quad \Big(\,\widetilde{H}_u^0\,\widetilde{H}_d^0 \;-\; \widetilde{H}_u^+\,\widetilde{H}_d^-\,\Big) \;+\; c.c.\end{aligned} \tag{1.47}$$

The first three vertices in Eq.(1.47) are represented in Figure 1.1. The rest are equivalent but exchanging the up-type particle by down-type or leptons and the up-Higgs by the down-Higgs. Similarly, the scalar potential defined in Eq.(1.42) contains interactions involving exclusively scalar fields such as mass-like contributions for the Higgs bosons

$$-\,\mathcal{L}_\mu \;=|\mu|^2\left(\left|\Phi_u^0\right|^2 \;+\; \left|\Phi_d^0\right|^2 \;+\; \left|\Phi_u^+\right|^2 \;+\; \left|\Phi_d^-\right|^2\right) \tag{1.48}$$

triple vertices for sfermions and Higgses

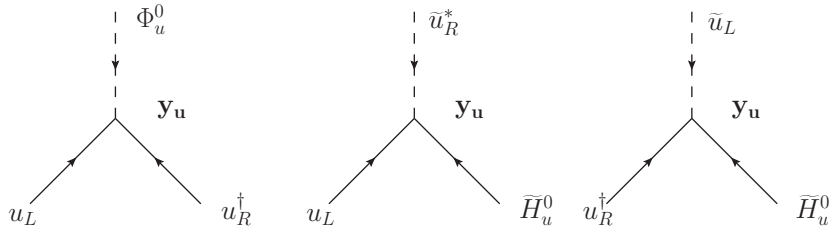

Figure 1.1: The usual Yukawa vertex *Higgs-quark-quark* for the up-quark and its "supersymmetrizations" *squark-quark-Higgsino* in Eq.(1.47). All these vertices have strength y_u.

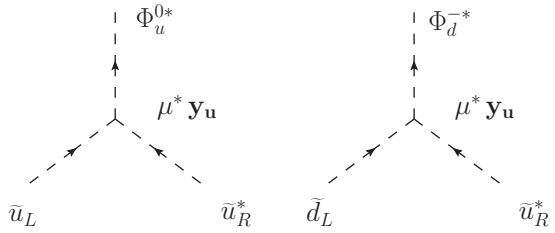

Figure 1.2: ϕ^3 vertices for the up-quark in Eq.(1.49) coming from the scalar potential. These vertices have strength $\mu^* \, y_u$.

$$
\begin{aligned}
\mathcal{L}_{\phi^3} &= \mu^* \, (\mathbf{Y_u})_{ij} \, \left(\widetilde{u}_R^{i^*} \, \widetilde{u}_L^j \, \Phi_d^{0*} \, + \, \widetilde{u}_R^{i^*} \, \widetilde{d}_L^j \, \Phi_d^{-*} \right) \\
&+ \mu^* \, (\mathbf{Y_d})_{ij} \, \left(\widetilde{d}_R^{i^*} \, \widetilde{d}_L^j \, \Phi_u^{0*} \, + \, \widetilde{d}_R^{i^*} \, \widetilde{u}_L^j \, \Phi_u^{+*} \right) \\
&+ \mu^* \, (\mathbf{Y_e})_{ij} \, \left(\widetilde{e}_R^{i^*} \, \widetilde{e}_L^j \, \Phi_u^{0*} \, + \, \widetilde{e}_R^{i^*} \, \widetilde{\nu}^j \, \Phi_u^{+*} \right) \, + \, c.c.
\end{aligned}
\tag{1.49}
$$

and quartic couplings with four sfermions and two sfermions plus two Higgses

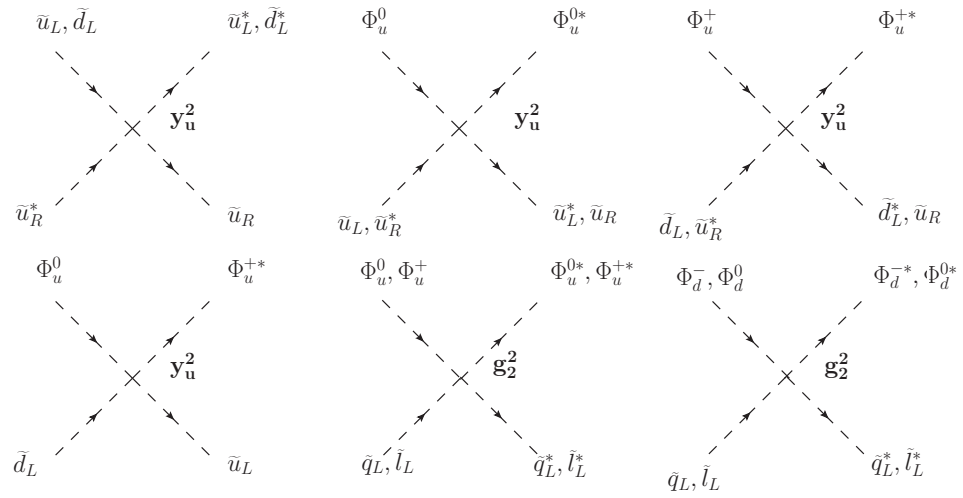

Figure 1.3: Typical ϕ^4 vertices in Eq.(1.50) coming from the F-terms and D-terms. These vertices have strength y_u^2.

$$
\begin{aligned}
-\mathcal{L}_{\phi^4} &= (\mathbf{Y_u})^*_{ij}\,(\mathbf{Y_u})_{kl}\left(\widetilde{u}^{i^*}_R\,\widetilde{u}^j_L\,\widetilde{u}^k_R\,\widetilde{u}^{l^*}_L \;+\; \widetilde{u}^{i^*}_R\,\widetilde{d}^j_L\,\widetilde{u}^k_R\,\widetilde{d}^{l^*}_L\right)\\
&+ |\mathbf{Y_u}|^2_{ij}\left(\widetilde{u}^{i^*}_L\,\widetilde{u}^j_L\,\left|\Phi^0_u\right|^2 \;+\; \widetilde{u}^{i^*}_R\,\widetilde{u}^j_R\,\left|\Phi^0_u\right|^2 \;+\; \widetilde{d}^{i^*}_L\,\widetilde{d}^j_L\,\left|\Phi^+_u\right|^2\right.\\
&\qquad \left. + \widetilde{u}^{i^*}_R\,\widetilde{u}^j_R\,\left|\Phi^+_u\right|^2 \;+\; \left(\widetilde{d}^{k^*}_L\,\widetilde{u}^j_L\,\Phi^0_u\,\Phi^{+^*}_u \;+\; c.c.\right)\right) \;+\; \ldots\\
&+ \frac{g_3^2}{8}\left(\sum_{\phi=\widetilde{q}} \phi^{i*}\,\lambda^a_{ij}\,\phi_j\right)^2 \;+\; \frac{g_2^2}{8}\left(\sum_{\substack{\phi=\Phi_u,\\ \Phi_d,\widetilde{L},\widetilde{Q}}} \phi^{i*}\,\sigma^a_{ij}\,\phi_j\right)^2\\
&+ \frac{g_1^2}{2}\left(\sum_{\substack{\phi=\Phi_u,\\ \Phi_d,\widetilde{f}}} \phi^*\,Y_\phi\,\phi\right)^2
\end{aligned}
\tag{1.50}
$$

where σ^a and λ^a are the $SU(2)$ and $SU(3)$ generators and correspond to the Pauli and Gell-Mann matrices, respectively. Figures 1.2 and 1.3 show some of the vertices in Eqs.(1.49) and (1.50) for up-type quarks. In the case of ϕ^3 vertices, for each vertex, there are two more where the up-type quark is a down-quark or lepton and the Higgs changes. For the quartic couplings, there are two different origins: on the one hand, the Yukawa squared interactions coming from the superpotential and, on the other hand, the gauge-coupling squared interactions originated in the D-terms, Eq.(1.41). Note that after electroweak symmetry breaking (SSB) these terms in Eqs.(1.49) and

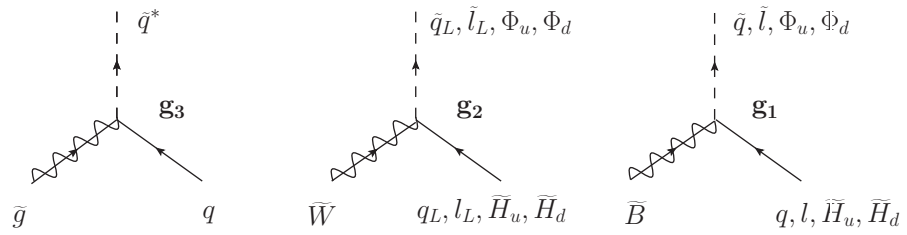

Figure 1.4: *Scalar-fermion-gaugino* vertices in Eq.(1.51) coming from the covariant derivatives of the chiral superfields. These vertices have strength g_a.

(1.50) will contribute to the sfermions mass matrices; the ϕ^3 interactions will induce $\widetilde{f}_L - \widetilde{f}_R$ mixing through off-diagonal terms whereas the ϕ^4 interactions will generate diagonal mass terms. Finally, gaugino-fermion-sfermion interactions are originated from the gauge-invariant kinetic term for chiral supermultiplets, Eq.(1.28). Usually, they will dominate over the superpotential dimensionless interactions because of the gauge-coupling strength

$$\begin{aligned} -\mathcal{L}_{\text{gauge}} &= \frac{g_3}{\sqrt{2}} \sum_{\substack{\mathsf{Q},\mathsf{D},\\ \mathsf{U}}} \left(\widetilde{\phi}^{i*}\, \lambda_i^{a\ j}\, \psi_j \right) \widetilde{g}^a \ + \ c.c. \\ &+ \frac{g_2}{\sqrt{2}} \sum_{\substack{\Phi_u,\\ \Phi_d,\mathsf{L},\mathsf{Q}}} \left(\phi^{i*}\, \sigma_i^{a\ j}\, \psi_j \right) \widetilde{W}^a \ + \ c.c. \\ &+ \sqrt{2}\, g_1 \sum_{\forall\, \text{chiral}} (\phi^*\, Y_\phi\, \psi\,)\, \widetilde{B} \ + \ c.c. \end{aligned} \tag{1.51}$$

1.3.3 Soft supersymmetry breaking interactions

Nature does not seem to be supersymmetric. Otherwise particles cohabiting into the same supermultiplet would have equal masses and the whole compendium of superpartners would have been already measured. So supersymmetry should be a broken symmetry, although the precise mechanism responsible for it is not known yet. In this situation, the wisest way to proceed is through the parametrization of our ignorance introducing nonrenormalizable terms which explicity breaks supersymmetry, supposing that they are induced by some mechanism. Normally these terms should be *soft*, in the sense of positive mass dimension. In the MSSM, the minimal number of soft-breaking contributions includes mass-like terms for scalars and gauginos, and

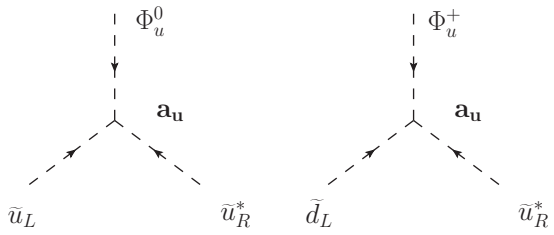

Figure 1.5: *Higgs-scalar-scalar* vertices for the up-quark in Eq.(1.52) coming from the soft-breaking Lagragian. These vertices have strength a_u.

trilinar interactions between sfermions and Higgses

$$
\begin{aligned}
-\mathcal{L}^{\text{soft}}_{\text{MSSM}} \;=\;& \frac{1}{2}\Big(M_3\,\widetilde{g}\widetilde{g} \;+\; M_2\,\widetilde{W}\widetilde{W} \;+\; M_1\,\widetilde{B}\widetilde{B} \;+\; \text{c.c.}\Big) \\
+\;& m^2_{H_u}\,\Phi_u^\dagger\Phi_u \;+\; m^2_{H_d}\,\Phi_d^\dagger\Phi_d \;+\; (\,b\,\Phi_u\Phi_d \;+\; \text{c.c.}\,) \\
+\;& \widetilde{Q}^\dagger\,\mathbf{m^2_Q}\,\widetilde{Q} \;+\; \widetilde{L}^\dagger\,\mathbf{m^2_L}\,\widetilde{L} \;+\; \widetilde{u}_R^*\,\mathbf{m^2_u}\,\widetilde{u}_R \;+\; \widetilde{d}_R^*\,\mathbf{m^2_d}\,\widetilde{d}_R \;+\; \widetilde{e}_R^*\,\mathbf{m^2_e}\,\widetilde{e}_R \\
+\;& \Big(\widetilde{u}_R^*\,\mathbf{a_u}\,\widetilde{Q}\,\Phi_u \;-\; \widetilde{d}_R^*\,\mathbf{a_d}\,\widetilde{Q}\,\Phi_d \;-\; \widetilde{e}_R^*\,\mathbf{a_e}\,\widetilde{L}\,\Phi_d \;+\; \text{c.c.}\Big)
\end{aligned}
\tag{1.52}
$$

where the product $\Phi_u\Phi_d = \epsilon_{\alpha\beta}\Phi_u^\alpha\Phi_d^\beta$. Clearly, these contributions break supersymmetry since the correspondent term for the superpartner fields do not appear. Some of the trilinear vertices given in the last line are represented in Figure 1.5. Note that after SSB these terms will induce sfermions mixing.

2

Higgs phenomenology with explicit CP violation

As presented in the previous section, the Higgs sector of the MSSM is a type-II 2HdM [33–35] in which two Higgs isodoublets are required to break the electroweak symmetry. Each of them couples uniquely to down-type fermions and leptons or up-type quarks. Among other reasons -see discussion in Section 1.3.1- this mechanism avoids the appearance of flavour-changing neutral currents (FCNC) at tree-level. In fact, as we will see, the Higgs sector of the MSSM is a type-II 2HdM that conserves CP at tree-level.

In its more general version, the MSSM introduces many new parameters which are absent in the SM and could, theoretically, carry complex phases. In particular, the MSSM accounts for 43 new phases coming from: i) the superpotential, through the mass parameter μ of the Higgs, and from ii) the soft-breaking Lagrangian through the gaugino masses M_1 and M_2, the dimensionless bilinear squark parameters $\mathbf{m}^{\mathbf{2}}_{\tilde{\mathbf{f}}}$ and through the trilinear couplings $\mathbf{a}_{\tilde{\mathbf{f}}}$[1]. This large number of complex phases generates in supersymmetry the so-called *supersymmetric CP problem* [37–49], mainly related to the strong tension between the flavour experimental data and the large contributions generated by $\mathcal{O}(1)$ CP phases. Particularly, the electron and neutron EDMs greatly constrain the complex phases associated with the bilinear μ-term of

[1] Observe that in the limit where $\mu = b = M_3 = M_2 = M_1 = 0$ and all matrix trilinear $\mathbf{a}_{\mathbf{f}}$-parameters are set to zero, the theory possesses two global $U(1)$ symmetries: a continuous R-symmetry and a Peccei-Quinn symmetry. Thus, a $U(1)_R$ rotation of the fields can make the gluino mass real and positive whereas a $U(1)_{PQ}$ rotation can be performed in order to remove the complex phase of b [36]

the superpotential and the diagonal entries of the trilinear matrices belonging to the first- and second-generation of fermions. Fortunately, these bounds are relaxed in the case of third-generation trilinear couplings, which could still have sizeable phases even for soft sfermion masses $\mathcal{O}(1)$ TeV. Here, without loss of generality, we take phases order unity only in $a_{t,b,\tau}$, leaving the rest of parameters real. This way, a sizeable scalar-pseudoscalar mixing is generated in the Higgs spectrum whereas the flavour phenomenology remains in perfect agreement with experiment.

2.1 Electroweak symmetry breaking

In the MSSM, the scalar Higgs potential has three different sources: i) mass-like terms coming from the scalar potential after integrating out the auxiliary fields F_i Eq.(1.48), ii) bilinears terms in the soft-breaking Lagrangian Eq.(1.52), and iii) quartic couplings in the scalar potential once the auxiliary fields D^a have been removed using their equations of motion in Eq.(1.50). These last contributions will be given by

$$\mathrm{U(1)_Y} \;:\; \frac{1}{2}D^1D^1 = \frac{g_1^2}{8}\left(\Phi_u^{0*}\Phi_u^0 \,+\, \Phi_u^{+*}\Phi_u^+ \,-\, \Phi_d^{0*}\Phi_d \,-\, \Phi_d^{-*}\Phi_d^- \,+\, \ldots\right)^2 \tag{2.1}$$

$$\mathrm{SU(2)_L} \;:\; \frac{1}{2}D^2D^2 = \frac{g_2^2}{8}\left(\Phi_u^{*i}\,\sigma_{ij}^a\,\Phi_u^j \,+\, \Phi_d^{*i}\,\sigma_{ij}^a\,\Phi_d^j \,+\, \ldots\right)^2 \tag{2.2}$$

where ellipses means additional terms belonging to squarks and sleptons that do not participate in the symmetry breaking and can be ignored now. Expanding Eqs.(2.1) and (2.2) and making some arrangement, the scalar Higgs potential can be written as

$$\begin{aligned} V_H \;&=\; (\,|\mu|^2 + m_{H_u}^2\,)\,|\Phi_u|^2 \;+\; (\,|\mu|^2 + m_{H_d}^2\,)\,|\Phi_d|^2 \;+\; (\,b\,\mu\,\Phi_u\Phi_d \,+\, \text{c.c.}\,) \\ &+\; \frac{g_1^2 \,+\, g_2^2}{8}\,\left(\,|\Phi_u|^2 \,-\, |\Phi_d|^2\,\right)^2 \;+\; \frac{g_2^2}{2}\,|\Phi_u^\dagger\Phi_d|^2 \end{aligned} \tag{2.3}$$

The only term in this potential that depends on the phases of the fields is the $b\mu$-term. However, it is always possible to perform a global Peccei Quinn rotation of the fields reabsorbing its complex phase[1]. Consequently, $b\mu$ can always be taken real and positive and the Higgs potential is CP-preserving in the Born approximation. Thence, the Higgs mass eigenstates can be assigned well-defined values of CP, at tree-level. Unfortunately, going beyond the leading order, this CP invariance of the Higgs potential may be explicitly broken through radiative corrections due to the presence

of complex phases in the soft-breaking Lagrangian [50–52]. In particular, after SSB, CP-violating phases in the trilinear couplings of sfermions may induce a large mixing between scalar and pseudoscalar states at one-loop level originating substantial modifications in the Higgs mass spectrum as well as in the associated couplings.
The $SU(2)_L \otimes U(1)_Y$ group gets spontaneously broken to the electromagnetic subgroup $U(1)_Q$ when the neutral components of the Higgs doublets acquire a vacuum expectation value (VEV). Since observation tells us that $U(1)_Q$ is a true symmetry of the theory, one should be able to ensure the absence of charge-breaking minima: $\partial V_H/\partial \Phi_u^+ = 0 = \partial V_H/\partial \Phi_d^-$. And, in fact, it can be easily guarantee thanks to the freedom of realizing $SU(2)_L$ transformations, which always permit rotating away one of the possible VEVs. Eventually, one may take $\langle \Phi_u^+ \rangle$ equal to zero and, as a consequence, it can be shown that $\langle \partial V_H/\partial \Phi_d^- \rangle = 0$ with $\langle \Phi_u^+ \rangle = 0$ implies $\langle \Phi_d^- \rangle = 0$, as desired. Therefore, without loss of generality, we can assume at the minimum

$$\langle \Phi_u^0 \rangle \;=\; \frac{v_u}{\sqrt{2}} \qquad\qquad \langle \Phi_d^0 \rangle \;=\; \frac{v_d}{\sqrt{2}} \tag{2.4}$$

where $v_u = v \sin\beta$, $v_d = v \cos\beta$ and $v \simeq 246$ GeV. In our case, excitations over the ground state of the Higgs doublets will be parametrized as

$$\Phi_d \;=\; \frac{1}{\sqrt{2}} \begin{pmatrix} v_d \;+\; \phi_d^0 \;+\; i\, P_d^0 \\ \phi_d^- \end{pmatrix} \qquad \Phi_u \;=\; e^{i\xi} \begin{pmatrix} \phi_u^+ \\ v_u \;+\; \phi_u^0 \;+\; i\, P_u^0 \end{pmatrix} \tag{2.5}$$

where ξ represents the relative phase between the doublets. All these parameters are determined by the minimization conditions of V_H. In the limit of CP-conservation [17, 35, 53], the breaking of the symmetry leads to two neutral Higgs scalars h^0 and H^0 (with $m_{h^0} < m_{H^0}$ by convention), a pseudoscalar Higgs state A^0, two charged Higgs scalars $H^\pm$ and three would-be Nambu-Goldstone bosons, which become the longitudinal modes of the (now) massive gauge bosons Z^0 and $W^\pm$. When violation of CP is included via complex phases in the trilinear couplings, mass terms merging scalar and pseudscalar states arise as a result of diagrams like those represented in Figure 2.1 [51]. Then, the neutral mass matrix may be written as [51, 52]

$$\mathcal{M}_H^2 = \begin{pmatrix} \mathcal{M}_S^2 & \mathcal{M}_{SP}^2 \\ \mathcal{M}_{PS}^2 & \mathcal{M}_P^2 \end{pmatrix} \tag{2.6}$$

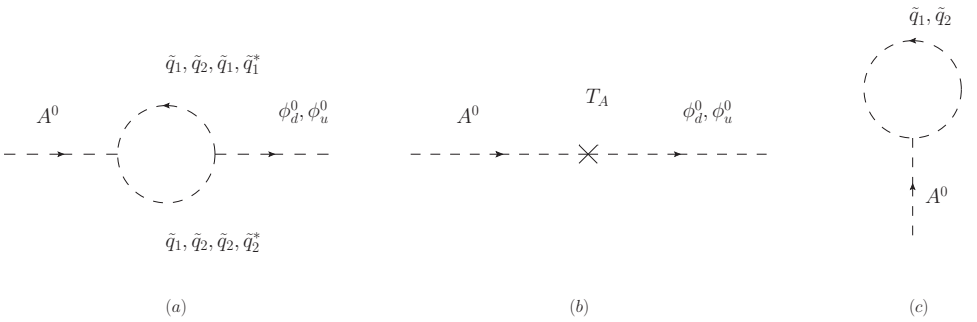

Figure 2.1: Feynman diagrams contributing to the scalar-pseudoscalar off-diagonal terms in the neutral mass matrix: (a) One-loop self-energy graph, (b) CP-odd tadpole renormalization, (c) Tadpole graph of the A^0 boson.

in the weak basis given by $(\phi_d\ \phi_u\ A^0)$, where $A^0 = -\sin\beta\, P_d^0 + \cos\beta\, P_u^0$ and in which the massless Goldstone boson G^0 associated with the flat direction of the potential $\langle \partial V_H / \partial G^0 \rangle = 0$ has been removed. As the notation suggest, $\mathcal{M}_S^2$ contains the mixing between CP-even states ($\phi_{d,u}^0$), $\mathcal{M}_P^2$ contains the pseudoscalar mass part (A^0) and $\mathcal{M}_{SP}^2$ is linked to the mixing between CP-even and CP-odd states. The condition to recover the CP-conserving limit would be

$$\Im m[\,\mu\, a_f\,] \;=\; 0, \qquad\qquad f = \tilde{t},\ \tilde{b},\ \tilde{\tau} \tag{2.7}$$

As $\mathcal{M}_H^2$ is symmetric, it can be diagonalized through an orthogonal rotation O

$$O^T \cdot \mathcal{M}_H^2 \cdot O \;=\; \mathrm{Diag}\left(m_{H_1}^2, m_{H_2}^2, m_{H_3}^2\right) \tag{2.8}$$

where by convention $m_{H_1}^2 \leq m_{H_2}^2 \leq m_{H_3}^2$. Then, the mass eigenstates will be given by

$$\phi_d \;=\; O_{1i}\, H_i\,, \qquad\qquad \phi_u \;=\; O_{2i}\, H_i\,, \qquad\qquad A^0 \;=\; O_{3i}\, H_i\,. \tag{2.9}$$

2.2 Higgs interactions

In the MSSM, the Higgs fields couple to every massive particle in the spectrum except for gluinos. In this section, following [54], we will review the most important Higgs interactions in the presence of explicit CP-violation.

Higgs interactions to vector bosons

In Table 1.1 the quantum numbers associated with each Higgs supermultiplet are shown. The Higgs superfields carry charges under the $SU(2)_L \otimes U(1)_Y$ group so that the correspondent covariant derivatives will be given by

$$\nabla_\mu \Phi_i \;=\; \left[\partial_\mu \;-\; i\, g_1\, Y_i B_\mu \;-\; i\, \frac{g_2}{2} \begin{pmatrix} W_\mu^0 & \sqrt{2} W_\mu^+ \\ \sqrt{2} W_\mu^- & -W_\mu^0 \end{pmatrix} \right] \Phi_i \tag{2.10}$$

with $W_\mu^\pm = (W_\mu^1 \mp i\, W_\mu^2)/\sqrt{2}$. Both, gauge boson masses and their interactions with the Higgs bosons, originate from the covariant derivatives in the Higgs field kinetic terms, Eq.(1.39), once the symmetry is broken and the Higgs particles emerge as perturbations around the minimum as presented in Eq.(2.5). Then, taking into account that B_μ and W_μ^3 mix with an angle θ_W to give the massless photon A_μ^0 and Z_μ^0, one will obtain the following triple couplings

$$\begin{aligned} \mathcal{L}_{\mathrm{H_i VV}} \;&=\; (v_u\, \phi_u^0 \;+\; v_d\, \phi_d^0) \left(\frac{g_2^2}{2}\, W_\mu^+ W^{-\mu} \;+\; \frac{g_2^2}{4\cos^2\theta_W}\, Z_\mu Z^\mu \right) \\ &=\; g_2\, M_W \left(W_\mu^+ W^{-\mu} + \frac{1}{2\cos^2\theta_W} Z_\mu Z^\mu \right) \sum_{i=1}^{3} g_{\mathrm{H_i VV}}\, H_i \end{aligned} \tag{2.11}$$

where $M_W = g_2\, v/2$ and the *Higgs-vector-vector* coupling is given by

$$g_{\mathrm{H_i VV}} \;=\; \cos\beta\, O_{1i} \;+\; \sin\beta\, O_{2i} \tag{2.12}$$

Note that gauge bosons only couple with the CP-even part of each Higgs mass eigenstate. In addition to these couplings, two more triple couplings emerge: H_i-H_j-Z and H_i-$H^\mp$-$W^\pm$. However, processes involving these vertices will be subdominant in our study so that we do not present them here.

Higgs interactions to sfermions

The *Higgs-sfermion-sfermion* interactions will be given by several contributions from both, the superpotential and the soft-breaking Lagrangian: the cubic vertices in Eq.(1.49) and the trilinear couplings in Eq.(1.52) induce mixing between left- and right-handed sfermions whereas the quartic vertices in Eq.(1.50), after SSB, generate

interactions between same-chirality squarks. Thus, the interactive Lagrangian can be written as

$$\mathcal{L}_{\mathrm{H_i\tilde{f}\tilde{f}}} \;=\; v\,\left(g_{\mathrm{H_i\tilde{f}\tilde{f}}}\right)_{jk}\,H_i\,\tilde{f}_j^*\,\tilde{f}_k \tag{2.13}$$

where $j,k=1,2$ (referring to the mass eigenstate) and $g_{\mathrm{H_i\tilde{f}\tilde{f}}}$ is a 2×2 matrix containing the H_i-$\tilde{f}_j$-$\tilde{f}_k$ vertices and the correspondent dependence on the rotation-matrix elements for Higgs bosons and sfermions. Hence

$$v\,\left(g_{\mathrm{H_i\tilde{f}\tilde{f}}}\right)_{jk} \;=\; \left(\widetilde{\Gamma}^{\rho}_{\tilde{f}\tilde{f}}\right)_{\kappa\nu}\,O_{\rho i}\,\mathcal{R}^{\tilde{f}*}_{\kappa j}\mathcal{R}^{\tilde{f}}_{\nu k} \tag{2.14}$$

where κ and ν are related to the chirality, L or R, $\mathcal{R}^f$ is the sfermion mixing matrix and $\widetilde{\Gamma}^{\alpha}_{ff}$ is the 2×2 matrix consisting of all the contributions from the superpotential and the soft-breaking Lagrangian. The explicit expression can be found in Appendix B.2.

Higgs interactions to charginos

Interactions between neutral Higgses and charginos emerge from the Higgs kinetic terms in Eq.(1.39) and are given in Eq.(1.51). Some of these vertices are represented in Figure 1.4. After SSB, and following the convention detailed in Appendix B.3, the interactive Lagrangian can be written as

$$\mathcal{L}_{\mathrm{H_i\tilde{\chi}^+\tilde{\chi}^-}} \;=\; -\frac{g_2}{\sqrt{2}}\,H_i\,\overline{\tilde{\chi}_j^-}\,\left(g^S_{\mathrm{H_i\chi_j^+\chi_k^-}}\;+\;i\,\gamma^5\,g^P_{\mathrm{H_i\chi_j^+\chi_k^-}}\right)\,\tilde{\chi}_k^- \tag{2.15}$$

where the scalar and pseudoscalar couplings $g^{S,P}_{\mathrm{H_i\chi^+\chi^-}}$ depend on the mixing-matrix elements associated with charginos and Higgses in the following way

$$g^S_{\mathrm{H_i\chi_j^+\chi_k^-}} \;=\; \frac{1}{2}\left[V^*_{j1}U^*_{k2}\,G_i^{\Phi_d^0}\;+\;V^*_{j2}U^*_{k1}\,G_i^{\Phi_u^0}\;+\;(j\leftrightarrow k)^*\right] \tag{2.16}$$

$$g^P_{\mathrm{H_i\chi_j^+\chi_k^-}} \;=\; \frac{i}{2}\left[V^*_{j1}U^*_{k2}\,G_i^{\Phi_d^0}\;+\;V^*_{j2}U^*_{k1}\,G_i^{\Phi_u^0}\;-\;(j\leftrightarrow k)^*\right] \tag{2.17}$$

$G_i^{\Phi_d^0}$ and $G_i^{\Phi_u^0}$ are the abbreviated notation for the Φ_d^0 and Φ_u^0 composition in terms of H_i

$$G_i^{\Phi_d^0} \;=\; O_{1i} \;+\; i\,\sin\beta\, O_{3i} \qquad\qquad G_i^{\Phi_u^0} \;=\; O_{2i} \;+\; i\,\cos\beta\, O_{3i} \tag{2.18}$$

Higgs self-interactions

We are also interested in the neutral-Higgs bosons couplings to the charged Higgses. They can be computed from the quartic couplings in the Higgs potential Eq.(2.3) after SSB

$$\mathcal{L}_{\mathrm{H_i H^+ H^-}} \;=\; v \sum_{\alpha=1}^{3} g_{\alpha \mathrm{H^+ H^-}}\; O_{\alpha i}\; H_i\, H^+ H^- \;\equiv\; v\, g_{_{\mathrm{H_i H^+ H^-}}}\; H_i\, H^+ H^- \tag{2.19}$$

with $g_{\alpha H^+ H^-}$ containing all the contributions from the potential. They are given in Appendix B.4.

Neutral-Higgs interactions to SM fermions

In the MSSM, the Higgs interactions with SM fermions emerge directly from the superpotential as showed in Eq.(1.47). At tree-level, SM-like Yukawa interactions are reproduced with the difference that now up-type quarks couple to Φ_u^0 whereas down-type quarks and leptons couple to Φ_d^0. However, beyond the leading order, non-logarithmic threshold corrections to the fermions couplings are induced by the decoupling of heavy SUSY states at a high scale [55–63]. For instance, diagrams like those represented in Figure 2.2 for the b-quark are responsible for additional contributions to the fermion mass and its couplings to the Higgs states. Moreover, these quantum corrections may induce effective couplings between fermions and the *wrong* Higgs, the Hall-Rattazi-Sarid effect [56], Figure 2.3. In this context, the following effective Lagrangian can be considered [64]

$$\begin{aligned} -\,\mathcal{L}_{\mathrm{H_i \bar{f} f}} \;&=\; u_R^\dagger\, \mathbf{Y}_u \left(\mathbf{1} \;+\; \mathbf{\Delta}_u^{\Phi_u^0}\right) \Phi_u^0\, u_L \;+\; u_R^\dagger\, \mathbf{Y}_u\, \mathbf{\Delta}_u^{\Phi_d^0}\, \Phi_d^0\, u_L \\ &+\; d_R^\dagger\, \mathbf{Y}_d \left(\mathbf{1} \;+\; \mathbf{\Delta}_d^{\Phi_d^0}\right) \Phi_d^0\, d_L \;+\; d_R^\dagger\, \mathbf{Y}_d\, \mathbf{\Delta}_d^{\Phi_u^0}\, \Phi_u^0\, d_L \\ &+\; e_R^\dagger\, \mathbf{Y}_e \left(\mathbf{1} \;+\; \mathbf{\Delta}_e^{\Phi_d^0}\right) \Phi_d^0\, e_L \;+\; e_R^\dagger\, \mathbf{Y}_e\, \mathbf{\Delta}_e^{\Phi_u^0}\, \Phi_u^0\, e_L \;+\; \mathrm{c.c.} \end{aligned} \tag{2.20}$$

where $\mathbf{\Delta}_j^{\Phi_i^0}$ contains all the loop contributions generating the correction. The complete expression for them can be found in Appendix B.5. Once the symmetry is broken and $\Phi_f^0 \to 1/\sqrt{2}(v_f + \phi_f^0 + iP_f^0)$, the mass terms are obtained from Eq.(2.20) by

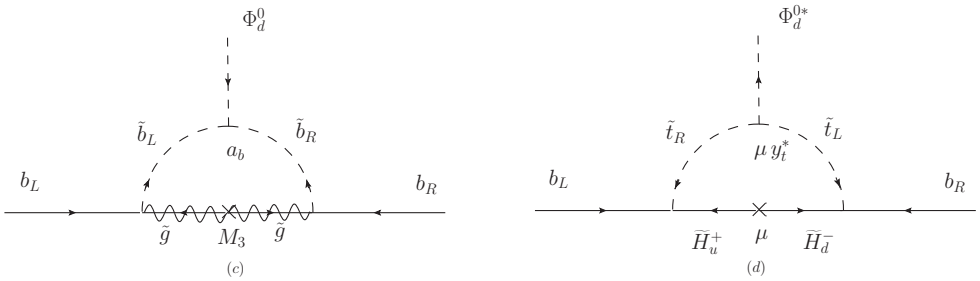

Figure 2.2: Some of the diagrams inducing non-logarithmic corrections to the bottom quark mass and its couplings to Φ_d^0 through (a) gluino exchange and (b) higgsino exchange.

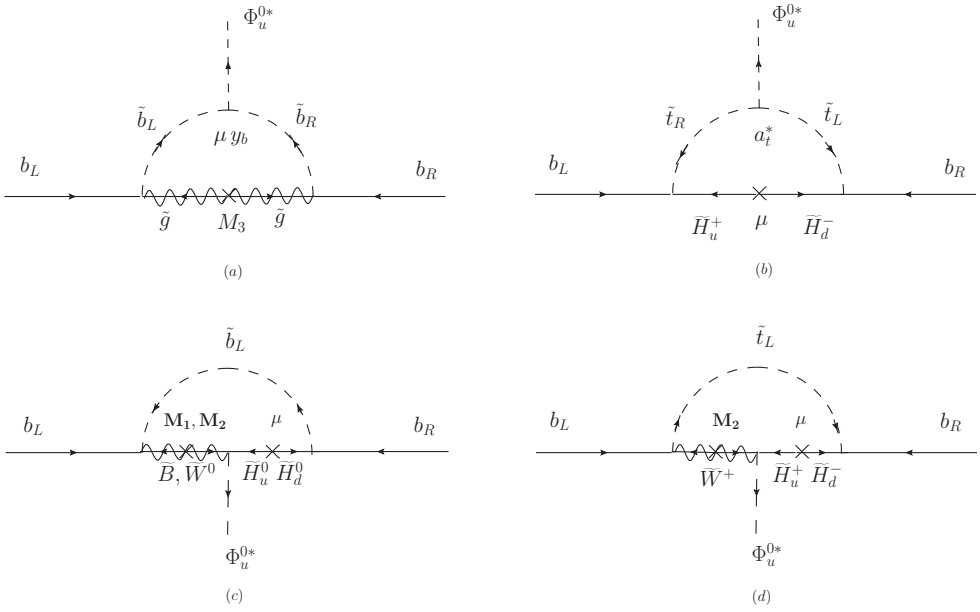

Figure 2.3: Some of the Feynman graphs involved in the threshold corrections to the bottom quark mass and its couplings to Φ_u^0 through (a) gluino exchange, (b) higgsino exchange, (c) neutral gaugino-higgsino exchange and (d) charged gaugino-higgsino exchange.

rotating the states to the mass basis. In particular, we can work in the basis where $\mathcal{U}_L^Q = \mathcal{U}_R^u = \mathcal{U}_R^d = \mathbf{1} = \mathcal{U}_L^l = \mathcal{U}_R^e$. Thus,

$$-\mathcal{L}_{\rm mass} \;=\; u_R^\dagger\, \widehat{\mathbf{M}}_u\, u_L \;+\; d_R^\dagger\, \widehat{\mathbf{M}}_d\, d_L \;+\; e_R^\dagger\, \widehat{\mathbf{M}}_l\, e_L \;+\; \text{c.c.} \tag{2.21}$$

with $\widehat{M}_u = \mathrm{diag}(m_u, m_c, m_t)$, $\widehat{M}_d = \mathrm{diag}(m_d, m_s, m_b)$ and $\widehat{M}_e = \mathrm{diag}(m_e, m_\mu, m_\nu)$ related to the correspondent Yukawa coupling according to

$$\widehat{\mathbf{M}}_u \equiv \frac{v_u}{\sqrt{2}}\,\mathbf{Y}_u\left(\mathbf{1} + \mathbf{\Delta}_u^{\Phi_u^0} + \cot\beta\,\mathbf{\Delta}_u^{\Phi_d^0}\right) \equiv \frac{v_u}{\sqrt{2}}\,\mathbf{Y}_u\,\mathbf{R}_u \tag{2.22}$$

$$\widehat{\mathbf{M}}_d \equiv \frac{v_d}{\sqrt{2}}\,\mathbf{Y}_d\left(\mathbf{1} + \mathbf{\Delta}_d^{\Phi_d^0} + \tan\beta\,\mathbf{\Delta}_d^{\Phi_u^0}\right)\mathbf{V} \equiv \frac{v_d}{\sqrt{2}}\,\mathbf{Y}_d\,\mathbf{R}_d\,\mathbf{V} \tag{2.23}$$

$$\widehat{\mathbf{M}}_e \equiv \frac{v_d}{\sqrt{2}}\,\mathbf{Y}_e\left(\mathbf{1} + \mathbf{\Delta}_e^{\Phi_d^0} + \tan\beta\,\mathbf{\Delta}_e^{\Phi_u^0}\right) \equiv \frac{v_d}{\sqrt{2}}\,\mathbf{Y}_e\,\mathbf{R}_e \tag{2.24}$$

where $\mathbf{R}_u$, $\mathbf{R}_d$ and $\mathbf{R}_e$ have been introduced. Notice that for down-type quarks (and leptons) one of the terms is proportional to $\tan\beta$ and, therefore, it can be important for medium and large $\tan\beta$ values. It is straightforward to obtain from Eq.(2.20) the following effective Lagrangian, using Eqs.(2.22)-(2.24) to rewrite the Yukawa couplings and going to the mass basis for the Higgs fields,

$$\mathcal{L}^{\mathrm{eff}}_{\mathrm{H_i\bar{f}f}} = -\frac{g_2}{2\,M_W}\,H_i\,\bar{f}\left(\widehat{\mathbf{M}}_f\,\mathbf{g}^L_{H_i\bar{f}f}\,P_L + \mathbf{g}^R_{H_i\bar{f}f}\,\widehat{\mathbf{M}}_f\,P_R\right)f \tag{2.25}$$

The effective couplings are given by

$$\begin{aligned}\mathbf{g}^L_{H_i\bar{u}u} &= \frac{\mathcal{O}_{1i}}{\sin\beta}\,\mathbf{R}_u^{-1}\mathbf{\Delta}_u^{\Phi_d^0} + \frac{\mathcal{O}_{2i}}{\sin\beta}\,\mathbf{R}_u^{-1}\left(\mathbf{1} + \mathbf{\Delta}_u^{\Phi_u^0}\right)\\ &\quad + i\,\mathcal{O}_{3i}\cot\beta\,\mathbf{R}_u^{-1}\left(\mathbf{1} - \Delta_u^{\Phi_d^0} + \tan\beta\mathbf{\Delta}_u^{\Phi_d^0}\right)\end{aligned} \tag{2.26}$$

$$\begin{aligned}\mathbf{g}^L_{H_i\bar{d}d} &= \frac{\mathcal{O}_{1i}}{\cos\beta}\,\mathbf{V}^\dagger\mathbf{R}_d^{-1}\left(\mathbf{1} + \mathbf{\Delta}_d^{\Phi_d^0}\right)\mathbf{V} + \frac{\mathcal{O}_{2i}}{\cos\beta}\,\mathbf{V}^\dagger\mathbf{R}_d^{-1}\mathbf{\Delta}_d^{\Phi_u^0}\mathbf{V}\\ &\quad + i\,\mathcal{O}_{3i}\tan\beta\,\mathbf{V}^\dagger\mathbf{R}_d^{-1}\left(\mathbf{1} + \Delta_d^{\Phi_d^0} - \frac{1}{\tan\beta}\mathbf{\Delta}_d^{\Phi_u^0}\right)\mathbf{V}\end{aligned} \tag{2.27}$$

$$\begin{aligned}\mathbf{g}^L_{H_i\bar{e}e} &= \frac{\mathcal{O}_{1i}}{\cos\beta}\,\mathbf{R}_e^{-1}\left(\mathbf{1} + \mathbf{\Delta}_e^{\Phi_d^0}\right) + \frac{\mathcal{O}_{2i}}{\cos\beta}\,\mathbf{R}_e^{-1}\mathbf{\Delta}_e^{\Phi_u^0}\\ &\quad + i\,\mathcal{O}_{3i}\tan\beta\,\mathbf{R}_d^{-1}\left(\mathbf{1} + \Delta_e^{\Phi_d^0} - \frac{1}{\tan\beta}\mathbf{\Delta}_e^{\Phi_u^0}\right)\end{aligned} \tag{2.28}$$

$$\mathbf{g}^R_{H_i\bar{f}f} = \left(\mathbf{g}^L_{H_i\bar{f}f}\right)^\dagger \tag{2.29}$$

In the case of equal fermions, the Lagrangian in Eq.(2.25) can be rewritten in terms of four-component spinors and scalar-pseudoscalar effective couplings as

$$\mathcal{L}^{\rm eff}_{\rm H_i\bar{f}f} \;=\; -\frac{g_2\, m_f}{2\, M_W}\, H_i\, \bar{f}\, \Big(g^S_{H_i\bar{f}f} \;+\; i\, g^P_{H_i\bar{f}f}\, \gamma^5 \Big)\, f \tag{2.30}$$

$$g^S_{\rm H_i\bar{f}f} \;=\; \frac{1}{2}\, \Big(g^L_{H_i\bar{f}f} \;+\; g^R_{H_i\bar{f}f} \Big) \tag{2.31}$$

$$g^P_{\rm H_i\bar{f}f} \;=\; \frac{i}{2}\, \Big(g^L_{H_i\bar{f}f} \;-\; g^R_{H_i\bar{f}f} \Big) \tag{2.32}$$

For our analysis, we mainly focus on the Higgs decay into third-generation fermions, since they couple stronger to the Higgs due to their larger masses. Threshold-corrections to their couplings may be important although, in our case, it is enough to consider the dominant corrections to the bottom quark, determined by the gluino and Higgsino exchanges showed in Figure 2.3, while leaving the tree-level couplings for the top and the τ-lepton [65]. Then

$$g^S_{\rm H_i\bar{t}t} \;\simeq\; \frac{O_{2i}}{\sin\beta} \qquad g^P_{\rm H_i\bar{t}t} \;\simeq\; -\,\cot\beta\, O_{3i} \tag{2.33}$$

$$g^S_{\rm H_i\bar{\tau}\tau} \;\simeq\; \frac{O_{1i}}{\cos\beta} \qquad g^P_{\rm H_i\bar{\tau}\tau} \;\simeq\; -\,\tan\beta\, O_{3i} \tag{2.34}$$

whereas for the b-quark

$$\mathbf{\Delta}_b^{\Phi_d^0} \;\simeq\; -\frac{2\alpha_s}{3\pi}\, M_3^*\, a_d\, I(m^2_{\tilde{b}_1}, m^2_{\tilde{b}_2}, |M_3|^2) - \frac{|y_t|^2}{16\pi^2} |\mu|^2\, I(m^2_{\tilde{t}_1}, m^2_{\tilde{t}_2}, |\mu|^2) \tag{2.35}$$

$$\mathbf{\Delta}_b^{\Phi_u^0} \;\simeq\; \frac{2\alpha_s}{3\pi}\, M_3^*\, \mu^*\, I(m^2_{\tilde{b}_1}, m^2_{\tilde{b}_2}, |M_3|^2) + \frac{|y_t|^2}{16\pi^2} a_t^*\, \mu^*\, I(m^2_{\tilde{t}_1}, m^2_{\tilde{t}_2}, |\mu|^2) \tag{2.36}$$

with $\alpha_s = g_3/4\pi$ and the loop function $I(a,b,c)$ given in Appendix C. Defining $\kappa_b = \mathbf{\Delta}_b^{\Phi_u^0}/(1 + \mathbf{\Delta}_d^{\Phi_d^0})$, the effective scalar and pseudoscalar couplings are giving by

$$g^S_{\mathrm{H_i\bar{b}b}} = \Re e\left[\frac{1}{1+\kappa_b\tan\beta}\right]\frac{O_{1i}}{\cos\beta} + \Re e\left[\frac{\kappa_b}{1+\kappa_b\tan\beta}\right]\frac{O_{2i}}{\cos\beta} + \Im m\left[\frac{\kappa_b\left(\tan^2\beta+1\right)}{1+\kappa_b\tan\beta}\right]O_{3i} \tag{2.37}$$

$$g^P_{\mathrm{H_i\bar{b}b}} = -\Re e\left[\frac{\tan\beta-\kappa_b}{1+\kappa_b\tan\beta}\right]O_{3i} + \Im m\left[\frac{\kappa_b\tan\beta}{1+\kappa_b\tan\beta}\right]\frac{\mathcal{O}_{1i}}{\cos\beta} - \Im m\left[\frac{\kappa_b}{1+\kappa_b\tan\beta}\right]\frac{\mathcal{O}_{2i}}{\cos\beta} \tag{2.38}$$

The general Lagrangian in Eq.(2.30) is also valid to study flavour-changing (FC) neutral processes like $H_i \to \bar{b}s, \bar{s}b$. Making use of the effective couplings obtained in Eqs.(2.26)-(2.29), one has

$$-\mathcal{L}_{H_ibs} = \frac{g_2}{2\,M_W}\,H_i\,\bar{b}\left(g^S_{\mathrm{H_i\bar{b}s}} + i\,g^P_{\mathrm{H_i\bar{b}s}}\,\gamma_5\right)s + \text{c.c.} \tag{2.39}$$

with the effective scalar and pseudoscalar couplings

$$g^S_{\mathrm{H_i\bar{b}s}} = \frac{1}{2}\left(m_b\,g^L_{\mathrm{H_i\bar{b}s}} + m_s\,g^R_{\mathrm{H_i\bar{b}s}}\right) \equiv \frac{v}{2}\left(y^L_i + y^R_i\right) \tag{2.40}$$

$$g^P_{\mathrm{H_i\bar{b}s}} = \frac{i}{2}\left(m_b\,g^L_{\mathrm{H_i\bar{b}s}} - m_s\,g^R_{\mathrm{H_i\bar{b}s}}\right) \equiv \frac{i\,v}{2}\left(y^L_i - y^R_i\right) \tag{2.41}$$

and where the dimensionless couplings $y^L_i = m_b\,g^L_{\mathrm{H_i\bar{b}s}}/v$ and $y^R_i = m_s\,g^R_{\mathrm{H_i\bar{b}s}}/v$ have been introduced.

Charged-Higgs interactions to SM fermions

As before, one can deduce the interactive Lagrangian for the charged-Higgs boson and the charged-Goldstone boson with SM fermions from Eq.(1.47) taken into account that

$$\begin{pmatrix}\Phi^+_u\\ \Phi^{-*}_d\end{pmatrix} = \begin{pmatrix}\cos\beta & \sin\beta\\ -\sin\beta & \cos\beta\end{pmatrix}\begin{pmatrix}H^+\\ G^+\end{pmatrix} \tag{2.42}$$

Then, the resulting Lagrangian is given by [64]

$$\begin{aligned}\mathcal{L} &= -\frac{g_2}{2\,M_W}\, H^- \bar{d}\left(\widehat{\mathbf{M}}_d\, \mathbf{g}^L_{H^-\bar{d}u}\, P_L + \mathbf{g}^R_{H^-\bar{d}u}\, \widehat{\mathbf{M}}_u\, P_R\right) u \\ &\quad -\frac{g_2}{2\,M_W}\, G^- \bar{d}\left(\widehat{\mathbf{M}}_d\, \mathbf{V}^\dagger\, P_L - \mathbf{V}^\dagger\, \widehat{\mathbf{M}}_u\, P_R\right) u \;+\; \text{h.c.} \end{aligned} \tag{2.43}$$

The complete expression for the couplings considering all possible loop contributions can be found in [64]. Here, we restrict the analysis to the threshold corrections which are $\tan\beta$-enhanced, that is those in the down sector represented in Figure 2.3. Thus

$$\mathbf{g}^L_{H^-\bar{d}u} = -\tan\beta\, \mathbf{V}^\dagger \mathbf{R}_d^{-1} \;+\; \mathbf{V}^\dagger \mathbf{R}_d^{-1} \mathbf{\Delta}_d^{\Phi_u^0} \qquad\qquad \mathbf{g}^R_{H^-\bar{d}u} = -\frac{1}{\tan\beta}\mathbf{V}^\dagger \tag{2.44}$$

The single-Higgs-insertion (SHI) approximation [64] is assumed where: $\mathbf{\Delta}_d^{\Phi_u^+} = \mathbf{\Delta}_u^{\Phi_u^0}$.

2.3 Higgs decays

The dominant decay channels for a Higgs state with no well-defined CP and mass between one and several hundred GeVs will be reviewed here [54].

Higgs decay into SM fermions

First, we consider the decay width into a pair of SM fermions. The interactions between quarks/leptons and neutral Higgses are shown in the Lagrangian of Eq.(2.30). At leading order, the partial decay width of a Higgs into two fermions with the same flavour is given by

$$\Gamma^{LO}_{\mathrm{H_i}\to\mathrm{f\bar{f}}} \;=\; N_C\, \frac{g_2^2}{32\,\pi}\, \frac{m_f^2}{M_W^2}\, m_{H_i}\, \beta_f \,\left(\beta_f^2\, |g^S_{\mathrm{H_i f\bar{f}}}|^2 \;+\; |g^P_{\mathrm{H_i f\bar{f}}}|^2\right) \tag{2.45}$$

where N_C is the color factor (three for quarks and one for leptons) and $\beta_f = \sqrt{1-\tau_f^{-1}}$ with $\tau_f = m^2_{H_i}/(4m_f^2)$ the fermions velocity in the final state. For strongly interactive particles, QCD corrections to the leading-order process like those in Figure 2.4 are important. A useful way to improve the tree-level cross section including NLO corrections is using the so-called K-factors , which parametrise the ratio of the higher

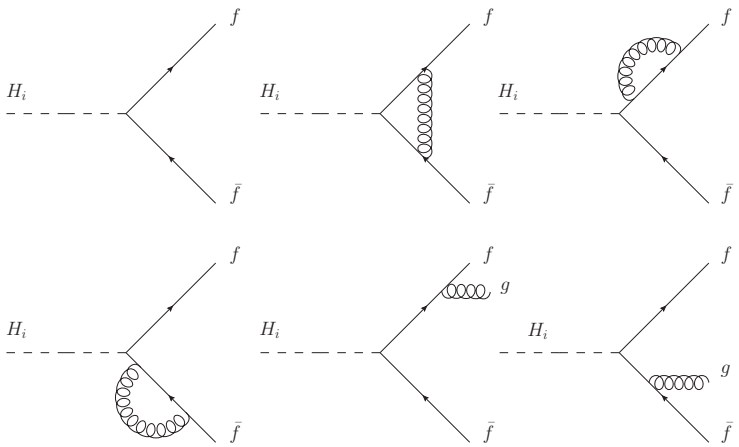

Figure 2.4: Feynman graphs for the tree-level Higgs decay into two fermions and some of the QCD corrections at higher order.

order cross section to the leading order one. In particular for $H_i \to q\bar{q}$, the next-to-leading order (NLO) decay when $m_f \ll m_{H_i}$ can be obtained including the K-factor $K^f_{H_i} = 1 + 5.67\,\alpha_s(m^2_{H_i})/\pi$ and replacing the quark pole mass with the renormalized mass calculated at the Higgs mass scale. This way, NLO-logarithmic corrections are resumed to all orders [35, 66, 67]. Hence

$$\Gamma^{QCD}_{\mathrm{H_i}\to\mathrm{f\bar{f}}} \;=\; K^f_i \left(\frac{m_f(m_{H_i})}{m_f(m_t)}\right)^2 \Gamma_{\mathrm{H_i}\to\mathrm{f\bar{f}}} \tag{2.46}$$

In the case of two different flavours in the final state, like in the study of flavour-violating decays such as those defined by the Lagrangian in Eq.(2.39), the decay width will be given by

$$\begin{aligned}\Gamma\left(H_i \to \bar{b}s, \bar{s}b\right) \;&=\; \frac{N_c}{8\,\pi}\,\frac{g_2^2}{4\,M_W^2}\,m_{H_i}\,\lambda^{1/2}\left(1, x_b, x_s\right)\,\kappa_{QCD}\,\times \\ &\left[\left(1 - x_b - x_s\right)\left(\left|g^S_{\mathrm{H_i\bar{b}s}}\right|^2 + \left|g^P_{\mathrm{H_i\bar{b}s}}\right|^2\right) \;-\; 2\sqrt{x_b x_s}\,\left(\left|g^S_{\mathrm{H_i\bar{b}s}}\right|^2 - \left|g^P_{\mathrm{H_i\bar{b}s}}\right|^2\right)\right]\end{aligned}$$

where again $\kappa_{QCD} \;=\; 1 + 5.67\,\alpha_S\left(m^2_{H_i}\right)/\pi$ includes the QCD corrections, $x_f \;=$

$m_f^2/m_{H_i}^2$ and $\lambda\,(1,a,b) = (1-a-b)^2 - 4ab$. Introducing $y_i^{L,R}$ in Eqs.(2.40) and (2.41), the decay will be

$$\begin{aligned}\Gamma\left(H_i \to \bar{b}s, \bar{s}b\right) &= \frac{N_c}{8\,\pi}\, m_{H_i}\, \lambda^{1/2}\,(1, x_b, x_s)\; \kappa_{QCD}\; \times \\ &\left[\,(1-x_b-x_s)\left(\left|y_i^L\right|^2 + \left|y_i^R\right|^2\right) \;-\; 4\sqrt{x_b x_s}\;\Re e\left[\,y_i^L\, y_i^{R*}\,\right]\right]\end{aligned} \tag{2.47}$$

Note that again the masses in $y_i^{L,R}$ are $m_{b,s} = m_{b,s}\,(m_{H_i})$ due to the inclusion of NLO QCD-corrections.

Higgs decay to vector bosons

If $m_H \geq 162$ GeV, the two body decay to gauge bosons is open and gives [54]

$$\Gamma(H_i \to VV) \;=\; \frac{g_2^2}{128\,\pi}\frac{m_{H_i}^3}{M_W^2}\,\delta_V\, g^2_{\mathrm{H_i VV}}\sqrt{1-\frac{4}{\omega_i}}\left(1-\frac{4}{\omega_i}+\frac{12}{\omega_i^2}\right) \tag{2.48}$$

where $\delta_W = 2$, $\delta_Z = 1$ and $\omega_i = m_{H_i}^2/M_V^2$. However, for Higgs masses below 160 GeV, the decay channel to two real vector bosons is forbidden and the three body decay through a virtual vector boson should be considered instead. Thus, the Higgs decay into one real and one virtual gauge boson can be written as [68–70]

$$\begin{aligned}\Gamma(H_i \to VV^*) \;&=\; \frac{g_2^2\,\delta_V}{64\,\pi}\,\frac{m_{H_i}^3}{M_W^2}\; g^2_{\mathrm{H_i VV}}\;\times \\ &\int_0^{(\sqrt{\omega_i}-1)^2} dx\,\frac{\epsilon_V\,\lambda^{1/2}(\omega_i,x,1)\;[\,\lambda(\omega_i,x,1)+12x\,]}{\omega_i^3\,\pi\;[\,(x-1)^2+\epsilon_V^2\,]}\end{aligned} \tag{2.49}$$

where $\epsilon_V = \Gamma_V/M_V$ and $\lambda(1,x,y) = (1-x-y)^2 - 4xy$. The effective coupling $g_{\mathrm{H_i VV}}$ for CP-mixed states is given in Eq.(2.12).

Higgs decay into two photons

One of the most important processes in the study of Higgs bosons is the decay to two photons. In the case of neutral Higgses that do not carry electric carge, the process only occurs at one-loop level by diagrams like those depicted in Fig.2.5. Every

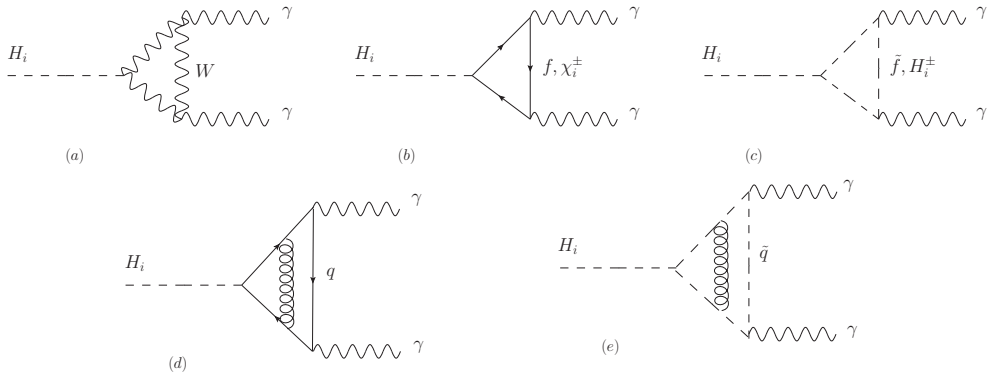

Figure 2.5: Feynman graphs for the one-loop Higgs decay into two photons mediated by: (a) the $W^\pm$ boson, (b) SM charged fermions or charginos, (c) charged squarks or the charged Higgs. Diagrams (d) and (e) in the second line show QCD corrections at NLO.

massive charged particle that couples with both, the Higgs bosons and photons, must be consider in the loop. Then, the decay width can be written as [54]

$$\Gamma\left(H_i \to \gamma\gamma\right) \;=\; \frac{\alpha^2}{256\,\pi^3}\frac{m_{H_i}^3}{v^2}\left(\left|S_i^\gamma\left(m_{H_i}\right)\right|^2 \;+\; \left|P_i^\gamma\left(m_{H_i}\right)\right|^2\right) \tag{2.50}$$

where $\alpha = g_2^2/4\pi$, $S_i^\gamma\left(m_{H_i}\right)$ is the scalar amplitude and $P_i^\gamma\left(m_{H_i}\right)$ refers to the pseudoscalar one. In the MSSM, besides the fermion and gauge boson contributions, the scalar part contains additional SUSY terms including charginos, the charged Higgs boson and sfermions. Thus

$$\begin{aligned} S_i^\gamma\left(m_{H_i}\right) \;=\; & 2\sum_{f=b,t,\tilde{\chi}_1^\pm,\tilde{\chi}_2^\pm} N_C\, Q_f^2\, J_f^\gamma\; g_f\, g^S_{\mathrm{H_i\bar{f}f}}\, F_f^S(\tau_f) \\ & - \sum_{\tilde{f}} N_C\, Q_{\tilde{f}}^2\, J_{\tilde{f}}^\gamma\, \frac{v^2}{2m_{\tilde{f}_j}^2}\;\left(g_{\mathrm{H_i\tilde{f}\tilde{f}}}\right)_{jj}\; F_0(\tau_{\tilde{f}}) \\ & - g_{\mathrm{H_iVV}}\, F_1(\tau_V) \;-\; \frac{v^2}{2m_{H^\pm}^2}\, g_{\mathrm{H_iH^+H^-}}\; F_0(\tau_{H^+}) \end{aligned} \tag{2.51}$$

where $g_f = 1$ for SM fermions and $g_{\chi^\pm} = \sqrt{2}M_W/m_{\chi^\pm}$, $\tau_X = m_{H_i}^2/(4\,m_X^2)$, F_0 and F_f^S

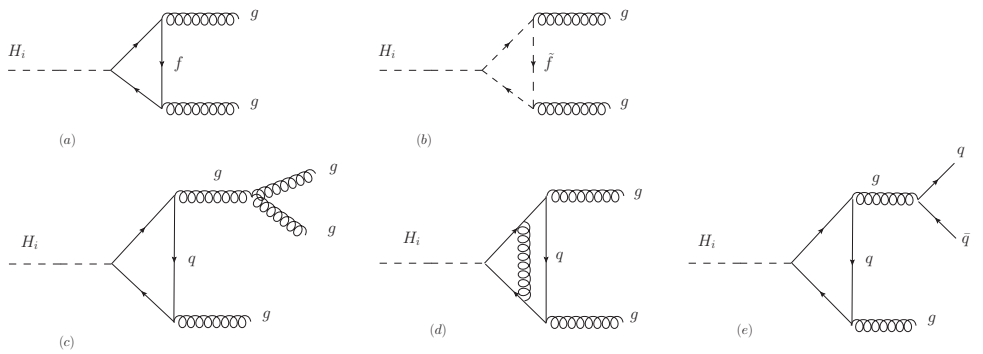

Figure 2.6: Feynman graphs for the one-loop Higgs decay into two gluons mediated by: (a) quarks, (b) squarks. Diagrams in the second line (c), (d) and (e) are related to NLO QCD-corrections.

are the loop function collected in Appendix C and J_f^γ refers to QCD corrections that we detail below in Eq.(2.53). Notice that terms due to first- and second-generation of fermions can be safety neglected in the first piece of Eq.(2.51) because of their small masses. In contrast to the scalar part, the pseudoscalar amplitude only receives contributions from SM fermions and charginos

$$P_i^\gamma\left(m_{H_i}\right) \;=\; 2 \sum_{f=b,t,\tilde{\chi}_1^\pm,\tilde{\chi}_2^\pm} N_C\, Q_f^2\, J_f^\gamma\, g_f\, g^P_{\mathrm{H_i\bar{f}f}}\, F_f^P(\tau_f) \tag{2.52}$$

As commented before, the rescaling factors J_X^γ in Eq.(2.51) and (2.52) contains QCD corrections built up by virtual gluon exchanges inside the quark/squark loops, second line in Fig.(2.5). In the large loop-mass limit, they are given by [71, 72]

$$J_\chi^\gamma \;=\; 1 \qquad\qquad J_t^\gamma \;=\; 1 - \frac{\alpha_s\left(m^2_{H_i}\right)}{\pi} \qquad\qquad J_{\tilde{q}}^\gamma \;=\; 1 + \frac{8\alpha_s\left(m^2_{H_i}\right)}{3\pi} \tag{2.53}$$

Higgs decay into two gluons

Finally, another essential decay for Higgs states in a hadron collider is the decay into two gluons, which also occurs at one-loop since Higgs supermultiplets carry no colour. Similarly to the $H_i \to \gamma\gamma$ case, in order to compute the decay width, all the

contributions from massive coloured particles that couple to the Higgs bosons must be taken into account, Figure 2.6. Therefore

$$\Gamma\left(H_i \to gg\right) \;=\; \frac{\alpha_s^2}{32\,\pi^3}\,\frac{m_{H_i}^3}{v^2}\,\left(\,K_S^g\,|S_i^g|^2 \;+\; K_P^g\,|P_i^g|^2\,\right) \tag{2.54}$$

where S_i^g and P_i^g are the scalar and pseudoscalar amplitudes

$$S_i^g \;=\; \sum_{f=b,t} g^S_{\mathrm{H_i ff}}\,F_f^S(\tau_f) \;-\; \sum_{\substack{\tilde{f}_i=\tilde{b}_1,\\ \tilde{b}_2,\tilde{t}_1,\tilde{t}_2}} \frac{v^2}{4m_{\tilde{f}_j^2}}\,\left(g_{\mathrm{H_i}\tilde{\mathrm{f}}\tilde{\mathrm{f}}}\right)_{jj}\,F_0(\tau_{\tilde{f}}) \tag{2.55}$$

$$P_i^g \;=\; \sum_{f=b,t} g^P_{\mathrm{H_i}\bar{\mathrm{f}}\mathrm{f}}\,F_f^P(\tau_f) \tag{2.56}$$

and $K^g_{S,P}$ are the leading-order QCD corrections due to virtual corrections and real emissions of gluons and quark-antiquark pairs in the final state [71, 72]

$$K_S^g = 1 + \frac{\alpha_s(M^2_{H_a})}{\pi}\left(\frac{95}{4} - \frac{7}{6}N^F\right) \qquad K_P^g = 1 + \frac{\alpha_s(M^2_{H_a})}{\pi}\left(\frac{97}{4} - \frac{7}{6}N^F\right) \tag{2.57}$$

with N^F the number of quark flavours at work, namely the number of quark flavours which remains lighter than the Higgs boson in consideration.

2.4 Higgs production at the LHC

In principle, the basic production processes in pp collisions at the LHC for MSSM Higgs bosons with explicit CP-violation are the same as in the SM [35, 73]

Associated production with vector bosons:	$q\bar{q} \to V \;+\; H_i$
Vector boson fusion:	$qq \to VV^* \to qq \;+\; H_i$
Gluon fusion:	$gg \to H_i$
Associated production with heavy quarks:	$gg,\, q\bar{q} \to Q\overline{Q} \;+\; H_i$

In Figure 2.7, illustrative values for the cross sections are shown in the case of a SM Higgs at $\sqrt{s} = 8$ TeV. Even so, quantitative differences may stem in our case

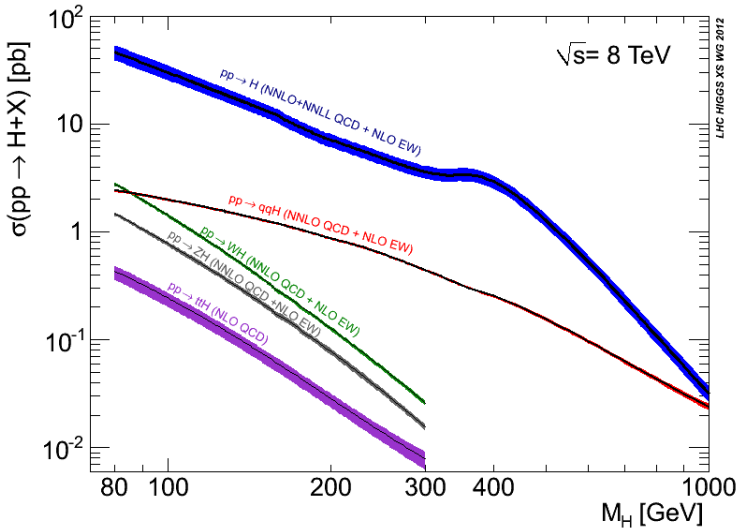

Figure 2.7: Main productions channels for a Standard Model Higgs at the LHC for $\sqrt{s} = 8$ TeV: blue line is for gluon fusion, dark red is for associated production with quarks, green lines are related to associated production with vector bosons and purple line is for the associated production with the top quark [74].

from the modified couplings, specially in the case of $\tan\beta$ dependences, the CP-mixed character of the particles and the extended SUSY spectrum. Nevertheless, for Higgs masses up to several hundred GeV the dominant mechanisms will still being the same: gluon fusion production and associated production with b-quarks for large $\tan\beta$ values [75, 76]. In contrast, vector boson fusion and associated production with gauge bosons will remain subdominant due to the electroweak character of the reactions together with the low parton distribution functions (PDFs) for quarks in this energy range.

Similarly to the Higgs decay into two gluons, the production of a Higgs state through gluon fusion occurs at one-loop level by processes like those in Fig.(2.6) but inverted. At the partonic level, the LO cross section can be expressed as

$$\sigma^{LO}_{gg\to H_i} = \hat{\sigma}^{LO}_{gg\to H_i}\, \delta\left(1 - \frac{m^2_{H_i}}{\hat{s}}\right) \tag{2.58}$$

where $\hat{s}$ refers to the partonic center-of-mass (c.m.) energy squared, δ is the zero-width distribution that should be replaced by the Breit-Wigner form of the Higgs

boson width and $\hat{\sigma}^{LO}_{gg\to H_a}$ is directly related to the decay width in Eq.(2.54)

$$\hat{\sigma}^{LO}_{gg\to H_a} \;=\; \frac{\pi^2}{8\,m_{H_i}}\,\Gamma^{LO}_{H_i\to gg} \;=\; \frac{\alpha_s^2\,(Q)}{256\,\pi}\,\frac{m^2_{H_i}}{v^2}\,\Big(\;|S^g_a|^2 \;+\; |P^g_a|^2\;\Big) \tag{2.59}$$

As before, the scalar and pseudoscalar amplitudes, which are given in eqs.(2.55) and (2.56), enclose the complete set of contributions due to the different particles running in the loop. On the grounds of the QCD factorization theorem, the hadronic cross section, at LO in the narrow-width approximation, can be computed by weighting the subprocess cross section at parton level, $\hat{\sigma}^{LO}_{gg\to H_i}$, with the parton distribution functions (PDFs), which contains the knowledge of the momentum distribution of every parton (gluons and quarks) inside the proton in the relevant kinematic range. Thus

$$\sigma^{LO}_{pp\to H_i}\Big|_{gg} \;=\; \hat{\sigma}^{LO}_{gg\to H_a}\;\tau_{H_i}\;\frac{d\mathcal{L}^{gg}_{LO}}{d\tau_{H_i}} \tag{2.60}$$

where $\tau_{H_i} = m^2_{H_i}/s$ is the Drell-Yan variable. The gluon luminosity, $d\mathcal{L}^{gg}_{LO}/d\tau$, bears the PDF dependence at some factorization scale M

$$\frac{d\mathcal{L}^{gg}_{LO}}{d\tau} \;=\; \int_\tau^1 \frac{dx}{x}\,g(x,M^2)\,g(\tau/x,M^2) \tag{2.61}$$

where $g(a,M^2)$ is the PDF described above. For our numerical analysis, the MSTW2008 [77] PDFs have been used. Again, QCD corrections to the tree-level process due to higher order processes like $gg \to H_i g$, $gq \to H_i q$ and $q\bar{q} \to H_i g$ in Figure 2.8 ought to be considered. Using the associated K-factor, the total hadronic cross section at NLO can written as [68, 72, 78, 79]

$$\sigma^{NLO}_{pp\to H_i}\Big|_{gg} \;=\; K\;\hat{\sigma}^{LO}_{gg\to H_a}\;\tau_{H_i}\;\frac{d\mathcal{L}^{gg}_{LO}}{d\tau_{H_i}} \tag{2.62}$$

It is important to include this factor since next-to-leading-order QCD effects, which affect both quark and squark contributions similarly [79, 80], can be significantly large. Such effects are essentially independent of the Higgs mass but exhibit a $\tan\beta$ dependence so that, in the low $\tan\beta$ region, K can be approximated by 2 while, for large $\tan\beta$, its value gets closer to unity [81]. In our study we have taken K to be constant for a given $\tan\beta$ in the considered range of masses.

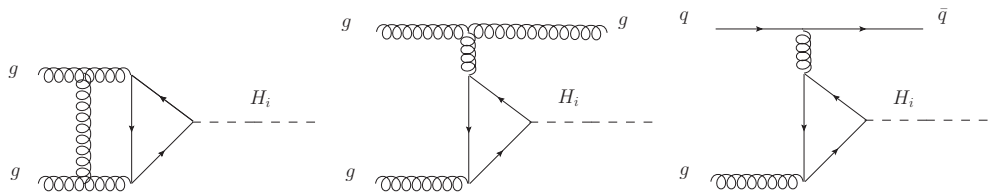

Figure 2.8: Typical diagrams contributing to the virtual and real QCD corrections to the Higgs production through gluon fusion.

For $\tan\beta \gtrsim 7$, the Higgs production in association with b-quarks may also contribute [76,81–86] due to the aforementioned $\tan\beta$-enhanced factors in the Higgs couplings to down-type quarks, Eqs.(2.37) and (2.38). Associated Higgs production with bottom quarks $gg/q\bar{q} \to b\bar{b} + H_i$ is equivalent to the $b\bar{b} \to H_i$ inclusive process when it is not required to observe any final b-jets, if one considers the b-quark as a massless parton and uses heavy quark distribution functions in a five active flavour scheme [35,76,87]. In this way, large logarithms $\log(s/m_b^2)$ are resummed to all orders. As in the previous process, the leading order partonic cross section is directly related to the fermionic decay width

$$\hat{\sigma}^{LO}_{b\bar{b}\to H_i} = \frac{4\pi^2}{9\, m_{H_i}}\, \Gamma^{LO}_{H_i\to b\bar{b}} = \frac{g_2^2\,\pi}{24}\,\frac{m_b^2}{M_W^2}\,\beta_b\left(\beta_b^2\left|g^S_{\mathrm{H_i\bar{b}b}}\right|^2 + \left|g^P_{\mathrm{H_i\bar{b}b}}\right|^2\right) \quad (2.63)$$

Regarding QCD corrections, it is enough to introduce the QCD enhancing factor K_i^f in the decay width $H_i \to b\bar{b}$, the running bottom mass evaluated at m_{H_i} and the threshold-corrected bottom couplings in Eqs.(2.37) and (2.38). Thus

$$\begin{aligned}\hat{\sigma}^{QCD}_{b\bar{b}\to H_a} &= \frac{4\pi^2}{9\, m_{H_i}}\,\Gamma(H_i\to b\bar{b})_{QCD} \\ &= \frac{g_2^2\, m_b^2}{4\, M_W^2}\,\frac{\pi}{6}\,K_i^b\left(\frac{m_b(m_{H_i})}{m_b(m_t)}\right)^2\,\beta_b\left(\beta_b^2\left|g^S_{\mathrm{H_i\bar{b}b}}\right|^2 + \left|g^P_{\mathrm{H_i\bar{b}b}}\right|^2\right) \quad (2.64)\end{aligned}$$

The hadronic cross section in the narrow-width approximation can be obtained in terms of the $b\bar{b}$ luminosity. As before, we use for our numerical calculation the

MSTW2008 five flavour PDFs. Then, the total production cross section (without tagged b-jets) will be given by

$$\sigma(pp \to H_i) \;=\; K\;\hat{\sigma}^{LO}_{gg\to H_i}\;\tau_{H_i}\;\frac{d\mathcal{L}^{gg}_{LO}}{d\tau_{H_i}} \;+\; \hat{\sigma}^{QCD}_{bb\to H_i}\;\tau_{H_i}\;\frac{d\mathcal{L}^{bb}_{LO}}{d\tau_{H_i}} \tag{2.65}$$

In the case of associated Higgs production with $b-$quarks but requiring a final b-jet, one have to consider the NLO correction to the LO process, that is $gb \to bH_i$. The differential partonic cross section for it is [82]

$$\frac{d\hat{\sigma}_{gb\to H_i b}}{dt} = -\frac{1}{s^2}\frac{\alpha_3(m_{H_i})}{24}\left(\frac{y_b(m_{H_i})}{\sqrt{2}}\right)^2\frac{m^4_{H_i}+u^2}{st} \tag{2.66}$$

where s, t, u are the Mandelstan variables. The total pp cross section is then obtained as

$$\sigma(pp \to H_i b) = 4\;\hat{\sigma}_{gb\to H_i b}\int_\tau^1 \frac{dx}{x}\,b(x,M^2)\,g(\tau/x,M^2) \tag{2.67}$$

where now $\tau = (p_g + p_b)^2/s$ and the factor 4 is due to the b-quark coming from one of the two protons and the conjugated process $g\bar{b} \to H_i\bar{b}$.

3

Flavour Phenomenology

The discussion in the previous section has revealed the large number of new parameters introduced by the MSSM in comparison with the SM. In particular, numerous complex phases and flavour violating terms arise in the soft SUSY breaking Lagrangian being highly constrained from experiment, since no significant deviation from the SM has been observed so far.
The strongest assumption that one may make in order to keep under control all these contributions is the hypothesis of Minimal Flavour Violation (MFV), which considers the Yukawa couplings as the unique non-trivial flavour structure of the model. Under this assumption, the sfermion masses and trilinear couplings can be written as expansions in terms of the Yukawa matrices. In principle, we will not consider significant deviations from MFV. Only in the last analysis off-diagonal entries in the trilinears and soft-mass matrices for third-generation squarks will provide an additional source of flavour violation, which may have their origin in the RG running of the soft-breaking parameters.
Therefore, the most stringent flavour constrains for us will come from electric dipole moments (EDM), helicity suppressed $b \to s$ transitions, B-meson oscillation and, specially for medium and large $\tan\beta$, the B_s-meson decay $B_s \to \mu^+\mu^-$.

3.1 Electric dipole moments

In physics, the electric dipole moment (EDM) of a system is a measure of the separation between positive and negative electric charge within it. The presence of non-zero EDMs implies the violation of parity (P) and time-reversal (T) symmetries so that

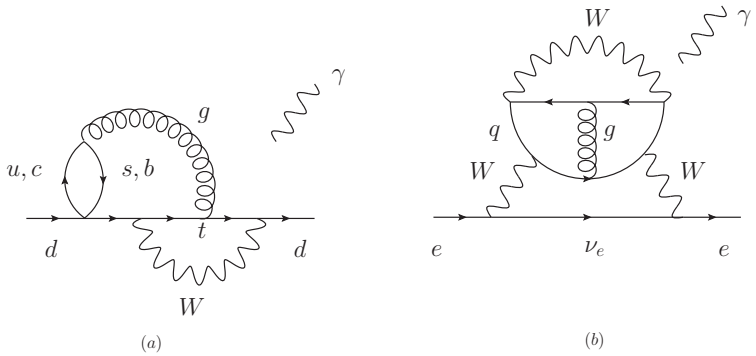

Figure 3.1: (a) Three-loop diagram for the d-quark EDM in the SM. Two additional diagrams can be drawn with the gluon line attached before and after the W loop. The photon can be radiated by any quark in the diagram or the W-boson. (b) Four-loop diagram for the electron EDM in the SM. Two-loop diagrams for the W EDM were demonstrated to cancel so this would be the first contribution different from zero. Again, the photon can be radiated by any quark, charged lepton or W-boson in the diagram.

they act as precision observables of fundamental CP violation in Nature, if one assumes CPT as a valid symmetry. In the context of beyond the SM theories, the neutron and electron EDMs serve as powerful bounds over new complex phases [37–42]. In the SM, EDMs are strongly suppressed since the CKM phase is the unique source of CP violation and consequently EDM interactions only appear at three-loop level for quarks and through four-loop diagrams for leptons [88–93], Figure 3.1. The electron EDM is directly caused by the W-boson EDM at three loops (d_W) and the theoretical prediction for its value can be estimated as

$$d_e \;\simeq\; \frac{g_2^2}{32\,\pi^2}\,\frac{m_e}{M_W}\,d_W \;\simeq\; 8\times 10^{-41}\,\text{e.cm} \tag{3.1}$$

The neutron EDM receives the dominant contribution at "two loops" by the diagram represented in Figure 3.2. The $\otimes$ is an effective vertex enclosing the *strong penguin* diagram which is given in the right part of the picture [92]. Thus, the neutron EDM is calculated taking into account the short-distance effects given by the quark EDMs as in Figure 3.1 and long-distance effects due to the diagram commented above. The predicted value is

$$d_n \;=\; d_n^{\text{short}} \;+\; d_n^{\text{long}} \;\simeq\; 10^{-32}\,\text{e.cm} \tag{3.2}$$

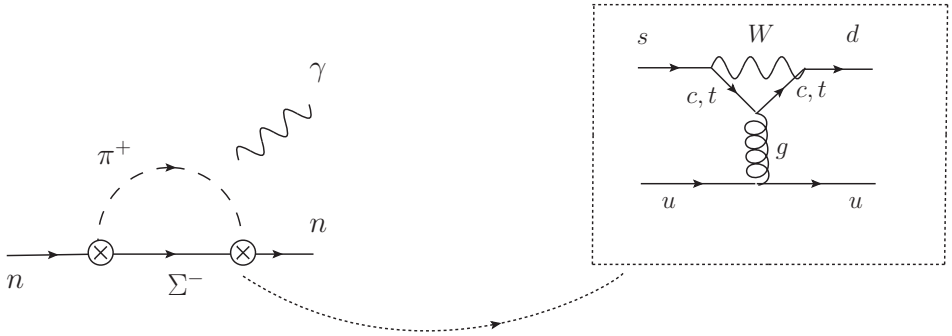

Figure 3.2: "Two-loop" effective diagram for the neutron EDM in the SM. The effective vertex is given by the diagram expanded in the right side of the picture. The external photon can be emitted by any quark within π^+ or Σ^- and the W-boson in the vertex.

In a general MSSM where the presence of complex phases is not constrained, new contributions to EDMs are induced at one-loop level by charginos, neutralinos and gluinos in processes like the one in Figure 3.3. At higher orders, two-loop diagrams from the W-boson [94–96], Barr-Zee graphs [97] or four-fermion interactions may have sizeable contributions to the process. However, it is not our goal to perform an exhaustive analysis of these interactions here, since we are just interested in the constraints that they impose over the presence of new CP-violating phases. Thus, in the following, we make use of these compact results at leading order in $v^2/M^2_{\rm SUSY}$ and for all 5 operators in the case of the electron and light quark EDMs [98]

$$\frac{d_e}{e} \simeq 7\times 10^{-26}\,\text{cm}\left(0.01\sin\varphi_{\mathbf{a_e}} + 0.09\sin\varphi_\mu\,\tan\beta\right)\left(\frac{1\text{TeV}}{M_{\rm SUSY}}\right)^2 \tag{3.3}$$

$$\frac{d_u}{e} \simeq 5\times 10^{-26}\,\text{cm}\left(\sin\varphi_\mu\,\cot\beta - \sin\varphi_{\mathbf{a_u}}\right)\left(\frac{1\text{TeV}}{M_{\rm SUSY}}\right)^2 \tag{3.4}$$

$$\frac{d_d}{e} \simeq 1\times 10^{-26}\,\text{cm}\left(\sin\varphi_\mu\,\tan\beta - \sin\varphi_{\mathbf{a_d}}\right)\left(\frac{1\text{TeV}}{M_{\rm SUSY}}\right)^2 \tag{3.5}$$

where φ_i refers to the phase of the correspondent parameter and M_{SUSY} reflects the mass scale for supersymmetric particles.

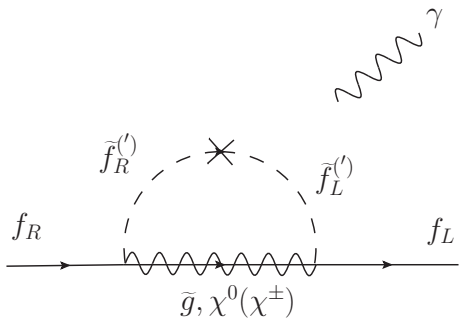

Figure 3.3: One-loop contribution to the EDM of quarks and leptons in the MSSM with MFV. The external photon can be emitted by any quark, squark or by the chargino.

3.2 $B \to X_s\gamma$

Rare processes such as the inclusive radiative decay $B \to X_s\gamma$ provides an excellent experimental ground where detect New Physics (NP) beyond the SM. In general, these processes involve high-order diagrams with several loops that makes them very sensitive to new particle virtual effects. A convenient way to compute these graphs is by means of effective operators and Wilson coefficients, which allow us to separate the relevant physics at each energy scale while keeping the high-energy information encoded into the coefficients. In this context, we can describe the $b \to s\gamma$ transition through the following effective Hamiltonian [64, 99, 100]

$$\mathcal{H}^{\text{eff}}_{b\to s\gamma} \;=\; -\,\frac{4\,G_F}{\sqrt{2}}\,\mathbf{V}_{33}\mathbf{V}^*_{32}\left(\sum_{i=2,7,8} C_i(\mu_b)Q_i(\mu_b) \;+\; C_7^{'}(\mu_b)Q_7^{'} \;+\; C_8^{'}(\mu_b)Q_8^{'}(\mu_b)\right)$$

where Q_2, Q_7 and Q_8 are the usual *current-current*, *magnetic-penguin* and *chromomagnetic-penguin* operators, respectively. Typical diagrams associated with them are represented in Figure 3.4. $Q_7^{'}$ and $Q_8^{'}$ are equivalent to Q_7 and Q_8 but exchanging P_R for P_L. In four-component notation (see Appendix A.5), their expressions are

$$Q_2 \;=\; (\bar{s}\,\gamma_\mu P_L\,c)\,(\bar{c}\,\gamma^\mu P_L\,b) \tag{3.6}$$

$$Q_7 \;=\; \frac{e\,m_b}{16\pi^2}\,(\bar{s}\,\sigma^{\mu\nu}P_R b)\,F_{\mu\nu} \qquad Q_7^{'} \;=\; \frac{e\,m_s}{16\pi^2}(\bar{s}\sigma^{\mu\nu}P_L b)\,F_{\mu\nu} \tag{3.7}$$

$$Q_8 \;=\; \frac{g_3\,m_b}{16\pi^2}\,(\bar{s}\,\sigma^{\mu\nu}P_R b)\,T^a G^a_{\mu\nu} \qquad Q_8^{'} \;=\; \frac{g_3\,m_s}{16\pi^2}(\bar{s}\sigma_{\mu\nu}P_L b)\,T^a G^a_{\mu\nu} \tag{3.8}$$

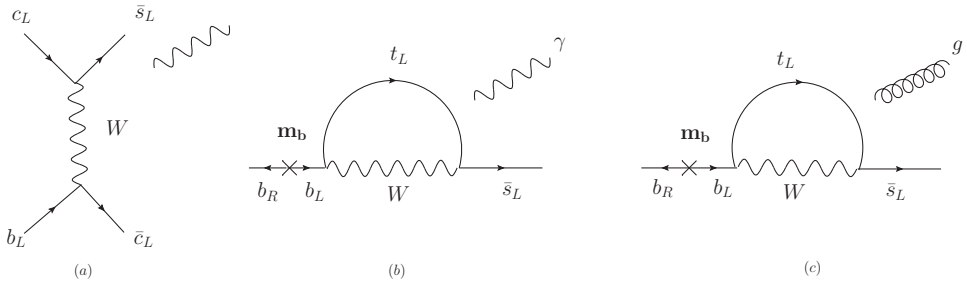

Figure 3.4: Typical diagrams in the SM for the the inclusive process $B \to X_s\gamma$: (a) four-fermion diagram contributing to the *current-current* operator, (b) magnetic-penguin diagram mediated by a W-boson, (c) chromomagnetic-penguin diagram mediated by a W-boson.

with $\sigma^{\mu\nu} = \frac{i}{2}[\gamma^\mu, \gamma^\nu]$. In the SM, processes are mediated by W-bosons just like in Figure 3.4. Going to the MSSM, new contributions to the magnetic and chromomagnetic operators arise owed to the exchange of charginos, the charged Higgs and gluinos. On top of that, some of these terms contains a dependence on $\tan\beta$ which can be important for medium and large $\tan\beta$ values. Following references [99–101], the branching ratio can be parametrised as

$$\mathrm{BR}(B \to X_s\gamma) \simeq a + a_{77}\delta\mathcal{C}_7^2 + a_{88}\delta\mathcal{C}_8^2 + \Re e\,[a_7\delta\mathcal{C}_7] + \Re e\,[a_8\delta\mathcal{C}_8] + \Re e\,[a_{78}\delta\mathcal{C}_7\delta\mathcal{C}_8^*]$$

with the numerical values

$$\begin{aligned} a &= 3.0 \times 10^{-4} & a_7 &= (-7.2 + 0.6\,i) \times 10^{-4} \\ a_{77} &= 4.7 \times 10^{-4} & a_8 &= (-2.2 - 0.6\,i) \times 10^{-4} \\ a_{88} &= 0.8 \times 10^{-4} & a_{78} &= (2.5 - 0.9\,i) \times 10^{-4} \end{aligned} \tag{3.9}$$

Written in this form, a is equivalent to the SM part mediated by the W-boson whilst $\delta\mathcal{C}_{7,8}$ refer to SUSY contributions. Under the assumption of MFV, only charginos and the charged-Higgs contribute. Therefore, $\delta\mathcal{C}_{7,8} = \mathcal{C}_{7,8}^{H^+} + \mathcal{C}_{7,8}^{\chi^+}$. In the case of the chargino at one-loop level, the dominant diagrams are those where a $\langle\phi_u^0\rangle$ insertion in the gaugino-higgsino mixing or in the stop left-right mixing signals the $\tan\beta$ enhancement. The computation of the correspondent Wilson coefficient gives [102]

$$\mathcal{C}_{7,8}^{\chi^+} = \frac{1}{\cos\beta}\sum_{a=1,2}\frac{U_{a2}^* V_{a1}}{\sqrt{2}}\frac{M_W}{m_{\chi_a^+}}\,\mathcal{F}_{7,8}\left(x_{\tilde{q}\chi_a^+},\, x_{\tilde{t}_1\chi_a^+},\, x_{\tilde{t}_2\chi_a^+}\right) + \frac{U_{a2}^* V_{a2}}{2\,\sin\beta}\frac{\overline{m}_t}{m_{\chi_a^+}}\,\mathcal{G}_{7,8}\left(x_{\tilde{t}_1\chi_a^+},\, x_{\tilde{t}_2\chi_a^+}\right) \tag{3.10}$$

where $x_{\alpha\beta} = m_\alpha^2/m_\beta^2$ and the functions $\mathcal{F}_{7,8}(x,y,z)$ and $\mathcal{G}_{7,8}(x,y)$ are defined in terms of the rotation matrix elements for squarks and loop functions as

$$\mathcal{F}_{7,8}(x,y,z) = f_{7,8}^{(3)}(x) - \left|\mathcal{R}_{11}^{\tilde{t}}\right|^2 f_{7,8}^{(3)}(y) - \left|\mathcal{R}_{21}^{\tilde{t}}\right|^2 f_{7,8}^{(3)}(z) \tag{3.11}$$

$$\mathcal{G}_{7,8}(x,y) = \mathcal{R}_{11}^{\tilde{t}}\,\mathcal{R}_{12}^{*\tilde{t}}\,f_{7,8}^{(3)}(x) \;-\; \mathcal{R}_{21}^{\tilde{t}}\,\mathcal{R}_{22}^{*\tilde{t}}\,f_{7,8}^{(3)}(y) \tag{3.12}$$

The loop functions $f_7^{(3)}(x)$ and $f_8^{(3)}(x)$ are given in Appendix C. For our analysis, it is convenient to implement the function expansion given in Appendix D in order to have a better understanding of the dominant terms in the Wilson coefficients defined in Eq.(3.10). The result is

$$\mathcal{C}_{7,8}^{\chi^+} \simeq \tan\beta\; M_W^2\,\frac{\mu\, M_2}{m_{\chi_1^+}^2 - m_{\chi_2^+}^2}\,F_{7,8}^{(3)}\left(x_{\tilde{q}\chi^+},\, x_{\tilde{t}_1\chi^+}\right) + \tan\beta\; M_W^2\,\frac{m_t^2}{m_{\tilde{t}_1}^2 - m_{\tilde{t}_2}^2}\,\frac{\mu\, A_t}{m_{\chi_1^+}^2 - m_{\chi_2^+}^2}\,F_{7,8}^{(3)}\left(x_{\tilde{t}_1\chi^+},\, x_{\tilde{t}_2\chi^+}\right) \tag{3.13}$$

where $F_{7,8}^{(3)}(x_{f_1\chi^+}, x_{f_2\chi^+})$ are defined by

$$F_{7,8}^{(3)}(x_{f_1\chi^+}, x_{f_2\chi^+}) = \frac{f_{7,8}^{(3)}(x_{f_1\chi_1^+}) - f_{7,8}^{(3)}(x_{f_2\chi_1^+})}{m_{\chi_1^+}^2} - \frac{f_{7,8}^{(3)}(x_{f_1\chi_2^+}) - f_{7,8}^{(3)}(x_{f_2\chi_2^+})}{m_{\chi_2^+}^2}$$

Besides, in the limit where the first and second charginos are nearly wino and higgsino i.e. $m_{\chi_1^+} \simeq M_2 \ll m_{\chi_2^+} \simeq \mu$, the previous expression can be simplified as

$$\mathcal{C}_{7,8}^{\chi^+} \simeq -\tan\beta\,\frac{M_W^2}{M_2^2}\,\frac{M_2}{\mu}\,\left[f_7^{(3)}\left(x_{\tilde{q}\chi_1^+}\right) - f_7^{(3)}\left(x_{\tilde{t}_1\chi_1^+}\right)\right] - \tan\beta\,\frac{M_W^2}{M_2^2}\,\frac{A_t}{\mu}\,\frac{m_t^2}{m_{\tilde{t}_1}^2 - m_{\tilde{t}_2}^2}\,\left[f_8^{(3)}\left(x_{\tilde{t}_1\chi_1^+}\right) - f_8^{(3)}\left(x_{\tilde{t}_2\chi_1^+}\right)\right] \tag{3.14}$$

This last expression will be very useful when analysing the results. The carged-Higgs contribution, including the would-be Goldstone-boson corrections to the W-boson contribution, can be written as [103]

$$\begin{aligned} \mathcal{C}_{7,8}^{H^\pm} &= \frac{1}{3\tan^2\beta}\, f_{7,8}^{(1)}(y_t) \\ &+ \frac{f_{7,8}^{(2)}(y_t) \,+\, f_{7,8}^{(2)}(x_t)\,\left(\,\mathbf{\Delta}_b^{\Phi_u^0}\,(1+\tan\beta) - \mathbf{\Delta}_b^{\Phi_d^0}\,(1-\cot\beta)\,\right)}{1 \,+\, \mathbf{\Delta}_b^{\Phi_d^0} \,+\, \tan\beta\mathbf{\Delta}_b^{\Phi_u^0}} \end{aligned} \tag{3.15}$$

with $y_t = m_t^2/m_{H^\pm}^2$ and $x_t = m_t^2/m_W^2$. The loop functions $f_{7,8}^{(1),(2)}$ are in Appendix C.

3.3 $B_s^0 \to \mu^+\mu^-$

The meson decay $B_s^0 \to \mu^+\mu^-$ occurs in the SM dominantly through Z^0-penguin and box diagrams with t-quarks in the loop, Figure 3.5. In the MSSM, making use of the effective description given in the Lagrangian of Eq.(2.25), additional contributions emerge from the exchange of neutral Higgses as in Figure 3.5(c). Note that in this case the $g^L_{H_i\bar{s}b}$ term is ms/mb suppressed with respect to $g^R_{H_i\bar{s}b}$. Thus, the effective Hamiltonian can be written as

$$H_{\Delta B=1}^{\text{eff}} \,=\, -2\sqrt{2}\,G_F\,V_{33}V_{32}^*\,\Big(\,C_S\,Q_S \,+\, C_P\,Q_P \,+\, C_{10}\,Q_{10}\,\Big) \tag{3.16}$$

where the relevant operators in Dirac-spinor notation are

$$Q_S = \frac{e^2}{16\pi^2} m_b\,(\bar{q}P_R b)\,(\bar{\mu}\mu) \tag{3.17}$$

$$Q_P = \frac{e^2}{16\pi^2} m_b\,(\bar{q}P_R b)\,(\bar{\mu}\gamma_5\mu) \tag{3.18}$$

$$Q_{10} = \frac{e^2}{16\pi^2}\,(\bar{q}\gamma^\mu P_L b)\,(\bar{\mu}\gamma_\mu\gamma_5\mu) \tag{3.19}$$

The branching ratio is given by [64]

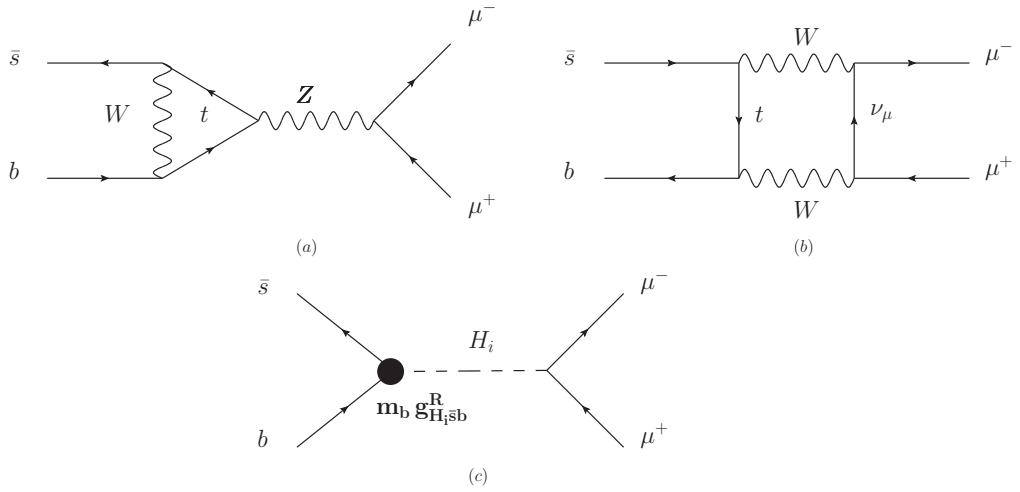

Figure 3.5: Diagrams contributing to the process $B_s^0 \to \mu^+\mu^-$: (a) peguin diagram mediated by a Z^0-boson, (b) W-boson box-diagram and (c) effective process with the exchange of a neutral-Higgs boson.

$$\begin{aligned} \mathrm{BR}\left(B_s^0 \,\to\, \mu^+\mu^-\right) \;&=\; \frac{G_F^2\,\alpha_{\mathrm{em}}^2}{16\,\pi^3}\, M_{B_s}\tau_{B_s}\, |V_{33}V_{32}^*|^2 \sqrt{1-\frac{4\,m_\mu^2}{M_{B_s}^2}}\;\times \\ &\left[\left(1-\frac{4m_\mu^2}{M_{B_s}^2}\right)|F_S^s|^2 \;+\; |F_P^s \;+\; 2m_\mu F_A^s|^2\right] \end{aligned} \tag{3.20}$$

with τ_{B_s} the total lifetime and the form factors given by

$$F_{S,P}^s \;=\; -\frac{i}{2}\, M_{B_s}^2 F_{Bs}\, \frac{m_b}{m_b \,+\, m_q}\, C_{S,P} \qquad\qquad F_A^s = \,-\frac{i}{2}\, F_{B_s}\, C_{10} \tag{3.21}$$

The Wilson coefficients can be calculated from the FCNC Lagrangian given in Eq.(2.30) as

$$C_S \;=\; \frac{2\pi m_\mu}{\alpha_{\mathrm{em}}}\,\frac{1}{V_{33}V_{32}^*}\,\sum_{i=1}^{3}\,\frac{g^R_{H_i\bar{s}b}\, g^S_{H_i\bar{\mu}\mu}}{m^2_{H_i}} \tag{3.22}$$

$$C_P \;=\; i\,\frac{2\pi m_\mu}{\alpha_{\mathrm{em}}}\,\frac{1}{V_{33}V_{32}^*}\,\sum_{i=1}^{3}\,\frac{g^R_{H_i\bar{s}b}\, g^P_{H_i\bar{\mu}\mu}}{m^2_{H_i}} \tag{3.23}$$

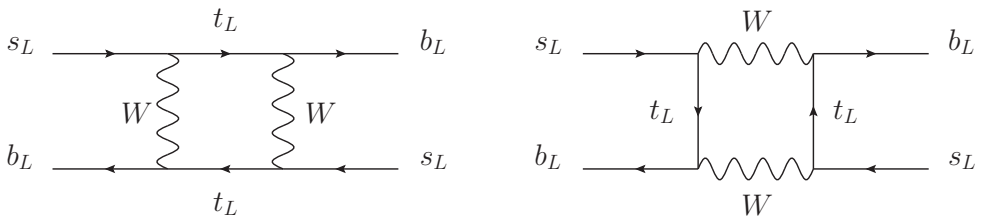

Figure 3.6: Dominant box-diagrams in the SM contributing to the B_s^0-$\bar{B}_s^0$ mixing. They involve the exchange of W-bosons and top quarks.

$$C_{10} \quad = \quad -4.221 \tag{3.24}$$

with C_{10} the leading SM contribution, $g^R_{H_i \bar{s} b}$ given in Eq.(2.29) and $g^{S,P}_{H_i \bar{\mu} \mu}$ the scalar and pseudoscalar couplings between neutral Higgses and μ-leptons given in Eqs.(2.31) and (2.32). Again, non-holomorphic corrections to the vertices on the leptonic sector have been neglected here for being unobservable small. Therefore, at tree-level, the leptonic couplings are exactly equal to the τ-lepton couplings given in Eq.(2.34).

3.4 ΔM_{B_s}

The effective Lagrangian for $\Delta B = 2$ interactions is given by

$$\mathcal{H}^{\text{eff}}_{\Delta B=2} \quad = \quad \frac{G_F^2 \, M_W^2}{16 \, \pi^2} \sum C_i \, Q_i \tag{3.25}$$

where the dominant contributions come from the following operators, written in terms of four-component spinors

$$Q_1^{\text{VLL}} \quad = \quad (\bar{b} \gamma_\mu P_L s)(\bar{b} \gamma^\mu P_L s) \tag{3.26}$$

$$Q_1^{\text{SLL}} \quad = \quad (\bar{b} P_L s)(\bar{b} P_L s) \tag{3.27}$$

$$Q_1^{\text{SRR}} \quad = \quad (\bar{b} P_R s)(\bar{b} P_R s) \tag{3.28}$$

$$Q_2^{\text{LR}} \quad = \quad (\bar{b} P_L s)(\bar{b} P_R s) \tag{3.29}$$

In the SM, $\bar{B}_s^0$-B_s^0 oscillations occur through W-box diagrams involving top quarks like in Figure 3.6. They contribute to the Q_1^{VLL} operator. In the MSSM, new transitions

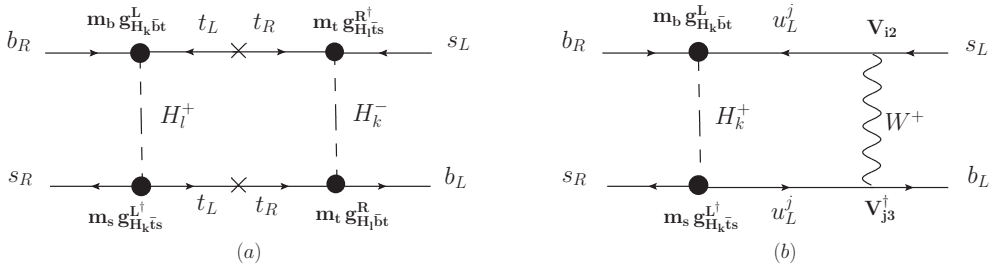

Figure 3.7: Box diagrams contributing to the B_s^0-$\bar{B}_s^0$ mixing in the MSSM through (a) the exchange of two charged-Higgs bosons and (b) the exchange of a charged Higgs and a W-boson.

are generated due to the exchange of charged-Higgs bosons in box diagrams like in Figure 3.7 and double-penguin diagrams with neutral Higgses exchanged at tree level through the effective vertices obtained in Eqs.(2.27) and (2.29), Figure 3.8. The B_s^0-meson difference of mass can be written as [64]

$$\Delta M_{B_s} \;=\; 2\,\Big|\,\langle \bar{B}_s^0|H^{\rm eff}_{\Delta B=2}|B_s^0\rangle_{SM} \;+\; \langle \bar{B}_s^0|H^{\rm eff}_{\Delta B=2}|B_s^0\rangle_{SUSY}\,\Big| \tag{3.30}$$

The SM theoretical prediction is [104]

$$\langle \bar{B}_s^0|H^{\rm eff}_{\Delta B=2}|B_s^0\rangle_{SM} \;=\; 17.3\ {\rm ps}^{-1} \tag{3.31}$$

whereas the SUSY diagrams give [64]

$$\begin{aligned}\left\langle \bar{B}_s^0|H^{\Delta B=2}_{eff}|B_s^0\right\rangle_{SUSY} \;&=\; 2310\,{\rm ps}^{-1}\left[\frac{\widehat{B}^{1/2}_{B_s}\,F_{B_s}}{265\,{\rm MeV}}\right]^2\left[\frac{\nu_B}{0.55}\right]\;\times \\ &\left[0.88\left(C^{(DP)}_{2,LR}+C^{(2HDM)}_{2,LR}\right)\;-\;0.52\left(C^{(DP)}_{1,SLL}+C^{(DP)}_{1,SRR}\right)\right]\end{aligned} \tag{3.32}$$

The Wilson coefficients for the double-penguin (DP) and box (2HDM) diagrams are given by

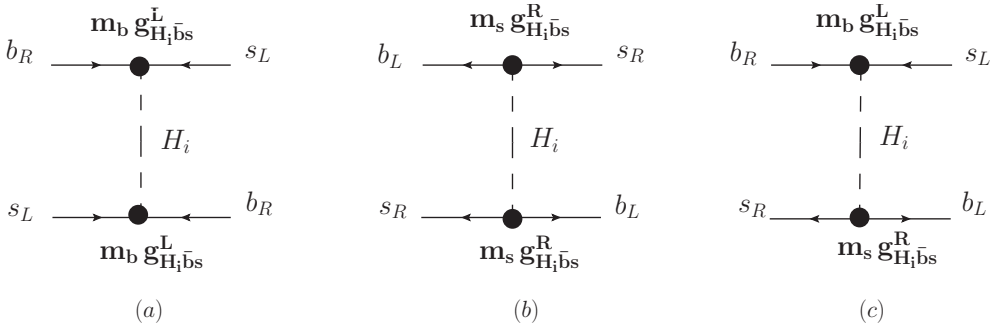

Figure 3.8: Double-penguin diagrams contributing to the B_s^0-$\bar{B}_s^0$ mixing in the MSSM through the flavour-violating effective vertices deduced in Eqs.(2.27) and (2.29).

$$C^{(DP)}_{1,SLL} = -\frac{16\pi^2 m_b^2}{\sqrt{2}G_F M_W^2}\sum_{i=1}^{3}\frac{g^L_{H_i\bar{b}s}\,\mathbf{g}^L_{H_i\bar{b}s}}{m_{H_i}} \tag{3.33}$$

$$C^{(DP)}_{1,SRR} = -\frac{16\pi^2 m_s^2}{\sqrt{2}G_F M_W^2}\sum_{i=1}^{3}\frac{g^R_{H_i\bar{b}s}\,\mathbf{g}^R_{H_i\bar{b}s}}{m_{H_i}} \tag{3.34}$$

$$C^{(DP)}_{2,LR} = -\frac{32\pi^2 m_b m_s}{\sqrt{2}G_F M_W^2}\sum_{i=1}^{3}\frac{g^L_{H_i\bar{b}s}\,\mathbf{g}^R_{H_i\bar{b}s}}{m_{H_i}} \tag{3.35}$$

$$C^{(2HDM)}_{2,LR} = C^{(2HDM)}_{2,LR}\Big|_{H^\pm H^\mp} + C^{(2HDM)}_{2,LR}\Big|_{W^\pm H^\mp} \tag{3.36}$$

As can be seen in Figure 3.7, the last coefficient in Eq.(3.36) contains two different contributions associated with the double charged-Higgs box-diagram and the graph where one W-boson and one charged Higgs are exchanged. They are given by [105]

$$C^{(2HDM)}_{2,LR}\Big|_{H^\pm H^\mp} = \frac{8\, m_b\, m_s\, m_t^4}{m_W^2}\sum_{\substack{k,l=\\ H,G}}\mathbf{g}^L_{H_l^-\,33}\,\mathbf{g}^{L\dagger}_{H_l^-\,32}\,\mathbf{g}^R_{H_k^-\,33}\,\mathbf{g}^{R\dagger}_{H_k^-\,32}\times D_0\left(M^2_{H_l^-},\, M^2_{H_k^-},\, m_t^2,\, m_t^2\right) \tag{3.37}$$

$$C_{2,LR}^{(2HDM)}\Big|_{W^{\pm}H^{\mp}} = -8\, m_b\, m_s \sum_{i,j=1}^{3} \sum_{k=H,G} \mathbf{g}^{L}_{H_k^- 3i}\, \mathbf{g}^{L\dagger}_{H_k^- j2}\, \mathbf{V}^{\dagger}{}_{3j}\, \mathbf{V}_{i2} \times D_2\left(M_W^2,\, M_{H_k^-}^2,\, m_{q_i}^2,\, m_{q_j}^2\right) \tag{3.38}$$

with $D_0(a,b,c,d)$ and $D_2(a,b,c,d)$ the loop functions in Appendix C.

4

Experimental bounds

4.1 Higgs signal at LHC

For our analysis, we use the experimental results provided by ATLAS and CMS experiments regarding the Higgs-like signal with the full pp collision data sample at 7 and 8 TeV. Specifically, the ATLAS analysis [106] uses a integrated luminosities of 4.8 fb^{-1} for $\sqrt{s} = 7$ TeV and 20.7 fb^{-1} for $\sqrt{s} = 8$ TeV in the most sensitive channels, $H \to \gamma\gamma$, $H \to ZZ^* \to 4l$ and $H \to WW^* \to l\nu l\nu$, whereas for the $H \to \tau\tau$ and $H \to b\bar{b}$ the integrated luminosity is of 4.7 fb^{-1} at $\sqrt{s} = 7$ TeV and 13 fb^{-1} at $\sqrt{s} = 8$ TeV. Similarly CMS [107] uses 5.1 fb^{-1} at $\sqrt{s} = 7$ TeV and 19.6 fb^{-1} at $\sqrt{s} = 8$ TeV in all the channels. The most important channels contributing to the observed signal are those associated with decays into two photons and two Z-bosons whilst the most relevant channel constraining the presence of additional Higgs-bosons is the decay into two τ leptons. ATLAS and CMS agree on the mass of the observed state which is $m_h = 125.5 \pm 0.2(\text{stat})^{+0.5}_{-0.6}(\text{sys})$ GeV for ATLAS [108] and $m_h = 125.7 \pm 0.3(\text{stat}) \pm 0.3(\text{syst})$ GeV for CMS [107], Figure 4.1. However, there are some tensions regarding the signal strength of one the channels. The signal strength μ_X for a Higgs decaying to X is defined as

$$\mu_X = \frac{\sigma(pp \to H) \times \text{BR}(H \to X)}{\sigma(pp \to H)_{\text{SM}} \times \text{BR}(H \to X)_{\text{SM}}}, \tag{4.1}$$

such that $\mu = 0$ corresponds to the background-only hypothesis and $\mu = 1$ corresponds to a SM Higgs signal. The combined signal-strength for the channels $H \to \gamma\gamma$, $H \to ZZ^*$, $H \to WW^*$, $H \to \tau\tau$ and $H \to b\bar{b}$ is $\mu^{\text{ATLAS}} = 1.23 \pm 0.18$ for ATLAS [108]

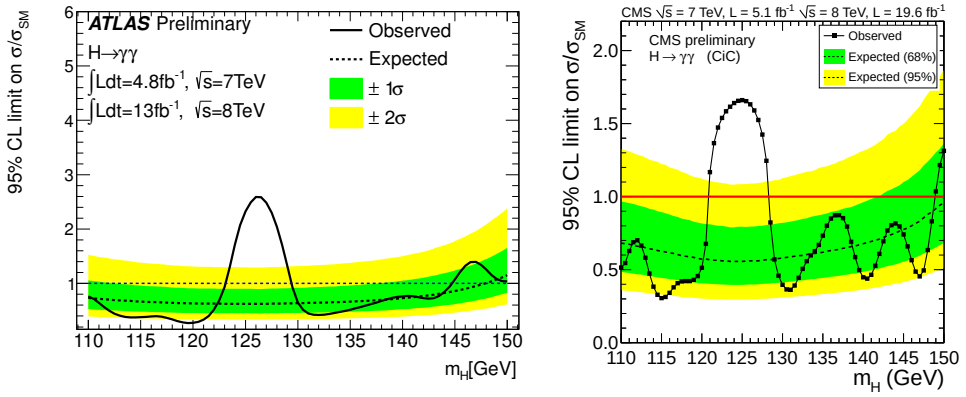

Figure 4.1: Observation of the Higgs state in the $H \to \gamma\gamma$ channel in terms of $\sigma/\sigma_{\rm SM}$ at (a) ATLAS [109] and (b) CMS [110].

and $\mu^{\rm CMS} = 0.80 \pm 0.14$ for CMS [107]. The diphoton channel has a measured signal strength of $\mu^{\rm ATLAS}_{\gamma\gamma} = 1.6 \pm 0.3$ [108] and $\mu^{\rm CMS}_{\gamma\gamma} = 0.78^{+0.28}_{-0.26}$ [110]. In both cases the signal is consistent with the SM, although ATLAS points to a slight excess over the SM expectations. In any case, both results agree on the fact that the diphoton signal must be of the order of the SM prediction, which is an important fact to take into account in the context of multi-Higgs models, as the MSSM, where the Higgs couplings to the d-quark and charged leptons are usually enhanced by $\tan\beta$ factors decreasing the $H \to \gamma\gamma$ branching ratio and consequently the signal strength. In this regard, we adopt as a conservative approach the weighted average of ATLAS and CMS results at 2σ

$$0.5 \leq \mu^{\rm LHC}_{\gamma\gamma} \leq 1.9 \tag{4.2}$$

The signal strengths for the $H \to ZZ^*$ channel are $\mu^{\rm ATLAS}_{ZZ^*} = 1.5 \pm 0.4$ [108] and $\mu^{\rm CMS}_{ZZ^*} = 0.92 \pm 0.28$ [113] so we require

$$0.78 \leq \mu^{\rm LHC}_{ZZ^*} \leq 1.58 \tag{4.3}$$

Finally, we include the bounds on charged Higgses produced in the top decay $t \to H^+ b$ with the subsequent decay $H^+ \to \tau\nu$ [114, 115]. These analysis set upper bounds on $BR(t \to H^+ b)$ in the range 2-3% for masses between 80 and 160 GeV under the assumption that $BR(H^+ \to \tau\nu) = 1$, which is a very good hypothesis unless the decay channels to lighter Higgses and W-bosons are kinematically open the .

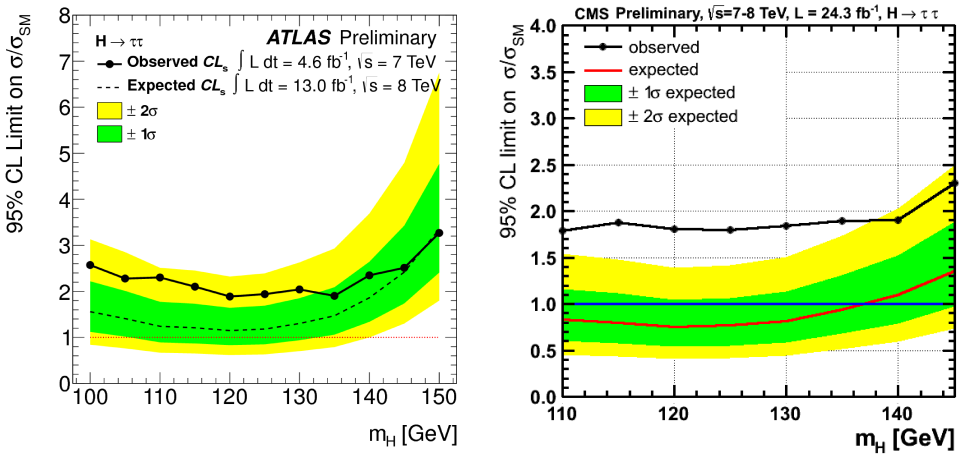

Figure 4.2: Higgs searches in the $H \to \tau\tau$ channel for 100 GeV $\leq m_H \leq$ 150 GeV at (a) ATLAS [111] and (b) CMS [112].

4.2 Improved $\tau\tau$ searches for additional Higgs states

The most restrictive constraint on the presence of additional heavy Higgses comes from ATLAS and CMS searches of a Higgs boson decaying into a pair of τ-leptons. Since in the MSSM the production cross section of τ-pairs through a heavy Higgs would be enhanced by powers of $\tan\beta$, these bounds on $\sigma_\phi \times \mathrm{BR}(\phi \to \tau\tau)$ are very important in the medium-large $\tan\beta$ region.

ATLAS and CMS provide limits on $\sigma(pp \to H) \times \mathrm{BR}(H \to \tau\tau)$ for different mass ranges. For masses up to 150 GeV, ATLAS has analysed the collected data samples of 4.6 fb^{-1} at $\sqrt{s}$ =7 TeV and 13.0 fb^{-1} at $\sqrt{s}$ =8 TeV [111] while CMS used 4.9 fb^{-1} at $\sqrt{s}$ =7 TeV and 19.4 fb^{-1}at $\sqrt{s}$ =8 TeV [112]. The bounds on the $\tau\tau$-cross section normalised to the SM cross section as a function of the Higgs mass are shown in Figure 4.2. In this case, CMS sets the strongest bound for m_H below 150 GeV: for m_H = 110 GeV, $\mu_{\tau\tau} = \sigma\left(H \to \tau\tau\right)/\sigma_{SM} \leq 1.8$ at 95% C.L. and this limit remains nearly constant, $\mu_{\tau\tau} \leq 2.0$, up to m_H = 140 GeV; for a neutral Higgs of mass m_H = 150 GeV, $\mu_{\tau\tau} \leq 2.3$. In our scenario, this limit can be imposed to any Higgs state with a mass below 150 GeV. For heavier masses, there exist a previous search in ATLAS for MSSM Higgs bosons with masses up to 500 GeV [116] which is presented in Figure 4.3 as an upper limit on the $\tau\tau$ and $\mu\mu$ production cross-section for 4.9 fb^{-1} at $\sqrt{s}$ =7 TeV.

In addition, updated analysis haven been released by both collaborations for masses

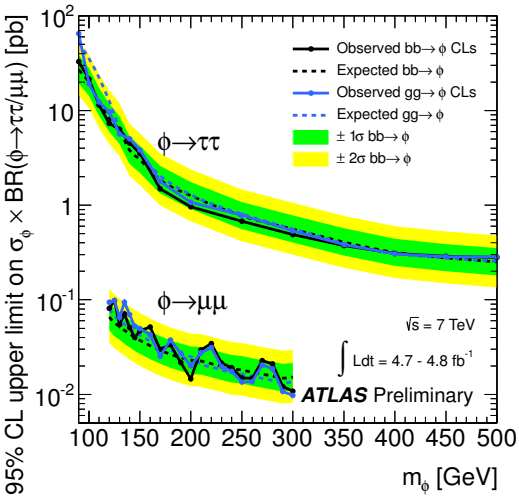

Figure 4.3: Upper limit on the $\tau\tau$ production cross section through heavy Higgs states from ATLAS with 4.8 fb^{-1} at $\sqrt{s} = 7$ TeV [116]

up to 1 TeV [117, 118]. The ATLAS analysis was performed on data collected for 8 TeV collisions with integrated luminosities in the range 19.5-20.3 fb^{-1}. CMS analysed the full data set with a total integrated luminosity of 24.6 fb^{-1}, 4.9 fb^{-1} at 7 TeV and 19.7 fb^{-1} at 8 TeV. Both analysis discriminated between Higgses produced through gluon fusion and $b\bar{b}$ fusion with two extra b-jets. These latest results are presented in Figure 4.4. In our studio these bounds are imposed at 95% C.L. on the theoretical cross sections obtained in our generic MSSM.

4.3 SUSY searches at LHC

Simultaneously to the Higgs searches described above, LHC has been looking for signatures on new physics beyond the SM. A large effort has been devoted to search for supersymmetric extensions of the SM. These studies focus the searches on jets/leptons plus missing energy (possible evidence of the LSP) and, so far, agree with the SM expectations in all the explored region. Therefore they can be implemented to set bounds on masses for supersymmetric particles. The most stringent constraints from LHC experiments are set on gluinos and first-generation squarks produced through strong interactions in pp collisions. We use for our analysis gluino searches performed by ATLAS [119–122] and CMS [123–125] at 8 TeV that have driven to the exclusion

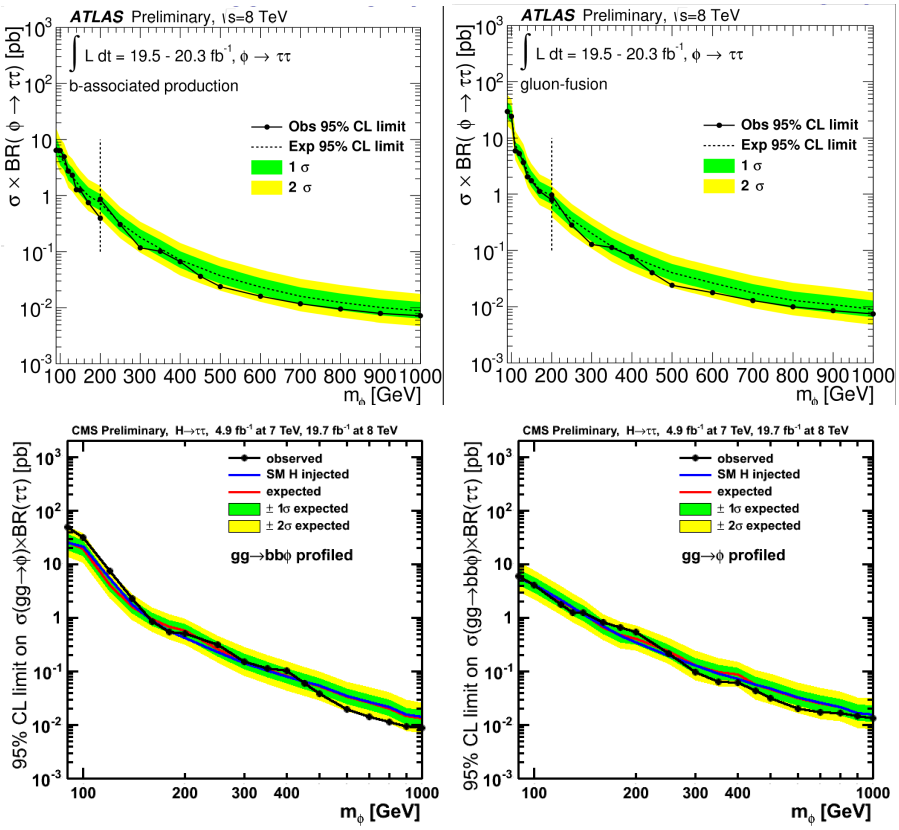

Figure 4.4: Latest ATLAS and CMS results on the $\tau\tau$ production cross section through heavy Higgs states [117, 118]. Figures on the left correspond to $b\bar{b}$ production mode with two additional b-jets whereas figures on the right are obtained from gluon-fusion produced Higgs.

of masses up to 1.3 TeV for (neutralino) LSP masses below 500 GeV, Figure 4.5. The limits on first-generation squarks directly produced are $m_{\tilde{q}} \gtrsim 740$ GeV for squarks decaying as $\tilde{q} \to q\chi_1^0$ with $m_{\chi_1^0} = 0$ GeV [126][1].

However, the most important players in Higgs physics are third-generation squarks because of their large Yukawa couplings. In this case, stop masses are required to be above ~ 650 GeV for $m_{\chi^0} \lesssim 200$ GeV [127–130] with the exception of small regions of nearly degenerate stop-neutralino, Figure 4.5. Regarding limits on sbottom, we use ATLAS bounds on sbottom masses up to 620 GeV at 95% C.L. from direct production

[1]Limits on masses could be softer if these squarks are nearly degenerate with the LSP, but this does not affect our analysis below

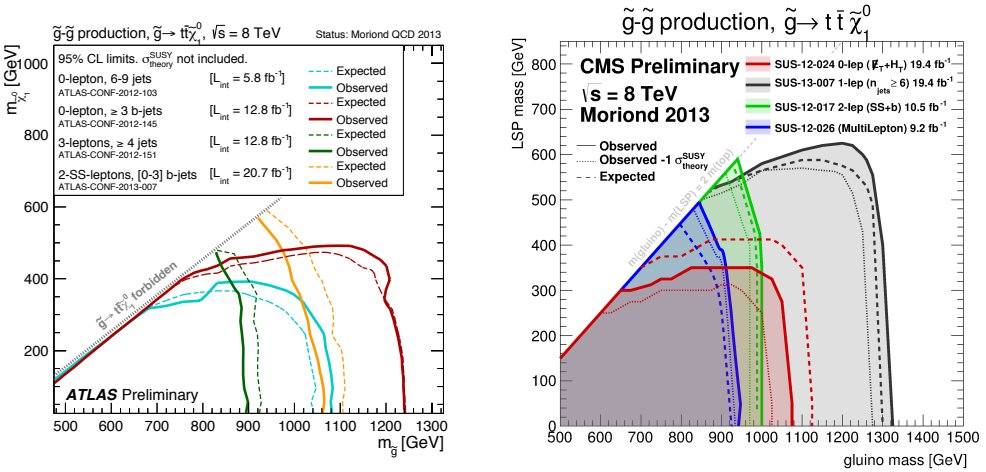

Figure 4.5: Summary of the different limits on gluino masses versus the LSP mass from experimental observations at (a) ATLAS and (b) CMS.

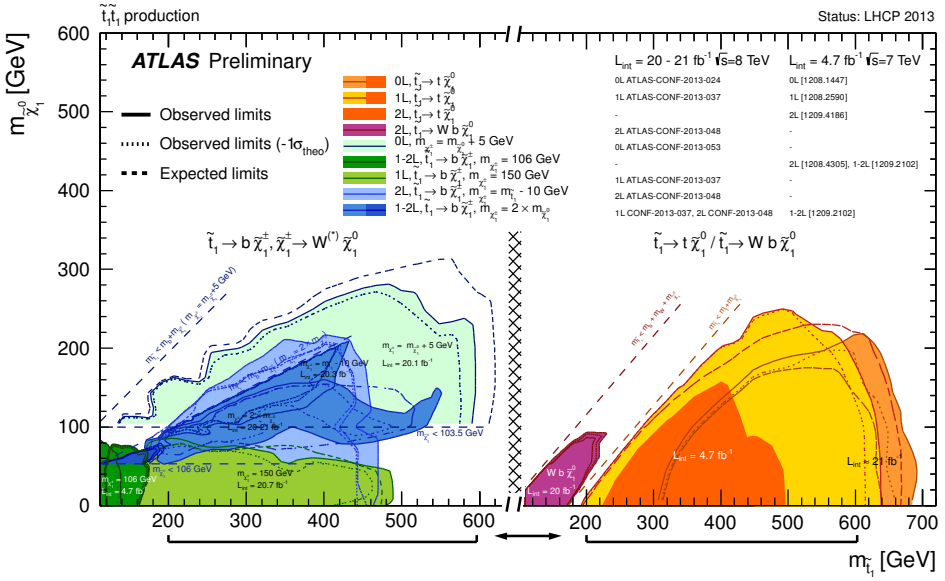

Figure 4.6: Summary of the present limits on stop masses versus lightest neutralino masses from ATLAS.

and $m_{\chi^0} < 150$ GeV, with the exception of $m_{\tilde{b}_1} - m_{\chi^0} < 70$ GeV for which sbottom masses are excluded only up to 250 GeV [129]. Similar results are obtained by CMS in [126, 131].

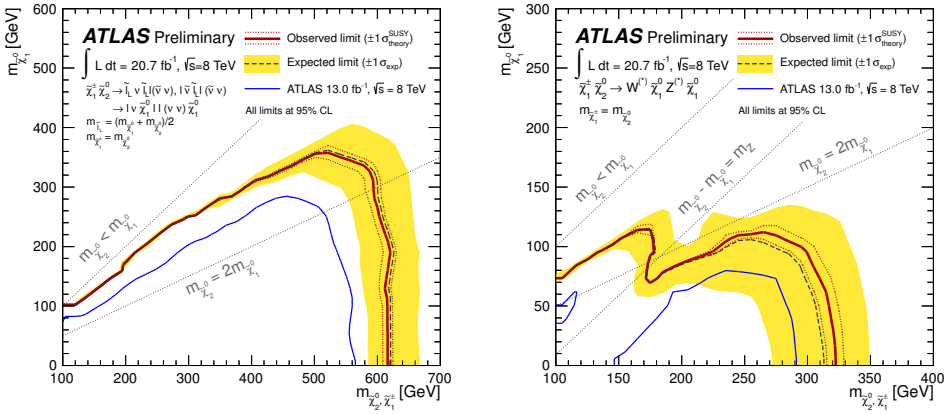

Figure 4.7: Limits on chargino masses from searches of particles directly produced through electroweak interactions at ATLAS [132].

Finally, ATLAS and CMS have presented limits on chargino masses from direct EW production [132, 133], Figure 4.7. In both cases the limits depend strongly on the slepton masses and the braching ratios of chargino and second neutralino, which are supposed to be degenerated. When the decays to charged sleptons are dominant, chargino masses are excluded up to $\sim$ 600 GeV for large mass differences with χ_1^0. Even in the case when the slepton channels are closed, decays to weak bosons plus lightest neutralino exclude chargino masses up to $\sim$ 350 GeV for $m_{\chi_1^0} \lesssim 120$ GeV[2].
As a conclusion, it is interesting noting that limits on SUSY particles from LHC are already fairly strong with the exceptions of sparticle masses rather degenerate with the lightest supersymmetric particle.

4.4 Flavour constraints

Indirect probes of new physics in low energy experiments still play a relevant role in the search for extensions of the SM [135–137]. Even in the absence of new flavour structures beyond the SM Yukawa couplings, in a MFV scheme, decays like $B_s^0 \to \mu^+\mu^-$, $B \to X_s\gamma$ or EDMs put strong limits for the whole $\tan\beta$ range.
For instance, the inclusion of EDM bounds is mandatory within a complex MSSM

[2] As pointed out in [134], these bounds with the slepton channel closed are only valid in a simplified model that assumes $BR(\chi_2^0 \to Z\chi_1^0)$. This bound is strongly relaxed once the decay $\chi_2^0 \to \chi_1^0 h$ is included. However, in our analysis, this limit is only taken into account as a reference value for chargino masses and has no effect regarding the feasibility of this scenario.

in order to have CP-violating parameters consistent with the available experimental data. Nowadays, a remarkable precision has been achieved in the measurement of the electron, neutron, heavy atoms, and molecules EDMs and, indeed, the accuracy to which they are known to vanish is exceptional [98]. In particular, the most stringent bounds come from Thallium (Tl) [138], the neutron (n) [139] and Mercury (Hg) [140], which can be expressed in terms of the electron EDM (d_e) and the EDMs of the constituent quarks for the neutron (d_d and d_u) [98] as

$$\begin{aligned} d_{\rm Tl} &= -585\, d_e \,-\, e\, 43\,{\rm GeV}\,(C_S^{(0)} - 0.2 C_S^{(1)}) \;\leq\; 9\times 10^{-25}\ {\rm e\ cm} \\ d_{\rm H_g} &= 10^{-2}\, d_e \,-\, (1.8\times 10^{-4}\,{\rm GeV}^{-1})\, e\, \bar{g}^{(1)}_{\pi NN} \;\leq\; 3\times 10^{-29}\ {\rm e\ cm} \\ d_n &= (1\pm 0.5)\left[1.4\,(d_d - 0.25\, d_u) \,+\, 1.1\, e\,(d_d^c + 0.5\, d_u^c)\right] \;\leq\; 3\times 10^{-26}\ {\rm e\ cm} \end{aligned} \tag{4.4}$$

where $C_S^{(0)}$ and $C_S^{(1)}$ are CP-odd electron-nucleon couplings and $g_{\pi NN}$ is the CP-odd pion-nucleon coupling due to CP-odd interactions among quarks and gluons. Their expressions can be found in [98, 141]. Recalling Eqs.(3.3)-(3.5), one can plug these expressions into Eq.(4.4) -after evolving them down to the low-enery range- and arrives to the known result of "overproduction" of EDMs in supersymmetric models [98, 142, 143]. The plausible solutions are three: CP-violating phases are small for the first two generations, the scale of the soft-breaking masses is significantly larger than 1 TeV, or accidental cancellations happens. For our analysis, we assume CP-violating phases of order unity only for $\mathbf{a}_t$, $\mathbf{a}_b$ and $\mathbf{a}_\tau$. We also work with arbitrary masses for squarks in the GeV scale, always within the limits imposed by direct searches.

Regarding the present status of the decay $B_s^0 \to \mu^+\mu^-$, we use the LHCb data with 1.1 fb^{-1} of proton-proton collisions at $\sqrt{s} = 8$ TeV and 1.0 fb^{-1} at $\sqrt{s} = 7$ TeV. The observed value for the branching ratio is [144]

$$\mathrm{BR}\left(B_s^0 \to \mu^+\mu^-\right) = \left(2.9^{+1.1}_{-1.0}\right) \times 10^{-9}\,. \tag{4.5}$$

We also consider the CMS measurement given by [145]

$$\mathrm{BR}\left(B_s^0 \to \mu^+\mu^-\right) = \left(3.0^{+1.0}_{-0.9}\right) \times 10^{-9} \tag{4.6}$$

Limits on the decay $B \to X_s\gamma$ come principally from BaBar and Belle B-factories and CLEO [146–151] so that the current world average for $E_\gamma > 1.6$ GeV given by HFAG [152, 153] is

$$\mathrm{BR}\,(B \to X_s\gamma) = (3.43 \pm 0.21 \pm 0.07) \times 10^{-4} \tag{4.7}$$

This result will be essential in the study of the low $\tan\beta$ region where other supersymmetric contributions are rather small. Finally, in our last analysis where the FC decay $H_i \to \bar{b}s, \bar{s}b$ is considering, another interesting bound comes from the $\mathrm{B_s}$-meson mass difference ΔM_{B_s}. The present experimental value is [154]

$$\Delta M_{B_s} \;=\; (17.757 \;\pm\; 0.021) \quad \mathrm{ps}^{-1} \tag{4.8}$$

Thus, we will require in our analysis

$$15.94\,\mathrm{ps}^{-1} \;\leq\; \Delta M_{B_s} \;\leq\; 19.83\,\mathrm{ps}^{-1} \tag{4.9}$$

where we have included the theoretical error on $f_{B_s}\sqrt{B_s} = 262 \pm 10$ [155].

5

Results

Since the detection of the 125 GeV scalar boson at the LHC in 2012 [156,157], the SM picture seems to be completed. The key role of the Higgs boson in the structure of the model makes its detection a big success for the theory of electroweak interactions and the mechanism of spontaneous symmetry breaking. However, in all SM extensions, other similar scalars play equally important roles and, actually, to verify that this resonance corresponds to the SM Higgs boson or it belongs to one of these extensions, it will be necessary to measure its properties and couplings with high precision [106–108,158–165]. At this stage, the observed production cross section and decay channels are consistent with a SM Higgs boson, although inevitably fluctuations are relatively large and there is still room for it to pertain to one of the different extensions of the SM [107,108].

In this work [166–168], we intend to shed some light on the status of the Higgs sector in general MSSM models with explicit CP-violation. In particular, we investigate the cases in which the discovered scalar is identified as the lightest or the second-lightest Higgs. The possibility of being the heaviest Higgs implies equivalent conclusions to those of the second case so it will be commented too. Finally, we believe it is worth studying some potentially measurable flavour-violating processes which might reveal the presence of new particles whose direct production can be out of reach until the next generation of colliders.

The way to proceed for all these analysis is quite similar; we do not simply scan the parameter space in order to find permitted regions but rather choose the most important experimental signatures from both high- and low-energy experiments and perform a semianalytical approach. Thus, we gain understanding on the physics of

the model while avoiding missing fine-tuned areas where unexpected cancellations might occur.

5.1 Eviction of a 125 GeV "heavy" Higgs

In this analysis [166] we study whether it would be possible to interpret the Higgs resonance observed at LHC with mass 125 GeV as the second lightest Higgs (H_2) in a generic MSSM framework with explicit CP-violation. In this context, H_1 would have evaded detection at LEP and Tevatron whereas, as we will see, the third neutral Higgs (H_3) would have a mass below 200 GeV. Notice that we do not impose any mass relations obtained through the RG running from a high scale, as it is usually the case in models such as the Constrained MSSM (CMSSM), but keep all MSSM parameters free and independent at M_W. Furthermore, as we are principally interested in the Higgs sector of the model, we analyse it assuming generic Higgs masses and mixings in the presence of complex phases for the squark sector.
In order to carry out this program, we begin making some observations about the Higgs spectrum of the model under the assumptions of explicit violation of CP and $m_{H_2} = 125$ GeV in Section 5.1.1. For the analysis, the parameter space is divided in two regions -low and medium-large $\tan\beta$- and, in Section 5.1.2, the $\gamma\gamma$ signal for H_2 is examined by means of analytical expressions and numerical simulations. From it, a very specific pattern of mixing for the neutral scalars is deduced. Once this is known, the compatibility among additional Higgs collider limits and indirect bounds is tested. In Section 5.1.4, our conclusions are drawn.

5.1.1 Mass spectrum

In Section 2.1, the Higgs spectrum for a MSSM with explicit CP-violation has been reviewed with the conclusion that radiative corrections strongly modifies the neutral-Higgs mass matrix generating non well-defined CP Higgs states. Here, we aim to be more precise and carefully examine analytic expressions in order to gain knowledge about the masses of the Higgs bosons predicted in our model.
We consider the scalar part of the squared-mass matrix first. As it is well-known, even in the absence of complex phases, the different MSSM particles enter in the Higgs masses and mixings through one-loop corrections and, in particular, M_S^2 receive important contributions that may increase the lightest Higgs mass from M_Z to ~ 130 GeV [18–20]. The most important ones come from the top-stop sector and are given by

$$\delta M_S^2 \simeq \frac{3\, m_t^4}{2\,\pi^2\, v^2\, \sin^2\beta}\left[\log\frac{M_{SUSY}^2}{m_t^2} + \frac{X_t^2}{2\, M_{SUSY}^2}\left(1 - \frac{X_t^2}{6\, M_{SUSY}^2}\right)\right] \tag{5.1}$$

with M_{SUSY} the geometric mean of the two stop masses and $X_t = A_t - \mu\cot\beta$. On the other hand, the pseudoscalar mass M_A^2 can be related with the charged-Higgs mass through [52]

$$M_{H^\pm}^2 = M_A^2 + \frac{1}{2}\,\lambda_4\, v^2 - \Re e\left[\lambda_5 e^{2i\xi}\right] v^2 \tag{5.2}$$

where $\lambda_{4,5}$ are the two-loop corrected parameters of the Higgs potential [52,169] that, at tree-level, are given by $\lambda_4 = g_w^2/2$, such that $\lambda_4 v^2/2 = M_W^2$, and $\lambda_5 = 0$. In any case, what looks reasonable is to expect $\lambda_i \lesssim 1$. This implies that, for the complex MSSM, the squared charged Higgs mass can never be heavier that the largest neutral Higgs (H_3) by a difference much larger than M_Z^2. This is equivalent to say that loop corrections are of the same order as $\sim \delta M_S^2$.
Similarly, we can expect the mass of the second neutral Higgs, which in our scenario is $m_{H_2} \simeq 125$ GeV, only to differ from the heavier eigenvalue by terms of order v^2. This can be seen from the trace of the neutral Higgs masses that, in the basis of CP eigenstates and considering the decoupling limit, would be at tree-level $\mathrm{Tr}\left(M_H^2\right) = 2M_A^2 + M_Z^2$. Loop corrections to the diagonal elements are expected to be order the corrections to the lightest Higgs mass, $O(M_Z^2)$, so that a light second-Higgs can be obtained either for low M_A or for a large scalar-pseudoscalar mixing. The different contributions to scalar-pseudoscalar mixing, M_{SP}^2, are approximately given by [52]

$$M_{SP}^2 = \mathcal{O}\left(\frac{m_t^4\,|\mu|\,|A_t|}{32\,\pi^2\, v^2\, M_{SUSY}^2}\right)\sin\phi_{CP} \times \left[6,\ \frac{|A_t|^2}{M_{SUSY}^2},\ \frac{|\mu|^2}{\tan\beta\, M_{SUSY}^2}\right] \tag{5.3}$$

which again are of the same order as $\delta M_S^2 \simeq O(M_Z^2)$ for $\sin\phi_{CP} \sim O(1)$. Therefore, taking also into account that in the decoupling limit, and in the absence of scalar-pseudoscalar mixing, $M_H \simeq M_A$, we must require M_A^2 not to be much larger than M_Z^2. Taking $M_A^2 \lesssim 3M_Z^2$, the invariance of the trace tells us that $m_{H_1}^2 + m_{H_2}^2 + m_{H_3}^2 = 2M_A^2 + M_Z^2 + O(M_Z^2)$ in such a way that with 90 GeV $\lesssim m_{H_1} \lesssim m_{H_2} \simeq 125$ GeV, we get an upper limit for $m_{H_3}^3 \lesssim 2M_A^2 + 2M_Z^2 - \left(m_{H_2}^2 + m_{H_1}^2\right) \lesssim (200\ \mathrm{GeV})^2$[1].

[1] Allowing the heaviest neutral-Higgs to be 200 GeV with a second-lightest Higgs of 125 GeV is a

5.1.2 Medium–large $\tan\beta$ regimen

Once the Higgs spectrum for our model have been examined, we aim to analyse different processes in the medium-large $\tan\beta$ regime defined by $\tan\beta \gtrsim 5$. For these values of $\tan\beta$, the following approximations can be safely taken: $\sin\beta \simeq 1$ and $\cos\beta \simeq (1/\tan\beta) \ll 1$. First, we examine the model predictions for the process $pp \to H_2 \to \gamma\gamma$, which is requested to satisfy the experimental constraints exposed in Section 4.1 of $0.5 \leq \mu_{\gamma\gamma}^{\rm LHC} \leq 1.9$. Then, we investigate the constraints from $pp \to H_a \to \tau\tau$ checking whether both results are compatible for $m_{H_2} = 125$ GeV.

Two photon cross section

In the narrow-width approximation, the production cross section of two photons through a Higgs boson is given by the Higgs production cross section and the branching ratio of the Higgs decay to the two photon final state: $\sigma_{\gamma\gamma} = \sigma(pp \to H_2) \times \mathrm{BR}(H_2 \to \gamma\gamma)$. Thus we have to analyze three elements, *i.e.* $\sigma(pp \to H_2)$, $\Gamma(H_2 \to \gamma\gamma)$ and Γ_{H_2}. In first place, we consider the decay width of the Higgs boson into two photons. As a reference value, we compare our MSSM prediction with the SM value given by the loop contributions of the heavier quarks, bottom and top, and the W-boson

$$\begin{aligned} S^{\gamma}_{\rm H_{SM}} &= \frac{2}{3} F_b^S(\tau_b) + \frac{8}{3} F_t^S(\tau_t) - F_1(\tau_W) \simeq (-0.025 + i\,0.034) + 1.8 - 8.3 \\ &\simeq -6.54 \end{aligned} \tag{5.4}$$

with $\tau_f = m_f^2/m_H^2$. The MSSM decay width has been presented in Eq.(2.50) and it consists of a scalar and a pseudoscalar part, receiving each of them different contributions according to the virtual particles that run in the loop. In particular

$$S^{\gamma}_{H_2} = S^{\gamma}_{H_2,b} + S^{\gamma}_{H_2,t} + S^{\gamma}_{H_2,W} + S^{\gamma}_{H_2,\tilde{b}} + S^{\gamma}_{H_2,\tilde{t}} + S^{\gamma}_{H_2,\tilde{\tau}} + S^{\gamma}_{H_2,\tilde{\chi}} + S^{\gamma}_{H_2,H^{\pm}} \tag{5.5}$$

$$P^{\gamma}_{H_2} = P^{\gamma}_{H_2,b} + P^{\gamma}_{H_2,t} + P^{\gamma}_{H_2,\tilde{\chi}} \tag{5.6}$$

Once the Higgs mass is fixed as $m_{H_2} = 125$ GeV, the contributions from W-bosons and SM fermions are completely determined at tree level in terms of the Higgs mixings

very conservative assumption that actually looks very difficult to be realised in any realistic MSSM construction.

and $\tan\beta$, which are taken as free parameters here. The W-boson scalar amplitude would be

$$\begin{aligned} S^{\gamma}_{H_2,W} &= -\, g_{H_2WW}\, F_1(\tau_W) \;=\; -\,(\,\mathcal{O}_{12}\,\cos\beta \;+\; \mathcal{O}_{22}\,\sin\beta\,)\; F_1(\tau_W) \\ &\simeq -\,8.3\left(\mathcal{O}_{22}+\frac{\mathcal{O}_{12}}{\tan\beta}\right) \end{aligned} \tag{5.7}$$

where we have used that $F_1(\tau_W) = F_1(0.61) \simeq 8$. Regarding third generation fermions, as emphasized before in Section 2.2, it is very important to take into account the non-holomorphic threshold corrections from gluino and chargino loops to the Higgs-fermionic couplings. Their expression have been given in Eqs.(2.33), (2.37) and (2.38). Then, the top and bottom quark contributions entering in both the scalar and pseudoscalar pieces can be written as

$$\begin{aligned} S^{\gamma}_{H_2,b+t} &\simeq \frac{2}{3}\left(\Re e\left[\frac{\mathcal{O}_{12}+\mathcal{O}_{22}\,\kappa_d}{1+\kappa_d\,\tan\beta}\right]\tan\beta \;+\; \Im m\left[\frac{\kappa_d\,(\tan^2\beta+1)}{1+\kappa_d\tan\beta}\right]\mathcal{O}_{32}\right) F_b^S(\tau_{2b}) \\ &\quad + \frac{8}{3}\,\mathcal{O}_{22}\,F_t^S(\tau_{2t}) \end{aligned} \tag{5.8}$$

with $\kappa_b = \mathbf{\Delta}_b^{\Phi_u}/(1+\mathbf{\Delta}_d^{\Phi_d})$ the parameter associated to the finite loop-induced threshold corrections that are generally much lower than 1. In Eq.(5.8), $\tan\beta \simeq 1/\cos\beta$ has been assumed. The loop functions for $m_t = 173,1$ GeV (pole mass) and $m_b = 4.33$ GeV (mass at m_t scale) are just about $F_b^S \simeq -0.04 + i0.05$ and $F_t^S \simeq 0.7$. Hence, Eq.(5.8) can be approximated as

$$\begin{aligned} S^{\gamma}_{H_2,b+t} &\simeq 1.8\;\mathcal{O}_{22} \;+\; (\,-0.025+\,i\,0.034\,)\;\times\left(\Re e\left[\frac{\tan\beta}{1+\kappa_d\tan\beta}\right]\mathcal{O}_{12}\right. \\ &\quad \left. +\,\Im m\left[\frac{\kappa_d\tan^2\beta}{1+\kappa_d\tan\beta}\right]\mathcal{O}_{32}\right) \end{aligned} \tag{5.9}$$

Going to the supersymmetric spectrum, the first contribution we consider is the one associated with the charged-Higgs boson. As already seen in Eq.(2.51), it only takes part in the scalar part of the decay width as

$$S^{\gamma}_{H_2,H^{\pm}} \;=\; -\,g_{_{H_2H^+H^-}}\,\frac{v^2}{2\,m^2_{H^{\pm}}}\,F_0(\tau_{H^{\pm}}) \tag{5.10}$$

The self-couplings has been collected in Appendix B.4. For our medium-large $\tan\beta$ regimen, the self-coupling to the second neutral-Higgs can be approximated as follows

$$\begin{aligned} g_{_{H_2H^+H^-}} &\simeq \mathcal{O}_{12}\ (\,2\,\lambda_1\,\cos\beta\ -\ \lambda_4\,\cos\beta\ -\ 2\,\cos\beta\,\Re e\,[\lambda_5]\ +\ \Re e\,[\lambda_6]\,) \\ &+ \mathcal{O}_{22}\ (\,\lambda_3\ +\ \cos\beta\,\Re e\,[\lambda_6]\ -\ 2\,\cos\beta\,\Re e\,[\lambda_7]\,) \\ &+ \mathcal{O}_{32}\ (\,2\,\cos\beta\,\Im m\,[\lambda_5]\ -\ \Im m\,[\lambda_6]\,) \end{aligned} \tag{5.11}$$

where only the leading terms in $\cos\beta$ have been kept. Regarding the loop function $F_0\,(\tau)$, it is quite stable for small τ values: for 150 GeV $\leq m_{H^\pm} \leq$ 200 GeV, $0.17 \simeq (125/300)^2 \leq \tau_{H^\pm} \leq 0.097 \simeq (125/400)^2$ and we obtain $F_0\,(\tau_{H^\pm}) \simeq 0.34$. Then

$$\begin{aligned} S^{\gamma}_{H_2,H^\pm} &\lesssim -0.45\,\left\{\mathcal{O}_{12}\,\left(\frac{2\,\lambda_1-\lambda_4-2\,\Re e\,[\lambda_5]}{\tan\beta}+\Re e\,[\lambda_6]\right)\right. \\ &+ \left.\mathcal{O}_{22}\,\left(\lambda_3+\frac{\Re e\,[\lambda_6]-2\,\Re e\,[\lambda_7]}{\tan\beta}\right)\ +\ \mathcal{O}_{32}\,\left(\frac{2\,\Im m\,[\lambda_5]}{\tan\beta}-\Im m\,[\lambda_6]\right)\right\} \end{aligned} \tag{5.12}$$

At tree-level the Higgs potential couplings are given in Appendix B.4, although we refer to [52] for the two-loop corrected expressions. In any case, they can be safely considered $\lambda_i \lesssim 1$ and, in particular, we find a numerical maximum of $\lambda_i^{max} \sim 0.25$ for some of them. However, the dominant terms will be those not suppressed by $\tan\beta$ factors, that is λ_3 and λ_6. For them, we find $\lambda_3 \simeq -0.074$ at tree-level (the one-loop values would be even smaller due to the opposite sign of the fermionic corrections) and $\lambda_6 \simeq -0.14\,e^{i\alpha}$, where $\alpha = \arg(a_t)$. Thus, our conclusion is that the charged-Higgs contribution will be always negligible in comparison with the SM contributions given in Eqs.(5.7) and (5.9), even for $m_{H^\pm} \simeq 150$ GeV. Consequently, a signal slightly above the SM expectations (as presented by ATLAS in [108]) can not have its origin in the charged-Higgs boson.

Considering squarks, those with larger Yukawa couplings will be important in the two photon decay width. They are the sbottom and the stop squarks. Their contribution in the scalar amplitude is specified in Eq.(2.51) and, writing explicitly their couplings to the Higgs, they are given by

$$S^{\gamma}_{H_2,\tilde{b}} = -\sum_{i=1,2} \frac{v}{6\,m^2_{\tilde{b}_i}} \left(\tilde{\Gamma}^{\alpha}_{\tilde{b}\tilde{b}}\right)_{\beta\gamma} \mathcal{O}_{\alpha 2}\, \mathcal{R}^{\tilde{b}*}_{\beta i}\, \mathcal{R}^{\tilde{b}}_{\gamma i}\; F_0\left(\tau_{\tilde{b}_i}\right) \tag{5.13}$$

$$S^{\gamma}_{H_2,\tilde{t}} = -\sum_{i=1,2} \frac{2\,v}{3\,m^2_{\tilde{t}_i}} \left(\tilde{\Gamma}^{\alpha}_{tt}\right)_{\beta\gamma} \mathcal{O}_{\alpha 2}\, \mathcal{R}^{\tilde{t}*}_{\beta i}\, \mathcal{R}^{\tilde{t}}_{\gamma i}\; F_0\left(\tau_{\tilde{t}_i}\right) \tag{5.14}$$

The sbottom contribution can be expanded following the approximation of Appendix D for Hermitian matrices, since in this case the off-diagonal terms of the mass matrix are much smaller than the diagonal ones. Then, it is obtained

$$\begin{aligned} S^{\gamma}_{H_2,\tilde{b}} &\simeq 0.12\,\tan^2\beta\,\frac{m_b^2}{m^2_{\tilde{b}_1}}\left(\mathcal{O}_{12}\,\frac{\Re e\,[A_b^*\,\mu\,]}{m^2_{\tilde{b}_2}} - \mathcal{O}_{22}\,\frac{\mu^2}{m^2_{\tilde{b}_2}} + \mathcal{O}_{32}\,\frac{\Im m\,[A_b^*\,\mu\,]}{m^2_{\tilde{b}_2}\,\tan\beta}\right) \\ &\simeq 1.2\times 10^{-5}\,\tan^2\beta\left(\frac{300\ \text{GeV}}{m_{\tilde{b}_1}}\right)^2 \times \\ &\quad \left(\mathcal{O}_{12}\,\frac{\Re e\,[A_b^*\,\mu]}{m^2_{\tilde{b}_2}} - \mathcal{O}_{22}\,\frac{\mu^2}{m^2_{\tilde{b}_2}} + \mathcal{O}_{32}\,\frac{\Im m\,[A_b^*\,\mu\,]}{m^2_{\tilde{b}_2}\,\tan\beta}\right) \end{aligned} \tag{5.15}$$

where $F_0\left(\tau_{2\tilde{b}_i}\right) \simeq 0.34$ have been considered for both, right and left-handed sbottoms. In the case that $A_b/m_{\tilde{b}_2}, \mu/m_{\tilde{b}_2} \simeq O(1)$, the sbottom contribution can be safely neglected since, even for $\tan\beta \sim 50$, it would be two orders of magnitude below the top-quark contribution in Eq.(5.8).

Incidentally, the stau contribution can be obtained from above with the replacement $b \leftrightarrow \tau$. However, it is expected to be negligible for stau masses above 100 GeV.

On the other hand, we have the top squark case where the large off-diagonal terms in the mass matrix do not allow us to use the Appendix D approximation in such a straightforward way. Nevertheless, we can still expand the chargino mass-matrix, while keeping the stop mixing matrices, $\mathcal{R}$, and write Eq.(5.14) as

$$
\begin{aligned}
S^{\gamma}_{H_2,\tilde{t}} \;\simeq\; & -0.45\;\mathcal{O}_{12}\;\;\Re e\left[\frac{\mu\, m_t}{m^2_{\tilde{t}_1}}\mathcal{R}^*_{11}\,\mathcal{R}_{21}\right] \\
& +0.45\;\mathcal{O}_{32}\;\;\Im m\left[\frac{\mu\, m_t}{m^2_{\tilde{t}_1}}\,\mathcal{R}^*_{11}\,\mathcal{R}_{21}\right] \\
& +0.45\;\mathcal{O}_{22}\;\;\left\{\Re e\left[\frac{A^*_t\, m_t}{m^2_{\tilde{t}_1}}\,\mathcal{R}^*_{11}\,\mathcal{R}_{21}\right]\left(1-\frac{m^2_{\tilde{t}_1}}{m^2_{\tilde{t}_2}}\right)\right. \\
& \left.+\frac{m^2_t}{m^2_{\tilde{t}_1}}\left(|\mathcal{R}_{11}|^2+|\mathcal{R}_{12}|^2\right)+\frac{m^2_t}{m^2_{\tilde{t}_2}}\left(|\mathcal{R}_{22}|^2+|\mathcal{R}_{21}|^2\right)\right\}
\end{aligned}
\tag{5.16}
$$

where again $F_0\left(\tau_{2\tilde{t}_1}\right) \simeq F_0\left(\tau_{2\tilde{t}_2}\right) \simeq 0.34$. The limits for the stop mass have been provided by ATLAS and CMS and presented here in Figure 4.6. They set $m_{\tilde{t}} \geq$ 650 GeV in the general case where the lightest neutralino mass is $m_{\tilde{\chi}^0_1} \lesssim 250$ GeV [127–130]. Therefore, if we typically consider upper values for $A_t, \mu \lesssim 3m_{\widetilde{Q}_3} \sim 3000$ GeV and for $m_{\widetilde{Q}_3} \lesssim 1000$ GeV (higher values may have naturalness and charge and color breaking problems), the size of the coefficients in the equation above will be $m^2_t/m^2_{\tilde{t}_2}$, $m^2_t/m^2_{\tilde{t}_1} < 0.1$ qnd $A_t m_t/m^2_{\tilde{t}_1}$, $\mu m_t/m^2_{\tilde{t}_1} \lesssim 1.2$. Recalling that $\mathcal{R}^*_{11}\mathcal{R}_{21} \leq \frac{1}{2}$, $|\mathcal{R}_{ij}|^2 \leq 1$ and $(1 - m^2_{\tilde{t}_1}/m^2_{\tilde{t}_2}) < 1$, it is obtained that

$$
S^{\gamma}_{H_2,\tilde{t}} \;\lesssim\; 0.26\;\left[\,-\mathcal{O}_{12}+1.7\,\mathcal{O}_{22}+\mathcal{O}_{32}\,\right], \tag{5.17}
$$

This prediction is typically an order of magnitude smaller than the t- and b-quarks and W-boson contributions computed in Eqs.(5.7) and (5.8). However, it is interesting to keep it because it can be important in the case of light stop masses nearly degenerated with the LSP. As presented in Figure 4.6, a small region in the 160-200 GeV range is not excluded by data in this special case of quasi-degeneration.
Finally, the chargino contribution is given by

$$
S^{\gamma}_{H_2,\tilde{\chi}^+} \;=\; \sqrt{2}\,g\sum_{i=1,2}\Re e\left[V^*_{i1}\,U^*_{i2}\,G_2^{\phi_1}+V^*_{i2}\,U^*_{i1}\,G_2^{\phi_2}\right]\frac{v}{m_{\chi^+_i}}\,F^S_f\left(\tau_{2\tilde{\chi}_i}\right) \tag{5.18}
$$

with $G_2^{\phi_1} = (\mathcal{O}_{12} - i\sin\beta\mathcal{O}_{32})$ and $G_2^{\phi_2} = (\mathcal{O}_{22} - i\cos\beta\mathcal{O}_{32})$. Using again the expansion of the chargino mass matrices in Appendix D, we have

$$S^{\gamma}_{H_2,\tilde{\chi}^+} \;\simeq\; 2.8\left[\cos\beta\,\frac{m_W^2}{\mu^2}\,O_{12} \;+\; \frac{m_W^2}{M_2^2}\,O_{22}\right] \tag{5.19}$$

under the following assumptions

$$\begin{aligned} & m_{\chi_1^+} \simeq M_2 \ll m_{\chi_2^+} \simeq \mu \qquad \text{and} \qquad \sin\beta \simeq 1 \\ & F_f^S\left(\tau_{H_2\chi_2^+}\right) \simeq F_f^S\left(\tau_{H_2\chi_1^+}\right) \simeq 0.7 \\ & \frac{F_f^S\left(\tau_{H_2\chi_1^+}\right) - F_f^S\left(\tau_{H_2\chi_2^+}\right)}{m^2_{\chi_1^+} - m^2_{\chi_2^+}} \simeq 0 \end{aligned} \tag{5.20}$$

Taking $M_W^2/M_2^2 \lesssim 0.05$ for $m_{\chi_1^+} < 350$ GeV from the LHC limits [132, 133], we have

$$S^{\gamma}_{H_2,\tilde{\chi}^+} \lesssim 0.15\left[\;\mathcal{O}_{22} + \frac{M_2^2}{\mu^2}\;\mathcal{O}_{12}\right] \tag{5.21}$$

Thus, the chargino contribution is also negligible compared to the W-boson, top and bottom contributions. In summary, we can safely neglect the charged Higgs, chargino and sbottom contributions to the two-photon decay width and approximate the scalar amplitude by

$$\begin{aligned} S^{\gamma}_{H_2} \;\simeq\;& \mathcal{O}_{12}\left\{-\frac{8.3}{\tan\beta} + (-0.025 + i\,0.034)\;\Re e\left[\frac{\tan\beta}{1+\kappa_d\tan\beta}\right]\right. \\ & \left. -\;0.45\,\Re e\left[\frac{\mu\, m_t\,\mathcal{R}^*_{11}\,\mathcal{R}_{21}}{m^2_{\tilde{t}_2}}\right]\left(\frac{m^2_{\tilde{t}_2}}{m^2_{\tilde{t}_1}} - 1\right)\right\} \\ +\;& \mathcal{O}_{22}\left\{-6.5 + 0.45\Re e\left[\frac{A_t^*\, m_t\,\mathcal{R}^*_{11}\,\mathcal{R}_{21}}{m^2_{\tilde{t}_2}}\right]\left(\frac{m^2_{\tilde{t}_2}}{m^2_{\tilde{t}_1}} - 1\right)\right. \\ & \left. +\;0.45\left(\frac{m_t^2\,|\mathcal{R}_{11}|^2}{m^2_{\tilde{t}_1}} + \frac{m_t^2\,|\mathcal{R}_{22}|^2}{m^2_{\tilde{t}_2}}\right)\right\} \\ +\;& \mathcal{O}_{23}\left\{(-0.025 + i\,0.034)\;\Im m\left[\frac{\kappa_d\tan^2\beta}{1+\kappa_d\tan\beta}\right] + 0.45\,\Im m\left[\frac{\mu\, m_t\,\mathcal{R}^*_{11}\,\mathcal{R}_{21}}{m^2_{\tilde{t}_2}}\right]\right\} \end{aligned} \tag{5.22}$$

From here, it looks very difficult to obtain a scalar amplitude for the two photons process significantly larger than the SM value, taking into account that the stop contribution can be at most order one. The same discussion applies to the pseudoscalar amplitude, although in this case it only receives the fermionic terms, which are effectively equivalent to the top and bottom contributions, and thus it is much smaller than the scalar term. The possibility of large SUSY contributions as advocated in [170,171] seems closed, at least in the MSSM with $m_{H_2} \simeq 125$ GeV.
Next, we compute the Higgs production cross section that has been already presented in Section 2.4. At the partonic level, the cross section is determined by the gluon-fusion and $b\bar{b}$-fusion processes. The $b\bar{b}$-fusion, considering only the main threshold-corrections to the bottom couplings, is given by

$$\begin{aligned}\hat{\sigma}_{b\bar{b}\to H_2} &\simeq \frac{\pi}{6}\,\frac{g^2\,m_b^2}{4\,M_W^2}\,\left[\frac{\tan^2\beta}{(1+\kappa_d\tan\beta)^2}\,\left(|\mathcal{O}_{12}|^2+|\mathcal{O}_{32}|^2\right)\right] \\ &\simeq 6.8\times 10^{-5}\,\frac{\tan^2\beta}{(1+\kappa_d\tan\beta)^2}\,\left(|\mathcal{O}_{12}|^2+|\mathcal{O}_{32}|^2\right) \end{aligned} \tag{5.23}$$

The dimensionless partonic cross section must be multiplied now by the $b\bar{b}$ luminosity in the proton in order to get the hadronic cross section. Taking $m_{H_2} = 125$ GeV and for $\sqrt{s} = 8$ TeV, $\tau d\mathcal{L}^{b\bar{b}}/d\tau \simeq 2300$ pb considering the MSTW2008 parton distributions at LO. Thus, the $b\bar{b}$ hadronic contribution to the pp cross section is given by

$$\sigma(pp\to H_2)_{bb} \simeq 0.16\,\frac{\tan^2\beta}{(1+\kappa_d\tan\beta)^2}\,\left(|\mathcal{O}_{12}|^2+|\mathcal{O}_{32}|^2\right)\ \text{pb} \tag{5.24}$$

The gluon fusion cross section is a loop process and can be calculated as

$$\hat{\sigma}^{LO}_{gg\to H_2} = \frac{\alpha_s^2\,(M_{H_2})}{256\,\pi}\,\frac{m_{H_2}^2}{v^2}\left(|S_2^g|^2+|P_2^g|^2\right) \simeq 4\times 10^{-6}\left(|S_2^g|^2+|P_2^g|^2\right) \tag{5.25}$$

where the scalar coupling S_2^g gets contributions from both quarks and squarks, while the pseudoscalar one P_2^g receives contributions only from quarks. Squark contributions can be easily obtained from Eqs.(5.15 and (5.16) taking into account that, for $J^\gamma_{\tilde{f}} = 1$, $S^g_{2,\tilde{b}} = 3/2\ S^\gamma_{2,\tilde{b}}$ and $S^g_{2,\tilde{t}} = 3/8\ S^\gamma_{2,\tilde{t}}$. Therefore, analogously to the photonic amplitudes, the sbottom and stop contributions to gluon fusion production can be neglected. Hence, the scalar and pseudoscalar contributions to the gluon-fusion production may be approximated as

$$S^g_{2,b+t} \simeq 1.35\ \mathcal{O}_{22} + (-0.04 + i\,0.05)\ \times \left(\mathcal{O}_{12}\ \Re e\left[\frac{\tan\beta}{1+\kappa_d\tan\beta}\right] + \mathcal{O}_{32}\ \Im m\left[\frac{\kappa_d\tan^2\beta}{1+\kappa_d\tan\beta}\right]\right) \quad (5.26)$$

$$P^g_{2,b+t} \simeq (-0.04 + i\,0.05)\left(\mathcal{O}_{22}\ \Im m\left[\frac{\kappa_d\tan\beta}{1+\kappa_d\tan\beta}\right] + \mathcal{O}_{12}\ \Im m\left[\frac{\kappa_d\tan^2\beta}{1+\kappa_d\tan\beta}\right]\right) + \mathcal{O}_{32}\left((-0.04 + i\,0.05)\,\Re e\left[\frac{\tan\beta}{1+\kappa_d\tan\beta}\right] - \frac{1}{\tan\beta}\right) \quad (5.27)$$

The gluon-fusion hadronic contribution to the pp cross section is obtained by multiplying the gluon luminosity, $\tau_{H_2}\ d\mathcal{L}^{gg}_{LO}/d\tau_{H_2} \simeq 3\times 10^6$ pb and the K-factor ($K = 2$ corresponding to the low $\tan\beta$ region and close to one for large $\tan\beta$ [81])

$$\begin{aligned}\sigma(pp\to H_2)_{gg} &\simeq 25\ \left(|S^g_2|^2 + |P^g_2|^2\right)\\ &\simeq 45\ \mathcal{O}^2_{22} - \mathcal{O}_{12}\,\mathcal{O}_{22}\ \frac{1.4\,\tan\beta}{1+\kappa_d\tan\beta}\\ &+ \mathcal{O}^2_{12}\ \frac{0.1\tan^2\beta}{(1+\kappa_d\tan\beta)^2}\\ &+ \mathcal{O}^2_{32}\left(\frac{2}{(1+\kappa_d\tan\beta)} + \frac{0.1\tan^2\beta}{(1+\kappa_d\tan\beta)^2} + \frac{25}{\tan^2\beta}\right)\end{aligned} \quad (5.28)$$

where κ_d has been taken real for simplicity. Here, we see that the gluon fusion production is dominated by the top quark contribution if $\mathcal{O}_{12}, \mathcal{O}_{22} = O(1)$ up to $\tan\beta \gtrsim 20$. In fact, the SM prediction would correspond to simply take $\kappa = 0$, $\tan\beta = 1$, $\mathcal{O}_{12} = \mathcal{O}_{22} = 1$ and $\mathcal{O}_{32} = 0$ and therefore, it can be seen that the gluon fusion cross section is typically smaller than the SM cross section for medium-low $\tan\beta$. Besides, comparing Eqs.(5.24) and (5.28), one may observe that gluon-fusion dominates over $b\bar{b}$-fusion except for large $\tan\beta$ or small $\mathcal{O}_{22}$.

Finally, we check the total width Γ_{H_2}. The main decay channels for $m_{H_2} \simeq 125$ GeV are $H_2 \to b\bar{b}$, $H_2 \to WW^*$ and $H_2 \to \tau\tau$ ($H_2 \to gg$ can of the same order as $H_2 \to \tau\tau$ in some cases, but, being comparatively small with respect to $b\bar{b}$ and WW, it is not necessary to consider it in the following discussion). In particular, the decay width is

usually dominated by the $b\bar{b}$-channel which in the MSSM may be enhanced by $\tan\beta$ factors with respect to the SM one (as well as the $\tau\tau$ channel). The main contribution to the decay width to $b\bar{b}$ is captured by the tree-level Higgs-bottom couplings in the limit $\kappa_d \to 0$ (although in our numerical analysis threshold corrections have been always taken into account)

$$\begin{aligned}\Gamma_{H_2} \;\simeq\; & \frac{g^2\, m_{H_2}}{32\,\pi\, m_W^2}\left(\left(|\mathcal{O}_{12}|^2 + |\mathcal{O}_{32}|^2 \right) \left(3\, m_b^2 + m_\tau^2\right) \tan^2\beta \right. \\ & \left. + \left(\mathcal{O}_{22} + \frac{\mathcal{O}_{12}}{\tan\beta} \right)^2 m_{H_2}^2\; I_{PS} \right) \end{aligned} \tag{5.29}$$

where $I_{PS} \simeq 6.7 \times 10^{-4}$ for $m_H \simeq 125$ GeV refers to the phase-space integral that can be found in [54]. It must be compared with the SM decay width, which would correspond to the usual MSSM decoupling limit if we replace $H_1 \leftrightarrow H_2$, $\tan\beta \to 1$, $\mathcal{O}_{12}, \mathcal{O}_{22} \to 1$ and $\mathcal{O}_{32} = 0$. This implies that for sizable $\mathcal{O}_{12}, \mathcal{O}_{32} > \tan^{-1}\beta$, the total width will be much larger than the SM width. Then, taking into account that it has been shown that $\Gamma_{H_2\to\gamma\gamma} \simeq \Gamma^{SM}_{h\to\gamma\gamma}$, our conclusion is that, for $\mathcal{O}_{22} \leq 1$, the diphoton branching ratio will be smaller than the SM one. The only way to achieve a large branching ratio is taking $\mathcal{O}_{12}, \mathcal{O}_{32} \lesssim 1/\tan\beta$ so that the total width is reduced and $\Gamma_{H_2\to\gamma\gamma}$ remains similar to the SM prediction. On the other hand, it has been commented that the H_2 production cross section is typically smaller than the SM unless $\mathcal{O}_{22} \simeq 1$, and the the gluon-fusion process is the dominant production mechanism, or $\tan\beta \gtrsim 20$ with sizeable $\mathcal{O}_{12}, \mathcal{O}_{32}$, and the production is dominated by $b\bar{b}$ fusion. Even for this last case, the $\tan\beta$ enhancement of the production cross section is exactly compensated by the suppression on the $H_2 \to \gamma\gamma$ branching ratio. For the gluon fusion, there is no $\tan\beta$ enhancement and thus in both cases the $\gamma\gamma$-production cross section is smaller than the SM one.

Therefore, we arrive to the conclusion that the only way to increase the $\gamma\gamma$-production cross section to reproduce the LHC results in our scenario is to **decrease the total width by suppressing the b-quark and the τ-lepton decay widths**. This implies having a second Higgs H_2 predominantly H_u^0 so that the couplings associated to these fermions are suppressed and, consequently, the two photons branching ratio will be increased. This condition means, in terms of the mixing matrix elements

$$\mathcal{O}_{22} \sim 1, \qquad \mathcal{O}_{12} \simeq \mathcal{O}_{32} \leq \frac{1}{\tan\beta} \ll \mathcal{O}_{22} \tag{5.30}$$

Tau-tau cross section

The above analysis has led us to the conclusion that to reproduce the $\gamma\gamma$-production cross section we need the second lightest Higgs to be almost purely up-type. As a consequence, H_2 nearly decouples from tau fermions and, consequently, other neutral Higgses must unavoidably inherit large down-type components increasing their decays into τ-fermions. Therefore, we need to compute the decay $H_i \to \tau\tau$.
Once more, in the narrow width approximation, the $\tau\tau$-production cross section through a Higgs is given in terms of $\sigma(pp \to H_i)$, $\Gamma(H_i \to \gamma\gamma)$ and Γ_{H_i}. The decay width $H_i \to \tau\tau$ has been presented in Eq.(2.45) whereas the τ scalar and pseudoscalar couplings were given in Eq.(2.34). It has been pointed out before that threshold corrections for leptons are usually negligible, although $\tan\beta$-enhanced terms are involved. Let us see this with more detail. Noting that the corrected scalar and pseudoscalar couplings for the τ-lepton follow the same pattern than the down-type quark, they would be

$$g^S_{\tau i} \simeq \frac{\tan\beta}{1+\epsilon_\tau \tan\beta}\,\mathcal{O}_{1i} + \frac{\epsilon_\tau \tan\beta}{1+\epsilon_\tau \tan\beta}\,\mathcal{O}_{2i} \tag{5.31}$$

$$g^P_{\tau i} \simeq -\frac{\tan\beta - \epsilon_\tau}{1+\epsilon_\tau \tan\beta}\,\mathcal{O}_{3i} \tag{5.32}$$

with $\epsilon_\tau \simeq g_2^2/16\pi^2\,(\mu M_1/m^2_{\tilde{\tau}_2}) \simeq 2\times 10^{-3}$ (taking it real). Thus, taking into account that $g_1^2 \ll g_2^2$, $\epsilon_\tau \simeq \epsilon_b/20$ and, as predicted, this is just a sub-leading correction which can be safely neglected. Therefore, in the case of H_1 and H_3, we get

$$\Gamma_{H_i\to\tau\tau} \;\simeq\; \frac{m_{H_i}}{8\pi}\left(\frac{g\,m_\tau}{2\,m_W}\right)^2 \Big[\tan^2\beta\left(|\mathcal{O}_{1i}|^2 + |\mathcal{O}_{3i}|^2\right)\Big] \;\simeq\; \frac{g^2\,m_{H_i} m_\tau^2}{32\,\pi\,m_W^2}\;\tan^2\beta \tag{5.33}$$

where $\mathcal{O}_{22} \simeq 1$ and $\mathcal{O}_{12}, \mathcal{O}_{32} \ll 1$ has been introduced. Now, the production cross section for H_1 and H_3 can be obtained from Eqs.(5.24) and (5.28) replacing $\mathcal{O}_{j2} \to \mathcal{O}_{ji}$. Recalling that $|\mathcal{O}_{1i}|^2 + |\mathcal{O}_{3i}|^2 \simeq 1$ and $\mathcal{O}_{2i} \simeq 1/\tan\beta$, we have

$$\begin{aligned}
\sigma(pp \to H_i)_{gg} &\simeq 25 \left(|S_2^g|^2 + [|P_2^g|^2 \right) \\
&\simeq 45\ \mathcal{O}_{2i}^2 \ -\ \mathcal{O}_{1i}\mathcal{O}_{2i}\ \frac{1.4\tan\beta}{1+\kappa_d\tan\beta}\ +\ \mathcal{O}_{1i}^2\ \frac{0.1\tan^2\beta}{(1+\kappa_d\tan\beta)^2} \\
&+ \mathcal{O}_{3i}^2\ \left(\frac{2}{(1+\kappa_d\tan\beta)} + \frac{0.1\tan^2\beta}{(1+\kappa_d\tan\beta)^2} + \frac{25}{\tan^2\beta} \right) \\
&\simeq \frac{0.1\tan^2\beta}{(1+\kappa_d\tan\beta)^2}\ +\ \frac{45+25\ \mathcal{O}_{3i}^2}{\tan^2\beta} + \frac{2\ \mathcal{O}_{3i}^2 - 1.4\ \mathcal{O}_{1i}}{1+\kappa_d\tan\beta}
\end{aligned} \tag{5.34}$$

$$\sigma(pp \to H_i)_{bb}\ \simeq 0.16\ \left(|\mathcal{O}_{1i}|^2 + |\mathcal{O}_{3i}|^2 \right)\ \frac{\tan^2\beta}{(1+\kappa_d\tan\beta)^2}\ \simeq\ 0.16\ \frac{\tan^2\beta}{(1+\kappa_d\tan\beta)^2} \tag{5.35}$$

Therefore, for $\tan\beta \gtrsim 5$ and $\mathcal{O}_{2i} \lesssim 1/\tan\beta$, the bottom contribution to gluon fusion is larger than the top contribution and only slightly smaller than the $b\bar{b}$-fusion. Then, total production cross section for H_1 and H_3 can be approximated as

$$\sigma(pp \to H_i) \simeq\ \left[0.16\ \left(\frac{\tau_{H_i}\, d\mathcal{L}^{bb}/d\tau_{H_i}}{2300\ \text{pb}} \right) + 0.10\ \left(\frac{\tau_{H_i}\, d\mathcal{L}^{gg}_{LO}/d\tau_{H_i}}{3\times 10^6\ \text{pb}} \right) \right]\ \frac{\tan^2\beta}{(1+\kappa_d\tan\beta)^2}\ \text{pb}$$

Finally, we need the total width for these two bosons, H_1 and H_3. For them, the dominant contributions still come from $b\bar{b}$, $\tau\tau$ and WW^* providing that their masses are below 160 GeV. For masses above 160 GeV, the width is usually dominated by real W-production and ZZ/ZZ^*. Therefore, below 160 GeV, the total width can be directly read from Eq.(5.29) replacing $H_2 \to H_i$ and $\mathcal{O}_{j2} \to \mathcal{O}_{ji}$. For Higgs masses above 160 GeV, but always below 200 GeV as argued before for our scenario, the total width will be larger than Eq.(5.29) and thus, taking only $b\bar{b}$, $\tau\tau$ and WW^*, we obtain a lower limit to Γ_i. For H_1 and H_3, it has been shown that $\mathcal{O}_{2i} \ll 1$ and $|\mathcal{O}_{1i}|^2 + |\mathcal{O}_{3i}|^2 \simeq 1$ in order to be in agreement with the experimental data available for the $\gamma\gamma$ signal. Then the total width is

$$\Gamma_i\ \gtrsim\ \frac{g^2 m_{H_i}}{32\,\pi m_W^2} \left(\frac{3\,m_b^2}{1+\kappa_d\tan\beta} + m_\tau^2 \right) \tan^2\beta \tag{5.36}$$

and the branching ratio is

$$\mathrm{BR}\left(H_i \to \tau\tau\right) \lesssim \frac{m_\tau^2 \left(1+\kappa_d \tan\beta\right)^2}{3\, m_b^2 + m_\tau^2 \left(1+\kappa_d \tan\beta\right)^2} \tag{5.37}$$

So, for the $\tau\tau$-production cross section trough H_1 and H_3 we have

$$\begin{aligned}
\sigma(pp \xrightarrow{H_i} \tau\tau) &\lesssim \frac{\tan^2\beta}{\left(1+\kappa_d \tan\beta\right)^2} \frac{m_\tau^2 \left(1+\kappa_d \tan\beta\right)^2}{3, m_b^2 + m_\tau^2 \left(1+\kappa_d \tan\beta\right)^2} \times \\
&\quad \left[0.16 \left(\frac{\tau_{H_i}\, d\mathcal{L}^{bb}/d\tau_{H_i}}{2300 \text{ pb}}\right) + 0.10 \left(\frac{\tau_{H_i}\, d\mathcal{L}^{gg}_{LO}/d\tau_{H_i}}{3\times 10^6 \text{ pb}}\right)\right] \text{ pb} \\
&\simeq \frac{\tan^2\beta}{8.4 + 2\kappa_d \tan\beta + \kappa_d^2 \tan^2\beta} \times \\
&\quad \left[0.16 \left(\frac{\tau_{H_i}\, d\mathcal{L}^{bb}/d\tau_{H_i}}{2300 \text{ pb}}\right) + 0.10 \left(\frac{\tau_{H_i}\, d\mathcal{L}^{gg}_{LO}/d\tau_{H_i}}{3\times 10^6 \text{ pb}}\right)\right] \text{ pb}
\end{aligned} \tag{5.38}$$

Combining the bounds for the $\gamma\gamma$ and $\tau\tau$ production cross sections, we show in Figure 5.1 the $\tau\tau$ production cross sections at LHC for $m_{H_1} \simeq 110$ GeV and $m_{H_3} \simeq 160$ GeV with (squares in blue) or without (circles in red) fulfilling the requirement of $0.5 \leq \mu_{\gamma\gamma}^{\mathrm{LHC}} \leq 1.9$. The green line is the CMS limit on the $\tau\tau$ production cross section for Higgs masses below 150 GeV and green points represent the points where, in addition to the $\tau\tau$ cross-section limit, the observation of the Higgs, H_2 in our scenario, at $m_{H_2} \simeq 125$ GeV is also fulfilled. Even though this plot is for a fixed value $m_{H_1} = 110$ GeV, the situation does not change at all for any value in the range $m_{H_1} = (100, 120)$ GeV.
Therefore, we see that there are no points consistent with the LHC constraints on $\sigma(pp \to H_1 \to \tau\tau)$ for $\tan\beta \geq 7.8$ and 100 GeV $< m_{H_1} <$ 125 GeV. In the following, we will see that even the surviving points for low $\tan\beta$ are on conflict with another bounds.

5.1.3 Low $\tan\beta$ regime

We have just seen that LHC constraints on $\sigma(pp \to H_1 \to \tau\tau)$ rule out the possibility of $m_{H_2} \simeq 125$ GeV for $\tan\beta \geq 7.8$. Still, the situation for $\tan\beta \lesssim 8$ is quite different because, for low $\tan\beta$ values, a $\gamma\gamma$-signal strength compatible with the LHC result $\mu_{\gamma\gamma} \gtrsim 0.5$ is easier to obtain.
A similar discussion to the one had for the medium-large $\tan\beta$ regime can be applied

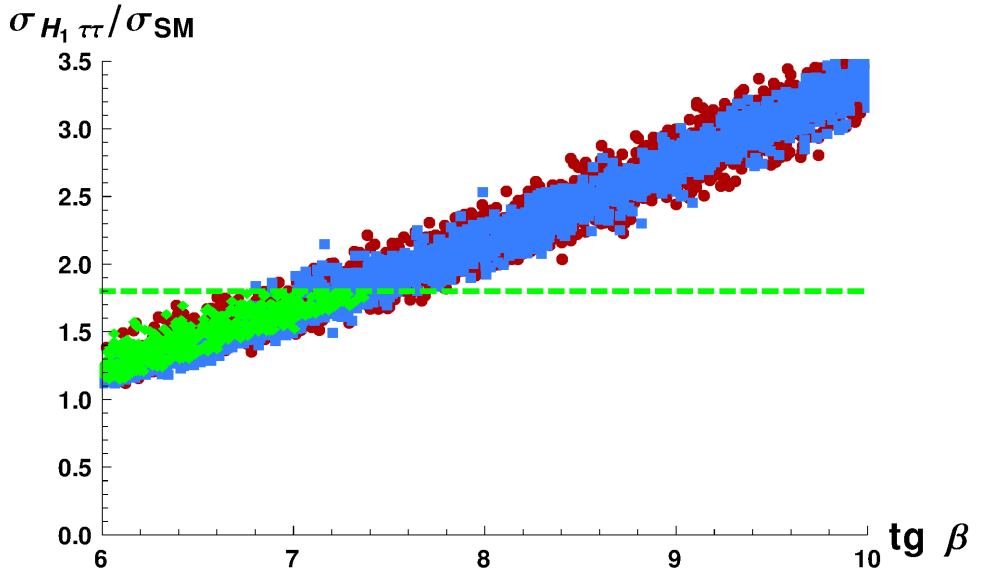

Figure 5.1: $\tau\tau$ production cross-section at $m_{H_1} = 110$ GeV as a function of $\tan\beta$, with the CMS limit on $\tau\tau$ production in green.

here for the $\gamma\gamma$-decay width. For low $\tan\beta$ values, it remains again of the same order as the SM one $\Gamma_{H_2\to\gamma\gamma} \simeq \Gamma^{SM}_{h\to\gamma\gamma}$. The same can be said for the production cross section, which will be approximately order SM since the $b\bar{b}$-fusion process and the b-quark contribution to the gluon-fusion process are proportional to $\tan\beta$, which is now smaller, leaving the top contribution very close to the SM for $\mathcal{O}_{22} \simeq O(1)$. In fact, the total decay width is still larger than the SM value if O_{12} and O_{13} are sizeable because $b\bar{b}$ and $\tau\tau$ widths are still enhanced by $\tan^2\beta$. Therefore, the same requirements on Higgs mixings in Eq.(5.30) hold true now, although they are less suppressed due to the smaller $\tan\beta$ values. On the other hand, the $\tau\tau$ production cross section through the three neutral Higgses remains an important constraint, but it is much easier to satisfy for low $\tan\beta$ values, as we can see in Figure 5.1.
However, as previously noted, our scenario requires a rather light charged Higgs to be realised, $m_{H^\pm} \lesssim 220$ GeV. In this context, and for $\tan\beta \lesssim 8$, indirect constraints from BR($B \to X_s\gamma$) will have a role to play.

Constraints from BR($B \to X_s\gamma$)

The decay $B \to X_s\gamma$ is an important constraint on the presence of light charged Higgs particles such as in our scenario. In the computation of this branching ratio one may

observe that the charged Higgs contribution interferes always constructively with the SM W-boson. See their correspondent Wilson coefficients in Eqs.(3.9) and (3.15). However, in the MSSM, this contribution can be compensated by an opposite sign term originated in the stop-chargino loop when $\mathrm{Re}\,(\mu A_t)$ is negative.
The dominant contribution in $\mathcal{C}_7^{H^\pm}$ is the one associated with $f_7^{(2)}(m_t^2/m_{H^\pm}^2)$ and, thus, the typical size of the Wilson coefficient may be estimated as

$$\mathcal{C}_7^{H^\pm} \;\simeq\; \frac{f_7^{(2)}(y_t)}{1 \;+\; \mathbf{\Delta}_d^{\Phi_d^0} \;+\; \tan\beta\, \mathbf{\Delta}_d^{\Phi_u^0}} \tag{5.39}$$

For $m_{H^\pm} \in [150, 200]$ GeV, we get $f_7^{(2)}(y_t) \in [-0.22, -0.18]$ while the coefficient $\mathcal{C}_7^{H^\pm}$ grows with lower $\tan\beta$. The stop-chargino contribution given in Eq.(3.14) was

$$\begin{aligned} \mathcal{C}_{7,8}^{\chi^+} \;\simeq\; & -\frac{m_W^2}{M_2^2}\,\frac{M_2}{\mu}\,\tan\beta\,\left[\, f_{7,8}^{(3)}\left(x_{\tilde{q}\tilde{\chi}_1^+}\right) - f_{7,8}^{(3)}\left(x_{\tilde{t}_1\tilde{\chi}_1^+}\right)\right] \\ & -\frac{A_t}{\mu}\,\frac{m_W^2}{M_2^2}\,\tan\beta\,\frac{m_t^2}{m_{\tilde{t}_1}^2 - m_{\tilde{t}_2}^2}\,\left[\, f_{7,8}^{(3)}\left(x_{\tilde{t}_1\tilde{\chi}_1^+}\right) - f_{7,8}^{(3)}\left(x_{\tilde{t}_2\tilde{\chi}_1^+}\right)\right] \end{aligned} \tag{5.40}$$

Taking the present limits on stop and chargino masses, $m_{\tilde{t}_1} \geq 650$ GeV and $m_{\chi^\pm} \geq 350$ GeV, $f_7^{(3)}\,(x \simeq 1) \simeq 0.44$ and

$$\mathcal{C}_7^{\chi^+} \;\simeq 0.02\; M_2/\mu\;\tan\beta \ll \mathcal{C}_{7,8}^{H^\pm} \tag{5.41}$$

Thus, it looks very difficult to compensate the charged Higgs contribution for low $\tan\beta$ and, indeed, this is confirmed in the numerical analysis.
Figure 5.2 collects this numerical result. There, the computed $\mathrm{BR}(B \to X_s\gamma)$ is shown where the blue squares fulfill the requirements of $0.5 \leq \mu_{\gamma\gamma}^{\mathrm{LHC}} \leq 1.9$, $\sigma_{H_1\tau\tau}/\sigma_{\mathrm{SM}} \leq 1.8$ and $\sigma_{H_2\tau\tau}/\sigma_{\mathrm{SM}} \leq 1.8$ while the red dots violate some of them. The experimentally allowed region for $B \to X_s\gamma$ at 1-σ and 2-σ is coloured in green and yellow, respectively[2]. Notice that the reduction of the BR with $\tan\beta$ is mainly due to the decrease of the charged-Higgs contribution observed in Eq.(5.39) and not to the negative interference with the chargino diagram. Therefore, the only option left is having a light stop which had escaped detection at LHC because of a small mass difference with the lightest neutralino as LSP. To explore numerically this possibility, we select the

[2]Even allowing a three-σ range, we find no allowed points when $m_{\tilde{t}_1} \geq 650$ GeV and $m_{\chi^\pm} \geq 350$ GeV

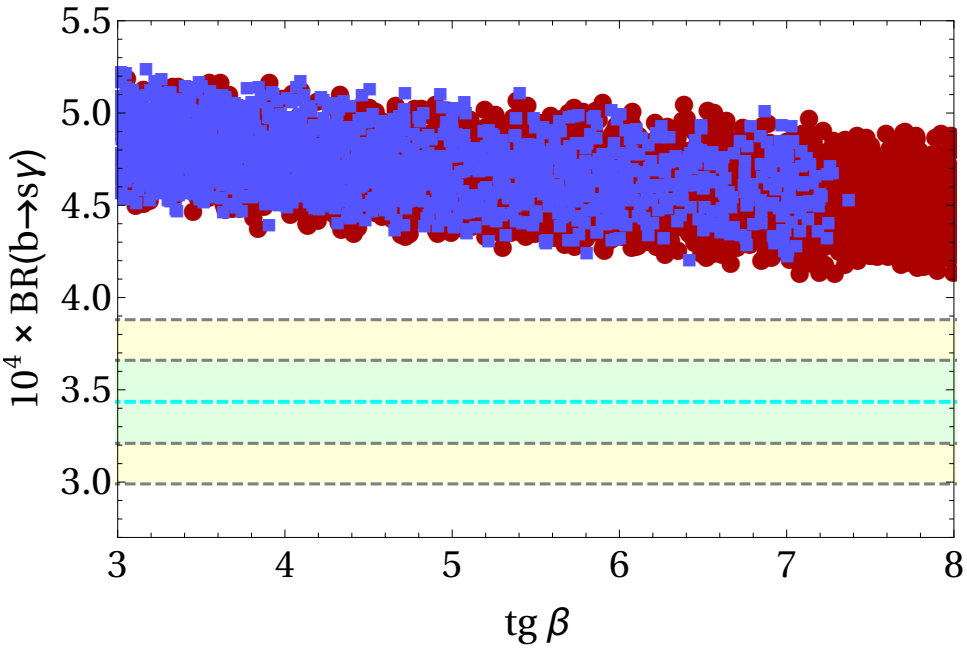

Figure 5.2: Branching ratio of the $B \to X_s\gamma$ decay as a function of $\tan\beta$. Blue squares fulfill the $\mu_{\gamma\gamma}^{\rm LHC}$ and $\sigma_{H_i\tau\tau}/\sigma_{\rm SM}$ constraints, as explained in the text. Green and yellow regions are the one and two-σ experimentally allowed regions.

lightest stop mass to be $m_{\chi_1^0} \leq m_{\tilde{t}_1} \leq m_t + m_{\chi_1^0}$. The result is shown in Figure 5.3, where we plot again BR($B \to X_s\gamma$) as a function of $\tan\beta$.

In this case the range of BR($B \to X_s\gamma$) for a given $\tan\beta$ has decreased, as expected, because of a possible destructive interference with the stop-chargino diagram. Nevertheless, we can see that there are no points allowed by collider constraints that reach the 2-σ permitted region for the flavour bound[3].

As a by-product, we can emphasize here the difficulty to possibly accommodate two sizeable Higgs-like peaks for the $\gamma\gamma$ production cross section within an MSSM context, as was announced by the CMS collaboration in [161]. The CMS analysis has an integrated luminosity of 5.1 (19.6) fb^{-1} at a center of mass energy of 7 (8) TeV and clearly reveals an excess near $m_H = 136.5$ GeV, aside from the 125-126 GeV Higgs boson that has already been discovered, with a local significance of 2.73 σ combining the data from Higgs coming from vector-boson fusion and vector-boson associated

[3]Allowing points within the three-σ region, BR($B \to X_s\gamma$) $\leq 4.1 \times 10^{-4}$, several points would survive. However, for all of them, a very large $\sigma_{H_3\tau\tau}$ is obtained so that recent ATLAS analysis on heavy MSSM Higgses rule out them [116]

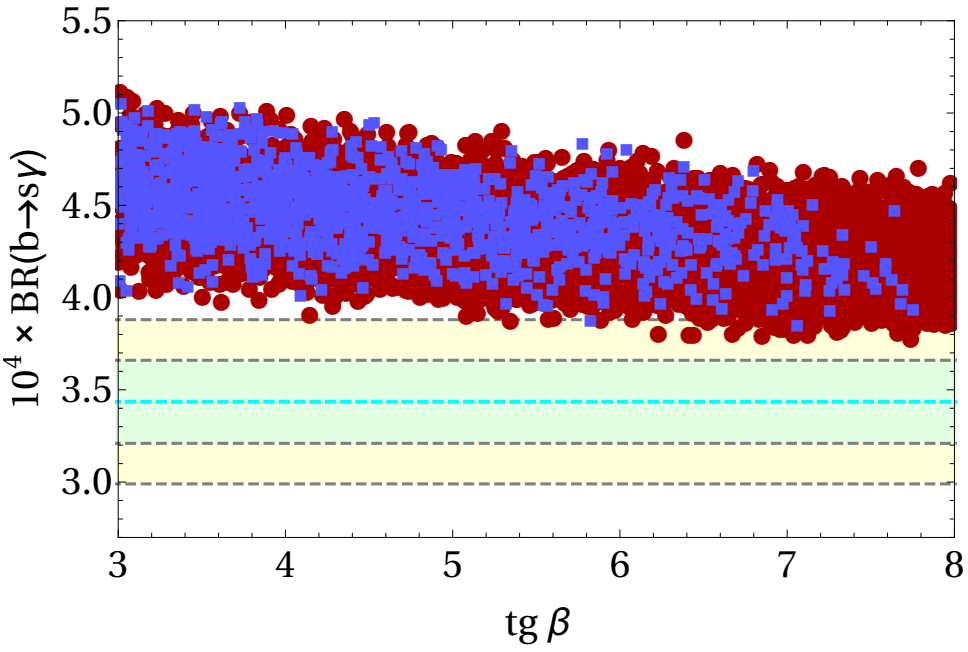

Figure 5.3: Branching ratio of the $B \to X_s\gamma$ decay as a function of $\tan\beta$, for $m_{\tilde{t}_1} \leq 650$ and $m_{\chi_1^0} \leq m_{\tilde{t}_1} \leq m_t + m_{\chi_1^0}$. The color coding is the same as in Fig. 5.2

production (each of which shows the excess individually). Even in the case where 125 GeV resonance was identified as the lightest Higgs in the spectrum, H_2 and H_3 would inherit all the pseudoscalar and down-type Higgs components in such a way that the branching ratio of these Higgses to $\gamma\gamma$ would be brutally inhibited. Additionally, such a light Higgs with a mass of 136.5 GeV, would produce a signal in the $\tau\tau$-channel which is already excluded by [112, 116, 172]. The only way to evade that would be remain in the low $\tan\beta$ regime, but also in this case constraints from the flavour transition $b \to s\gamma$ would be in conflict. Therefore, we conclude that there is no way to accommodate two Higgs peaks in the $\gamma\gamma$ spectrum with a signal strength of the order of the SM model one.

Finally, for the sake of completeness, we would like to comment the possibility of having a heaviest Higgs corresponding to the 125 GeV resonance. In this case, H_3 would be predominantly up-type whereas H_1 and H_2, with masses below 125 GeV or practically degenerated with H_3, would inherit the down-type and pseudoscalar components. In this case, again, the current $\tau\tau$ limits for such a light masses would constrain enormously the parameter space for medium and large $\tan\beta$ values. On

the other hand, the low $\tan\beta$ region would be excluded due to $b \to s\gamma$ for the same reason than in the previous case: a charged Higgs boson unavoidable light, due to its relation with the pseudoscalar part, producing a large contribution in the $B \to X_s\gamma$ process.

5.1.4 Conclusions

In this analysis, we have seen that the discovered 125 GeV Higgs is forced to be the lightest Higgs in a MSSM framework due to the present constraints in the $H_i \to \tau\tau$ channel together with those associated with the flavour process $B \to X_s\gamma$. In particular, we have seen that for the proposed spectrum, where H_2 was the 126 GeV discovered boson, $m_{H_3} < 180$ GeV and $m_{H^+} < 200$ GeV. Then, to reproduce the observed signal strength in the $\gamma\gamma$-channel for the 126 GeV peak in the medium-large $\tan\beta$ regime, we had to eliminate all the pseudoscalar and down-type content from the second Higgs state. Specifically, we obtained $\mathcal{O}_{22} \approx 1$ and $\mathcal{O}_{12}, \mathcal{O}_{32} \ll 1$ so that the lightest and heaviest Higgses will necessarily couple, with $\tan\beta$-enhancement, to down-type fermions. At the same time, the $H_i \longrightarrow \tau\tau$ decay width for $i = 1, 3$ is $\propto (O_{1i}^2 + O_{3i}^2) \approx (1 - O_{2i}^2) \approx O_{22}^2 \simeq 1$ meaning that any MSSM setting would predict a $H_i \longrightarrow \tau\tau$ peak at a level that is already excluded [112,116,172]. The only possible escape to this situation would be to stay in the (very) low $\tan\beta$ region but then, given the low mass of the charged Higgs, the constraints from $\mathrm{BR}(B \to X_s\gamma)$ would eliminate completely this possibility. Therefore, our conclusion is that in case of a MSSM Higgs resonance at 125 GeV, it should correspond to H_1 being this boson almost completely up-type in order to reproduce a SM signal in the $\gamma\gamma$ channel.

5.2 Constraining the presence of extra Higgs states

Here a similar analysis is performed but identifying the lightest Higgs of the complex MSSM as the detected scalar at 125 GeV [167]. Again, the main channels used to constrain the parameter space are $pp \to H_1 \to \gamma\gamma$, $pp \to H_i \to \tau^+\tau^-$ and indirect probes such as $b \to s\gamma$ and $B_s \to \mu^+\mu^-$. The analysis is divided in two different regions: i) *the light MSSM Higgs sector* defined by $m_{H^+} < m_t$, which can be considered the non-decoupling regime, and ii) *the heavy Higgs sector* given by $m_{H^+} > m_t$, which would correspond to the usual decoupling limit where $M_A^2 > v^2$.
In our numerical analysis, we basically follow the method described in [173, 174] (see Appendix A in [173]) to determine the regions of the model excluded at 95% CL. This roughly amounts to identify the most sensitive observable for a given point in the parameter space using the expected experimental limits and then using the observed limit at 95% C.L. to exclude the corresponding region in case of disagreement. The situation becomes more subtle in the presence of a positive signal where the above procedure may lead to fake surviving regions which contain the 126 Higgs state whenever its decay channels are the most sensitive observables. In this case, the described procedure is applied to each individual Higgs state independently. The excluded regions are then ruled out at a level slightly stronger than 95% [174][4]. This procedure will be strictly followed to deliver the final 95% C.L. allowed regions. Besides, in the intermediate steps we discuss the impact of the individual constraints separately to allow the reader to understand how the excluded regions are obtained.

5.2.1 Two photon cross section

As before, our analysis starts considering the Higgs decay amplitude into photons for the discovered boson which now corresponds to H_1 with $m_{H_1} = 125$ GeV. The $\gamma\gamma$-production through a Higgs, in the narrow width approximation, depends on the Higgs production cross section and on the $H \to \gamma\gamma$ branching ratio, which in turn depends both on the decay width into two photons and on the total decay width. The decay width into two photons is given in Eq.(2.50) and receive contributions from gauge bosons, fermions, sfermions and the charged Higgs. The full expressions for the scalar S_i^γ and pseudoscalar P_a^γ amplitudes are given in Eqs.(2.51) and (2.52). In the following, as in the previous analysis, we consider approximate formulae to

[4]With regard to indirect bounds we take the SM prediction as the expected value to asses the sensitivity of the given mode. For example, in the case of $\mathrm{BR}(B \to X_s\gamma)$ we use $\mathrm{BR}(B \to X_s\gamma) = (3.15 \pm 0.23) \times 10^{-4}$ for photon energies of $E_\gamma > 1.6$ GeV [175].

understand the numerical results obtained from the full expressions. The dominant contributions to the diphoton scalar amplitude are those due to the W-boson and the top quark, with the b-quark contributing only for very large $\tan\beta$. Thus

$$S^{\gamma}_{H^0_1,W} \simeq -8.3 \left(\mathcal{O}_{21} + \frac{\mathcal{O}_{11}}{\tan\beta}\right) \tag{5.42}$$

$$S^{\gamma}_{H^0_1,b+t} \simeq 1.8\,\mathcal{O}_{21} + (-0.025 + i\,0.034) \times \left(\mathcal{O}_{11}\,\Re e\left[\frac{\tan\beta}{1+\kappa_d\tan\beta}\right] + \mathcal{O}_{31}\,\Im m\left[\frac{\kappa_d\tan^2\beta}{1+\kappa_d\tan\beta}\right]\right) \tag{5.43}$$

The MSSM contributions to the amplitude are restricted to the charged Higgs, charginos and third generation sfermions. However, as previously seen in Eqs.(5.21) and (5.12), the charged Higgs and chargino contributions can always be neglected in comparison to the SM one in Eq.(5.43). In the case of the stop, imposing the LHC bound on the stop mass for a large mass difference to the LSP $m_{\tilde{t}} \gtrsim 650\,\text{GeV}$, its contribution is also much smaller than the dominant SM contributions. However, this contribution can be somewhat larger for lighter stops with a small mass difference with the LSP, although there exists an absolute lower bound of $m_{\tilde{t}} \gtrsim 250\,\text{GeV}$ from single jet searches [176] and another excluded region for stop masses $m_{\tilde{t}_1} < 200$ GeV at 95% C.L. if $m_{\tilde{t}_1} - m_{\chi^0_1} < 85$ GeV [177]. Therefore, we keep stop contributions in our approximated expression since for low masses it can be important.

Finally, we have the sbottom and stau contributions. They are usually negligible at medium-low $\tan\beta$, say $\tan\beta \lesssim 8$, compared to those coming from the SM particles due to the smallness of the Yukawa couplings in this regime. However, they can be sizeable for very large $\tan\beta$ or very light sparticles. In fact, in [170, 171, 178] the stau contribution was proposed as a way to increase the diphoton decay rate without affecting the Higgs production cross section[5] and therefore not modifying the successful predictions in other channels. However, this would require large $\tan\beta$ values and, as we will show below, this is incompatible with the bounds from $H_2, H_3 \to \tau\tau$ for $M_{H_{2,3}} \leq 1$ TeV. Nevertheless, for such heavy Higgs masses, a light stau could contribute considerably to the scalar amplitude for large $\tan\beta$. The stau contribution to $S^{\gamma}_{H^0_1}$, neglecting as always the relatively small non-holomorphic corrections to the τ-lepton Yukawa (see Eqs.(5.31) and (5.32) and the discussion below), can be approximated by

[5] Notice that a large sbotton contribution would enhance both the Higgs production and the diphoton decay width, and thus modify also the successful ZZ and WW predictions.

$$
\begin{aligned}
S^{\gamma}_{H^0_1,\tilde{\tau}} &\simeq 0.36\,\tan^2\beta\,\frac{m_\tau^2}{m^2_{\tilde{\tau}_1}}\left(\mathcal{O}_{11}\,\frac{\Re e\,[A_\tau^*\,\mu]}{m^2_{\tilde{\tau}_2}}-\mathcal{O}_{21}\,\frac{\mu^2}{m^2_{\tilde{\tau}_2}}+\mathcal{O}_{31}\,\frac{\Im m\,[A_\tau^*\,\mu]}{m^2_{\tilde{\tau}_2}\tan\beta}\right)\\
&\simeq 3\times10^{-5}\,\tan^2\beta\left(\frac{200\,\text{GeV}}{m_{\tilde{\tau}_1}}\right)^2\,\times\\
&\quad\left(\mathcal{O}_{11}\,\frac{\Re e\,[A_\tau^*\,\mu]}{m^2_{\tilde{\tau}_2}}-\mathcal{O}_{21}\,\frac{\mu^2}{m^2_{\tilde{\tau}_2}}+\mathcal{O}_{31}\,\frac{\Im m\,[A_\tau^*\,\mu]}{m^2_{\tilde{\tau}_2}\tan\beta}\right)
\end{aligned}
\tag{5.44}
$$

where we used that the loop function is approximately 0.35 (and tends to 1/3) for $m_{\tilde{\tau}} \gtrsim 200\,\text{GeV}$. From here it is clear that an $O(1)$ stau contribution, which would be required to enhance the diphoton rate, is only possible for $\tan\beta \geq 80$ and $m_{\tilde{\tau}} \leq 100$ GeV if $A_\tau^*/m_{\tilde{\tau}_2}, \mu/m_{\tilde{\tau}_2} \simeq O(1)$. Even the extreme case where $A_\tau^*/m_{\tilde{\tau}_2},\ \mu/m_{\tilde{\tau}_2} \lesssim 3$ would require $\tan\beta \geq 50$ and $m_{\tilde{\tau}} \leq 150$ GeV to get an $O(1)$ contribution. This can be seen in Figure 5.4 where the stau and the W-boson contributions are compared up to $\tan\beta$ values of 50. In any case, these large $\tan\beta$ values can increase the diphoton width at most a 10-30% but such large $\tan\beta \gtrsim 50$ values are strongly constrained by the $H_i \to \tau\tau$ channel. Besides, these large $\tan\beta$ values would not be enough to increase the $H_1 \to \gamma\gamma$ branching ratio, as they would simultaneously increase the H_1 total width. Therefore, in this work, we do not consider such large $\tan\beta$ values and we neglect stau and sbottom contributions. Thus, keeping just the dominant W-boson, quark and stop contributions, the scalar amplitude can be approximate by

$$
\begin{aligned}
S^{\gamma}_{H^0_1} &\simeq \mathcal{O}_{11}\left\{-\frac{8.3}{\tan\beta}+(-0.025+i\,0.034)\,\Re e\left[\frac{\tan\beta}{1+\kappa_d\tan\beta}\right]\right.\\
&\qquad\left.-0.45\,\Re e\left[\frac{\mu\,m_t\,\mathcal{R}^*_{11}\,\mathcal{R}_{21}}{m^2_{\tilde{t}_2}}\right]\left(\frac{m^2_{\tilde{t}_2}}{m^2_{\tilde{t}_1}}-1\right)\right\}\\
&+\ \mathcal{O}_{21}\left\{-6.5+0.45\,\Re e\left[\frac{A_t^*\,m_t\,\mathcal{R}^*_{11}\,\mathcal{R}_{21}}{m^2_{\tilde{t}_2}}\right]\left(\frac{m^2_{\tilde{t}_2}}{m^2_{\tilde{t}_1}}-1\right)\right.
\end{aligned}
\tag{5.45}
$$

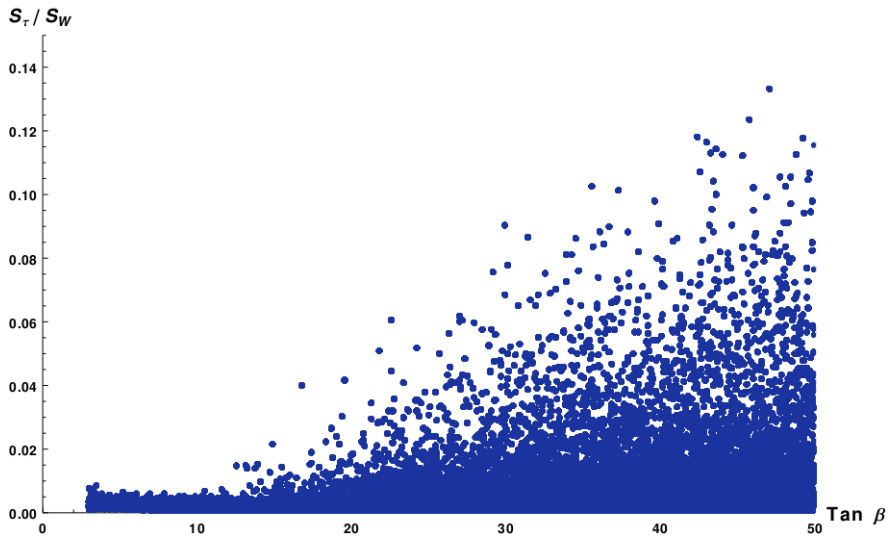

Figure 5.4: $\tilde{\tau}$ scalar contribution to the two photons decay width compared to the and W-boson contribution as a function of $\tan\beta$

$$
\begin{aligned}
&\quad + 0.45 \left(\frac{m_t^2 \, |\mathcal{R}_{11}|^2}{m_{\tilde{t}_1}^2} + \frac{m_t^2 \, |\mathcal{R}_{12}|^2}{m_{\tilde{t}_2}^2} \right) \Bigg\} \\
+ \quad \mathcal{O}_{31} &\left\{ (-0.025 + i\, 0.034) \; \Im m \left[\frac{\kappa_d \tan^2\beta}{1 + \kappa_d \tan\beta} \right] \right. \\
&\left. \quad + 0.45 \, \Im m \left[\frac{\mu \, m_t \, \mathcal{R}_{11}^* \, \mathcal{R}_{21}}{m_{\tilde{t}_2}^2} \right] \left(\frac{m_{\tilde{t}_2}^2}{m_{\tilde{t}_1}^2} - 1 \right) \right\}
\end{aligned}
\tag{5.46}
$$

This amplitude has to be compared with the SM value calculated in Eq.(5.4) for a SM-like Higgs: $S^{\gamma}_{\mathrm{H_{SM}}} \simeq -6.55$. The pseudoscalar amplitude absent in the SM is typically much smaller since it receives contributions only from fermions, mainly top and bottom quarks, and they are usually of the same order as fermionic contributions to the scalar amplitude. Then, the total Higgs decay width receives contributions mainly from $H_1 \to WW^*$ and the down-type fermion, $H_1 \to b\bar{b}$ and $H_1 \to \tau\tau$ which, compared to the SM predictions, are enhanced by $\tan^2\beta$. The $H_1 \to gg$ decay can be of the same order of $H_1 \to \tau\tau$ for low $\tan\beta$, but it can be safely neglected as it is always subdominant with respect to $b\bar{b}$ and WW^* and does not influence significantly the total width. Hence

$$\Gamma_{H_1} \simeq \frac{g^2 m_{H_1}}{32\,\pi\, m_W^2}\left[\left(\mathcal{O}_{11}^2+\mathcal{O}_{31}^2\right)\left(3m_b^2+m_\tau^2\right)\tan^2\beta+\left(\mathcal{O}_{21}+\frac{\mathcal{O}_{11}}{\tan\beta}\right)^2 I_{PS}\, m_{H_1}^2\right] \quad (5.47)$$

with $I_{PS} \simeq 6.7\times 10^{-4}$ the phase-space integral. Then, the BR($H_1 \to \gamma\gamma$) can be written as

$$\begin{aligned}\mathrm{BR}(H_1\to\gamma\gamma) &\simeq \frac{\alpha^2}{32\,\pi^2\,(3x_b+x_\tau)}\,\frac{|S_1^\gamma|^2+|P_1^\gamma|^2}{\left(\mathcal{O}_{11}^2+\mathcal{O}_{31}^2\right)\tan^2\beta+\left(\mathcal{O}_{21}+\frac{\mathcal{O}_{11}}{\tan\beta}\right)^2\frac{I_{PS}}{(3x_b+x_\tau)}} \\ &\simeq 4.65\times 10^{-3}\,\frac{|S_1^\gamma/6.5|^2+|P_1^\gamma/6.5|^2}{\left(\mathcal{O}_{11}^2+\mathcal{O}_{31}^2\right)\tan^2\beta+0.38\left(\mathcal{O}_{21}+\frac{\mathcal{O}_{11}}{\tan\beta}\right)^2} \quad (5.48)\end{aligned}$$

From here, we can see that it is very difficult to obtain a diphoton branching ratio larger than the SM value given by $\sim 3\times 10^{-3}$. In fact, as the branching ratio is inversely proportional to $\tan^2\beta$, for $\mathcal{O}_{11}\sim O(1)$ and recalling the diphoton scalar amplitude in Eq.(5.46), we conclude that there is no way to compensate this enhancement in the total width through a $\tan\beta$-enhanced contribution or through the stop contribution to S_1^γ in the numerator consistently with present bounds on sfermion masses [166].

Finally, the last ingredient we need is the Higgs production cross section. This cross section is dominated by gluon-fusion and $b\bar{b}$-fusion. As before, the result can be expressed in terms of our free parameters: the Higgs mixings and $\tan\beta$. The hadronic tree-level $b\bar{b}$-fusion cross section, being calculated with the $b\bar{b}$ luminosity of the 5-flavour MSTW2008 parton distributions functions [77], gives

$$\sigma\left(pp\to H_1\right)_{b\bar{b}} \simeq 0.16\,\frac{\tan^2\beta}{\left(1+\kappa_d\tan\beta\right)^2}\left(\left|\mathcal{O}_{11}\right|^2+\left|\mathcal{O}_{31}\right|^2\right) \quad \text{pb} \quad (5.49)$$

Whereas the gluon fusion contribution, with the gluon luminosity from MSTW2008, will be

$$\begin{aligned}\sigma\left(pp\to H_1\right)_{gg} &\simeq \mathcal{O}_{11}^2\,\frac{0.1\tan^2\beta}{\left(1+\kappa_d\tan\beta\right)^2}-\mathcal{O}_{11}\,\mathcal{O}_{21}\,\frac{1.4\tan\beta}{1+\kappa_d\tan\beta}+13\,\mathcal{O}_{21}^2 \\ &+ \mathcal{O}_{31}^2\left(\frac{2}{\left(1+\kappa_d\tan\beta\right)}+\frac{0.1\tan^2\beta}{\left(1+\kappa_d\tan\beta\right)^2}+\frac{27}{\tan^2\beta}\right) \quad (5.50)\end{aligned}$$

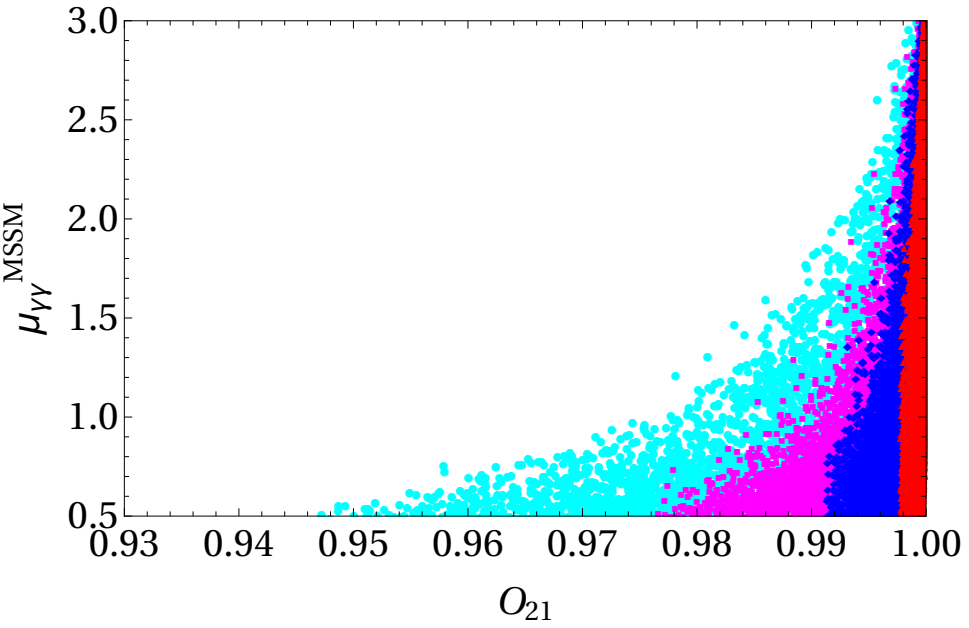

Figure 5.5: Number of events (normalized to SM) in $H_1 \to \gamma\gamma$ respect to the Higgs up mixing component in a generic MSSM as described in the text.

It can be observed that the top quark contribution in the gluon-fusion process (proportional to O_{21}) is the dominant amplitude, except for large $\tan\beta$ and $\mathcal{O}_{11}$, $\mathcal{O}_{31} \sim O(1)$ where bottom fusion and the bottom contributions to gluon-fusion may become important and overcome it. Nevertheless, experimental results in other Higgs search channels require a Higgs production cross section close to the SM values.
In conclusion, from Eq.(5.47) we have seen that the total decay width is larger than the SM one if $\mathcal{O}_{11}$, $\mathcal{O}_{31} > \tan^{-1}\beta$. Thus, what one would need is having $\mathcal{O}_{11}$, $\mathcal{O}_{31} \lesssim \tan^{-1}\beta$ in order to reduce the total width and increase $\mathrm{BR}(H_1 \to \gamma\gamma)$. On the other hand, from Eqs.(5.49) and (5.50), one may notice that for small $\mathcal{O}_{11}$, $\mathcal{O}_{31}$ the Higgs production is dominated by gluon fusion. In this way, it will be possible to reproduce the observed signal strength in the different Higgs decay channels and the following Higgs mixing components will appear naturally

$$\mathcal{O}_{21} \simeq 1 \quad \text{and} \quad \mathcal{O}_{11}, \mathcal{O}_{31} < \frac{1}{\tan\beta} \tag{5.51}$$

Figure 5.5 shows the allowed $\mathcal{O}_{21}$ values as a function of the diphoton signal strength. The different colours correspond to different $\tan\beta$ values: blue for $\tan\beta < 5$, magenta

for $5 < \tan\beta < 9$, navy for $9 < \tan\beta < 30$ and red for $30 < \tan\beta$. From here, it is clear that O_{21} is required to be close to one being always larger than $1 - (1/\tan\beta)^2$. Notice that this result simply generalizes the usual real MSSM result in the decoupling limit, which implies that $\mathcal{O}_{21} = \cos\alpha \simeq \sin\beta$.
Now that our model satisfies the requirement of the observed signal strength in the diphoton channel, we should analyse the limits on $H_a \to \tau\tau$, $t \to H^+ b$ and BR($B \to X_s\gamma$).

5.2.2 $H_a \to \tau\tau$ production cross section

As we have already discussed, the $pp \to H \to \tau\tau$ production cross section is one of the main channels used to search for extra Higgs boson states at LHC [116, 118]. We have already seen that the lightest Higgs with $M_{H_1} = 126$ GeV must be mainly up-type to reproduce the observed signal strength. Thus, the $\tan\beta$ enhancement of the decay width of H_1 into tau fermions is controlled by this small mixing. However, for the heavier neutral Higgses, we have the opposite effect being the down-type or pseudoscalar content of the heavier Higgses high and, consequently, the $H_{2,3} \to \tau^+\tau^-$ decay width proportional to $\tan^2\beta$ at tree level and neglecting the relatively small non-holomorphic corrections to the tau Yukawa

$$\Gamma_{i,\,\tau\tau} \;\simeq\; \frac{g^2\, m_{H_i}\, m_\tau^2}{32\pi\, m_W^2}\, \tan^2\beta\,. \tag{5.52}$$

Here, it is important to remember from Eq.(5.37) that the relevant quantity in the $pp \to \tau\tau$ production cross section is the H_i branching ratio to $\tau\tau$, which has an identical leading-order $\tan\beta$-enhancement than that of the dominant decay width which is into $b\bar{b}$. Therefore, the total production cross sections be almost independent of $\tan\beta$, with only a small dependence due to the different higher-order corrections to the bottom and tau Yukawa couplings. On the other hand, for medium-large $\tan\beta$, the production of these Higgs bosons will also be mainly due to $b\bar{b}$-fusion and the $b\bar{b}$ contribution to the gluon-fusion loop[6] and can be approximated by

$$\sigma(pp \to H_i) \;\simeq\; \left[0.07\, \left(\frac{\tau_{H_i}\; d\mathcal{L}^{bb}/d\tau_{H_i}}{1000\ \text{pb}}\right) + 0.04\, \left(\frac{\tau_{H_i}\; d\mathcal{L}^{gg}_{LO}/d\tau_{H_i}}{1.1\times 10^6\ \text{pb}}\right)\right] \frac{\tan^2\beta}{(1+\kappa_d\tan\beta)^2}\ \ \text{pb}$$

[6] In our numerical analysis, all contributions to gluon fusion are always included and we include also the gluon-b production channel, although it is always subdominant if b-jets are not tagged

with $\mathcal{O}_{22}^2 + \mathcal{O}_{32}^2 \simeq \mathcal{O}_{23}^2 + \mathcal{O}_{33}^2 \simeq 1$ and the gluon and $b\bar{b}$ luminosities at $M_{H_i} = 150$ GeV (corresponding to the light Higgs region) and $\sqrt{s} = 7$ TeV. Therefore, we can see that the $\tau\tau$ production cross section of H_2 and H_3 will be

$$\sigma(pp \xrightarrow{H_i} \tau\tau) \lesssim \frac{\tan^2\beta}{8.4 + 10.4\,\kappa_d \tan\beta + \kappa_d^2 \tan^2\beta} \times \left[0.07\left(\frac{\tau_{H_i}\, d\mathcal{L}^{bb}/d\tau_{H_i}}{1000 \text{ pb}}\right) + 0.04\left(\frac{\tau_{H_i}\, d\mathcal{L}^{gg}_{LO}/d\tau_{H_i}}{1.1\times 10^6 \text{ pb}}\right)\right] \text{ pb} \tag{5.53}$$

The latest CMS constraints discriminate between Higgs bosons produced through gluon fusion and through $b\bar{b}$ fusion in association with two b-jets. A p_T-cut of 30 GeV is imposed in at least one b-jet in order to identify the $b\bar{b}$ origin. As commented in Section 2.4, the theoretical production cross section with b-jets can be obtained using the MSTW2008 pdf in the 5-flavour scheme [77] with the $bg \to h_i b$ cross section and a 30 GeV p_T cut on the final b-jet. Then, the differential partonic cross section will be [82]

$$\frac{d\hat{\sigma}_{gb\to H_i b}}{dt} = -\frac{1}{s^2}\frac{\alpha_S(\mu)}{24}\left(\frac{y_b(\mu)}{\sqrt{2}}\right)^2 \frac{m_{H_i}^4 + u^2}{st}\,, \tag{5.54}$$

and the total pp cross section given by

$$\sigma(pp \to H_i b) = 4\;\hat{\sigma}_{gb\to H_i b}\int_\tau^1 \frac{dx}{x}\, b(x, M^2)\, g(\tau/x, M^2) \tag{5.55}$$

5.2.3 Indirect bounds

After applying the constraints on the Higgs mixings from the $H_1 \to \gamma\gamma$ and the $H_i \to \tau^+\tau^-$ decay, the most important constraints come now from the two indirect flavour bounds $B \to X_s\gamma$ and, in the light charged-Higgs region, $t \to b\,H^+$. The experimental limits on the $B \to X_s\gamma$ decay as well as the 95% C.L. range to be compared to the model predictions have been given in Eq.(4.7). Regarding the top decay to the charged Higgs, we use the ATLAS results released on [179]. Besides, in our calculation we include also other indirect constraints on additional Higgs states, as the $B^+ \to \tau^+\nu$ decay and, specially the rare decay $B_s \to \mu^+\mu^-$ which could play a significant role for large $\tan\beta$.

As it has been already commented, the BR $(B \to X_s\gamma)$ receives contributions mainly

from W-boson, charged Higgs and stop-chargino loops within a MFV scenario. As shown in Eq.(5.39), the branching ratio receives a sizeable contribution coming from the light charged-Higgs for low $\tan\beta$. This large charged-Higgs contribution cannot be compensated by the stop-chargino contribution, given in Eq.(5.41), with opposite sign because of the $\tan\beta$ proportionality of this contribution and the small $\tan\beta$ values in consideration. Even forcing the stop mass into the region below $m_{\tilde{t}_1} = 650\,\text{GeV}$ experimentally allowed for small stop-neutralino mass differences, this contribution would be still too small. Obviously, this is the region where this process becomes determinant to exclude important parts of the Higgs sector's parameter space. Therefore, it is expected that $\text{BR}\,(B \to X_s\gamma)$ plays a fairly limited role in large $\tan\beta$ regime.
Regarding the ATLAS bounds in [179] for the $t \to H^+ b$ decay, we observe that it becomes an important discriminating channel for very light charged Higgs masses (up to $m_H^+ = 160$ GeV). However, even for such low Higgs masses, we will see that $\text{BR}\,(B \to X_s\gamma)$ imposes stronger bounds.

5.2.4 Light MSSM Higgs masses

We define the light Higgs region as $M_{H^+} < m_t$, being the charged Higgs heavier than the neutral scalars of our model. In this regime, Higgs states are strongly constrained by the present experimental results, in particular by the process $pp \to H_i \to \tau^+\tau^-$ [116,118]. Furthermore, as pointed out above, such light charged-Higgs produce rather large contributions to the FC observable $B \to X_s\gamma$ originating incompatible results with the experimental limits.
As seen in Eq.(5.53), the $\tau\tau$ production cross section is proportional to $\tan^2\beta$ so we can expect that the presence of additional Higgs bosons to be strongly constrained by the current searches, which are sensitive to cross sections of the order of the SM cross section for $m_H \lesssim 150$ GeV. In Figure 5.6, the allowed Higgs masses as a function of $\tan\beta$ are presented, where all the points satisfy the ATLAS and CMS searches up to 150 GeV plus their searches up to 1 TeV on the $H_i \to \tau\tau$ channel. The ATLAS bounds due to the $t \to H^+ b$ decay are only fulfilled for the blue points. From this figure one may conclude that $\tau\tau$ bounds eliminate completely the possibility of having extra Higgs states with masses below 145 GeV for $\tan\beta \gtrsim 7$ and below 180 GeV when considering $\tan\beta \gtrsim 10$. Moreover, ATLAS bounds on the top decay eliminate Higgs masses below 140 GeV for any $\tan\beta$ value. However, masses such as $145\,\text{GeV} \leq M_{H_i} \leq 175\,\text{GeV}$ are perfectly in agreement with all these collider limits as long as $\tan\beta \lesssim 10$.
Adding the rare decay $B \to X_s\gamma$ bounds, this narrow region is completely ruled out

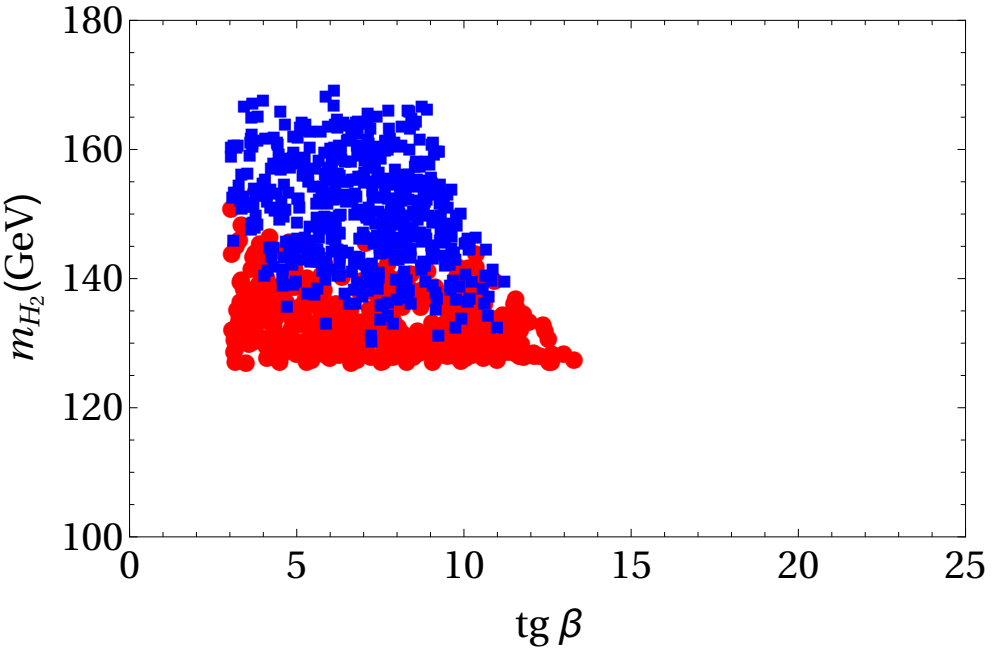

Figure 5.6: Allowed Higgs masses in the plane $(\tan\beta,\ M_{H_2})$ in the light Higgs scenario. Red (dark grey) points satisfy the ATLAS and CMS $pp \to \tau\tau$ bounds in SM Higgs searches and MSSM neutral Higgs searches. Blue (black) points satisfy ATLAS $t \to H^+ b$ constraints in addition. However, if we consider $B \to X_s\gamma$ bounds, this region of the parameter space is ruled out.

closing the door on the possibility of having extra Higgs states below m_t.

5.2.5 Heavy MSSM Higgs masses

Next, we consider second and third neutral-Higgs masses much larger than the lightest Higgs mass, which is fixed at the experimental value of $m_{H_1} = 125\,\text{GeV}$. In this limit, already approaching the decoupling limit in the MSSM, the heaviest mass of the scalar sector is the charged-Higgs mass, which is taken now $m_{H^\pm} > m_t$.

As we did in the previous case, the lightest Higgs is required to reproduce the observed signal strength in the $\gamma\gamma$-channel. This implies that H_1 must have a dominant up-type component and therefore, the heavier Higgs states must be dominantly down-type or pseudoscalar. So, the $H_{2,3} \to \tau\tau$ decay width is expected to be important. However, once the neutral- and charged-Higgs acquire large masses, new decay channels are opened and that will reduce the branching ratio of $H_{2,3} \to \tau\bar{\tau}$. Nevertheless, in the

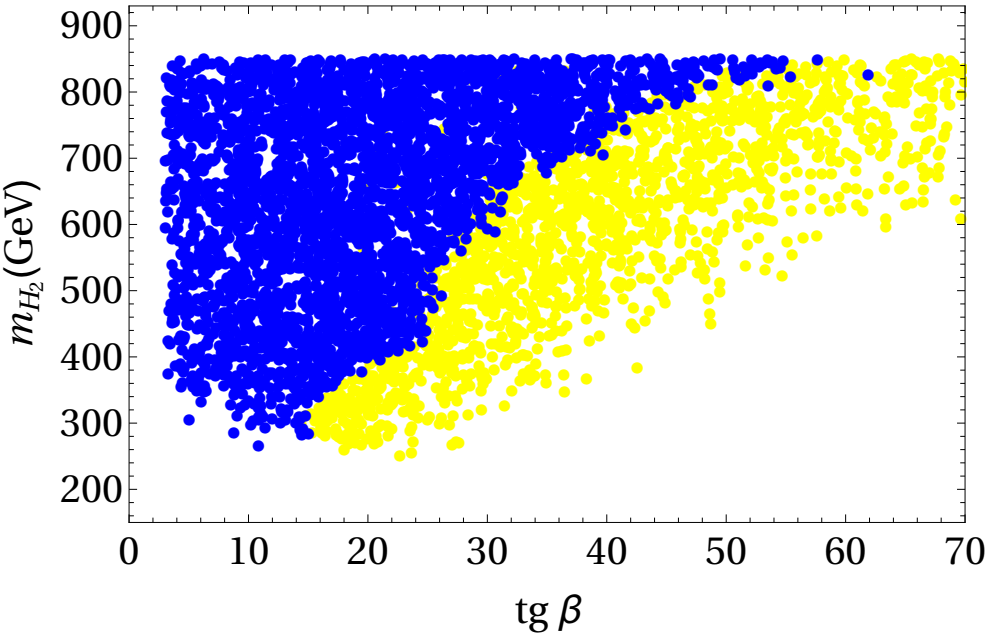

Figure 5.7: Allowed Higgs masses in the plane $(\tan\beta, M_{H_2})$ taking into account the diphoton signal strength, $\tau\tau$ bounds and BR$(B \to X_s\gamma)$. Yellow (light grey) points are those that satisfy ATLAS bounds at 95% C.L., whereas blue (dark grey) points fulfil CMS constraints at 95% C.L. too

limit of large $\tan\beta$ both, the (mostly) down-type Higgs and the pseudoscalar Higgs, decay dominantly to $b\bar{b}$ and $\tau^+\tau^-$ and we have that BR$(H_{2,3} \to \tau^+\tau^-)$ is typically ~ 0.1. In the low $\tan\beta$ region, and once $m_{H_i} \geq 2m_t$, the $t\bar{t}$ channel is sizeable too and can dominate the total Higgs width reducing in this way the $H_{2,3} \to \tau^+\tau^-$ branching ratio. But, as we will see, in this low $\tan\beta$ region the strong constraints from $B \to X_s\gamma$ on charged Higgs masses will reduce significantly the allowed parameter space.

As we have seen before, the $\tau\tau$ constraints are very effective in the large $\tan\beta$ region and, indeed, the result from imposing these bounds can be seen in Figure 5.7. Yellow points in this plot means allowed by ATLAS $\tau\tau$ constraints while blue points satisfy also the stronger CMS bounds. All of them satisfy the BR$(B \to X_s\gamma)$ bounds and other indirect constraints such as $B \to \tau\nu$ and $B_s \to \mu^+\mu^-$.

Therefore, we observe that the combination of direct and indirect constraints is quite effective in the search for additional neutral Higgs bosons at low Higgs masses and/or large $\tan\beta$. In fact, CMS constraints which discriminate different production mechanisms reduce the permitted area previously allowed by ATLAS searches. At present,

the second neutral Higgs in a generic MSSM must be heavier than 250 GeV, and such low values for the Higgs mass are possible only for $\tan\beta \simeq 16$. Lower values of $\tan\beta$ require a heavier neutral Higgs around 300 GeV, due to the large charged Higgs contribution to $\mathrm{BR}(B \to X_s\gamma)$. Larger values of $\tan\beta$ are strongly constrained by CMS searches in the $H_i \to \tau\tau$ channel and would require much heavier Higgs states. For instance, a value of $\tan\beta = 30$ would be only possible for $M_{H_2} \gtrsim 600$ GeV. Comparing with the previous estimate based on the ATLAS results, the improvement becomes apparent.
On the other hand, as we have seen in section 5.2.3, at low $\tan\beta$, the constraints from $B \to X_s\gamma$ eliminate light Higgs masses. Then, the combination of $\tau\tau$ and $B \to X_s\gamma$ constraints implies that $H_{2,3}$ masses below 250 GeV are already ruled out. An improvement of the $\tau\tau$ bound by a factor of 10, which could be possible with the analysis of the stored LHC data, would eliminate the possibility of $M_{H_2} \leq 300$ GeV for all $\tan\beta$ values.

5.2.6 Conclusions

We have used the results from Higgs searches in the $\gamma\gamma$ and $\tau\tau$ decay channels at LHC and indirect bounds as $\mathrm{BR}(B \to X_s\gamma)$ to constrain the parameter space of a generic MSSM Higgs sector. In this case, we identified the scalar resonance at $m_H \simeq 126$ GeV with the lightest Higgs in a MSSM context with explicit CP-violation and we showed that the $\tau\tau$-channel is the best and most accurate weapon in the hunt for new Higgs states beyond the Standard Model. We obtained that present experimental results rule out additional neutral Higgs bosons in a generic MSSM below 300 GeV for any value of $\tan\beta$ and, for values of $\tan\beta$ above 30, only Higgs masses above 600 GeV are possible.

5.3 Flavour-violating Higgs decays

In this analysis [168], our proposal consists of searching for FC Higgs decays that do not exist in the SM and would undoubtedly signal the presence of new physics beyond the SM. Like in the past indirect searches have been extensively used to search for new physics, FC Higgs decays may point out to extensions of the SM containing additional scalars which mix with the lightest Higgs [180–185]. In this work, we will explore a generic supersymmetric scenario as well as the MSSM framework, both in the presence of non-minimal flavour structures. Our analysis will be focused on the process $H \to b\,s$, since one would expect on general grounds that, among FC Higgs decays, those involving third generation particles -whose Yukawa couplings are larger- are the most experimentally accessible. Besides, loop-induced FC proceses in the quark sector are typically larger by a factor α_3^2/α_2^2 for similar flavour changing entries in the lepton sector.
The main goal in this analysis is to find out the largest FC branching ratios for the different Higgs states attainable in a general supersymmetric scenario. First, we will introduce the framework in which the analysis will be carried out, with some compelling variations of it also addressed because of their interest. Then, the theoretical expressions for the FC Higgs decays into down-type quarks will be provided. In Section 5.3.2 the principal features of the numerical analysis are shown, concluding in Section 5.3.5 with the main results.

5.3.1 Higgs mixings

Our analysis is performed within a generic CP-violating MSSM framework and its extensions. In particular, to study Higgs flavour changing decays it is worth to introduce the following parametrization of the Higgs mixings

$$\delta_1 \equiv \left(\frac{\mathcal{O}_{11}}{\cos\beta} - \frac{\mathcal{O}_{21}}{\sin\beta}\right) \qquad\qquad \eta_1 \equiv \frac{\mathcal{O}_{31}}{\sin\beta\cos\beta}\,, \tag{5.56}$$

where δ_1 quantifies the distance of the lightest Higgs mixings from $\cos\beta$ and $\sin\beta$, and η_1 is directly related to the pseudoscalar content of H_1. We will distinguish two different situations in regard to the Higgs mixing: *full MSSM framework* and *generic supersymmetric SM*.
The full MSSM framework is associated with the usual MSSM Higgs potential [34] which breaks the electroweak symmetry radiatively. The minimization of this poten-

tial gives us the Higgs masses and mixings. Using $\mathcal{O}_{11}^2 + \mathcal{O}_{21}^2 + \mathcal{O}_{31}^2 = 1$, one may express the mixing angles, $\mathcal{O}_{\alpha 1}$, in terms of δ_1 and η_1 as follows

$$\begin{aligned}
\mathcal{O}_{11} &= \cos\beta \left[\sqrt{1 - (\delta_1^2 + \eta_1^2)\cos^2\beta \sin^2\beta} + \delta_1 \sin^2\beta \right] \\
\mathcal{O}_{21} &= \sin\beta \left[\sqrt{1 - (\delta_1^2 + \eta_1^2)\cos^2\beta \sin^2\beta} - \delta_1 \cos^2\beta \right] \\
\mathcal{O}_{31} &= \eta_1 \cos\beta \sin\beta
\end{aligned} \tag{5.57}$$

Then, the coupling of the lightest Higgs to a pair of massive vector bosons given in Eq.(2.12) can be rewritten as

$$g_{H_1VV} = \cos\beta\, \mathcal{O}_{11} + \sin\beta\, \mathcal{O}_{21} = \sqrt{1 - (\delta_1^2 + \eta_1^2)\cos^2\beta \sin^2\beta}\,. \tag{5.58}$$

LHC Higgs-data [186] constrain g_{H_1VV} to be close to its SM value, $g_{H_1VV} = 1$. The present best-fit values and uncertainties are $\kappa_V = g_{H_1VV} = 1.15 \pm 0.08$, if we assume there is no change in the Higgs total width, and $\kappa_{VV} = \kappa_V \cdot \kappa_V / \kappa_H = 1.28^{+0.16}_{-0.15}$, if we allow for a change in the total decay width. At present, the errors are still large, but requiring, for example, $g_{H_1VV} \gtrsim 0.9$, one needs to have $(\delta_1^2 + \eta_1^2)\cos^2\beta \sin^2\beta \lesssim 0.2$. As we will be show later, $\mathrm{BR}\left(H_1 \to \bar{b}s + \bar{s}b\right)$ is directly proportional to the quantity $(\delta_1^2 + \eta_1^2)$ which can be larger for larger $\tan\beta$-values while satisfying this constraint. On the other hand, large $\tan\beta$ values are constrained by the $\Delta B = 1$ and $\Delta B = 2$ processes such as $b \to s\gamma$, $B_s^0 \to \mu^+\mu^-$, $B_s^0 - \bar{B}_s^0$ mixing, etc. Taking into account all these constraint, we find that, $\mathrm{BR}\left(H_1 \to \bar{b}s + \bar{s}b\right)$ can be as large as 10^{-6} at most in an MSSM framework.

Given that no signs of supersymmetry have been found so far in collider experiments and taking into account the strong constraints on the parameter space of minimal models, it is interesting to examine more general models like the generic supersymmetric SM where we consider the possibility of having additional Higgses. In this case, the Higgs mass eigenstates H_i would be given by

$$H_i = \sum_{\alpha=1,2} \mathcal{O}_{\alpha i}\, \phi_\alpha + \mathcal{O}_{3i}\, a + \sum_{\beta \geq 4} \mathcal{O}_{\beta i}\, \varphi_\beta \tag{5.59}$$

where φ_β represent the additional CP-even and CP-odd Higgs states which could be charged or neutral under $\mathrm{SU}(2)_L$. We note that only the $\mathrm{SU}(2)_L$-charged CP-even states contribute to the tree-level g_{H_iVV} couplings and, due to the additional states,

we generically would have $\mathcal{O}_{11}^2 + \mathcal{O}_{21}^2 + \mathcal{O}_{31}^2 < 1$. As in the MSSM framework, these couplings are constrained by the experimental results on Higgs decays, but in the presence of other Higgs states close to the 125-GeV state, the mixing pattern could be different from that in the MSSM and δ_1 and/or η_1 can be sizeable. In this case, one may treat δ_1 and η_1 as free parameters effectively. We find that, in this case, BR $\left(H_1 \to \bar{b}s + \bar{s}b\right)$ can be as large as 10^{-4}.

5.3.2 FC phenomenology

Processes mediated by FCNCs involving down-type quarks have been largely studied in the context of 2HDM where significant contributions can be accommodated due to the $\tan\beta$-enhancement of their Yukawa couplings. Here, we aim to study the transitions $H_i \to bs$, keeping always under control processes like $B_s \to \mu^+\mu^-$ and the B-meson mass difference ΔM_{B_s} which usually impose strong experimental constraints.

First, we recall Eqs.(2.27) and (2.29) associated with the down-type quarks FC couplings. As can be check in Eq.(2.23), $\mathbf{R}_d$ contains the complete set of loop corrections to the d-quark couplings

$$\mathbf{R}_d \;=\; \mathbf{1} \;+\; \mathbf{\Delta}_d^{\Phi_d^0} \;+\; \tan\beta\, \mathbf{\Delta}_d^{\Phi_u^0} \tag{5.60}$$

where some of the diagrams associated with these terms are represented in Figures 2.2 and 2.3. For large $\tan\beta$ values, the Φ_d^0 corrections can be neglected in comparison with the $\tan\beta$-enhanced $\mathbf{\Delta}_d^{\Phi_u^0}$ term. Then

$$\mathbf{R}_d \;\simeq\; \mathbf{1} \;+\; \tan\beta\, \mathbf{\Delta}_d^{\Phi_u^0} \tag{5.61}$$

Consequently, the FC couplings would be approximately given by

$$\begin{aligned} \mathbf{g}^L_{H_i\bar{d}d} \;&\simeq\; \frac{O_{1i}}{\cos\beta}\mathbf{V}^\dagger\mathbf{R}_d^{-1}\mathbf{V} \;+\; \frac{O_{2i}}{\sin\beta}\left(\mathbf{1} \;-\; \mathbf{V}^\dagger\mathbf{R}_d^{-1}\mathbf{V}\right) \\ &+\; i\mathcal{O}_{3i}\tan\beta\left(\frac{1}{\sin^2\beta}\mathbf{V}^\dagger\mathbf{R}_d^{-1}\mathbf{V} \;-\; \frac{1}{\tan^2\beta}\right) \end{aligned} \tag{5.62}$$

$$\mathbf{g}^R_{H_i\bar{d}d} \;\simeq\; \left(\mathbf{g}^L_{H_i\bar{d}d}\right)^\dagger \tag{5.63}$$

where $\mathbf{V}^\dagger \mathbf{R}_d^{-1} \mathbf{\Delta}_d^{\Phi_u^0} \mathbf{V} = \left(\mathbf{1} - \mathbf{V}^\dagger \mathbf{R}_d^{-1} \mathbf{V}\right) / \tan\beta$ have been used. Note that the size of flavour-violation is strictly dictated by the off-diagonal components of the matrix product $\mathbf{V}^\dagger \mathbf{R}_d^{-1} \mathbf{V}$. Appendix B.5 collects the full expression for the $\mathbf{\Delta}_d^{\Phi_u^0}$ loop-contributions. They depends on the flavour structure in the soft-breaking mass matrices $\delta\widetilde{\mathbf{M}}^2_{Q,U,D}$ and trilinears couplings $\delta\mathbf{a}_u$. Assuming universality for the first two generations, the following flavour parametrization may be introduced [7]

$$\widetilde{\mathbf{M}}^2_X = \begin{pmatrix} \rho & 0 & 0 \\ 0 & \rho & \delta_X \\ 0 & \delta_X & 1 \end{pmatrix} \widetilde{M}^2_{X_3}\,, \qquad \mathbf{Y}_u^{-1}\mathbf{a}_u = \begin{pmatrix} \rho & 0 & 0 \\ 0 & \rho & \delta_{a_u} \\ 0 & \delta_{a_u} & 1 \end{pmatrix} a_{u_3} \tag{5.64}$$

where $X = Q, U, D$. $\delta\widetilde{\mathbf{M}}^2_{Q,U,D}$ and $\delta\mathbf{a}_u$ are simply given by

$$\delta\widetilde{\mathbf{M}}^2_{Q,U,D} = \widetilde{\mathbf{M}}^2_{Q,U,D} - \widetilde{M}^2_{Q,U,D}\,\mathbf{1} \qquad\qquad \delta\mathbf{a}_u = \mathbf{a}_u - \mathbf{Y}_u\, a_u \tag{5.65}$$

$$\widetilde{M}^2_{Q,U,D} = \frac{1}{3}\mathrm{Tr}\left(\widetilde{\mathbf{M}}^2_{Q,U,D}\right) = \frac{1}{3}\,(2\rho+1)\;\widetilde{M}^2_{Q_3,U_3,D_3} \tag{5.66}$$

$$a_u = \frac{1}{3}\mathrm{Tr}\left(\mathbf{Y}_u^{-1}\mathbf{a}_u\right) = \frac{1}{3}\,(2\rho+1)\;a_{u_3} \tag{5.67}$$

In the basis where the up-type Yukawa quarks are diagonal $\mathbf{Y}_u = \mathrm{diag}\,(y_u,\, y_c,\, y_t)$, we have

$$\delta\widetilde{\mathbf{M}}^2_X = \begin{pmatrix} \frac{\rho-1}{3} & 0 & 0 \\ 0 & \frac{\rho-1}{3} & \delta_X \\ 0 & \delta_X & -\frac{2}{3}\,(\rho-1) \end{pmatrix} \widetilde{M}^2_{X_3} \tag{5.68}$$

$$\delta\mathbf{a}_u = \begin{pmatrix} \frac{\rho-1}{3}\,y_u & 0 & 0 \\ 0 & \frac{\rho-1}{3}\,y_c & \delta_{a_u}\,y_c \\ 0 & \delta_{a_u}\,y_t & -\frac{2}{3}\,(\rho-1)\;y_t \end{pmatrix} a_{u_3} \tag{5.69}$$

Inserting the above expressions for $\delta\widetilde{\mathbf{M}}^2_{Q,U,D}$ and $\delta\mathbf{a}_u$ into Eqs.(B.8) and (B.9), one can express in a simplified form

[7] We are assuming, for simplicity, symmetric Yukawa and trilinear matrices at tree-level. In general, $\left(\mathbf{Y}_u^{-1}\mathbf{a}_u\right)_{23}$ and $\left(\mathbf{Y}_u^{-1}\mathbf{a}_u\right)_{32}$ can be different from each other and complex.

$$\mathbf{\Delta}_d^{\Phi_u^0} \simeq \begin{pmatrix} \epsilon & 0 & 0 \\ 0 & \epsilon & \delta\epsilon_{23} \\ 0 & \delta\epsilon_{32} & \epsilon+\eta \end{pmatrix} \tag{5.70}$$

with ϵ, η, $\delta\epsilon_{32}$, $\delta\epsilon_{23}$ containing the main loop contributions. Neglecting the EW corrections and approximating the down-type Yukawa couplings as $\mathbf{Y}_d \simeq \frac{\sqrt{2}}{v_1}\widehat{\mathbf{M}}_d\mathbf{V}^\dagger$, an analytic expression for the these elements can be found

$$\begin{aligned} \epsilon &= \frac{2\alpha_s}{3\pi}\,\mu^*\,M_3^*\,I\left(\tilde{M}_Q^2,\tilde{M}_D^2,|M_3|^2\right) \\ &+ \frac{\rho-1}{3}\left(\frac{2\alpha_s}{3\pi}\,\mu^*\,M_3^*\left(\tilde{M}_{D_3}^2+\tilde{M}_{Q_3}^2\right)\,K\left(\tilde{M}_Q^2,\tilde{M}_D^2,|M_3|^2\right)\right) \end{aligned} \tag{5.71}$$

$$\begin{aligned} \eta &= \frac{|y_t|^2}{16\pi^2}\,\mu^* A_u^*\,I\left(\tilde{M}_Q^2,\tilde{M}_U^2,|\mu|^2\right) \\ &- \delta_R\left[\frac{2\alpha_s}{3\pi}\,\mu^*\,M_3^*\,\frac{V_{23}^*}{V_{33}^*}\tilde{M}_{D_3}^2\,K\left(\tilde{M}_Q^2,\tilde{M}_D^2,|M_3|^2\right)\right] \\ &+ (1-\rho)\left\{\frac{2}{3}\frac{|y_t|^2}{16\pi^2}\,\mu^*\left(A_t^*\,I\left(\tilde{M}_Q^2,\tilde{M}_U^2,|\mu|^2\right)+A_u^*\left(\tilde{M}_{U_3}^2+\tilde{M}_{Q_3}^2\right)\,K\left(\tilde{M}_Q^2,\tilde{M}_U^2,|\mu|^2\right)\right)\right. \\ &\qquad \left.+\frac{2\alpha_s}{3\pi}\,\mu^*\,M_3^*\left(\tilde{M}_{D_3}^2+\tilde{M}_{Q_3}^2\right)\,K\left(\tilde{M}_Q^2,\tilde{M}_D^2,|M_3|^2\right)\right\} \end{aligned} \tag{5.72}$$

$$\begin{aligned} \delta\epsilon_{23} &= \delta_L\left(\frac{2\,\alpha_s}{3\pi}\mu^*\,M_3^*\,\tilde{M}_{Q_3}^2\,K\left(\tilde{M}_Q^2,\tilde{M}_D^2,|M_3|^2\right)+\frac{|y_t|^2}{16\pi^2}\,\mu^*\,A_t^*\,\tilde{M}_{Q_3}^2\,K\left(\tilde{M}_Q^2,\tilde{M}_D^2,|\mu|^2\right)\right) \\ &+ \delta_{a_u}\left(\frac{|y_t|^2}{16\,\pi^2}\mu^* A_t^* I\left(\tilde{M}_Q^2,\tilde{M}_U^2,|\mu|^2\right)\right) \\ &+ \delta_R\left(\frac{2\alpha_s}{3\pi}\,\frac{V_{33}^*\,y_b}{V_{22}^*\,y_s}\mu^*\,M_3^*\,\tilde{M}_{D_3}^2 K\left(\tilde{M}_D^2,\tilde{M}_Q^2,|M_3|^2\right)\right) \\ &+ (\rho-1)\left(\frac{2\alpha_s}{3\pi}\,\frac{V_{32}^*}{V_{22}^*}\mu^*\,M_3^*\,\tilde{M}_{D_3}^2 K\left(\tilde{M}_D^2,\tilde{M}_Q^2,|M_3|^2\right)\right) \end{aligned} \tag{5.73}$$

$$
\begin{aligned}
\delta\epsilon_{32} &= \delta_L \left(\frac{2\,\alpha_s}{3\pi}\,\mu^*\,M_3^*\,\tilde{M}^2_{Q_3}\,K\left(\tilde{M}^2_Q,\tilde{M}^2_D,|M_3|^2\right)\right) \\
&+ \delta_{a_u} \left(\frac{|y_c|^2}{16\pi^2}\mu^*\,A_t^*\,I\left(\tilde{M}^2_Q,\tilde{M}^2_U,|\mu|^2\right)\right) \\
&+ \delta_R \left(\frac{2\,\alpha_s}{3\pi}\left(\frac{V_{22}^*\,y_s}{V_{33}^*\,y_b} - \frac{V_{23}^{*^2}\,y_b}{V_{22}^*\,V_{33}^*\,y_s}\right)\mu^*\,M_3^*\,\tilde{M}^2_{D_3}\,K\left(\tilde{M}^2_D,\tilde{M}^2_Q,|M_3|^2\right)\right) \\
&+ (\rho-1)\left(\frac{2\alpha_s}{3\pi}\frac{V_{23}^*}{V_{33}^*}\,\mu^*\,M_3^*\,\tilde{M}^2_{D_3}\,K\left(\tilde{M}^2_D,\tilde{M}^2_Q,|M_3|^2\right)\right) \qquad (5.74)
\end{aligned}
$$

where $\delta_Q \equiv \delta_L$ and $\delta_U = \delta_D \equiv \delta_R$. Four types of flavour-violating terms proportional to δ_L, δ_{a_u}, δ_R, and $(\rho-1)$ arise for our model[8]. Then

$$
\mathbf{R}_d \;=\; \mathbf{1} + \tan\beta\,\mathbf{\Delta}_d^{\Phi_u^0} \;\simeq\; \begin{pmatrix} 1+\epsilon\tan\beta & 0 & 0 \\ 0 & 1+\epsilon\tan\beta & \delta\epsilon_{23}\tan\beta \\ 0 & \delta\epsilon_{32}\tan\beta & 1+(\epsilon+\eta)\tan\beta \end{pmatrix} \qquad (5.75)
$$

from which $\mathbf{R}_d^{-1}$ can be obtained as presented in Appendix E. For the decay $H_i \to bs$, the relevant matrix elements determining the effective couplings are $\left(\mathbf{V}^\dagger\mathbf{R}_\mathbf{d}^{-\mathbf{1}}\mathbf{V}\right)_{32}$ and $\left(\mathbf{V}^\dagger\mathbf{R}_\mathbf{d}^{-\mathbf{1}}\mathbf{V}\right)_{23}$. The former is given by

$$
\begin{aligned}
\left(\mathbf{V}^\dagger\mathbf{R}_d^{-1}\mathbf{V}\right)_{32} &= \sum_{i,j=1}^{3} \mathbf{V}_{i3}^*\left(\mathbf{R}_d^{-1}\right)_{ij}\mathbf{V}_{j2} \qquad (5.76)\\
&= \sum_{i=1}^{3}\left[\mathbf{V}_{i3}^*\left(\mathbf{R}_d^{-1}\right)_{ii}\mathbf{V}_{i2}\right] + \mathbf{V}_{23}^*\left(\mathbf{R}_d^{-1}\right)_{23}\mathbf{V}_{32} + \mathbf{V}_{33}^*\left(\mathbf{R}_d^{-1}\right)_{32}\mathbf{V}_{22}
\end{aligned}
$$

From Eq.(E.2) to (E.6) in Appendix E for $\mathbf{R}_d^{-1}$ and taking into account the unitarity of the CKM matrix, we can write

$$
\begin{aligned}
\sum_{i=1}^{3}\left[\mathbf{V}_{i3}^*\left(\mathbf{R}_d^{-1}\right)_{ii}\mathbf{V}_{i2}\right] &= \left(\mathbf{V}_{13}^*\mathbf{V}_{12} + \mathbf{V}_{23}^*\mathbf{V}_{22}\right)\frac{(1+\epsilon\tan\beta)\,\eta\,\tan\beta}{\mathrm{Det}\left(\mathbf{R}_d\right)} \\
&- \mathbf{V}_{13}^*\mathbf{V}_{12}\frac{\delta\epsilon_{23}\delta\epsilon_{32}\tan^2\beta}{\mathrm{Det}\left(\mathbf{R}_d\right)} \qquad (5.77)
\end{aligned}
$$

[8] Please note that our definition of δ_{a_u} in Eq.(5.69) makes it different from the δ_{LR} usually defined in the literature.

In this expresion, we can neglect all the terms proportional to $\mathbf{V}_{13}^{*}\mathbf{V}_{12} \sim 8 \times 10^{-4}$ with respect to $\mathbf{V}_{23}^{*}\mathbf{V}_{22} \sim 4 \times 10^{-2}$, even for the last term proportional to $\delta\epsilon_{23}\,\delta\epsilon_{32}$ that for sizeable mass insertions (MI), $\delta_{L,R} \geq \mathbf{V}_{23}^{*}\mathbf{V}_{22}$, would be of the same order as $\epsilon \times \eta$. Going back to Eq.(5.76) and noticing the the off-diagonal elements $\left(\mathbf{R}_{d}^{-1}\right)_{23}$ and $\left(\mathbf{R}_{d}^{-1}\right)_{32}$ should have similar values, the second term would be also suppressed with respect to the last one by roughly $|\mathbf{V}_{23}^{*}\mathbf{V}_{32}| \sim 2.10^{-3}$ and could be neglected. Therefore, under all these assumptions, we can safely take

$$\left(\mathbf{V}^{\dagger}\mathbf{R}_{\mathbf{d}}^{-\mathbf{1}}\mathbf{V}\right)_{32} \;\simeq\; \mathbf{V}_{33}^{*}\,\mathbf{V}_{22}\,\left(\mathbf{R}_{\mathbf{d}}^{-\mathbf{1}}\right)_{32} + \mathbf{V}_{23}^{*}\mathbf{V}_{22}\frac{(1+\epsilon\tan\beta)\,\eta\,\tan\beta}{\mathrm{Det}\,(\mathbf{R}_{d})} \simeq \left(\mathbf{R}_{\mathbf{d}}^{-\mathbf{1}}\right)_{32} \quad (5.78)$$

Repeating the same excercise with $\left(\mathbf{V}^{\dagger}\mathbf{R}_{\mathbf{d}}^{-\mathbf{1}}\mathbf{V}\right)_{23}$, it is found

$$\left(\mathbf{V}^{\dagger}\mathbf{R}_{\mathbf{d}}^{-\mathbf{1}}\mathbf{V}\right)_{23} \;\simeq\; \mathbf{V}_{22}^{*}\,\mathbf{V}_{33}\,\left(\mathbf{R}_{\mathbf{d}}^{-\mathbf{1}}\right)_{23} + \mathbf{V}_{22}^{*}\mathbf{V}_{23}\frac{(1+\epsilon\tan\beta)\,\eta\,\tan\beta}{\mathrm{Det}\,(\mathbf{R}_{d})} \simeq \left(\mathbf{R}_{\mathbf{d}}^{-\mathbf{1}}\right)_{23} \quad (5.79)$$

The study of these matrix elements is very interesting because of its dependence on δ_L, δ_R and δ_{a_u}. Looking at Eq.(5.74) for $\delta\epsilon_{32}$ and comparing the δ_L and δ_R contributions, one can observe that the δ_R term is suppressed by $\left(y_s/y_b - \mathbf{V}_{23}^{*\,2}y_b/y_s\right) \simeq -0.013$ with respect to the δ_L term. Therefore, the resulting matrix element will be very different depending on the insertion at work. Also from these equations it can be noted that if $\delta_L \simeq \delta_{a_u}$, similar results are obtained for $\delta\epsilon_{23}$ from each type of mass insertion. However, this is not still the case for $\delta\epsilon_{32}$, for which the δ_{a_u} insertion is suppressed by a factor $(y_c/y_t)^2$ compared to δ_L. In any case, the δ_{a_u} contributions to $\delta\epsilon_{23}$ and $\delta\epsilon_{32}$ are always subdominant to the δ_R contributions. For this reason, in our analysis, we only consider the cases where δ_L and δ_R contribute. All the results of the numerical simulation have been computed with the `CPsuperH2.3` code [54, 187, 188].

5.3.3 Full MSSM Framework

In the full MSSM framework, the effective FC Higgs couplings defined in Eqs.(2.40) and (2.41) are given by

$$y_{L_i} \equiv \frac{m_b}{v}\mathbf{g}^L_{H_i\bar{b}s} = \frac{m_b}{v}\left(\frac{\mathcal{O}_{1i}}{\cos\beta} - \frac{\mathcal{O}_{2i}}{\sin\beta} + i\tan\beta\frac{\mathcal{O}_{3i}}{\sin^2\beta}\right)\left(\mathbf{V}^\dagger\mathbf{R}_d^{-1}\mathbf{V}\right)_{32} \quad (5.80)$$

$$y_{R_i} \equiv \frac{m_s}{v}\mathbf{g}^R_{H_i\bar{b}s} = \frac{m_s}{v}\left(\frac{\mathcal{O}_{1i}}{\cos\beta} - \frac{\mathcal{O}_{2i}}{\sin\beta} - i\tan\beta\frac{\mathcal{O}_{3i}}{\sin^2\beta}\right)\left(\mathbf{V}^\dagger\mathbf{R}_d^{-1}\mathbf{V}\right)^*_{23} \quad (5.81)$$

The decay width given by Eq.(2.47) would be

$$\begin{aligned}\Gamma\left(H_i \to \bar{b}s + \bar{s}b\right) &\simeq \frac{3m_{H_i}}{8\pi}\kappa_{QCD}\left(|y_{L_i}|^2 + |y_{R_i}|^2\right) \quad (5.82)\\ &\simeq \frac{3m_{H_i}m_b^2}{8\pi v^2}\kappa_{QCD}\left[\left(\frac{\mathcal{O}_{1i}}{\cos\beta} - \frac{\mathcal{O}_{2i}}{\sin\beta}\right)^2 + \left(\tan\beta\frac{\mathcal{O}_{3i}}{\sin^2\beta}\right)^2\right] \times \\ &\quad \left(\left|\left(\mathbf{V}^\dagger\mathbf{R}_d^{-1}\mathbf{V}\right)_{32}\right|^2 + \frac{m_s^2}{m_b^2}\left|\left(\mathbf{V}^\dagger\mathbf{R}_d^{-1}\mathbf{V}\right)_{23}\right|^2\right)\end{aligned}$$

For δ_L insertions, as discussed in the previous section, $|y_{R_i}| \ll |y_{L_i}|$ due to the m_s/m_b suppression when $\left(\mathbf{V}^\dagger\mathbf{R}_d^{-1}\mathbf{V}\right)_{32} \sim \left(\mathbf{V}^\dagger\mathbf{R}_d^{-1}\mathbf{V}\right)^*_{23}$. In the presence of δ_R insertions the situation is more involved and both terms must be considered. The branching ratio for the process is calculated from the partial decay width, Eq.(5.82), and the total decay width of the correspondent bosons. We have already seen that the total decay width of a lightest Higgs of 125 GeV mass is dominated by the decay into two b-quarks, two W-bosons and two τ-leptons. Thus

$$\Gamma_{H_1} = \frac{m_{H_1}m_b^2}{8\pi v^2}\left[\left(3\,\kappa_{QCD} + \frac{m_\tau^2}{m_b^2}\right)\tan^2\beta\,\left(\mathcal{O}_{11}^2 + \mathcal{O}_{31}^2\right) + I_{PS}\frac{m_{H_1}^2}{m_b^2}\left(\mathcal{O}_{21} + \frac{\mathcal{O}_{11}}{\tan\beta}\right)^2\right]$$

where for the large $\tan\beta$ limit $\left(\mathcal{O}_{11}^2/\cos^2\beta + \tan^2\beta\,\mathcal{O}_{31}^2\right) \simeq \tan^2\beta\left(\mathcal{O}_{11}^2 + \mathcal{O}_{31}^2\right)$ and $\left(\sin\beta\,\mathcal{O}_{21} + \cos\beta\,\mathcal{O}_{11}\right)^2 \simeq \left(\mathcal{O}_{21} + \mathcal{O}_{11}/\tan\beta\right)^2$. I_{PS} in the second term refers to the phase-space integral in the Higgs decay into two W-bosons [54] and can be approximated by $I_{PS} \simeq 6.7 \times 10^{-4}$ when $m_{H_1} = 125$ GeV. Then, the branching ratio will be

$$\mathrm{BR}\left(H_1 \to \bar{b}s + \bar{s}b\right) \;=\; 3\,\kappa_{QCD}\left|\left(\mathbf{V}^{\dagger}\mathbf{R}_d^{-1}\mathbf{V}\right)_{32}\right|^2 \times \tag{5.83}$$

$$\frac{\left(\frac{\mathcal{O}_{11}}{\cos\beta} - \frac{\mathcal{O}_{21}}{\sin\beta}\right)^2 + \left(\frac{\mathcal{O}_{31}}{\sin\beta\cos\beta}\right)^2}{\left(3\,\kappa_{QCD} + \frac{m_\tau^2}{m_b^2}\right)\tan^2\beta\,(\mathcal{O}_{11}^2 + \mathcal{O}_{31}^2) + I_{PS}\frac{m_{H_1}^2}{m_b^2}\left(\mathcal{O}_{21} + \frac{\mathcal{O}_{11}}{\tan\beta}\right)^2}$$

For the heavier Higgses, and $\tan\beta \gtrsim 30$, the total decay width is dominated by the bottom and tau decays so

$$\Gamma_{H_2} \;\simeq\; \frac{m_{H_2} m_b^2}{8\pi v^2}\left(3\,\kappa_{QCD} \,+\, \frac{m_\tau^2}{m_b^2}\right)\tan^2\beta\left(\mathcal{O}_{12}^2 + \mathcal{O}_{32}^2\right) \tag{5.84}$$

since $\left(\mathcal{O}_{12}^2/\cos^2\beta + \tan^2\beta\,\mathcal{O}_{32}^2\right) \simeq \tan^2\beta\left(\mathcal{O}_{12}^2 + \mathcal{O}_{32}^2\right)$. Hence, the branching ratio is

$$\mathrm{BR}\left(H_2 \to \bar{b}s + \bar{s}b\right) \;=\; 3\,\kappa_{QCD}\left|\left(\mathbf{V}^{\dagger}\mathbf{R}_d^{-1}\mathbf{V}\right)_{32}\right|^2 \frac{\left(\frac{\mathcal{O}_{12}}{\cos\beta} - \frac{\mathcal{O}_{22}}{\sin\beta}\right)^2 \,+\, \left(\frac{\mathcal{O}_{32}}{\sin\beta\cos\beta}\right)^2}{\left(3\,\kappa_{QCD} \,+\, \frac{m_\tau^2}{m_b^2}\right)\tan^2\beta\,(\mathcal{O}_{12}^2 + \mathcal{O}_{32}^2)}$$

From Section 5.2, we know that the latest LHC data for the Higgs signal in the diphoton channel constrains strongly the Higgs mixing within a general CP-violating model. In particular that if we consider the lightest Higgs as the recently discovered boson at 126 GeV, its mixing conditions are $\left(\mathcal{O}_{11}^2 + \mathcal{O}_{31}^2\right) \sim 1/\tan^2\beta$ and $\mathcal{O}_{21}^2 \sim 1$. Therefore, using the parametrization presented in Eq.(5.56), we can write

$$\mathrm{BR}\left(H_1 \to \bar{b}s + \bar{s}b\right) \;=\; 3\,\kappa_{QCD}\left|\left(\mathbf{V}^{\dagger}\mathbf{R}_{\mathbf{d}}^{-\mathbf{1}}\mathbf{V}\right)_{32}\right|^2 \frac{(\delta_1^2 + \eta_1^2)}{\left(3\,\kappa_{QCD} + \frac{m_\tau^2}{m_b^2}\right) + I_{PS}\frac{m_{H_1}^2}{m_b^2}}$$

Still following the conclusions of Section 5.2, it was also showed that the diphoton condition establishes for the heavier Higgs mixings $\left(\mathcal{O}_{1i}^2 + \mathcal{O}_{3i}^2\right) \sim 1$ and $\mathcal{O}_{2i} \lesssim 1/\tan\beta$, $i = 2, 3$. Hence

$$\mathrm{BR}\left(H_2 \to \bar{b}s + \bar{s}b\right) \;\simeq\; \left|\left(\mathbf{V}^{\dagger}\mathbf{R}_{\mathbf{d}}^{-\mathbf{1}}\mathbf{V}\right)_{32}\right|^2 \frac{3\,\kappa_{QCD}}{3\,\kappa_{QCD} + \frac{m_\tau^2}{m_b^2}} \tag{5.85}$$

where $1/\cos\beta \simeq \tan\beta$ and $\sin\beta \simeq 1$ have been considered in good approximation.

LL insertion

We first analyse the case $\delta_L \neq 0$ and $\delta_R = 0$. Then

$$\delta\epsilon_{32(L)} \simeq \delta_L \frac{2\alpha_s}{3\pi} \mu^* M_3^* \tilde{M}_{Q_3}^2 K\left(\tilde{M}_Q^2, \tilde{M}_D^2, |M_3|^2\right) \sim -3 \cdot 10^{-3}\, \delta_L \quad (5.86)$$

where it can be seen that $\delta\epsilon_{32(L)}$ has a non-decoupling behaviour -as it depends only on ratios of sparticle masses- and we have used as numerical orientative values $\widetilde{M}_{Q,D,Q_3} \sim 5$ TeV, $M_3 \sim 7$ TeV and $\mu \sim 6$ TeV. Consequently, for the maximum value of $\tan\beta$ and δ_L considered during the scan $\delta_L \sim 0.5$ [9] and $\tan\beta \sim 60$, we obtain

$$\left(\mathbf{R_d^{-1}}\right)_{32(L)}^{\max} \simeq -\frac{\delta\epsilon_{32(L)}\,(1+\epsilon\tan\beta)\tan\beta}{\mathrm{Det}\,(\mathbf{R}_\mathrm{d})} \sim \frac{3\cdot 10^{-3} \times 1.5 \times 60}{4} \sim 0.03$$

where ϵ in Eq.(5.71) and $\mathrm{Det}(\mathbf{R}_\mathrm{d})$ for the masses specified above take the values $\epsilon \simeq 0.01$ and $\mathrm{Det}(\mathbf{R}_d) \simeq 4.7$. Therefore

$$\begin{aligned} \mathrm{BR}\left(H_1 \to \bar{b}s + \bar{s}b\right)_{(L)}^{\max} &\simeq \left|\left(\mathbf{V}^\dagger \mathbf{R_d^{-1}} \mathbf{V}\right)_{32(L)}\right|^2 \frac{3\,\kappa_{QCD} \times (\delta_1^2 + \eta_1^2)}{\left(3\,\kappa_{QCD} + \frac{m_\tau^2}{m_b^2}\right) + I_{PS}\frac{126^2}{m_b^2}} \\ &\sim 5\cdot 10^{-4}\,(\delta_1^2 + \eta_1^2) \end{aligned} \quad (5.87)$$

$$\mathrm{BR}\left(H_2 \to \bar{b}s + \bar{s}b\right)_{(L)}^{\max} \simeq \left|\left(\mathbf{V}^\dagger \mathbf{R_d^{-1}} \mathbf{V}\right)_{32(L)}\right|^2 \frac{3\,\kappa_{QCD}}{3\,\kappa_{QCD} + \frac{m_\tau^2}{m_b^2}} \sim 10^{-3} \quad (5.88)$$

Figure 5.8 shows the results of our scans. As in the previous analysis, flavour constraints associated with the processes $B_s \to \mu\mu$, $B \to X_s\gamma$ and ΔM_{B_s} are required to be accomplished. Thus, blue points satisfy the whole set of constraints whilst red points are excluded because of the violation of one of them or more. In the upper frames, the branching ratios for H_1 and H_2 versus $\tan\beta$ are represented. Notice that, for all considerations, H_3 will be equivalent to H_2 given that they are nearly degenerate for the range of masses considered here. In these two plots, one can see that, before applying the low-energy constraints, the branching ratio grows with $\tan\beta$

[9] Notice, effectively, that there is no bound from low-energy FC proceses on this MI for such heavy gluinos and squarks.

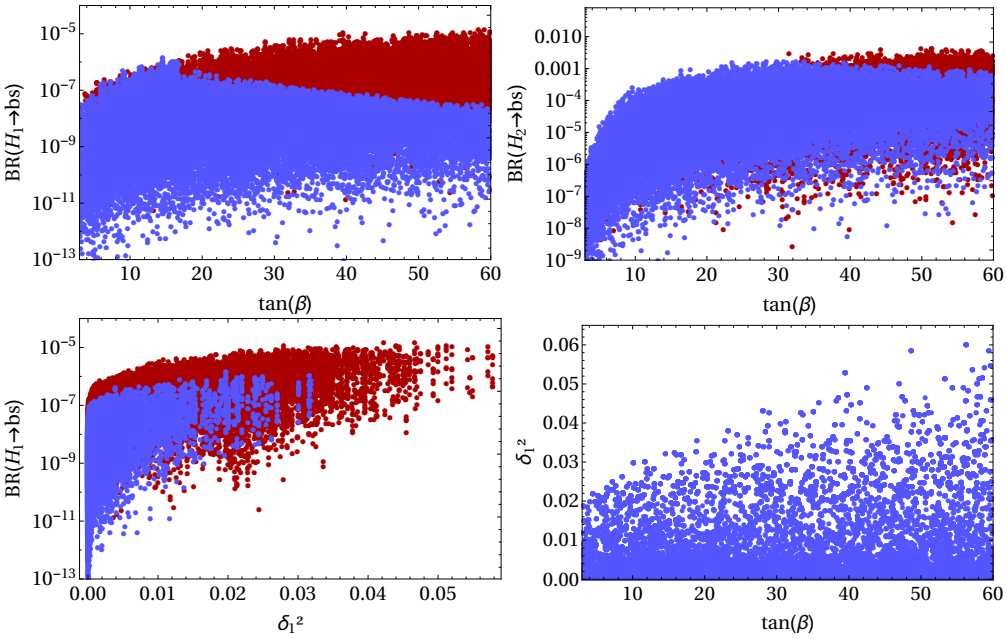

Figure 5.8: A full MSSM framework with LL insertion with $\delta_L \neq 0$ and $\delta_{A_u} = \delta_R = 0$: the upper frames show the dependence of the estimated branching ratios for $H_{1,2} \to \bar{b}s + \bar{s}b$ on $\tan\beta$. The lower-left frame is for the dependence of $\mathrm{B}(H_1 \to bs)$ on δ_1^2 and the lower-right frame for the δ_1^2 dependence on $\tan\beta$. Blue (dark) points satisfy all the constraints considered, while red (light) point violate one or several of these constraints.

(red points). However, the imposed experimental limits from B-mesons modify significantly the final result (blue points). Whereas for heavy Higgses few points become excluded, in the case of the lightest Higgs the effect is quite acute. Indeed, looking at the upper-left frame, the tendency is completely opposite and the branching ratio decreases for $\tan\beta > 20$.

The reason for this behaviour stems in the $B_s^0 \to \mu^+\mu^-$ constraint. This branching ratio is given in Eq.(3.20) with C_S in Eq.(3.22) and C_P in Eq.(3.23) containing the SUSY contributions. The dominant terms come from the heavy Higgses so

$$C_{S,P}^2 \;\propto\; 4\,\frac{\tan^4\beta}{m_{H_j}^4}\,\left|\left(\mathbf{V}^\dagger\mathbf{R}_d^{-1}\mathbf{V}\right)_{32}\right|^2\left[\left(\mathcal{O}_{1j}-\frac{\mathcal{O}_{2j}}{\tan^2\beta}\right)^2+\mathcal{O}_{3j}^2\right]\;\sim\;4\,\frac{\tan^4\beta}{m_{H_j}^4}\,\left|\mathbf{R}_{d,32}^{-1}\right|^2$$

with $j = 2, 3$. This dependence of $C_{S,P}$ on $\tan^3\beta$ -the matrix element $\left(\mathbf{R}_d^{-1}\right)_{32}^*$ carries an additional $\tan\beta$- and the heavy Higgs masses explains why this decay provides

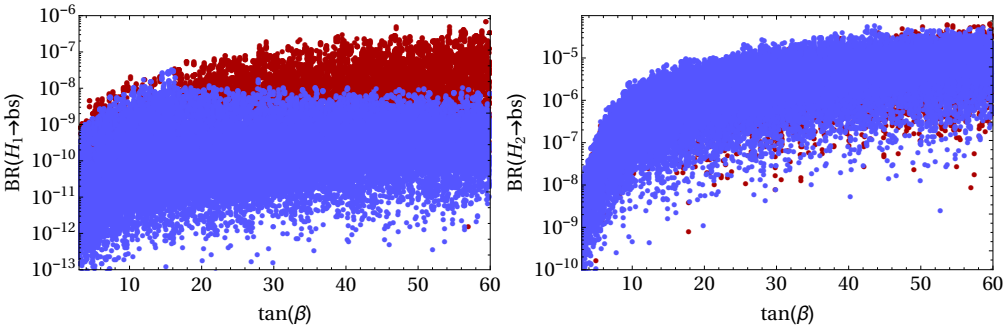

Figure 5.9: A full MSSM framework with RR insertion with $\delta_R \neq 0$ and $\delta_{A_u} = \delta_L = 0$: The left frame shows the dependence of BR($H_1 \to bs$) on $\tan\beta$ and the right one the dependence of BR($H_2 \to bs$) on $\tan\beta$. Again, blue (dark) points satisfy all the constraints considered, while red (light) point violate one or several of these constraints.

such a restrictive constraint for relatively small $m^2_{H_2(3)}$ and medium-to-large values of $\tan\beta$. As a matter of fact, it is BR($H_1 \to bs$) which is highly suppressed by this bound at medium and large $\tan\beta$ values in contrast to BR($H_2 \to bs$). This is because BR($H_1 \to bs$) is proportional to δ_1 and η_1 -see Eq.(5.83) and the lower-left frame in Figure 5.8-, which are order $v^2/M^2_{H_2}$ in the MSSM. Then, when H_2 is light, BR($H_1 \to bs$) is larger but also B-meson constraints are more restrictive. The only solution to be in agreement with the flavour bound would be remain in the low $\tan\beta$ region but, as can be seen in the lower-right frame of the picture, large values of (δ_1^2) -and therefore of BR($H_1 \to bs$)- are not possible when $\tan\beta$ is below 20.
Conversely, BR($H_2 \to bs$) is practically not affected for the rare decay limits. The reason is that BR($H_2 \to bs$) is independent of δ_1 or η_1 and, therefore, of the H_2 mass. Thus, for m_{H_2} large enough, B-meson constraints are not effective and large branching ratios can be reached for large $\tan\beta$ values. Besides, it can be observed in the upper-right frame of Figure 5.8 that this BR saturates for medium-large values of $\tan\beta$ since it is in this regimen when both, the FC decay width and the total decay width, tend to have the same $\tan\beta$ dependence.

RR insertion

We consider now $\delta_R \neq 0$ and $\delta_L = \delta_{a_u} = 0$. From Eqs.(5.74) we see that

$$\delta\epsilon_{32(R)} \;\simeq\; \delta_R \left(\frac{\mathbf{V}^*_{22}\, y_s}{\mathbf{V}^*_{33}\, y_b} - \frac{{\mathbf{V}^*_{23}}^2\, y_b}{\mathbf{V}^*_{22}\, \mathbf{V}^*_{33}\, y_s} \right) \frac{\delta\epsilon_{32(L)}}{\delta_L} \sim 0.013 \times 3 \times 10^{-3}\, \delta_R \sim 5 \cdot 10^{-5}\, \delta_R$$

Then, from Eq.(5.87), one may express $\left(\mathbf{R}_d^{-1}\right)_{32(R)}$ as

$$\left(\mathbf{R}_d^{-1}\right)_{32(R)} \simeq \left(\frac{\mathbf{V}_{22}^* y_s}{\mathbf{V}_{33}^* y_b} - \frac{\mathbf{V}_{23}^{*\,2} y_b}{\mathbf{V}_{22}^* \mathbf{V}_{33}^* y_s}\right) \left(\mathbf{R}_d^{-1}\right)_{32(L)} \sim 4 \cdot 10^{-4}\, \delta_R \tag{5.89}$$

In this case, the value of the off-diagonal element $(\mathbf{R}_d^{-1})_{32}$ is order 10^{-4} and this implies that the contributions $\mathbf{V}_{23}^* \mathbf{V}_{22}$ in Eq.(5.77) and $\left(\mathbf{R}_d^{-1}\right)_{23}$ in Eq.(5.76) or y_{R_i} in Eq.(5.81), can be important. Thus

$$\begin{aligned}\left(\mathbf{V}^\dagger \mathbf{R}_d^{-1} \mathbf{V}\right)_{32(R)}^{\max} &\simeq \left(\mathbf{R}_d^{-1}\right)_{32(R)} + 2 \cdot 10^{-3} \left(\mathbf{R}_d^{-1}\right)_{23(R)} + 0.04\, \frac{(1 + \epsilon \tan\beta)\, \eta\, \tan\beta}{\mathrm{Det}\,(\mathbf{R}_\mathrm{d})} \qquad (5.90)\\ &\sim -4 \cdot 10^{-4} \delta_R - 2 \cdot 10^{-3}\, \frac{\delta\epsilon_{23(R)} \times 1.5 \times 60}{4} + 0.04\, \frac{1.5 \times 4 \cdot 10^{-3} \times 60}{4}\end{aligned}$$

where we used the same values for the parameters as in Eq.(5.87). Note that now $\delta\epsilon_{23(R)}$ is enhanced by a factor y_b/y_s

$$\delta\epsilon_{23(R)} \sim \delta_R \frac{2\alpha_s}{3\pi} \frac{y_b}{y_s}\, \mu^*\, M_3^*\, \tilde{M}_{D_3}^2\, K\left(\tilde{M}_Q^2, \tilde{M}_D^2, |M_3|^2\right) \sim -0.1\, \delta_R \tag{5.91}$$

Therefore, we obtain

$$\left(\mathbf{V}^\dagger \mathbf{R}_d^{-1} \mathbf{V}\right)_{32(R)}^{\max} \sim 4(\delta_R + 1) \cdot 10^{-3} \tag{5.92}$$

For $\delta_R = 0.5$, the branching ratios are

$$\begin{aligned}\mathrm{BR}\left(H_1 \to \bar{b}s + \bar{s}b\right)_{(R)}^{\max} &\simeq \left|\left(\mathbf{V}^\dagger \mathbf{R}_d^{-1} \mathbf{V}\right)_{32(R)}\right|^2 \frac{3\,\kappa_{QCD}(\delta_1^2 + \eta_1^2)}{\left(3\,\kappa_{QCD} + \frac{m_\tau^2}{m_b^2}\right) + I_{PS}\frac{126^2}{m_b^2}} \qquad (5.93)\\ &\sim 1.5 \cdot 10^{-5}\, (\delta_1^2 + \eta_1^2) \qquad (5.94)\end{aligned}$$

$$\mathrm{BR}\left(H_2 \to \bar{b}s + \bar{s}b\right)_{(R)}^{\max} \simeq \left|\left(\mathbf{V}^\dagger \mathbf{R}_d^{-1} \mathbf{V}\right)_{32(R)}\right|^2 \frac{3\,\kappa_{QCD}}{3\,\kappa_{QCD} + \frac{m_\tau^2}{m_b^2}} \sim 2 \cdot 10^{-5} \tag{5.95}$$

The results of our scans for this case are shown in Figure 5.9. As before, they are in agreement with the numerical values if B-meson constraints are not taken into

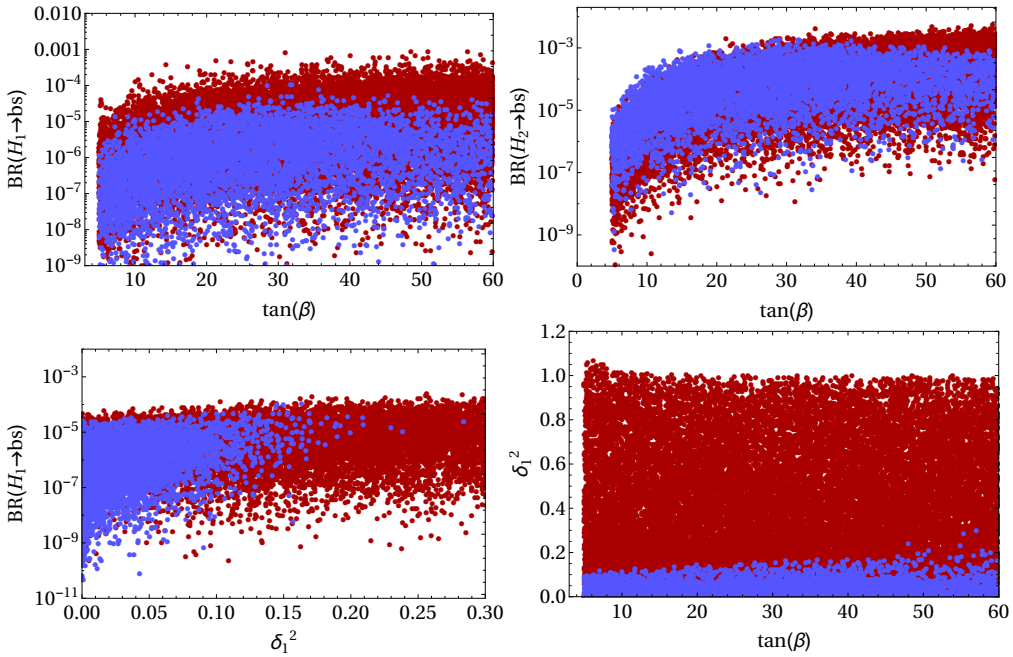

Figure 5.10: A generic supersymmetryic SM with LL insertion with $\delta_L \neq 0$ and $\delta_{A_u} = \delta_R = 0$: The upper frames show the dependence of the estimated branching ratios for $H_{1,2} \to \bar{b}s + \bar{s}b$ on $\tan\beta$. The lower frame is for the dependence of $\mathrm{B}(H_1 \to bs)$ on δ_1^2 and the lower-right frame for the δ_1^2 dependence on $\tan\beta$. Blue (dark) points satisfy all the constraints considered, while red (light) point violate one or several of these constraints.

account. Once they are incorporated to the analysis, the lightest Higgs branching ratio is reduced in more than one order of magnitude. Also, taking into account from Eq.(5.90) that both, the MI and the MI-independent contributions are of the same order only for large δ_R, the BR is completely independent of δ_R.

5.3.4 Generic Supersymmetric SM

After computing these branching ratios in the MSSM framework, we now perform our analysis in a generic supersymmetric model meaning that generic Higgs mixings are considered with the possible presence of extra Higgs states, Eq.(5.59). In this case, we have $\mathcal{O}_{11}^2 + \mathcal{O}_{21}^2 + \mathcal{O}_{31}^2 \leq 1$ and the parameters δ_1 and/or η_1 entering $\Gamma(H_1 \to \bar{b}s + \bar{s}b)$ can be sizeable. The expressions for the decay widths and branching ratios in Eqs.(5.82)-(5.85) are still valid, being the main difference that now the parameters δ_1 and η_1 are only constrained by experimental results on Higgs decays and low energy

FCNC processes. Notice, however, that the flavour changing entries in $\mathbf{R_d^{-1}}$ do not change in these two models.

In Figure 5.10, the FC branching ratios of H_1 and H_2 are shown when $\delta_L \neq 0$ and $\delta_{a_u} = \delta_R = 0$. These figures must be compared with Figure 5.8 in the MSSM framework. Whereas in the MSSM framework the mixing angles are obtained through a minimization of the scalar potential and both, δ_1 and η_1 are of order $v^2/m_{H_2}^2$ from the diagonalization of the neutral Higgs mass matrix, in the generic supersymmetric scenario δ_1 and η_1 are treated as free parameters that do not depend a priori on the ratio $v^2/m_{H_2}^2$ and are only constrained by the experimentally measured Higgs branching ratios and B-meson constraints. This is why $\mathrm{BR}(H_1 \to bs)$ in Figure 5.8 is two orders of magnitude smaller that the largest possible value in Figure 5.10. The different distribution of the points allowed by B-meson constraints is due to the same reason. In the MSSM scenario, Higgs flavour-changing processes are mediated by heavy Higgses and therefore are only important for light m_{H_2}, which correspond also to the largest δ_1 and η_1 and consequently to the largest branching ratios. In the generic supersymmetric SM it is, in principle, possible to have a large δ_1 with heavy H_2 and therefore the B-meson constraints are not so efficient. On the other hand, as the FC decays of heavy Higgses $H_{2,3}$ are independent of δ_1 and η_1, in this case, the upper-right frames of Figures 5.8 and 5.10 are very similar equivalent results are obtained for both scenarios. Also, as shown in the lower-right plot of Figure 5.10, the allowed values of $(\delta_1)^2$ are completely independent of $\tan\beta$ now and then the B-meson constraints, which deppend on $(\tan\beta)^n/m_{H_2}^4$, can always be satisfied adjusting conveniently the value of m_{H_2}. In this case, the upper limit for $(\delta_1)^2$ is fixed by the $H_1 \to \gamma\gamma$ decay, which as shown in Section 5.2 requires $\left(\mathcal{O}_{11}^2 + \mathcal{O}_{31}^2\right) \sim 1/\tan^2\beta$ and $\mathcal{O}_{21}^2 \sim 1 - 1/\tan^2\beta$. Using the definition of δ_1, and in the limit where $\mathcal{O}_{31} \ll 1$ with the above constraints, $(\delta_1)^2 \lesssim 0.17$ for $\tan\beta \gtrsim 10$. This value is almost one order or magnitude above the maximum possible one for the full MSSM.

In summary, the main difference in the generic supersymmetric SM is that $\mathrm{BR}(H_1 \to bs)$ could reach a value of $\sim 10^{-4}$ consistently with present experimental constraints. This value is still too small to be observed in the large background of an hadron collider, but could be tested in a leptonic linear collider in the near future.

5.3.5 Conclusions

In this work, we have explored the flavour-changing Higgs decays $H_i \to bs$ in a general supersymmetric scenario. The importance of these FC decays is that, although they arise at one loop-level, they originate from a dimension-four operator and therefore

the effect of additional heavy particles may not decouple, even when the masses are taken to infinity. This provides a unique opportunity to find a first sign of new physics beyond collider reach. In the framework of the minimal supersymmetric extension of the Standard Model (MSSM), we found that the largest branching ratio of the lightest Higgs (H_1) is $\mathcal{O}(10^{-6})$, after imposing present experimental constraints. Heavy Higgs states might still present branching ratios $\mathcal{O}(10^{-3})$. In a more general supersymmetric scenario, where additional Higgs states may modify the Higgs mixings, the branching ratio BR($H_1 \to bs$) could reach values $\mathcal{O}(10^{-4})$, while heavy Higgses remained at $\mathcal{O}(10^{-3})$. Although these values are clearly out of reach for the LHC, a full study in a linear collider environment could be worth.

6

The Origin of Flavour

Since the discovery of the muon in cosmic rays at the beginning of the 20th century, the flavour puzzle remains one of the biggest open questions in high-energy physics. This puzzle derives from the bizarre flavour structures present in the Standard Model (SM) and the mystery, if any, behind their origin. Although the SM is able to accommodate all known flavour parameters in its Yukawa matrices, the values of these parameters are completely arbitrary and can only be fixed from experimental measurements.

Using symmetries to interpret a large number of apparently arbitrary parameters is a strategy that has been remarkably successful for similar problems in the past. In this spirit, the Frogatt-Nielsen mechanism [189] uses a spontaneously-broken flavour symmetry to explain the large hierarchies observed in the fermionic masses and mixing angles. In this work we choose to focus on this mechanism as the solution to the flavour puzzle. Although perhaps the best way to test this idea would be to directly produce the flavour mediators, in practice this is impossible if the flavour symmetry is broken at energies much higher than the electroweak (EW) scale. Given the fact that the Yukawa couplings are dimensionless, in principle this symmetry could be broken at any scale above the EW scale, even close to the Planck scale: $\Lambda_{EW} \ll \Lambda_f \lesssim M_{Pl}$. And, in fact, if the Yukawa couplings are the only remnant of flavour symmetry breaking, we may never be able to unravel the origin of flavour.

Nevertheless, as the LHC continues to explore the TeV scale [190–201], we can hope that new physics associated with the breaking of the flavour symmetry may emerge in this energy region. In many extensions of the SM proposed in the literature, this new physics is not completely flavour-blind, and the new interactions have a non-trivial flavour dependence. This is indeed the case for supersymmetric extensions of the

Standard Model [17,33,34,202]. Whereas in the SM we can only measure the fermion masses and the left-handed mixings -the relative misalignment between Y_u and Y_d in the quark sector- in the Yukawa matrices, in SUSY extensions of the SM right-handed fields couple also through their trilinear interactions and may have non-trivial soft-mass matrices. In general, these three flavour structures can not be simultaneously diagonalized and their relative misalignment becomes observable [203], providing a way to explore whether the mixings in the right-handed sector are small (analogous to the case of the CKM left-handed mixings) or large (similar perhaps to the PMNS neutrino mixings). Similarly, the measure of left-handed mixings in the leptonic fields can clarify whether the large PMNS mixings are due to large Yukawa mixings or to the Majorana nature of the neutrino masses through a type-I seesaw mechanism.
Here, we will show that flavour non-universal couplings are unavoidable in the soft-breaking terms when $\Lambda_f \lesssim \Lambda_{\rm SUSY}$. We assume that SUSY breaking is primarily mediated by supergravity, and that the Yukawa structures arise from a broken flavour symmetry through the FN mechanism. We begin in Section 6.1 by providing a brief review of the necessary background. Through simplified examples we see that these effective theories generically introduce new sources of flavour non-universality to the scalar sector of the Lagrangian (soft terms). As an application of these results, we consider two instructive choices for the flavour symmetry, an Abelian $U(1)_f$ and a non-Abelian $SU(3)_f$ in Section 6.2. As these SUSY models predict the order of magnitude of the flavour violation expected at low-energies, we show how phenomenological bounds from flavour observables can be used to provide information on the expected scale of the soft terms in Section 6.3. We conclude in Section 6.4 with an overview of our results and prospects for further phenomenological studies.

6.1 Supersymmetry and Flavour

In Section 1.3 we saw that the MSSM Lagrangian is determined by the particle content (gauge representations), the superpotential and the soft supersymmetry-breaking terms. Regarding the first, the MSSM economically contains only the supersymmetric field content of the SM with an additional Higgs doublet. As its superpotential (up to the μ-term) is fixed by the Yukawa sector of the SM, the soft-breaking terms encode most of the new parameters of the Lagrangian, unfortunately introducing a huge number of unknowns to the theory that can potentially give rise to dangerous flavour-violation effects (see the initial discussion in Chapter 2).
It is possible, however, that the mechanism responsible for generating the soft-terms

preserves some or all of the structure of a flavour-symmetric ultraviolet completion to the MSSM. For instance, an underlying spontaneously-broken flavour symmetry may be *simultaneously* responsible for the fermion masses and mixing angles and the different flavour structures in the soft-breaking terms. In this case, the new flavour violating couplings in the SUSY Lagrangian provide a magnificent opportunity to measure new data on flavour, and may hopefully provide hints towards a fundamental theory of flavour.

As remarked in Section 1.3.3, if supersymmetry has to be realised it must be a broken symmetry. The precise mechanism through which the breaking occurs is not obvious, although what is clear is that it requires to extend the MSSM to a hidden sector of particles that have no (or only very small) direct couplings to the visible sector of chiral supermultiplets in the MSSM [17]. The breakdown takes place in the hidden sector and it is transmitted to the visible one through mediators, either radiatively or through non-renormalizable interactions. A minimal option to couple the hidden and visible sectors is gravity, typically referred to as a "gravity-mediation". That is the scenario we consider in this work.

A non-renormalizable gauge-invariant theory involving chiral and vector supermultiplets can be constructed from

$$\mathcal{L} \;=\; \Big[K(\Phi_i, \tilde{\Phi}^{j*})\Big]_D \;+\; \left(\left[\frac{1}{4}\,\mathsf{f}_{ab}(\Phi_i)\widehat{\mathcal{W}}^{a\alpha}\widehat{W}^{b}_{\alpha} \;+\; \mathsf{W}(\Phi)\right]_F \;+\; \text{c.c.}\right) \tag{6.1}$$

where the Lagrangian density depends on three functions: the superpotential, W, the *Kähler potential*, K and the *gauge kinetic function*, f_{ab}. As presented in Section 1.2.1, the superpotential is a general holomorphic function only dependent on the chiral superfields and invariant under gauge symmetries. It gives rise to the Yukawa couplings likewise in the MSSM seen in Section 1.3.2. The Kähler potential, conversely, is a function of both chiral and anti-chiral superfields, and includes vector superfields in order to be supergauge invariant. Finally, like the superpotential, the gauge kinetic function is an holomorphic function of the chiral supermultiplets and it is symmetric under the exchange of the indices $a \leftrightarrow b$. It encodes the non-renormalizable couplings of the gauge superfields to the chiral ones.

In a gravitational-strength mediation scheme, the non-renormalizable interactions described above also includes interactions with the hidden sector through $M_{\rm Pl}$ suppressed couplings. For instance, let us consider

$$\mathsf{W} = \mathsf{W}_{\rm MSSM} - \frac{1}{M_{\rm Pl}}\left(\frac{1}{6}\alpha y^{ijk}\, X\Phi_i\Phi_j\Phi_k + \frac{1}{2}\beta\mu^{ij}\, X\Phi_i\Phi_j\right) + \ldots \quad (6.2)$$

$$K = \Phi^{*i}\Phi_i + \frac{1}{M_{\rm Pl}^2}k\delta_i^j\,\Phi^{*i}\Phi_j\, XX^* + \ldots \quad (6.3)$$

$$\mathsf{f}_{ab} = \frac{\delta_{ab}}{g_a^2}\left(1 - \frac{2}{M_{\rm Pl}}f_a X + \ldots\right) \quad (6.4)$$

where Φ_i would be the MSSM chiral fields, $\mathsf{W}_{\rm MSSM}$ would contain the interactions specified in Eq.(1.45) and X would be the chiral superfield whose F-term auxiliary field will break supersymmetry. Since we are mainly interested in the visible sector, and given that the couplings between the two sectors are gravitationally small, we can in practice neglect most of these interactions and the energy transfer between the hidden and visible sector. However, some effects of the hidden sector may still be important at low energies, especially if they break a symmetry which remains exact in the visible sector. An example of this is SUSY breaking; after SUSY is broken in the hidden sector with a non vanishing F-term, $F \equiv \langle F_{\mathsf{X}}\rangle \neq 0$, the gravitational interactions communicate this breaking to the visible sector with a strength $m_{\rm soft} \sim F/M_{\rm Pl}$. The remnant of these interactions in the visible sector is the soft SUSY-breaking Lagrangian which includes the soft SUSY-breaking masses for gauginos and scalars as well as the scalar trilinear terms. From Eq.(6.2)-(6.4) above, it will be

$$\mathcal{L}_{\rm soft} = -\frac{1}{2M_{\rm Pl}}f_a\lambda^a\lambda^a - \frac{F}{6M_{\rm Pl}}\alpha y^{ijk}\,\phi_i\phi_j\phi_k - \frac{F}{2M_{\rm Pl}}\beta\mu^{ij}\phi_i\phi_j + \text{c.c.} \\ -\frac{|F|^2}{M_{\rm Pl}^2}k\,\phi^{*i}\phi_i \quad (6.5)$$

Comparing with Eq.(1.52) one observes that the second term in Eq.(6.5), emerging from the second term in the superpotential of Eq.(6.2), corresponds to the trilinear couplings whereas the last term, arising from the Kähler in Eq.(6.3), is associated with the soft masses. Then, it can be seen that in the case of a single F-term all the soft masses in the "full" theory are universal whereas the trilinear couplings remain just proportional to the Yukawa couplings. However, if a flavour symmetry is indeed present in the theory, its pattern of breaking and the details of the underlying theory will dictate new non-universal flavour structures in the low-energy effective theory below Λ_f.

To illustrate this point, let us consider an Abelian flavour symmetry $U(1)_f$ that breaks

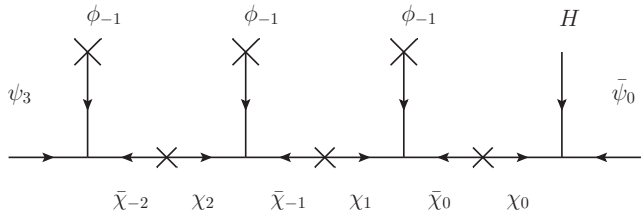

Figure 6.1: Contribution to the superpotential in superfield notation. The superpotential is holomorphic and therefore involves only fields and not daggered fields, *i.e.*, all arrows must enter the vertices in superfield notation.

spontaneously at a scale $\Lambda_f < M_{\rm Pl}$. Before the breaking of the flavour symmetry, our superpotential and Kähler potential are invariant under both the SM (or GUT) and flavour symmetries. Suppose that the relevant superpotential terms allowed by the symmetries of the theory and which couple the flavons and mediators to the SM fields is given by

$$\begin{aligned} \mathsf{W} &= g\left(\psi_3\bar{\chi}_{-2}\phi + \chi_2\bar{\chi}_{-1}\phi + \chi_1\bar{\chi}_0\phi + \chi_0\bar{\psi}_0 H + \psi_0\bar{\chi}_{-1}\bar{\phi}\right) \\ &\quad + M\left(\chi_0\bar{\chi}_0 + \chi_1\bar{\chi}_{-1} + \chi_2\bar{\chi}_{-2}\right) + m\,\phi\bar{\phi} + \dots \end{aligned} \tag{6.6}$$

where we have used subscripts to denote the $U(1)_f$-charges of the SM and mediator fields, and the flavon ϕ ($\bar{\phi}$) is taken to have charge -1 ($+1$). We assume a common coupling g and mediator mass M to simplify the discussion.
Supposing that at $\Lambda_f \sim \langle\phi\rangle$ the flavour symmetry is spontaneously broken, an effective Yukawa term in the superpotential will be generated upon integrating out the mediators as shown in the supergraph[1] of Figure 6.1

$$\mathsf{W}_{\rm eff} = g^4\left(\frac{\langle\phi\rangle}{M}\right)^3 \psi_3\bar{\psi}_0 H + \ \dots\ . \tag{6.7}$$

Further flavour structures will be generated in the soft-breaking terms. Before the flavour symmetry is broken, as saw before in Eq.(6.5), trilinear terms in the potential of the "full" theory are simply generated proportional to the superpotential in

[1] In superfield notation arrows pointing towards the vertex correspond to left-handed fields and those leaving from the vertex right-handed, or alternatively daggered, fields. Then the superpotential terms are vertices with all arrows entering (W) or leaving the vertex (W^*) while Kähler vertices have arrows both entering and leaving the vertex [205–207].

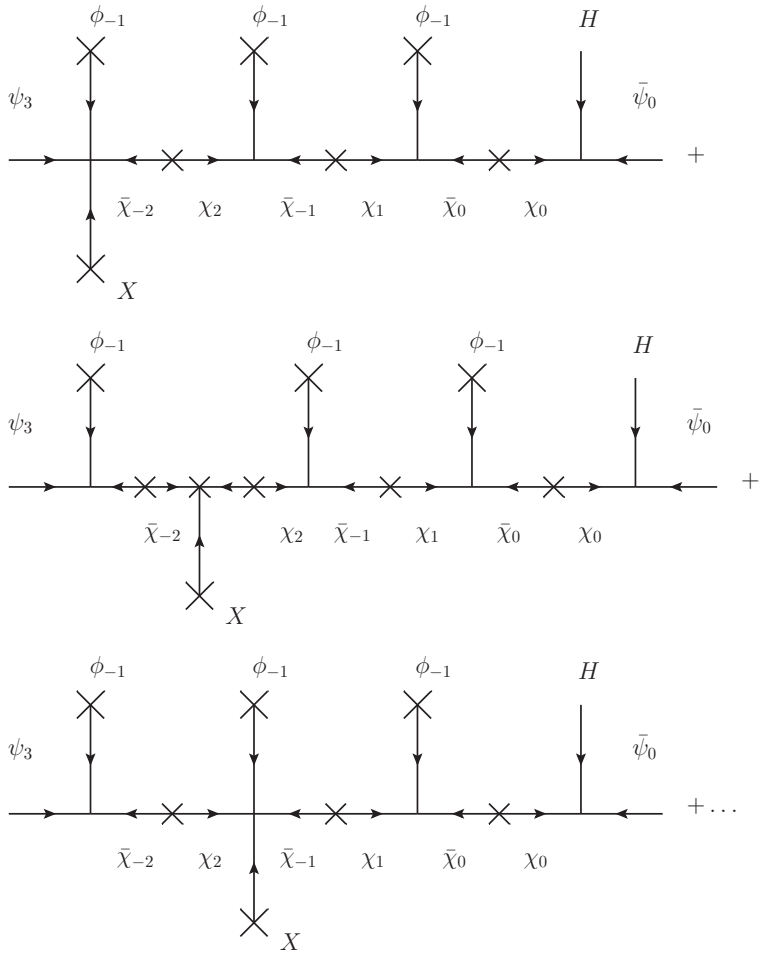

Figure 6.2: Contributions to the A-terms from Figure 6.1. As noted, for this diagram seven insertions of F_X are possible.

Eq. (6.6) from V = $m_{3/2} \times W$, where $m_{3/2} = \frac{F}{M_{\rm Pl}}$. When the flavour symmetry breaks, an effective potential for the trilinear terms will be generated $V_{\rm eff}$. However, unlike the contribution to $\mathsf{W}_{\rm eff}$, the trilinear scalar coupling in the effective theory at low energies coming from the effective Yukawa coupling of Figure 6.1 has seven different contributions; four with F_{X} inserted in any of the cubic vertices, plus three contributions with $F_{\rm X}$ in the superpotential mass, as shown in Figure 6.2.
The same diagrams drawn in terms of the component scalar fields are shown in Figure 6.3. The vertices proportional to M are obtained from the interference of the different

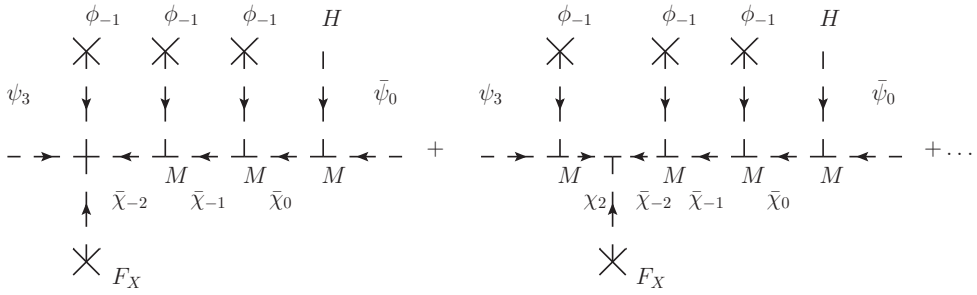

Figure 6.3: Figure 6.2 drawn in terms of the scalar component fields.

components of the F-terms from Eq. (6.6), which are $|F_{\chi_2}|^2$, $|F_{\chi_1}|^2$ and $|F_{\chi_0}|^2$. The term $F_{\mathsf{X}}/M_{\rm Pl} = m_{3/2}$ corresponds to the trilinear term $\frac{\mathsf{X}}{M_{\rm Pl}} \times W$. Integrating out the heavy fields and replacing the scalar propagators by $1/M^2$, we obtain 7 identical contributions with coupling $m_{3/2}(\langle\phi\rangle/M)^3$, generating a term $a_{3,0} = 7 \times m_{3/2}(\langle\phi\rangle/M)^3$ in the effective potential; this is to be compared with the Yukawa coupling of the effective superpotential, for which the single supergraph generates only $Y_{3,0} = (\langle\phi\rangle/M)^3$. By this simple example, it is clear that the proportionality factor will change depending on the number of vertices in the full theory and therefore, if we have a different number of flavon insertions generating the various Yukawa elements, *the trilinear matrices will never be proportional to Yukawa matrices* [208–210].

A similar mismatch occurs for the soft masses. Before flavour symmetry breaking, the soft-masses obtained from the Kähler potential are universal for all visible fields, see Eq.(6.5). This includes the SM, flavon and any mediator fields needed in the model. In terms of the spurion X, these flavour symmetric soft-terms would be represented through the supergraph of Figure 6.4 and the Kähler function would be

$$K = \psi_i^\dagger \psi_j \left(\delta_{ij} + \delta_{ij} \frac{X X^\dagger}{M_{\rm Pl}^2} \right) , \tag{6.8}$$

with ψ_i any of the visible fields. As was the case for the superpotential, after the flavour symmetry is broken, the Kähler potential receives new contributions. Since the Kähler potential includes the usual wave-function renormalization, the light-field two-point functions in the low energy effective theory receive new contributions mediated by the heavy fields, coupling fields with different flavour charges through an appropriate number of flavon insertions. An example of these two-point functions is shown in Figure 6.5. In this case, field redefinitions will be necessary to ensure canonical kinetic terms, see [211].

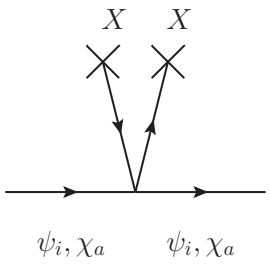

Figure 6.4: Contribution to the soft mass from the Kähler potential in superfield notation. Arrows entering the vertex represent fields, while arrows leaving the vertex are daggered fields; here $|\langle F_X \rangle|^2 / M_{\rm Pl}^2 = m_{3/2}^2$.

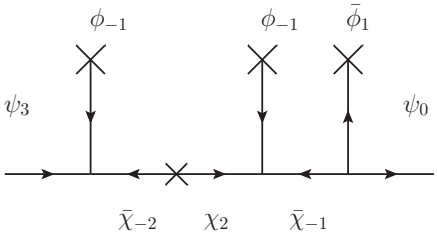

Figure 6.5: Supergraph illustrating a possible non-diagonal Kähler couplings induced by integrating out the heavy mediator superfields.

Following the same logic as for the trilinear interactions, inserting the SUSY breaking F-term in all possible ways at different points in the diagram makes a difference between the kinetic terms and the soft masses. Again we have several diagrams contributing equally to the soft-breaking masses for each diagram (if $\langle X \rangle \ll \langle F_X \rangle$) renormalizing the kinetic terms, Figure 6.6. In general, the Kähler potential after integrating the heavy mediator fields is now,

$$K = \psi_i^\dagger \psi_j \left(\delta_{ij} + c \left(\frac{\langle \phi \rangle}{M_\chi} \right)^{q_{ij}} + \left(\delta_{ij} + b \left(\frac{\langle \phi \rangle}{M_\chi} \right)^{q_{ij}} \right) \frac{|F|^2}{M_{\rm Pl}^2} + \text{h.c.} \right) \tag{6.9}$$

with $b \sim Nc$, where N is the number of internal lines we can insert the spurion field.[2] Given that the kinetic terms and the soft masses are not proportional, the field redefinition necessary to ensure canonical kinetic terms will not simultaneously diagonalize the soft masses, introducing new sources of flavour violation.

[2] As in the case of the trilinears, this may be expressed in terms of the component fields.

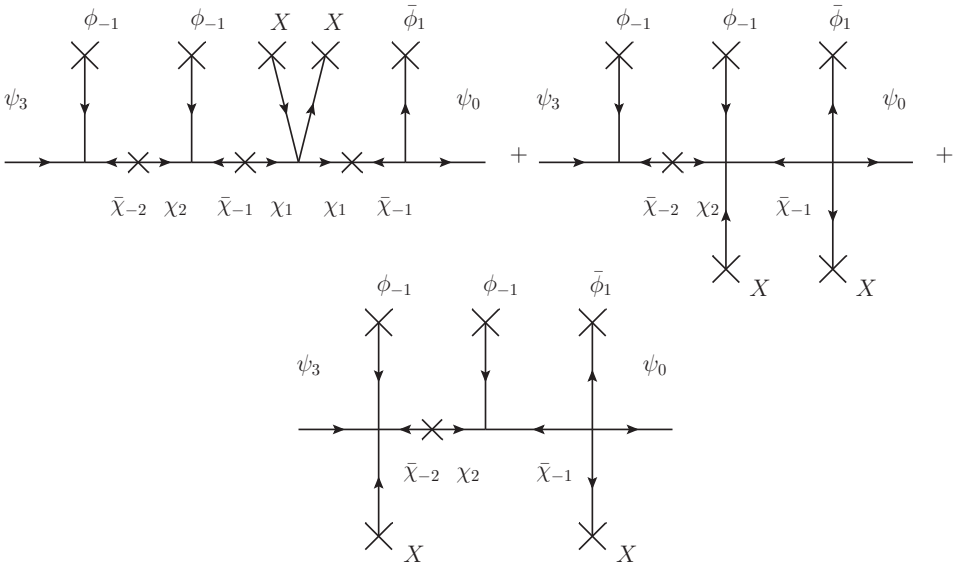

Figure 6.6: Off-diagonal contributions to the scalar soft-masses from the Kähler diagram of Figure 6.5. Again, multiple ossibilities exist for inserting the supersymmetry breaking term $XX^\dagger$.

These results, that trilinear interactions and soft masses are not proportional in the low-energy theory after integrating out heavy fields, apply generically to all supersymmetric effective theories of flavour with $\Lambda_f \lesssim \Lambda_{\rm SUSY}$.

6.2 Flavour Symmetries

As a first application of the results of the previous section, we consider now the effects of integrating out heavy mediator fields on the structure of the soft-breaking terms in two representative flavour models: a toy $U(1)_f$ model, as an example of an Abelian symmetry, and a non-Abelian $SU(3)_f$ model.
In the following, we assume the conditions on the breaking of SUSY of the previous section apply: i) gravity mediation and ii) a single F-term with universal couplings is responsible for generating all the soft-terms of the visible sector. Our goal is not to present completely realistic models, but to show that non-universal soft-terms are a generic prediction of these models, even starting with fully universal soft terms at the mediation scale. Realistic models will have to deal with other problems like Golstone bosons in the case of global symmetries or D-flatness in the case of gauged

non-Abelian symmetries, etc. Solutions to all these problems can be found in the literature [212, 213] or can be avoided altogether with discrete flavour symmetries [214–216].

6.2.1 Toy $U(1)_f$ Model

Under the conditions outlined above, our toy $U(1)_f$ model is completely defined by its superpotential, which generalizes the superpotential of Eq. (6.6)

$$\begin{aligned} W \;\supset\; & g\sum_q \left(\psi_q\bar{\chi}_{-q+1}\phi + \chi_q\bar{\chi}_{-q+1}\phi + \chi_{q-1}\bar{\chi}_{-q}\bar{\phi} + \chi_{-q}\bar{\psi}^u_q H_u + \chi_{-q}\bar{\psi}^d_q H_d\right) + \\ + \;& g\left(\bar{\psi}^u_q\bar{\chi}^u_{-q+1}\phi + \chi^u_q\bar{\chi}^u_{-q+1}\phi + \chi^u_{q-1}\bar{\chi}^u_{-q}\bar{\phi} + \bar{\psi}^d_q\bar{\chi}^d_{-q+1}\phi + \chi^d_q\bar{\chi}^d_{-q+1}\phi + \chi^d_{q-1}\bar{\chi}^d_{-q}\bar{\phi}\right) \\ + \;& M\sum_q \left(\chi_q\bar{\chi}_{-q} + \chi^u_q\bar{\chi}^u_{-q} + \chi^d_q\bar{\chi}^d_{-q}\right) + m\,\phi\bar{\phi} \end{aligned} \tag{6.10}$$

where the ψs ($\bar{\psi}$s) represent the left-handed (right-handed) SM superfields, χs and $\bar{\chi}$s the mediators, and ϕ and $\bar{\phi}$ are the flavons. As before, the subscripts for the ψs and χs denote their respective $U(1)_f$ charges, chosen positive for the SM fields. The flavon, ϕ ($\bar{\phi}$) is assigned to have $U(1)_f$ charge -1 ($+1$). For simplicity, we assume a common coupling, g, and a common mass, M, for all the mediators. In principle, however, each mediator particle can couple with its own $\mathcal{O}(1)$ coupling and can have a different mass. Similarly, it is well-known that one of the main problems of supersymmetric $U(1)_f$ models is that the equality of soft-masses of the different generations, even in the symmetric limit, is not guaranteed by symmetry. This inequality may generate large off-diagonal entries after rotating to the basis of diagonal Yukawa matrices. This problem is absent in our toy model due to our assumption of a single F-term with universal couplings to the visible sector, but should be addressed in a realistic Abelian model.

To obtain the low-energy Yukawa couplings and the soft-breaking trilinear interactions in the effective theory below Λ_f (or the soft-masses and the Kähler function), it is again easiest to work with supergraphs. Drawing supergraphs such as that of Figure 6.1, one finds that in terms of the small expansion parameter, $\varepsilon = g(\langle\phi\rangle/M) \ll 1$, integrating out the heavy messengers will generate Yukawa interactions of the form

$$Y_{ij} \;\sim\; \varepsilon^{n_{ij}}, \qquad n_{ij} = q_i + q_j\,. \tag{6.11}$$

For the trilinear couplings, we have to take into account that each supergraph generating the Yukawa terms will necessarily contain n_{ij} flavon insertions (cubic vertices) and n_{ij} messenger masses, with one additional vertex to couple the Higgs. This will result in $2n_{ij}+1$ possibilities to insert the SUSY breaking F_X term, so that the trilinear interactions are given by

$$a_{ij} \;\sim\; m_{3/2}\,(2n_{ij}+1)\,Y_{ij}. \tag{6.12}$$

The distinct prefactors, $\sim n_{ij}$, in the entries of the trilinear matrix make it *not proportional* to the Yukawa matrix, as advertised.
We can apply this to an explicit $SU(5)$-inspired pattern for the $U(1)_f$ charges of the SM fermions: $(Q_3,0)$, $(Q_2,2)$, $(Q_1,3)$, $(\overline{d}_3,0)$, $(\overline{d}_2,0)$, $(\overline{d}_1,1)$, $(\overline{u}_3,0)$, $(\overline{u}_2,2)$, $(\overline{u}_1,3)$. Given these charges, the Yukawa matrices are given by

$$\mathbf{Y_u} \sim y_t \begin{pmatrix} e\varepsilon^6 & \varepsilon^5 & \varepsilon^3 \\ \varepsilon^5 & d\varepsilon^4 & \varepsilon^2 \\ \varepsilon^3 & \varepsilon^2 & 1 \end{pmatrix}, \qquad \mathbf{Y_d} \sim y_b \begin{pmatrix} e'\varepsilon^4 & f'\varepsilon^3 & f\varepsilon^3 \\ \varepsilon^3 & d'\varepsilon^2 & h\varepsilon^2 \\ \varepsilon & k' & k \end{pmatrix}, \tag{6.13}$$

where we have taken the liberty to add $\mathcal{O}(1)$ coefficients in the different entries to reproduce the observed masses and mixings.[3] Using $\varepsilon = \lambda_C = 0.225$ as the expansion parameter and choosing $e = 1.1$, $e' = 1.8$, $d = 4.0$, $d' = 0.90$, $f = 1.3$, $f' = 0.82$, $h = 1.3$, $k = 0.69$ and $k' = 1.2$ gives a good fit to the measured quark masses, reproduces correctly the Cabibbo block of the CKM matrix and approximates the smaller CKM elements. Assuming the same $\mathcal{O}(1)$ coefficients appear in the graphs generating the trilinear couplings, we would obtain

$$\mathbf{a_u} \sim m_{3/2}\; y_t \begin{pmatrix} 13e\varepsilon^6 & 11\varepsilon^5 & 7\varepsilon^3 \\ 11\varepsilon^5 & 9d\varepsilon^4 & 5\varepsilon^2 \\ 7\varepsilon^3 & 5\varepsilon^2 & 1 \end{pmatrix} \qquad \mathbf{a_d} \sim m_{3/2}\; y_b \begin{pmatrix} 9e'\varepsilon^4 & 7f'\varepsilon^3 & 7f\varepsilon^3 \\ 7\varepsilon^3 & 5d'\varepsilon^2 & 5h\varepsilon^2 \\ 3\varepsilon & k' & k \end{pmatrix}$$

To get a sense for the flavour violation induced by this mismatch in order one coefficients, we must go to the Super-CKM (SCKM) basis[4], where the Yukawas are diagonal and in which $\mathbf{a_u}$ and $\mathbf{a_d}$ take the form

[3] This freedom is a general feature of Abelian models, and can be motivated by modifying our simplified superpotential to allow distinct $\mathcal{O}(1)$ couplings for each term.

[4] In principle, we should first redefine the fields and obtain canonical kinetic terms as discussed

$$\mathbf{a_u} \;\to\; U_u A_u V_u^\dagger \;\approx\; m_{3/2}\; y_t \begin{pmatrix} 14.6\varepsilon^6 & 10.9\varepsilon^5 & 7\varepsilon^3 \\ 10.9\varepsilon^5 & 35.9\varepsilon^4 & 4.9\varepsilon^2 \\ 7\varepsilon^3 & 4.9\varepsilon^2 & 1 \end{pmatrix}$$

$$\mathbf{a_d} \;\to\; U_d A_d V_d^\dagger \;\approx\; m_{3/2}\; y_b \begin{pmatrix} 11.3\varepsilon^4 & 4\varepsilon^3 & 6.5\varepsilon^3 \\ 4.9\varepsilon^3 & 3.2\varepsilon^2 & 4.3\varepsilon^2 \\ 2.1\varepsilon & 0.86 & 0.49 \end{pmatrix}$$

We see that indeed large flavour violating entries can be expected in the trilinear matrices of the low energy effective theory, even starting with completely universal soft terms in the full theory. This non-universality can constrain strongly the allowed squark and gluino masses of the model.
In addition to generating the Yukawa and trilinear interactions, integrating over the heavy mediators will also give new off-diagonal contributions to the Kähler function,

$$K \;=\; \psi_i^\dagger \psi_j \left(\delta_{ij} + c_{ij} \;+\; (\delta_{ij} + b_{ij}) \frac{X X^\dagger}{M_{\rm Pl}^2} + \text{c.c.} + \dots \right), \tag{6.14}$$

where the coefficients c_{ij} encode the supersymmetric off-diagonal entries in the kinetic terms while the b_{ij} give rise to the soft-breaking masses; the ellipses denote terms of higher order. The mismatch between the wave-function renormalization $(\delta_{ij} + c_{ij})$ and the soft masses $(\delta_{ij} + b_{ij})$ can again be calculated by drawing the appropriate supergraphs. Looking at Figure 6.5, for example, and remembering that the super-propagator of the mediator gives a factor of M^{-2} (left-right, uncrossed propagator) or M^{-1} (left-left or right-right, crossed propagator), it is tempting to guess that for the Kähler function, the leading corrections are proportional to $\varepsilon^{q_{ij}}$, where $q_{ij} = |q_i - q_j|$. This guess is indeed true, except for the special case of $q_{ij} = 1$. Given that our superpotential does not include direct couplings between the SM superfields ψ_q and the mediators $\bar{\chi}_{-q}$, one can only generate such a mixing through the supergraph of Figure 6.7, at the cost of a higher ε dependence than naively expected. Taking this subtlety into account, we find explicitly that

below. However, it can be shown that these fiels redefinitions introduce only subleading corrections in ε [211].

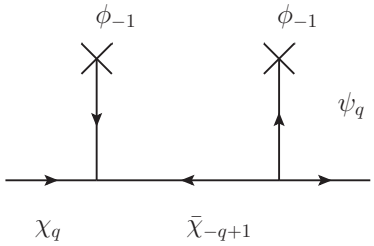

Figure 6.7: Supergraph giving an effective coupling between the messengers and the SM fields. Such a term is always present but in general gives only higher order ε corrections to the Kähler function.

$$c_{ij} \sim \begin{cases} (q_{ij}-1)\varepsilon^{q_{ij}} & \text{for } q_{ij} \geq 2 \\ 2\varepsilon^3 & \text{for } q_{ij} = 1 \\ \varepsilon^2 & \text{for } q_{ij} = 0\,. \end{cases} \tag{6.15}$$

where we included the leading correction to the diagonal terms that comes from the diagram with a single mediator super-propagator and two ϕ's, while the form of the coefficient for the off-diagonal terms stems from the number of different diagrams that can be drawn which contain only a single left-right super-propagator for the mediators.

For the soft masses, as remarked in the previous section, we will have $b_{ij} = Nc_{ij}$, where N is the number of SUSY breaking insertions, $X^\dagger X/M_{\rm Pl}^2$, we can make for a given supergraph. The counting for the number of possible insertions is straightforward. For a given supergraph contributing to the Kähler function, without increasing the powers of the flavour mediator mass, M, in the denominator, we can only insert $X^\dagger X/M_{\rm Pl}^2$ in the left-right propagator. However, there is also the possibility of inserting $X^\dagger$ in the single W^* vertex, with $(q_{ij}-1)$ options to insert the X in the remaining W vertices (see Figure 6.6). This gives $N = (q_{ij}-1)+1 = q_{ij}$ possibilities. Again, the subtlety for the case $q_{ij} = 1$ requires the additional mass insertion of Figure 6.7, so that in total we find,

$$N = \begin{cases} q_{ij} & \text{for } q_{ij} \geq 2 \\ 3 & \text{for } q_{ij} = 1 \\ 2 & \text{for } q_{ij} = 0\,. \end{cases} \tag{6.16}$$

An explicit example, using the same $SU(5)$-inspired charge assignment as before, would give the same coefficients c_{ij} and b_{ij} for Q, $\overline{u}$ and $\overline{d}$,

$$c_{ij}^{(Q,\overline{u},\overline{d})} = \begin{pmatrix} \varepsilon^2 & 2\varepsilon^3 & 2\varepsilon^3 \\ 2\varepsilon^3 & \varepsilon^2 & \varepsilon^2 \\ 2\varepsilon^3 & \varepsilon^2 & \varepsilon^2 \end{pmatrix} \qquad b_{ij}^{(Q,\overline{u},\overline{d})} = \begin{pmatrix} 2\varepsilon^2 & 6\varepsilon^3 & 6\varepsilon^3 \\ 6\varepsilon^3 & 2\varepsilon^2 & 2\varepsilon^2 \\ 6\varepsilon^3 & 2\varepsilon^2 & 2\varepsilon^2 \end{pmatrix} \tag{6.17}$$

Again, they are not proportional. One can see this explicitly by canonically normalizing the fields and diagonalizing the matrices $\delta_{ij} + c_{ij}$. As remarked in [211], this can always be achieved by an upper-triangular matrix T such as $\psi' = T\psi$

$$T = \begin{pmatrix} 1 + \frac{\varepsilon^2}{2} & 2\varepsilon^3 & 2\varepsilon^3 \\ 0 & 1 + \frac{\varepsilon^2}{2} & \varepsilon^2 \\ 0 & 0 & 1 + \frac{\varepsilon^2}{2} \end{pmatrix} \tag{6.18}$$

Aside from giving higher-order ε corrections to the Yukawa matrices, $Y \to (T^{-1})^\dagger Y T^{-1}$, this will give the soft masses in the canonical basis, $(m^2_{\text{soft}})_{ij} \equiv m^2_{3/2}(\delta_{ij} + b_{ij})$,

$$(m^2_{\text{soft}})_{ij} \to (T^{-1})^\dagger (m^2_{\text{soft}})_{ij} T^{-1} \sim m^2_{3/2} \begin{pmatrix} 1 + \varepsilon^2 - \frac{7}{4}\varepsilon^4 & 4\varepsilon^3 & 4\varepsilon^3 \\ 4\varepsilon^3 & 1 + \varepsilon^2 - \frac{7}{4}\varepsilon^4 & \varepsilon^2 - \frac{7}{4}\varepsilon^4 \\ 4\varepsilon^3 & \varepsilon^2 - \frac{7}{4}\varepsilon^4 & 1 + \varepsilon^2 - \frac{19}{4}\varepsilon^4 \end{pmatrix}$$

and due to the mismatch in the order one coefficients of c_{ij} and b_{ij}, off-diagonal entries in the soft masses remain after canonical normalization.[5]

6.2.2 $SU(3)_f$ Model

The situation is slightly different in the case of non-Abelian symmetries such as $SU(3)_f$, with flavon fields transforming as either a **3** or $\overline{\mathbf{3}}$. In this case, we must introduce several species of mediator fields, both singlets and triplets under $SU(3)_f$. We consider only $SU(2)_L$ singlet mediators, which always couple through a flavon to the right-handed SM fields and through the Higgs to the left-handed fields.
As an illustrative example, we take the model of I. de Medeiros Varzielas and G. G. Ross in [217], supplemented by the appropriate mediator sector. With the fields specified in Tables 6.1 and 6.2 from [217], the superpotential would be

[5] To compare with the usual mass insertion bounds present in the literature, one would need to go to the SCKM basis, *i.e.*, the basis of diagonal Yukawa couplings.

Field	ψ	$\bar{\psi}$	H	Σ	$\bar{\phi}_3$	$\bar{\phi}_{23}$	$\bar{\phi}_{123}$
R	1	1	0	0	0	0	0
U(1)	0	0	-4	2	2	1	3
$\mathbf{SU(3)}_f$	**3**	**3**	**1**	**1**	$\bar{\mathbf{3}}$	$\bar{\mathbf{3}}$	$\bar{\mathbf{3}}$

Table 6.1: Transformation of the matter superfields under the $SU(3)$ family symmetries.

Field	$\bar{\chi}_1$	χ_{-1}	$\bar{\chi}_2$	χ_{-2}	$\bar{\chi}_3$	χ_{-3}	$\bar{\chi}^k_4$	$\chi_{-4,k}$	$\chi_{-3,k}$	$\chi_{-5,k}$
R	1	1	1	1	1	1	1	1	1	1
U(1)	1	-1	2	-2	3	-3	4	-4	-3	-5
$\mathbf{SU(3)}_f$	**1**	**1**	**1**	**1**	**1**	**1**	$\bar{\mathbf{3}}$	**3**	**3**	**3**

Table 6.2: Transformation of the mediator superfields under the $SU(3)$ family symmetries.

$$
\begin{aligned}
W \;=\;& g\Big(\psi_i\,\bar{\chi}^i_4\,H + \chi_{-4,i}\,\bar{\chi}_1\,\bar{\phi}^i_{123} + \chi_{-4,i}\,\bar{\chi}_2\,\bar{\phi}^i_3 + \chi_{-4,i}\,\bar{\chi}_3\,\bar{\phi}^i_{23} + \chi_{-3}\,\bar{\chi}_1\,\Sigma \\
&\quad + \chi_{-3}\,\bar{\psi}_i\,\bar{\phi}^i_{123} + \chi_{-1}\,\bar{\psi}_i\,\bar{\phi}^i_{23} + \chi_{-2}\,\bar{\psi}_i\,\bar{\phi}^i_3 + \bar{\chi}_3\,\chi_{-5,i}\,\bar{\phi}^i_3 \\
&\quad + \bar{\chi}_2\,\chi_{-5,i}\,\bar{\phi}^i_{123} + \bar{\chi}_1\,\chi_{-3,i}\,\bar{\phi}^i_3 + \bar{\chi}_2\,\chi_{-3,i}\,\bar{\phi}^i_{23}\Big) \\
&+ M_u\Big(\chi^u_1\,\bar{\chi}^u_{-1} + \chi^u_2\,\bar{\chi}^u_{-2} + \chi^u_3\,\bar{\chi}^u_{-3} + \bar{\chi}^{u,i}_3\,\chi^u_{-3,i} + \bar{\chi}^{u,i}_4\,\chi^u_{-4,i} + \bar{\chi}^{u,i}_5\,\chi^u_{-5,i}\Big) \\
&+ M_d\Big(\chi^d_1\,\bar{\chi}^d_{-1} + \chi^d_2\,\bar{\chi}^d_{-2} + \chi^d_3\,\bar{\chi}^d_{-3} + \bar{\chi}^{d,i}_3\,\chi^d_{-3,i} + \bar{\chi}^{d,i}_4\,\chi^d_{-4,i} + \bar{\chi}^{d,i}_5\,\chi^d_{-5,i}\Big)
\end{aligned}
$$

suppressing the u and d indices on ψ and H, and where the flavons, $\bar{\phi}_3$, $\bar{\phi}_{23}$ and $\bar{\phi}_{123}$, are labelled with a subscript indicating the field component whose vev is non-zero. The messenger subscripts denote their charges under an additional $U(1)$ present in the superpotential, and we neglect contributions from the $SU(2)_L$ doublet-mediators, which are assumed to be much heavier.

The flavour symmetry is spontaneously broken in two steps: first $SU(3)_f \to SU(2)_f$, followed by the breaking of the residual $SU(2)_f$. We assume the following alignment of the flavon vevs

$$
\begin{aligned}
\langle\bar{\phi}_3\rangle &= \begin{pmatrix} 0 & 0 & 1 \end{pmatrix} \otimes \begin{pmatrix} \alpha_u & 0 \\ 0 & \alpha_d \end{pmatrix} \\
\langle\bar{\phi}_{23}\rangle &= \begin{pmatrix} 0 & \beta & -\beta \end{pmatrix} \\
\langle\bar{\phi}_{123}\rangle &= \begin{pmatrix} \gamma & \gamma & \gamma \end{pmatrix}
\end{aligned}
\tag{6.19}
$$

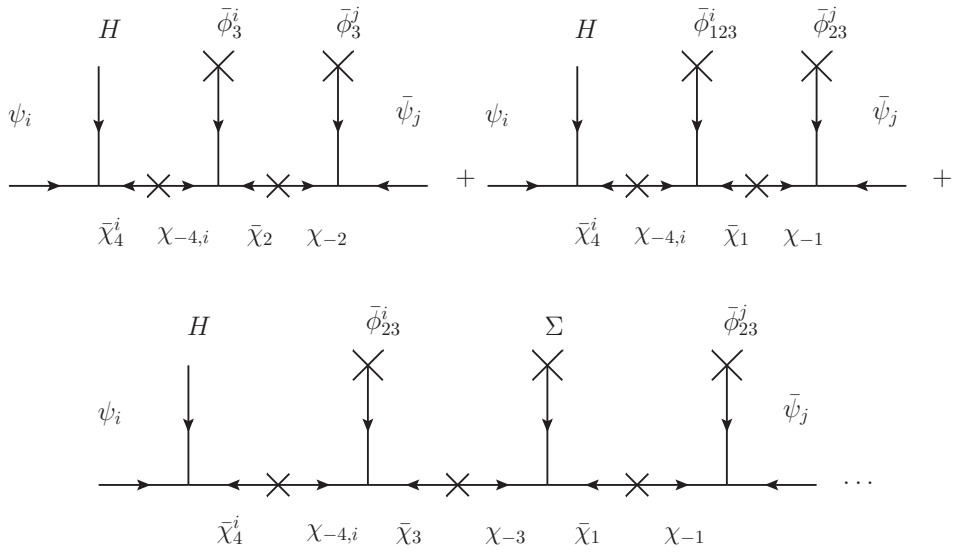

Figure 6.8: Contributions to the effective Yukawa couplings for the $SU(3)_f$ model in superfield notation.

where $\bar{\phi}_3$ transforms as a $\mathbf{3} \oplus \mathbf{1}$ under $SU(2)_R$, obtaining different vevs in the up (α_u) and down (α_d) sectors, while $\bar{\phi}_{23}$ and $\bar{\phi}_{123}$ are $SU(2)_R$ singlets; the vevs are assumed hierarchical, $\gamma \ll \beta \ll \alpha_u,\, \alpha_d$.

When the flavour symmetry is broken, the effective Yukawa couplings arise as the result of integrating out the heavy messengers in processes like those represented in Figure 6.8. For instance, the dominant contribution to Y_{33} will come from the first diagram, whereas the remaining terms in the 2×3 block will arise mostly from the third diagram. Similarly, Y_{12} and Y_{21} will be effectively generated by the second diagram and the analogous diagram obtained by changing the order of $\bar{\phi}_{23}$ and $\bar{\phi}_{123}$. The resulting Yukawa matrices are then

$$\mathbf{Y_u} \sim y'_t \begin{pmatrix} 0 & f\,\varepsilon_u^2\,\varepsilon_d & -f'\,\varepsilon_u^2\,\varepsilon_d \\ f\,\varepsilon_u^2\,\varepsilon_d & -\frac{2}{3}\,d\,\varepsilon_u^2 & \frac{2}{3}\,e\,\varepsilon_u^2 \\ -f'\,\varepsilon_u^2\,\varepsilon_d & \frac{2}{3}\,e\,\varepsilon_u^2 & 1 \end{pmatrix}$$

$$\mathbf{Y_d} \sim y'_b \begin{pmatrix} 0 & h\,\varepsilon_d^3 & -k\,\varepsilon_d^3 \\ h\,\varepsilon_d^3 & l\,\varepsilon_d^2 & -k'\,\varepsilon_d^2 \\ -k\,\varepsilon_d^3 & -k'\,\varepsilon_d^2 & 1 \end{pmatrix}$$

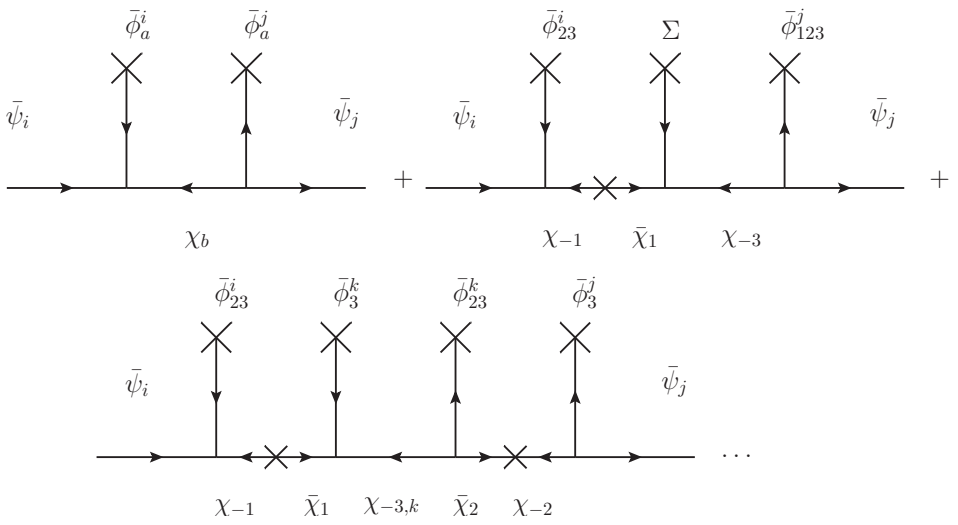

Figure 6.9: Contributions to the Kähler couplings in the $SU(3)_f$ model induced by integrating out the heavy mediator superfields.

where $\frac{\alpha_u}{M_u} \simeq \frac{\alpha_d}{M_d} \simeq 0.7 \equiv \alpha$, $\varepsilon_f \equiv \frac{\beta}{M_f}$, with $\varepsilon_d \simeq 3\,\varepsilon_u \sim 0.15$, $\frac{\gamma}{M_d} = \varepsilon_d^2$ and $\langle\Sigma\rangle/M_d \simeq \mathcal{O}(1)$ whereas $\langle\Sigma\rangle/M_u \simeq -2/3\,\langle\Sigma\rangle/M_d$. The couplings y'_t and y'_b refer to the top and bottom Yukawa couplings before rotating the matrices to the canonical basis. Again, we allow for order one coefficients in the Yukawa matrices in order to reproduce quark masses and the CKM matrix. Here, they are chosen to be: $f = 0.33$, $f' = 1.0$, $d = 1.62$, $e = 1.0$, $h = 1.14$, $k = 1.0$, $k' = 1.0$ and $l = 0.74$.
Once we know the diagrams which contribute to each effective Yukawa coupling, we may calculate the trilinear matrices, which are found to be

$$a_u \sim m_{3/2}\, y'_t \begin{pmatrix} 0 & 5\,f\,\varepsilon_u^2\,\varepsilon_d & -5\,f'\,\varepsilon_u^2\,\varepsilon_d \\ 5\,f\,\varepsilon_u^2\,\varepsilon_d & -\frac{14}{3}\,d\,\varepsilon_u^2 & \frac{14}{3}\,e\,\varepsilon_u^2 \\ -5\,f'\,\varepsilon_u^2\,\varepsilon_d & \frac{14}{3}\,e\,\varepsilon_u^2 & 5 \end{pmatrix}$$

$$a_d \sim m_{3/2}\, y'_b \begin{pmatrix} 0 & 5\,h\,\varepsilon_d^3 & -5\,k\,\varepsilon_d^3 \\ 5\,h\,\varepsilon_d^3 & 7\,l\,\varepsilon_d^2 & -7\,k'\,\varepsilon_d^2 \\ -5\,k\,\varepsilon_d^3 & -7\,k'\,\varepsilon_d^2 & 5 \end{pmatrix} \tag{6.20}$$

Going to the SCKM basis, after canonical normalization of the fields the trilinear matrices are given by

$$\mathbf{a_u} \longrightarrow U_u.A_u.V_u^\dagger \sim m_{3/2}\, y_t \begin{pmatrix} 0.3\,\varepsilon_u^2\,\varepsilon_d^2 & -0.7\,\varepsilon_u^2\,\varepsilon_d & 0.3\,\varepsilon_u^2\,\varepsilon_d \\ -0.7\,\varepsilon_u^2\,\varepsilon_d & -7.6\,\varepsilon_u^2 & \varepsilon_u^2 \\ 0.4\,\varepsilon_u^2\,\varepsilon_d & 1.3\,\varepsilon_u^2 & 5.0 \end{pmatrix}$$

$$\mathbf{a_d} \longrightarrow U_d.A_d.V_d^\dagger \sim m_{3/2}\, y_b \begin{pmatrix} -5.3\,\varepsilon_d^4 & -2.3\,\varepsilon_d^3 & 2.3\,\varepsilon_d^3 \\ -2.3\,\varepsilon_d^3 & 5.2\,\varepsilon_d^2 & -1.5\,\varepsilon_d^2 \\ 3.1\,\varepsilon_d^3 & -2.0\,\varepsilon_d^2 & 5.0 \end{pmatrix} \tag{6.21}$$

For the soft masses, the structure of the Kähler potential in the effective theory is given by Eq. (6.14), where as before, b_{ij} encodes the flavour effects in the soft masses while c_{ij} gives the form of the kinetic terms. Under our assumption that the $SU(2)_L$ doublet-messengers are much heavier than their singlet counterparts, their effects in the soft masses of the left-handed SM fields will be negligible; we therefore focus on the right-handed fields.

The leading supergraphs can be found in Figure 6.9. The first row of Figure 6.9 gives the dominant diagrams which contribute to the coefficients c_{ij}, while the second gives a subleading diagram which is supressed by α^2. In addition, these diagrams will always have α^{2n} corrections resulting from inserting pairs of $\bar{\phi}_3$ fields with the flavour indices contracted internally. These corrections can be factored out, amounting to a global rescaling of the fields that plays no role here. Taking all this into account, we obtain

$$c_{ij}^u \simeq \begin{pmatrix} \varepsilon_u^2\,\varepsilon_d^2 & -2\varepsilon_u^3 & 2\varepsilon_u^3 \\ -2\varepsilon_u^3 & \varepsilon_u^2 & -(1+\alpha^2)\varepsilon_u^2 \\ 2\varepsilon_u^3 & -(1+\alpha^2)\varepsilon_u^2 & \alpha^2 \end{pmatrix}$$

$$c_{ij}^d \simeq \begin{pmatrix} \varepsilon_d^4 & \varepsilon_d^3 & -\varepsilon_d^3 \\ \varepsilon_d^3 & \varepsilon_d^2 & -(1+\alpha^2)\varepsilon_d^2 \\ -\varepsilon_d^3 & -(1+\alpha^2)\varepsilon_d^2 & \alpha^2 \end{pmatrix}$$

Now, inserting the $XX^\dagger$ vertex in every possible position within the previous diagrams we can calculate the coefficients b_{ij}, which are found to be

$$b^u_{ij} \simeq \begin{pmatrix} 2\varepsilon_u^2\,\varepsilon_d & -6\varepsilon_u^3 & 6\varepsilon_u^3 \\ -6\varepsilon_u^3 & 2\varepsilon_u^2 & -(2+5\alpha^2)\varepsilon_u^2 \\ 6\varepsilon_u^3 & -(2+5\alpha^2)\varepsilon_u^2 & 2\alpha^2 \end{pmatrix}$$

$$b^d_{ij} \simeq \begin{pmatrix} 2\varepsilon_d^4 & 3\varepsilon_d^3 & -3\varepsilon_d^3 \\ 3\varepsilon_d^3 & 2\varepsilon_d^2 & -(2+5\alpha^2)\varepsilon_d^2 \\ -3\varepsilon_d^3 & -(2+5\alpha^2)\varepsilon_d^2 & 2\alpha^2 \end{pmatrix} \tag{6.22}$$

As before, knowing b_{ij}, the soft mass matrices are given by $(m^2_{\rm soft})_{ij} = m^2_{3/2}(\delta_{ij}+b_{ij})$. Then, the fields should be redefined first in the canonical basis and then in the SCKM basis. Finally, after these field redefinitions, the expression for the soft mass matrices for $\bar{u}$ and $\bar{d}$ will be

$$\left(m^2_{\rm soft}\right)_{\bar{u}} \simeq m^2_{3/2} \begin{pmatrix} 1+0.1\,\varepsilon_d^2 & -4\;\varepsilon_u^3 & 3\;\varepsilon_u^3 \\ -4\;\varepsilon_u^3 & 1+\varepsilon_u^2 & -3\;\varepsilon_u^2 \\ 3\;\varepsilon_u^3 & -3\;\varepsilon_u^2 & 1.3 \end{pmatrix}$$

$$\left(m^2_{\rm soft}\right)_{\bar{d}} \simeq m^2_{3/2} \begin{pmatrix} 1+2\;\varepsilon_d^4 & 0.5\;\varepsilon_d^3 & 2\;\varepsilon_d^3 \\ 0.5\;\varepsilon_d^3 & 1+3\;\varepsilon_d^2 & -2\;\varepsilon_d^2 \\ 2\;\varepsilon_d^3 & -2\;\varepsilon_d^2 & 1.3 \end{pmatrix}. \tag{6.23}$$

6.3 Flavour Phenomenology

In the previous sections, we obtained the soft-breaking matrices in two flavour symmetric models by simply assuming they were generated by the same mechanism responsible for generating the Yukawa couplings. Although these structures are to some extent dependent on the mediator sector, we have seen that integrating out the heavy mediator fields always generates non-universalities in the soft terms. In these flavour models, the structures of the soft matrices are fixed by symmetry, no longer unknowns of the (124-)SUSY model, but *predictions*.

Models in this spirit provide a new point of view for the phenomenology of flavour-supersymmetric models. Effectively, we have only the four parameters of the usual constrained MSSM, with m_0, $m_{1/2}$, $\tan\beta$ and $\mathrm{sgn}(\mu)$ serving as inputs, the order of

magnitude of the others being fixed by the flavour symmetry.[6] Our aim is therefore not to constrain the flavour violating entries as functions of the sfermion masses, but rather to constrain the sfermion masses of the model using flavour observables, checking whether these constraints are competitive with direct LHC searches.

To this end, we assume that the flavour symmetry is broken at a high scale of order $M_{\rm GUT}$, where the effective soft-breaking matrices are generated. These matrices must then be run using the MSSM renormalization group equations (RGE), in order to obtain the soft-breaking matrices at the electroweak scale and compared with the experimental constraints at low energies. The main effects of the RGE evolution are large contributions of order $\sim -2m_{1/2}$ to the diagonal elements in the trilinear matrices of the first two generations, with slightly smaller contributions to the third generation (stop) entries. The diagonal elements of the soft-mass matrices receive a large gluino contribution of order $\sim 6m_{1/2}^2$. On the other hand, off-diagonal entries in these matrices mostly remain unchanged by the running (possible exceptions are entries with $\mathcal{O}(1)$ Yukawa couplings) [218–221].

As an example of these ideas, we may apply the constraints provided by flavour observables to the toy $U(1)_f$ model of Section 6.2.1. In this model, all squark soft mass matrices, $m_{\tilde{Q}}^2$, $m_{\tilde{u}}^2$ and $m_{\tilde{d}}^2$ have similar non-universal structures given by Eq. (6.19), while the trilinear couplings, A_u and A_d also have sizeable off-diagonal entries as displayed in Eq. (6.14). After RGE evolution, the corresponding matrices at the electroweak scale can be extracted, and the off-diagonal elements compared with the usual Mass Insertion (MI) bounds [222–225]. Taking a fixed squark mass scale, we find that the best observables for this model are the ones associated with transitions between the first and second generations, *i.e.*, Δm_K and, if we take into account possible $\mathcal{O}(1)$ phases in these matrices, ε_K and ε'/ε [226]. To show the power of flavour observables in this $U(1)_f$ model, we will simply take the constraints from Δm_K.[7]

Although flavour symmetries fix the orders of magnitude of different entries in the soft-breaking matrices in powers of ε, unless we completely define the mediator sector, we cannot predict the $\mathcal{O}(1)$ coefficients. In particular, as we do not know the sign (phase) of these entries, both constructive or destructive interference with the SM contribution are possible. Taking a conservative approach following [224], we require that any supersymmetric contribution, (including both different mass insertions and additional supersymmetric particles such as the gluino and chargino), to a given observable must be smaller than the measured experimental value. In this way, we

[6] Due to our ignorance of the gauge kinetic function at $M_{\rm Pl}$, we take $m_{1/2}$ to be independent from $m_0 = m_{3/2}$.

[7] A full analysis using all available flavour observables is to appear in a future publication [227].

obtain the results given in Figure 6.10. Here, we consider only the dominant contribution given by the gluino, with $(\delta_{12})_{\mathrm{LL}} \times (\delta_{12})_{\mathrm{RR}}$ interference.
The region in red (darker shade) is excluded from Δm_K, while the region in grey (lighter rectangular shade) is ruled out from direct gluino searches [190, 191, 193–195, 197]. The contours in black give an estimate for the average squark masses, obtained from the approximate one-loop RGE relation $m_{\tilde{q}}^2 \sim 6m_{1/2}^2 + m_{3/2}^2$. As can be seen from the figure, the experimental bounds from Δm_K can be competitive with direct searches for a large range of gluino and gravitino masses for this simple $U(1)$ flavour symmetry. Taken in conjunction with the direct gluino bounds, the flavour constraints in the $U(1)_f$ model can also push up the lower bound for the gluino and squark masses as a function of $m_{3/2}$. The fact that the bounds are stronger for larger $m_{3/2}$ is simply due to the flavour-changing entries being proportional to $m_{3/2}$ and having taken the gluino mass independent from $m_{3/2}$. For the particular case of $m_{1/2} = m_{3/2}$ at M_{Pl}, we have $m_{\tilde{g}} \simeq 2.7 m_{3/2}$ and thus flavour bounds would require $m_{\tilde{g}}, m_{\tilde{q}} \gtrsim 2.1$ TeV, improving significantly bounds from direct searches in the $U(1)_f$ scenario. These bounds would be much stronger if these off-diagonal entries had sizeable imaginary parts and we were to apply the limits from ε_K.
We can apply the same procedure to the $SU(3)_f$ model. In this case, as we have taken the left-handed mediator masses $M_L \gg M_u, M_d$, we can neglect the flavour non-universality in $m_{\tilde{Q}}^2$, considering only $m_{\tilde{d}}^2$ and $m_{\tilde{u}}^2$ apart from the trilinear couplings A_u and A_d.
As before, the most sensitive observables are still Δm_K and ε_K, although the bounds from Δm_K are much weaker due to the absence of the left-handed mass insertions, which in the $U(1)$ model give the largest contribution to Δm_K through a mixed term $(\delta_{12})_{\mathrm{LL}}(\delta_{12})_{\mathrm{RR}}$. The dominant contribution is now given by the gluino with $(\delta_{12})_{\mathrm{LR}}^2 + (\delta_{12})_{\mathrm{RL}}^2$ mass insertions. In this case, Δm_K would exclude only a "small" region with $m_{\tilde{g}} \simeq m_{\tilde{q}} \lesssim 500$ GeV. However, if we assume that these flavour-changing entries have imaginary parts of $\mathcal{O}(1)$ [203, 228, 229], [8] we can apply the limits from ε_K. In this case, the bounds are much stronger and flavour limits can compete with direct LHC searches for the $SU(3)$ model as well. As we see, the $SU(3)_f$ model is safer than the $U(1)_f$ model, both due to the non-Abelian nature of the symmetry, which relates different generations, and to the small number of flavon insertions in the $SU(3)_f$ model, allowing flavour off-diagonal entries only at higher orders.
Although these bounds are model (and mediator) dependent, similar searches, using

[8] Sizeable phases in these mass matrices are found in models of spontaneous CP violation in the flavour sector [209, 210, 212] which naturally explain the presence of phases in the CKM matrix. However, due to re-phasing freedoms, the imaginary parts are typically subleading.

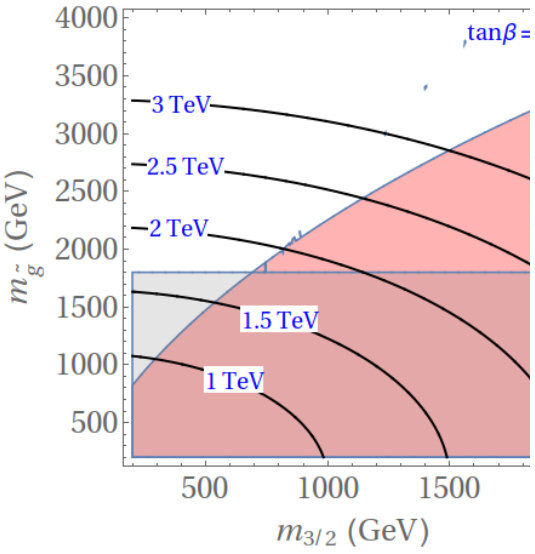

Figure 6.10: Δm_K exclusion plot for the toy $U(1)$ model of the previous section. Points in red (darker shade) exceed the current experimental bounds. The rectangle in gray (light rectangular shade) represents the direct bound on gluino masses from LHC searches and the black contours correspond to different values of the average squark masses. Although we have taken $\tan\beta = 2$ in this figure, the constraints are largely independent of $\tan\beta$.

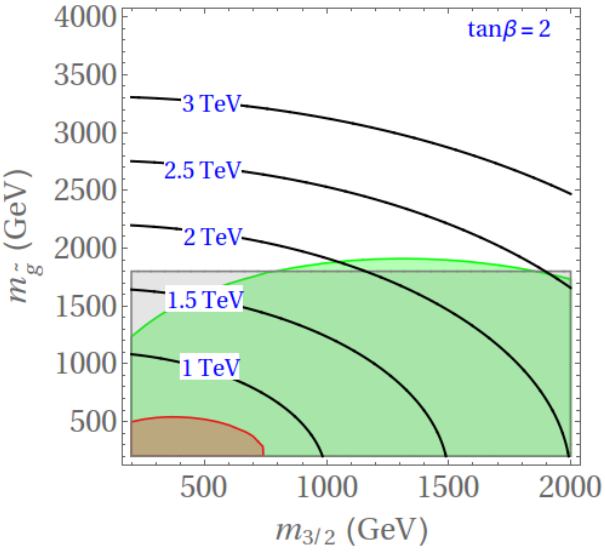

Figure 6.11: Δm_K (red/dark gray) and ε_K (green/light gray) exclusion plot for the $SU(3)_f$ model. Points in red (dark gray) or green (light gray) exceed the current experimental bounds. The rectangle in gray (shaded) represents the direct bound on gluino masses from LHC searches and the black contours correspond to different values of the average squark masses. Although we have taken $\tan\beta = 2$ in this figure, the constraints are largely independent of $\tan\beta$.

a complete set of flavour observables, may be applied to any supersymmetric flavour model. A more complete analysis of these effects for different flavour symmetries will be presented in a future work [227]. As we have shown for these simple models, these phenomenological studies may provide a very important tool in ruling out or discovering potential flavour symmetries.

6.4 Conclusions

The peculiar structure of the flavour sector remains one of the most puzzling and intriguing legacies of the SM. The question of whether these patterns arise from a deeper underlying theory, pointing the way to new physics, remains to be answered. Although the hope is that this will indeed be the case, it is clear that additional experimental inputs in the form of new observable flavour interactions would provide a clear boon towards unravelling this mystery.

New flavour interactions inherent in supersymmetric theories can provide an excellent laboratory in which to probe models where this underlying theory is governed by a flavour symmetry. Under our assumptions that the soft-breaking terms respect the flavour symmetry and that SUSY breaking is primarily communicated to the visible fields by gravity, these new flavour structures are calculable and governed by the flavour symmetry and the mediator sector of the underlying theory. The large number of parameters in the MSSM is thus vastly reduced.

The main result of this work is that even when the ultraviolet theory is flavour symmetric, the soft-terms of the effective theory below Λ_f can be strongly non-universal. We have demonstrated this explicitly in the case of two specific models: one with an Abelian $U(1)$ symmetry, the other an $SU(3)$.

As these effects are calculable, their phenomenological implications for flavour observables can in principle provide strong constraints on the parameter space of these models. In some cases, these constraints may be competitive with direct LHC searches. With the soft matrices given, indirect flavour measurements can provide a new tool to constrain parameters like the gluino mass or the average scale of the squark masses.

Unfortunately, these effects are model dependent, and an obvious extension of this work would be an application of these techniques to a representative set of popular flavour models available in the literature. This would require a more complete phenomenological analysis, taking into account all available flavour observables. We have also chosen to focus only on the quark sector, and it would be interesting to see whether these techniques can provide interesting constraints in lepton flavour models.

In highlighting these new sources of flavour violation, we hope to provide a new tool for tackling the flavour puzzle in one of the most well studied frameworks for new physics, SUSY.

A

Notation and conventions

A.1 Metric

The spacetime metric we use is

$$\eta_{\mu\nu} \;=\; \mathrm{diag}(-1,1,1,1)$$

The contravariant four-vector position and momentum of a particle are

$$x^\mu \;=\; (t,\, \overrightarrow{x}) \qquad\qquad p^\mu \;=\; (E,\, \overrightarrow{p})$$

So that $p^2 = -m^2$ for an on-shell particle of mass m.

A.2 Representation of γ matrices

We use the Weyl representation for the 4×4 gamma matrices

$$\gamma^\mu \;=\; \begin{pmatrix} 0 & \sigma^\mu \\ \overline{\sigma}^\mu & 0 \end{pmatrix} \qquad\qquad \gamma^5 \;=\; \begin{pmatrix} -\mathbf{1} & 0 \\ 0 & \mathbf{1} \end{pmatrix}$$

with $\sigma^\mu = (\mathbf{1}, \sigma^k)$, $\overline{\sigma} = (\mathbf{1}, -\sigma^k)$ and $\mathbf{1} = I_{2\times 2}$. The Pauli matrices are given by

$$\sigma^1 \;=\; \begin{pmatrix} 0 & 1 \\ 1 & 0 \end{pmatrix} \qquad \sigma^2 \;=\; \begin{pmatrix} 0 & -i \\ i & 0 \end{pmatrix} \qquad \sigma^3 \;=\; \begin{pmatrix} 1 & 0 \\ 0 & -1 \end{pmatrix}$$

A.3 Chirality projectors

The chirality projectors are defined as

$$P_R \;=\; \frac{1}{2}\left(\mathbf{1} + \gamma^5\right) \qquad\qquad P_L \;=\; \frac{1}{2}\left(\mathbf{1} - \gamma^5\right)$$

Note that, in this representation of the gamma matrices, every four-component Dirac spinor is directly written in terms of two two-component anticommuting Weyl spinors with opposite chirality, that is

$$\Psi_D \;=\; \begin{pmatrix} \psi_{L\,\alpha} \\ \psi_R^{\dot\alpha} \end{pmatrix}$$

And, indeed,

$$P_L\,\Psi_D \;=\; \begin{pmatrix} \psi_{L\,\alpha} \\ 0 \end{pmatrix} \qquad P_R\,\Psi_D \;=\; \begin{pmatrix} 0 \\ \psi_R^{\dot\alpha} \end{pmatrix}$$

with ψ_L and ψ_R the Weyl spinors. Besides, the Hermitian conjugate of any left-handed Weyl spinor is a right-handed Weyl spinor.

A.4 Antisymmetric symbol

The heights of the dotted and undotted spinor indices are important. The antisymmetric symbol defined as follows allow us to raise and lower indices

$$\epsilon^{\alpha\beta} \;=\; -\epsilon^{\beta\alpha} \;=\; -\epsilon_{\alpha\beta} \qquad \text{with} \qquad \epsilon^{12} = 1$$

Then

$$\psi^\alpha \;=\; \epsilon^{\alpha\beta}\,\psi_\beta \qquad \text{or} \qquad \psi_{\dot\alpha} \;=\; \epsilon_{\dot\alpha\dot\beta}\,\psi^{\dot\beta}$$

The Pauli matrices also carry spinor indices as $(\sigma^\mu)_{\alpha\dot\alpha}$ and $(\overline{\sigma}^\mu)^{\dot\alpha\alpha}$. As a convention, repeated indices are contracted

$$\psi^\alpha\,\xi_\alpha \;=\; \psi\xi \qquad \text{or} \qquad \psi_{\dot\alpha}\xi^{\dot\alpha} \;=\; \psi\xi$$

A.5 Dirac spinors

Given any expression involving four-component Dirac spinors, one can translate it into two-component Weyl spinor language. For instance, given the following conjugation of a Dirac spinor

$$\overline{\Psi}_D \;=\; \Psi_D^\dagger\,\gamma^0 \;=\; (\psi_R^\dagger \quad \psi_L^\dagger)$$

it can be shown that, for two Dirac spinors Ψ^a and Ψ^b

$$\begin{aligned} \overline{\Psi}^a\,P_L\,\Psi^b \;&=\; \psi_R^{a\dagger}\psi_L^b & \qquad \overline{\Psi}^a\,P_R\,\Psi^b \;&=\; \psi_L^{a\dagger}\psi_R^b \\ \overline{\Psi}^a\,\gamma^\mu P_L\,\Psi^b \;&=\; \psi_L^{a\dagger}\overline{\sigma}^\mu\psi_L^b & \qquad \overline{\Psi}^a\,\gamma^\mu P_R\,\Psi^b \;&=\; \psi_R^{a\dagger}\sigma^\mu\psi_R^b \end{aligned}$$

B

MSSM conventions

B.1 Chiral supermultiplets

In Section 1.3, when considering the particle content in the MSSM, we follow the standard convention in which all chiral supermultiplets should involve only left-handed Weyl fermions. Therefore, chirality-singlet supermultiplets such as E^{i}, D^{i} and U^{i} have as fermionic components the Hermitian conjugated of right-handed fermions $e_R^{i\dagger}$, $d_R^{i\dagger}$ and $u_R^{i\dagger}$, which are left-handed spinors (see Appendix A.3).

B.2 Sfermion couplings to neutral Higgses

In Section 2.2, the Higgs interactions with the MSSM spectrum are given. The *neutral Higgs-sfermion-sfermion* coulpings are written in Eq.(2.14) in terms of the rotation mass matrices and $\widetilde{\Gamma}^{\alpha ff}$. Here, the complete expressions for $\widetilde{\Gamma}^{\alpha}_{ff}$ in the case of third-generation squarks are collected. They are given in the weak basis $\left(\widetilde{f}_L, \widetilde{f}_R\right)$ [54]

$$\widetilde{\Gamma}^{1}_{\tilde{b}\tilde{b}} = \begin{pmatrix} -|y_b|^2\, v\, c_\beta + \frac{1}{4}\left(g_2^2 + \frac{1}{3}g_1^2\right) v\, c_\beta & -\frac{1}{\sqrt{2}}\, y_b^*\, a_b^* \\ -\frac{1}{\sqrt{2}}\, y_b\, a_b & -|y_b|^2\, v\, c_\beta + \frac{1}{6}\, g_1^2\, v\, c_\beta \end{pmatrix} \tag{B.1}$$

$$\widetilde{\Gamma}^{2}_{\tilde{b}\tilde{b}} = \begin{pmatrix} -\frac{1}{4}\left(g_2^2 + \frac{1}{3}\, g_1^2\right) v\, s_\beta & -\frac{1}{\sqrt{2}}\, y_b^*\, \mu \\ -\frac{1}{\sqrt{2}}\, y_b\, \mu^* & -\frac{1}{6}\, g_1^2\, v\, s_\beta \end{pmatrix} \tag{B.2}$$

$$\widetilde{\Gamma}^3_{\tilde{b}\tilde{b}} = \frac{1}{\sqrt{2}} \begin{pmatrix} 0 & -i\, h_b^* \,(s_\beta\, a_b^* + \mu\, c_\beta) \\ -i\, y_b\,(s_\beta\, a_b + c_\beta\, \mu^*) & 0 \end{pmatrix} \tag{B.3}$$

$$\widetilde{\Gamma}^1_{\tilde{t}\tilde{t}} = \begin{pmatrix} -\frac{1}{4}\left(g_2^2 - \frac{1}{3}\, g_1^2\right) v\, c_\beta & -\frac{1}{\sqrt{2}}\, y_t^*\, \mu \\ -\frac{1}{\sqrt{2}}\, y_t\, \mu^* & -\frac{1}{3}\, g_1^2\, v\, c_\beta \end{pmatrix} \tag{B.4}$$

$$\widetilde{\Gamma}^2_{\tilde{t}\tilde{t}} = \begin{pmatrix} -\left|y_t^2\right|\, v\, s_\beta + \frac{1}{4}\left(g_2^2 - \frac{1}{3} g_1^2\right) v\, s_\beta & -\frac{1}{\sqrt{2}}\, y_t^*\, a_t^* \\ -\frac{1}{\sqrt{2}}\, y_t\, a_t & -\left|y_t\right|^2 v\, s_\beta + \frac{1}{3}\, g_1^2\, v\, s_\beta \end{pmatrix} \tag{B.5}$$

$$\widetilde{\Gamma}^3_{\tilde{t}\tilde{t}} = \frac{1}{\sqrt{2}} \begin{pmatrix} 0 & i\, y_t^*\,(c_\beta\, a_t^* + s_\beta\, \mu) \\ -i y_t\,(c_\beta\, a_t + s_\beta\, \mu^*) & 0 \end{pmatrix} \tag{B.6}$$

B.3 Chargino mass matrix

Our convention for the diagonalization of the charginos mass matrix is the following: in the gauge-eigenstate basis $\psi^\pm = (\widetilde{W}^+, \widetilde{H}_u^+, \widetilde{W}^-, \widetilde{H}_d^-)$, the mass terms in the Lagrangian for the charginos are given by

$$\mathcal{L}_{\text{chargino mass}} = -\frac{1}{2}\, \psi^{\pm^T}\, \mathcal{M}_C\, \psi^\pm + \text{c.c.}$$

where the 4×4 mass matrix can be written in terms of 2×2 blocks as

$$\mathcal{M}_C = \begin{pmatrix} 0 & \mathbf{X}^T \\ \mathbf{X} & 0 \end{pmatrix}$$

where $\mathbf{X}$ is given by

$$\mathbf{X} = \begin{pmatrix} M_2 & \sqrt{2}\, M_W\, \sin\beta \\ \sqrt{2}\, M_W\, \cos\beta & \mu \end{pmatrix}$$

This matrix is diagonalised by two unitary 2×2 matrices $\mathbf{U}$ and $\mathbf{V}$,

$$\mathbf{U}^*\, \mathbf{X}\, \mathbf{V}^\dagger = \begin{pmatrix} m_{\chi_1^+} & 0 \\ 0 & m_{\chi_2^+} \end{pmatrix}$$

so that the mass eigenstates are related to the gauge eigenstates as

$$\begin{pmatrix} \chi_1^+ \\ \chi_2^+ \end{pmatrix} = \mathbf{V} \begin{pmatrix} \widetilde{W}^+ \\ \widetilde{H}_u^+ \end{pmatrix} \qquad \begin{pmatrix} \chi_1^- \\ \chi_2^- \end{pmatrix} = \mathbf{U} \begin{pmatrix} \widetilde{W}^- \\ \widetilde{H}_d^- \end{pmatrix}$$

For the interactive Lagrangian, Eq.(2.15), the four-component Dirac spinors in terms of mass-eigenstates are

$$\tilde{\chi}_1^- \equiv \begin{pmatrix} \chi_1^- \\ \chi_1^{+*} \end{pmatrix} \qquad \tilde{\chi}_2^- \equiv \begin{pmatrix} \chi_2^- \\ \chi_2^{+*} \end{pmatrix} \tag{B.7}$$

B.4 Charged Higgs couplings to neutral Higgses

In Eq.(2.19) the interactive Lagrangian between neutral and charged Higgses is given. The complete expressions for the couplings are presented here [54]

$$\begin{aligned} g_{\phi_d^0 H^+ H^-} &= 2\,\lambda_1\, s_\beta^2 c_\beta \;+\; \lambda_3\, c_\beta^3 \;-\; \lambda_4\, s_\beta^2 c_\beta \;-\; 2\,\Re e[\lambda_5]\, s_\beta^2 c_\beta \;+\; \Re e[\lambda_6]\, s_\beta (s_\beta^2 - 2c_\beta^2) \\ &+ \Re e[\lambda_7]\, s_\beta c_\beta^2 \end{aligned}$$

$$\begin{aligned} g_{\phi_u^0 H^+ H^-} &= 2\,\lambda_2\, c_\beta^2 s_\beta \;+\; \lambda_3\, s_\beta^3 \;-\; \lambda_4\, c_\beta^2 s_\beta \;-\; 2\,\Re e[\lambda_5]\, c_\beta^2 s_\beta \;+\; \Re e[\lambda_6]\, s_\beta^2 c_\beta \\ &+ \Re e[\lambda_7]\, c_\beta (c_\beta^2 - 2 s_\beta^2) \end{aligned}$$

$$g_{A^0 H^+ H^-} = 2\, s_\beta c_\beta \Im m[\lambda_5] \;-\; s_\beta^2 \Im m[\lambda_6] \;-\; \Im m[\lambda_7]$$

At tree-level, $\lambda_1 = \lambda_2 = -(g_1^2 + g_2^2)/8$, $\lambda_3 = -(g_2^2 - g_1^1)/4$, $\lambda_4 = g_2^2/2$ and $\lambda_5 = \lambda_6 = \lambda_7 = 0$. Beyond the leading order, these couplings receive corrections. In particular, radiative loops proportional to the stop and sbottom trilinear couplings emerge for λ_5-λ_7. In our analysis, two-loop analytic results were considered; they can be found in Appendix A of [52].

B.5 Threshold corrections to fermion couplings with the Higgs

The complete expression for the down-type quark threshold corrections that enter the effective Lagrangian in Eq.(2.20) are written here for the single-Higgs-insertion (SHI)

approximation. Up-type quarks and leptons corrections are completely symmetric to those given here. Their explicit expression as well as specific details regarding the formalism and calculation can be found in [64, 230, 231]. First, assuming flavour-diagonal soft SUSY-breaking terms

$$\begin{aligned}
\langle \mathbf{\Delta}_d^{\Phi_d^0} \rangle_0 &= -\mathbf{1}\,\frac{2\alpha_3}{3\pi}\,a_d\,M_3^*\,I\left(\widetilde{M}_Q^2,\widetilde{M}_D^2,|M_3|^2\right) + \mathbf{1}\,\frac{\alpha_1}{36\pi}a_d\,M_1^*\,I\left(\widetilde{M}_Q^2,\widetilde{M}_D^2,|M_1|^2\right) \\
&- \frac{\mathbf{Y}_u^\dagger\mathbf{Y}_u}{16\pi^2}\,|\mu|^2\,I\left(\widetilde{M}_Q^2,\widetilde{M}_U^2,|\mu|^2\right) + \mathbf{1}\,\frac{3\alpha_2}{8\pi}B_0\left(0,|M_2|^2,\widetilde{M}_Q^2\right) \\
&+ \mathbf{1}\,\frac{\alpha_1}{24\pi}B_0\left(0,|M_1|^2,\widetilde{M}_Q^2\right) + \mathbf{1}\,\frac{\alpha_1}{12\pi}\,B_0\left(0,|M_1|^2,\widetilde{M}_D^2\right)
\end{aligned}$$

$$\begin{aligned}
\langle \mathbf{\Delta}_d^{\Phi_u^0} \rangle_0 &= \mathbf{1}\,\frac{2\alpha_3}{3\pi}\,\mu^*\,M_3^*\,I\left(\widetilde{M}_Q^2,\widetilde{M}_D^2,|M_3|^2\right) - \mathbf{1}\,\frac{\alpha_1}{36\pi}\mu^*\,M_1^*\,I\left(\widetilde{M}_Q^2,\widetilde{M}_D^2,|M_1|^2\right) \\
&+ \frac{\mathbf{Y}_u^\dagger\mathbf{Y}_u}{16\pi^2}\,\mu^*\,a_u^*\,I\left(\widetilde{M}_Q^2,\widetilde{M}_U^2,|\mu|^2\right) - \mathbf{1}\,\frac{3\alpha_2}{8\pi}\mu^*\,M_2^*\,I\left(\widetilde{M}_Q^2,\widetilde{M}_D^2,|\mu|^2\right) \\
&- \mathbf{1}\,\frac{\alpha_1}{24\pi}\,\mu^*\,M_1^*\,I\left(\widetilde{M}_Q^2,|M_1|^2,|\mu|^2\right) - \mathbf{1}\,\frac{\alpha_1}{12\pi}\,\mu^*\,M_1^*\,I\left(\widetilde{M}_D^2,|M_1|^2,|\mu|^2\right)
\end{aligned} \tag{B.8}$$

Off-diagonal elements in the soft-breaking parameters also induce an additional source of flavour violation. In this case

$$\begin{aligned}
\langle \delta\mathbf{\Delta}_d^{\Phi_d^0} \rangle_0 &= -\frac{2\alpha_3}{3\pi}\,a_d\,M_3^*\left[\delta\widetilde{\mathbf{M}}_Q^2\,K\left(\widetilde{M}_Q^2,\widetilde{M}_D^2,|M_3|^2\right) + \mathbf{Y}_d^{-1}\delta\widetilde{\mathbf{M}}_D^2\mathbf{Y}_d\,K\left(\widetilde{M}_D^2,\widetilde{M}_Q^2,|M_3|^2\right)\right] \\
&- \frac{\alpha_3}{3\pi}\,\mathbf{Y}_d^{-1}\delta\mathbf{a}_d\,M_3^*\,I\left(\widetilde{M}_Q^2,\widetilde{M}_D^2,|M_3|^2\right) + \frac{\alpha_1}{36\pi}\mathbf{Y}_d^{-1}\delta\mathbf{a}_d\,M_1^*\,I\left(\widetilde{M}_Q^2,\widetilde{M}_D^2,|M_1|^2\right) \\
&+ \frac{\alpha_1}{36\pi}\,a_d\,M_1^*\left[\delta\widetilde{\mathbf{M}}_Q^2\,K\left(\widetilde{M}_Q^2,\widetilde{M}_D^2,|M_1|^2\right) + \mathbf{Y}_d^{-1}\delta\widetilde{\mathbf{M}}_D^2\mathbf{Y}_d\,K\left(\widetilde{M}_D^2,\widetilde{M}_Q^2,|M_1|^2\right)\right] \\
&- \frac{1}{16\pi^2}\,|\mu|^2\left[\mathbf{Y}_u^\dagger\delta\widetilde{\mathbf{M}}_U^2\mathbf{Y}_u\,K\left(\widetilde{M}_U^2,\widetilde{M}_Q^2,|\mu|^2\right) + \delta\widetilde{\mathbf{M}}_Q^2\mathbf{Y}_u^\dagger\mathbf{Y}_u\,K\left(\widetilde{M}_Q^2,\widetilde{M}_U^2,|\mu|^2\right)\right] \\
&+ \frac{3\alpha_2}{8\pi}\,\delta\widetilde{\mathbf{M}}_Q^2\,I\left(\widetilde{M}_Q^2,\left|\widetilde{M}_2\right|^2\right) - \frac{\alpha_1}{24\pi}\left[\delta\widetilde{\mathbf{M}}_Q^2\,I\left(\widetilde{M}_Q^2,|M_1|^2\right)\right. \\
&+ \left. 2\,\mathbf{Y}_d^{-1}\delta\widetilde{\mathbf{M}}_D^2\mathbf{Y}_d\,I\left(\widetilde{M}_D^2,|M_1|^2\right)\right] \\
\langle \delta\mathbf{\Delta}_d^{\Phi_u^0} \rangle_0 &= \frac{2\alpha_3}{3\pi}\,\mu^*\,M_3^*\left[\delta\widetilde{\mathbf{M}}_Q^2\,K\left(\widetilde{M}_Q^2,\widetilde{M}_D^2,|M_3|^2\right) + \mathbf{h}_d^{-1}\delta\widetilde{\mathbf{M}}_D^2\mathbf{h}_d\,K\left(\widetilde{M}_D^2,\widetilde{M}_Q^2,|M_3|^2\right)\right] \\
&- \frac{\alpha_1}{36\pi}\mu^*\,M_1^*\left[\delta\widetilde{\mathbf{M}}_Q^2\,K\left(\widetilde{M}_Q^2,\widetilde{M}_D^2,|M_1|^2\right) + \mathbf{h}_d^{-1}\delta\widetilde{\mathbf{M}}_D^2\mathbf{h}_d\,K\left(\widetilde{M}_D^2,\widetilde{M}_Q^2,|M_1|^2\right)\right] \\
&+ \frac{1}{16\pi^2}\,\mu^*\,A_u^*\left[\mathbf{h}_u^\dagger\delta\widetilde{\mathbf{M}}_U^2\mathbf{h}_u\,K\left(\widetilde{M}_U^2,\widetilde{M}_Q^2,|\mu|^2\right) + \delta\widetilde{\mathbf{M}}_Q^2\mathbf{h}_u^\dagger\mathbf{h}_u\,K\left(\widetilde{M}_Q^2,\widetilde{M}_U^2,|\mu|^2\right)\right] \\
&+ \frac{\delta\mathbf{a}_u^\dagger\mathbf{h}_u}{16\pi^2}\,\mu^*\,I\left(\widetilde{M}_Q^2,\widetilde{M}_U^2,|\mu|^2\right) - \frac{3\alpha_2}{8\pi}\,\mu^*M_2^*\delta\widetilde{\mathbf{M}}_Q^2\,K\left(\widetilde{M}_Q^2,\left|\widetilde{M}_2\right|^2,|\mu|^2\right) \\
&- \frac{\alpha_1}{24\pi}\,\mu^*\,M_1^*\delta\widetilde{\mathbf{M}}_Q^2\,K\left(\widetilde{M}_Q^2,|M_1|^2,|\mu|^2\right) \\
&- \frac{\alpha_1}{12\pi}\,\mu^*\,M_1^*\mathbf{h}_d^{-1}\delta\widetilde{\mathbf{M}}_D^2\mathbf{h}_d\,K\left(\widetilde{M}_D^2,|M_1|^2,|\mu|^2\right)
\end{aligned} \tag{B.9}$$

Loop functions are given in Appendix C

C

Loop functions

Loop functions associated with the non-logarithmic threshold corrections.

$$
\begin{aligned}
I\left(a,b,c\right) &= \frac{ab\,\ln\left(a/b\right)\,+\,bc\,\ln\left(b/c\right)\,+\,ac\,\ln\left(c/a\right)}{(a-b)(b-c)(a-c)} \\
K\left(a,b,c\right) &= \frac{b\ln\left(a/b\right)\,+\,c\ln\left(c/a\right)}{(a-b)(b-c)(a-c)}\,+\,\frac{\left(b+c-2a\right)I\left(a,b,c\right)+1}{(a-b)(a-c)} \\
B_0(0,a,b) &= 1\,-\,\ln\left(\frac{b}{Q^2}\right)\,+\,\frac{a}{a-b}\ln\left(\frac{b}{a}\right)
\end{aligned}
$$

Loop functions appearing in the scalar Eqs.(2.51)-(2.55) and pseudoscalar Eqs.(2.52)-(2.56) amplitudes for the decay rate of a neutral Higgs boson into two photons or gluons.

$$
\begin{aligned}
F_0\left(\tau\right) &= \tau^{-1}\,\left[\,-1+\tau^{-1}f\left(\tau\right)\,\right] \\
F_f^S\left(\tau\right) &= \tau^{-1}\,\left[\,1+\left(1-\tau^{-1}\right)f\left(\tau\right)\,\right] \\
F_f^P\left(\tau\right) &= \tau^{-1}\,f\left(\tau\right) \\
F_1\left(\tau\right) &= 2\,+\,3\tau^{-1}\,+\,3\tau^{-1}\,\left(2-\tau^{-1}\right)\,f\left(\tau\right)
\end{aligned}
$$

$$f(\tau) = -\frac{1}{2}\int_0^1 \frac{\mathrm{d}x}{x}\ln\left[1-4\tau x(1-x)\right] = \begin{cases} \arcsin^2\left(\sqrt{\tau}\right) & \text{if } \tau \leq 1 \\ -\frac{1}{4}\left[\ln\left(\frac{\sqrt{\tau}+\sqrt{\tau-1}}{\sqrt{\tau}-\sqrt{\tau-1}}\right) - i\pi\right]^2 & \text{if } \tau > 1 \end{cases}$$

Loop functions in Eqs.(3.10) and (3.15) associated with the carginos and charged Higgs contributions to $b \to s\gamma$.

$$\begin{aligned}
f_7^{(1)}(x) &= \frac{x\left(7-5x-8x^2\right)}{24(x-1)^3} + \frac{x^2(3x-2)}{4(x-1)^4}\ln x \\
f_7^{(2)}(x) &= \frac{x(3-5x)}{12(x-1)^2} + \frac{x(3x-2)}{6(x-1)^3}\ln x \\
f_7^{(3)}(x) &= \frac{5-7x}{6(x-1)^2} + \frac{x(3x-2)}{3(x-1)^2}\ln x \\
f_8^{(1)}(x) &= \frac{x\left(2+5x-x^2\right)}{8(x-1)^3} - \frac{3x^2}{4(x-1)^4}\ln x \\
f_8^{(2)}(x) &= \frac{x(3-x)}{4(x-1)^2} - \frac{x}{2(x-1)^3}\ln x \\
f_8^{(3)}(x) &= \frac{1+x}{2(x-1)^2} - \frac{x}{(x-1)^3}\ln x
\end{aligned}$$

Loop functions in Eqs.(3.37) and (3.38) associated with the charged-Higgs contributions to the B_s-meson difference of mass.

$$\begin{aligned}
D_0(a,b,c,d) &= \frac{b}{(b-a)(b-c)(b-d)}\,ln\left(\frac{b}{a}\right) + \frac{c}{(c-a)(c-b)(c-d)}\,ln\left(\frac{c}{a}\right) \\
&\quad + \frac{d}{(d-a)(d-b)(d-c)}\,ln\left(\frac{d}{a}\right) \\
D_2(a,b,c,d) &= \frac{b^2}{(b-a)(b-c)(b-d)}\,ln\left(\frac{b}{a}\right) + \frac{c^2}{(c-a)(c-b)(c-d)}\,ln\left(\frac{c}{a}\right) \\
&\quad + \frac{d^2}{(d-a)(d-b)(d-c)}\,ln\left(\frac{d}{a}\right)
\end{aligned}$$

D

Expansion of Hermitian matrices

Given a $n \times n$ hermitian matrix $A = A^0 + A^1$ with $A^0 = \text{diag}(a_1^0, ..., a_n^0)$ and A^1 completely off-diagonal that is diagonalized by an unitary matrix such as $\mathcal{U} \cdot A \cdot \mathcal{U}^\dagger = \text{diag}(a_1, ..., a_n)$, we have a first order in A^1 [232, 233]:

$$\sum_k \mathcal{U}_{ki}^* \, f\left(a_k\right) \mathcal{U}_{kj} \;\simeq\; \delta_{ij} \, f(a_i^0) \;+\; A_{ij}^1 \, \frac{f(a_i^0) - f(a_j^0)}{a_i^0 - a_j^0}$$

We use this formula to expand several terms in our analysis. For intance, it can be applied to Eq.(5.13) to obtain a simplified expression for the b-squark contribution to the $\gamma\gamma$-decay of the Higgs boson.

$$\begin{aligned} S_{H_2,\tilde{b}}^{\gamma} \;\simeq\; & -\frac{v}{6} \sum_{\alpha=1}^{3} O_{\alpha 2} \left\{ \left(\tilde{\Gamma}_{\tilde{b}\tilde{b}}^{\alpha}\right)_{11} \frac{F_0\left(\tau_{\tilde{b}_1}\right)}{m_{\tilde{b}_1}^2} \;+\; \left(\tilde{\Gamma}_{\tilde{b}\tilde{b}}^{\alpha}\right)_{22} \frac{F_0\left(\tau_{\tilde{b}_2}\right)}{m_{\tilde{b}_2}^2} \;+ \right. \\ & \left. \left[\left(\tilde{\Gamma}_{\tilde{b}\tilde{b}}^{\alpha}\right)_{12} \left(\mathcal{M}_{\tilde{b}}^2\right)_{12} \;+\; \left(\tilde{\Gamma}_{\tilde{b}\tilde{b}}^{\alpha}\right)_{21} \left(\mathcal{M}_{\tilde{b}}^2\right)_{21} \right] \frac{F_0(\tau_{\tilde{b}_1})/m_{\tilde{b}_1^2} - F_0(\tau_{\tilde{b}_2})/m_{\tilde{b}_2^2}}{m_{\tilde{b}_1^2} - m_{\tilde{b}_2^2}} \right\} \end{aligned}$$

From Eqs.(B.1)-(B.3), one can confirms that $\left(\tilde{\Gamma}_{\tilde{b}\tilde{b}}^{\alpha}\right)_{11} \simeq \left(\tilde{\Gamma}_{\tilde{b}\tilde{b}}^{\alpha}\right)_{22} \simeq 0$. Additionally, $F_0(\tau_{\tilde{b}_1}) \simeq F_0(\tau_{\tilde{b}_2}) \simeq 0.35$. Therefore

$$S_{H_2,\tilde{b}}^{\gamma} \;\simeq\; -\frac{2 \times 0.35 \, m_b^2 \, \tan^2\beta}{6 \, m_{\tilde{b}_1}^2 \, m_{\tilde{b}_2}^2} \left(O_{21} \, \Re e[A_b^* \mu] \;+\; O_{22} \, \Re e[\mu^2] \;-\; O_{23} \, \frac{\Im m[A_b^* \mu]}{\tan\beta} \right)$$

We use this formula again to expand the chargino Wilson coefficients, $\mathcal{C}_{7,8}^{\chi^+}$ in Eq.(3.10) with respect to the chargino mass matrix elements. In this case we have to be careful because the chargino mass matrix is not hermitian. However due to the necessary chirality flip in the chargino line $\mathcal{C}_{7,8}$ as a function of odd powers of M_{χ^+} [234] one may rewrite

$$\sum_{j=1}^{2} U_{j2}\, V_{j1}\, m_{\chi_j^+}\, A(m^2_{\chi_j^+}) \;=\; \sum_{j,k,l=1}^{2} U_{jk}\, m_{\chi_j^+}\, V_{j1}\, U_{l2}\, A(m^2_{\chi_l^+})\, U^*_{lk}$$

where $\sum_k U_{jk}\, U^*_{lk} = \delta_{jl}$ has been introduced. Then,

$$\mathcal{C}_{7,8}^{\chi^\pm(a)} \;=\; \frac{1}{\cos\beta} \sum_{a=1,2} \frac{U_{a2}\, V_{a1}\, m_W}{\sqrt{2}\, m_{\tilde{\chi}_a^\pm}}\, \mathcal{F}_{7,8}\left(x_{\tilde{q}\tilde{\chi}_a^\pm},\, x_{\tilde{t}_1\tilde{\chi}_a^\pm},\, x_{\tilde{t}_2\tilde{\chi}_a^\pm}\right) \;\sim$$

$$\sim \;\frac{m_W}{\sqrt{2}\,\cos\beta}\left[\,(\mathcal{M}_\chi)_{21}\,\frac{\mathcal{F}_{7,8}\left(x_{\tilde{q}\tilde{\chi}_2^\pm},\, x_{\tilde{t}_1\tilde{\chi}_2^\pm},\, x_{\tilde{t}_2\tilde{\chi}_2^\pm}\right)}{m^2_{\tilde{\chi}_2^\pm}} \;+\; (\mathcal{M}_\chi)_{11}\,\left(\mathcal{M}_\chi\mathcal{M}_\chi^\dagger\right)_{21}\times \right.$$
$$\left.\frac{m^2_{\tilde{\chi}_1^\pm}\,\mathcal{F}_{7,8}\left(x_{\tilde{q}\tilde{\chi}_2^\pm},\, x_{\tilde{t}_1\tilde{\chi}_2^\pm},\, x_{\tilde{t}_2\tilde{\chi}_2^\pm}\right) - m^2_{\tilde{\chi}_2^\pm}\,\mathcal{F}_{7,8}\left(x_{\tilde{q}\tilde{\chi}_1^\pm},\, x_{\tilde{t}_1\tilde{\chi}_1^\pm},\, x_{\tilde{t}_2\tilde{\chi}_1^\pm}\right)}{m^2_{\tilde{\chi}_1^\pm}\, m^2_{\tilde{\chi}_2^\pm}\left(m^2_{\tilde{\chi}_2^\pm} - m^2_{\tilde{\chi}_1^\pm}\right)}\,\right]$$

$$\mathcal{C}_{7,8}^{\chi^\pm(b)} = \frac{1}{\cos\beta} \sum_{a=1,2} \frac{U_{a2}\, V_{a2}\, \overline{m}_t}{2\, m_{\tilde{\chi}_a^\pm}\, \sin\beta}\, \mathcal{G}_{7,8}\left(x_{\tilde{t}_1\tilde{\chi}_a^\pm},\, x_{\tilde{t}_2\tilde{\chi}_a^\pm}\right)$$
$$\sim \frac{\overline{m}_t}{2\,\cos\beta\,\sin\beta}\left[(\mathcal{M}_\chi)_{22}\,\frac{\mathcal{G}_{7,8}\left(x_{\tilde{q}\tilde{\chi}_2^\pm},\, x_{\tilde{t}_1\tilde{\chi}_2^\pm},\, x_{\tilde{t}_2\tilde{\chi}_2^\pm}\right)}{m^2_{\tilde{\chi}_2^\pm}} + (\mathcal{M}_\chi)_{12}\left(\mathcal{M}_\chi\mathcal{M}_\chi^\dagger\right)_{21}\times \right.$$
$$\left.\frac{m^2_{\tilde{\chi}_1^\pm}\,\mathcal{G}_{7,8}\left(x_{\tilde{q}\tilde{\chi}_2^\pm},\, x_{\tilde{t}_1\tilde{\chi}_2^\pm},\, x_{\tilde{t}_2\tilde{\chi}_2^\pm}\right) - m^2_{\tilde{\chi}_2^\pm}\,\mathcal{G}_{7,8}\left(x_{\tilde{q}\tilde{\chi}_1^\pm},\, x_{\tilde{t}_1\tilde{\chi}_1^\pm},\, x_{\tilde{t}_2\tilde{\chi}_1^\pm}\right)}{m^2_{\tilde{\chi}_1^\pm}\, m^2_{\tilde{\chi}_2^\pm}\left(m^2_{\tilde{\chi}_2^\pm} - m^2_{\tilde{\chi}_1^\pm}\right)}\right]$$

Using again the same approximation in the case of t-squarks, we can expand the stop mixings in the $\mathcal{F}_{7,8}$ and $\mathcal{G}_{7,8}$ as

$$\mathcal{F}_{7,8}\left(x_{\tilde{q}\tilde{\chi}_a^\pm},\, x_{\tilde{t}_1\tilde{\chi}_a^\pm},\, x_{\tilde{t}_2\tilde{\chi}_a^\pm}\right) \;\simeq\; f^{(3)}_{7,8}\left(x_{\tilde{q}\tilde{\chi}_a^\pm}\right) \;-\; f^{(3)}_{7,8}\left(x_{\tilde{t}_1\tilde{\chi}_a^\pm}\right)$$
$$\mathcal{G}_{7,8}\left(x_{\tilde{t}_1\tilde{\chi}_a^\pm},\, x_{\tilde{t}_2\tilde{\chi}_a^\pm}\right) \;\simeq\; (\mathcal{M}_{\tilde{t}})_{21}\,\frac{f^{(3)}_{7,8}\left(x_{\tilde{t}_1\tilde{\chi}_a^\pm}\right) - f^{(3)}_{7,8}\left(x_{\tilde{t}_2\tilde{\chi}_a^\pm}\right)}{m^2_{\tilde{t}_1} - m^2_{\tilde{t}_2}}$$

Putting all together

$$\mathcal{C}_{7,8}^{\chi^{\pm}(a)} \sim \frac{m_W}{\sqrt{2}\,\cos\beta}\left[(\mathcal{M}_\chi)_{21}\,\frac{f_{7,8}^{(3)}\left(x_{\tilde{q}\tilde{\chi}_2^\pm}\right)-f_{7,8}^{(3)}\left(x_{\tilde{t}_1\tilde{\chi}_2^\pm}\right)}{m^2_{\tilde{\chi}_2^\pm}} + \frac{(\mathcal{M}_\chi)_{11}\,\left(\mathcal{M}_\chi\,\mathcal{M}_\chi^\dagger\right)_{21}}{m^2_{\tilde{\chi}_1^\pm}-m^2_{\tilde{\chi}_2^\pm}}\times \right.$$

$$\left.\left(\frac{f_{7,8}^{(3)}\left(x_{\tilde{q}\tilde{\chi}_1^\pm}\right)-f_{7,8}^{(3)}\left(x_{\tilde{t}_1\tilde{\chi}_1^\pm}\right)}{m^2_{\tilde{\chi}_1^\pm}} - \frac{f_{7,8}^{(3)}\left(x_{\tilde{q}\tilde{\chi}_2^\pm}\right)-f_{7,8}^{(3)}\left(x_{\tilde{t}_1\tilde{\chi}_2^\pm}\right)}{m^2_{\tilde{\chi}_2^\pm}}\right)\right]$$

$$\begin{aligned}\mathcal{C}_{7,8}^{\chi^{\pm}(b)} \;\sim\; & \frac{\overline{m}_t}{2\,\cos\beta\,\sin\beta}\left[(\mathcal{M}_\chi)_{22}\,\frac{(\mathcal{M}_{\tilde{t}})_{21}}{m^2_{\tilde{t}_1}-m^2_{\tilde{t}_2}}\left(\frac{f_{7,8}^{(3)}\left(x_{\tilde{t}_1\tilde{\chi}_2^\pm}\right)-f_{7,8}^{(3)}\left(x_{\tilde{t}_2\tilde{\chi}_2^\pm}\right)}{m^2_{\tilde{\chi}_2^\pm}}\right)\right. \\ & + \left.\frac{(\mathcal{M}_\chi)_{12}\,\left(\mathcal{M}_\chi\,\mathcal{M}_\chi^\dagger\right)_{21}}{m^2_{\tilde{\chi}_1^\pm}-m^2_{\tilde{\chi}_2^\pm}}\frac{(\mathcal{M}_{\tilde{t}})_{21}}{m^2_{\tilde{t}_1}-m^2_{\tilde{t}_2}}\times \right. \\ & \left.\left(\frac{f_{7,8}^{(3)}\left(x_{\tilde{t}_1\tilde{\chi}_1^\pm}\right)-f_{7,8}^{(3)}\left(x_{\tilde{t}_2\tilde{\chi}_1^\pm}\right)}{m^2_{\tilde{\chi}_1^\pm}} - \frac{f_{7,8}^{(3)}\left(x_{\tilde{t}_1\tilde{\chi}_2^\pm}\right)-f_{7,8}^{(3)}\left(x_{\tilde{t}_2\tilde{\chi}_2^\pm}\right)}{m^2_{\tilde{\chi}_2^\pm}}\right)\right]\end{aligned}$$

E

Flavour-changing inverse matrix

From $\mathbf{R}_d \simeq \mathbf{1} + \tan\beta \mathbf{\Delta}_d^{\Phi_u^0}$ obtained in Eq.(5.75) as

$$\mathbf{R}_d \;=\; \mathbf{1} + \tan\beta\, \mathbf{\Delta}_d^{\Phi_u^0} \;\simeq\; \begin{pmatrix} 1+\epsilon\tan\beta & 0 & 0 \\ 0 & 1+\epsilon\tan\beta & \delta\epsilon_{23}\tan\beta \\ 0 & \delta\epsilon_{32}\tan\beta & 1+(\epsilon+\eta)\tan\beta \end{pmatrix}$$

the inverse matrix calculated as $\mathbf{R}_d^{-1} \;=\; \frac{1}{\det(\mathbf{R}_d)}\mathrm{Adj}(\mathbf{R}_d)^T$ is given by

$$\mathbf{R}_d^{-1} \simeq \begin{pmatrix} R_{d,11}^{-1} & 0 & 0 \\ 0 & R_{d,22}^{-1} & R_{d,23}^{-1} \\ 0 & R_{d,32}^{-1} & R_{d,33}^{-1} \end{pmatrix} \tag{E.1}$$

with

$$R_{d,11}^{-1} \;=\; \frac{(1+\epsilon\tan\beta)\,(1+(\epsilon+\eta)\tan\beta) - \delta\epsilon_{23}\delta\epsilon_{32}\tan^2\beta}{\mathrm{Det}\,(\mathbf{R}_d)} \tag{E.2}$$

$$R_{d,22}^{-1} \;=\; \frac{(1+\epsilon\tan\beta)\,(1+(\epsilon+\eta)\tan\beta)}{\mathrm{Det}\,(\mathbf{R}_d)} \tag{E.3}$$

$$R_{d,23}^{-1} \;=\; -\frac{\delta\epsilon_{23}\,(1+\epsilon\tan\beta)\tan\beta}{\mathrm{Det}\,(\mathbf{R}_d)} \tag{E.4}$$

$$R^{-1}_{d,32} = -\frac{\delta\epsilon_{32}\,(1+\epsilon\tan\beta)\tan\beta}{\mathrm{Det}\,(\mathbf{R}_d)} \tag{E.5}$$

$$R^{-1}_{d,33} = \frac{(1+\epsilon\tan\beta)^2}{\mathrm{Det}\,(\mathbf{R}_d)} \tag{E.6}$$

where the determinant of $\mathbf{R}_d^{-1}$ is

$$\mathrm{Det}\,(\mathbf{R}_d) = (1+\epsilon\,\tan\beta)^2\;(1+(\epsilon+\eta)\tan\beta) \;-\; \delta\epsilon_{23}\,\delta\epsilon_{32}\,\tan^2\beta \tag{E.7}$$

Bibliography

[1] M. Kaku, *Quantum Field Theory: A Modern Introduction* (Oxford University Press, 1993) ISBN 9780195076523 (1 and 5)

[2] Hironari Miyazawa, "Baryon number changing currents," Progress of Theoretical Physics **36**, 1266–1276 (1966) (1)

[3] H. Miyazawa, "Spinor Currents and Symmetries of Baryons and Mesons," Physical Review **170**, 1586–1590 (Jun. 1968) (1)

[4] A. Neveu and J.H. Schwarz, "Factorizable dual model of pions," Nuclear Physics B **31**, 86 – 112 (1971) (1)

[5] P. Ramond, "Dual theory for free fermions," Phys. Rev. D **3**, 2415–2418 (May 1971) (1)

[6] Yu. A. Gol'fand and E. P. Likhtman, "Extension of the Algebra of Poincare Group Generators and Violation of p Invariance," JETP Lett. **13**, 323–326 (1971), [Pisma Zh. Eksp. Teor. Fiz.13,452(1971)] (1)

[7] J. Wess and B. Zumino, "Supergauge Transformations in Four-Dimensions," Nucl. Phys. **B70**, 39–50 (1974) (1)

[8] J. Wess and B. Zumino, "A Lagrangian Model Invariant Under Supergauge Transformations," Phys. Lett. **B49**, 52 (1974) (1)

[9] J. Wess and B. Zumino, "Supergauge Invariant Extension of Quantum Electrodynamics," Nucl. Phys. **B78**, 1 (1974) (1)

[10] Rudolf Haag, Jan T. Łopuszański, and Martin Sohnius, "All possible generators of supersymmetries of the s-matrix," Nuclear Physics B **88**, 257 – 274 (1975) (1)

[11] Pierre Fayet, "Supergauge Invariant Extension of the Higgs Mechanism and a Model for the electron and Its Neutrino," Nucl. Phys. **B90**, 104–124 (1975) (1)

[12] Pierre Fayet, "Supersymmetry and Weak, Electromagnetic and Strong Interactions," Phys. Lett. **B64**, 159 (1976) (1 and 13)

[13] Pierre Fayet, "Spontaneously Broken Supersymmetric Theories of Weak, Electromagnetic and Strong Interactions," Phys. Lett. **B69**, 489 (1977) (1 and 13)

[14] P. Fayet, "Mixing between gravitational and weak interactions through the massive gravitino," Physics Letters B **70**, 461 – 464 (1977) (1)

[15] William A. Bardeen, "On naturalness in the standard model," in *Ontake Summer Institute on Particle Physics Ontake Mountain, Japan, August 27-September 2, 1995* (1995) (2)

[16] John Ellis, "Prospects for Supersymmetry at the LHC & Beyond," *Proceedings, 18th International Conference From the Planck Scale to the Electroweak Scale (Planck 2015): Ioannina, Greece, May 25-29, 2015*, PoS **PLANCK2015**, 041 (2015), arXiv:1510.06204 [hep-ph] (3)

[17] Stephen P. Martin, "A supersymmetry primer," (1997), [Adv. Ser. Direct. High Energy Phys.18,1(1998)], arXiv:hep-ph/9709356 [hep-ph] (3, 5, 9, 23, 114 and 115)

[18] Howard E. Haber and Ralf Hempfling, "Can the mass of the lightest higgs boson of the minimal supersymmetric model be larger than m_z?." Phys. Rev. Lett. **66**, 1815–1818 (Apr 1991) (3 and 66)

[19] Yasuhiro Okada, Masahiro Yamaguchi, and Tsutomu Yanagida, "Upper bound of the lightest higgs boson mass in the minimal supersymmetric standard model," Progress of Theoretical Physics **85**, 1–5 (1991) (3 and 66)

[20] John Ellis, Giovanni Ridolfi, and Fabio Zwirner, "Radiative corrections to the masses of supersymmetric higgs bosons," Physics Letters B **257**, 83 – 91 (1991) (3 and 66)

[21] Joseph D. Lykken, "Introduction to supersymmetry," in *Fields, strings and duality. Proceedings, Summer School, Theoretical Advanced Study Institute in Elementary Particle Physics, TASI'96, Boulder, USA, June 2-28, 1996* (1996) pp. 85–153, arXiv:hep-th/9612114 [hep-th] (5)

[22] Ian J. R. Aitchison, "Supersymmetry and the MSSM: An Elementary introduction," (2005), arXiv:hep-ph/0505105 [hep-ph] (5)

[23] Sidney Coleman and Jeffrey Mandula, "All possible symmetries of the s matrix," Phys. Rev. **159**, 1251–1256 (Jul 1967) (5)

[24] Oskar Pelc and L. P. Horwitz, "Generalization of the Coleman-Mandula theorem to higher dimension," J. Math. Phys. **38**, 139–172 (1997), arXiv:hep-th/9605147 [hep-th] (5)

[25] Abdus Salam and J. Strathdee, "Super-gauge transformations," Nuclear Physics B **76**, 477 – 482 (1974) (5 and 7)

[26] S. Ferrara, B. Zumino, and J. Wess, "Supergauge multiplets and superfields," Physics Letters B **51**, 239 – 241 (1974) (5 and 7)

[27] W. Nahm, "Supersymmetries and their representations," Nuclear Physics B **135**, 149 – 166 (1978) (6)

[28] Glennys R. Farrar and Pierre Fayet, "Phenomenology of the production, decay, and detection of new hadronic states associated with supersymmetry," Physics Letters B **76**, 575 – 579 (1978) (13)

[29] Stephen P. Martin, "Implications of supersymmetric models with natural R-parity conservation," Phys. Rev. **D54**, 2340–2348 (1996), arXiv:hep-ph/9602349 [hep-ph] (14)

[30] Stephen L. Adler and William A. Bardeen, "Absence of higher-order corrections in the anomalous axial-vector divergence equation," Phys. Rev. **182**, 1517–1536 (Jun 1969) (15)

[31] David J. Gross Sam B. Treiman, Roman Jackiw, *Lectures on Current Algebra and Its Applications* (Princeton University Press, 1972) (15)

[32] Luis Alvarez-Gaumé and Edward Witten, "Gravitational anomalies," Nuclear Physics B **234**, 269 – 330 (1984) (15)

[33] H.P. Nilles, "Supersymmetry, supergravity and particle physics," Physics Reports **110**, 1 – 162 (1984) (21 and 114)

[34] H.E. Haber and G.L. Kane, "The search for supersymmetry: Probing physics beyond the standard model," Physics Reports **117**, 75 – 263 (1985) (21, 97 and 114)

[35] Abdelhak Djouadi, "The Anatomy of electro-weak symmetry breaking. II. The Higgs bosons in the minimal supersymmetric model," Phys. Rept. **459**, 1–241 (2008), arXiv:hep-ph/0503173 [hep-ph] (21, 23, 33, 37 and 40)

[36] Howard E. Haber, "The status of the minimal supersymmetric standard model and beyond," Nuclear Physics B - Proceedings Supplements **62**, 469 – 484 (1998) (21)

[37] F. del Águila, M.B. Gavela, J.A. Grifols, and A. Méndez, "Specifically supersymmetric contribution to electric dipole moments," Physics Letters B **126**, 71 – 73 (1983) (21 and 44)

[38] W. Buchmüller and D. Wyler, "Cp violation and r invariance in supersymmetric models of strong and electroweak interactions," Physics Letters B **121**, 321 – 325 (1983) (21 and 44)

[39] M. Dugan, B. Grinstein, and L. Hall, "Cp violation in the minimal n = 1 supergravity theory," Nuclear Physics B **255**, 413 – 438 (1985) (21 and 44)

[40] John Ellis, Sergio Ferrara, and D.V. Nanopoulos, "Cp violation and supersymmetry," Physics Letters B **114**, 231 – 234 (1982) (21 and 44)

[41] D.V. Nanopoulos and M. Srednicki, "The demon of local susy," Physics Letters B **128**, 61 – 64 (1983) (21 and 44)

[42] Yoshiki Kizukuri and Noriyuki Oshimo, "Neutron and electron electric dipole moments in supersymmetric theories," Phys. Rev. D **46**, 3025–3033 (Oct 1992) (21 and 44)

[43] Joseph Polchinski and Mark B. Wise, "The electric dipole moment of the neutron in low energy supergravity," Physics Letters B **125**, 393 – 398 (1983) (21)

[44] Toby Falk, Keith A. Olive, and Mark Srednicki, "Phases in the mssm, electric dipole moments and cosmological dark matter," Physics Letters B **354**, 99 – 106 (1995) (21)

[45] Toby Falk and Keith A. Olive, "More on electric dipole moment constraints on phases in the constrained MSSM," Phys. Lett. **B439**, 71–80 (1998), arXiv:hep-ph/9806236 [hep-ph] (21)

[46] Tarek Ibrahim and Pran Nath, "The chromoelectric and purely gluonic operator contributions to the neutron electric dipole moment in n=1 supergravity," Physics Letters B **418**, 98 – 106 (1998) (21)

[47] Michal Brhlik, Gerald J. Good, and G. L. Kane, "Electric dipole moments do not require the ***CP*** -violating phases of supersymmetry to be small," Phys. Rev. D **59**, 115004 (Apr 1999) (21)

[48] S. A. Abel and J.-M. Frère, "Could the mssm have no CP violation in the ckm matrix?." Phys. Rev. D **55**, 1623–1629 (Feb 1997) (21)

[49] Darwin Chang, Wai-Yee Keung, and Apostolos Pilaftsis, "New two-loop contribution to electric dipole moments in supersymmetric theories," Phys. Rev. Lett. **82**, 900–903 (Feb 1999) (21)

[50] Apostolos Pilaftsis, "CP odd tadpole renormalization of Higgs scalar - pseudoscalar mixing," Phys. Rev. **D58**, 096010 (1998), arXiv:hep-ph/9803297 [hep-ph] (23)

[51] Apostolos Pilaftsis, "Higgs scalar - pseudoscalar mixing in the minimal supersymmetric standard model," Phys. Lett. **B435**, 88–100 (1998), arXiv:hep-ph/9805373 [hep-ph] (23)

[52] Apostolos Pilaftsis and Carlos E. M. Wagner, "Higgs bosons in the minimal supersymmetric standard model with explicit CP violation," Nucl. Phys. **B553**, 3–42 (1999), arXiv:hep-ph/9902371 [hep-ph] (23, 67, 70 and 143)

[53] J.F. Gunion and H.E. Haber, "Higgs bosons in supersymmetric models (i)," Nuclear Physics B **402**, 567 – 568 (1993) (23)

[54] J. S. Lee, A. Pilaftsis, Marcela Carena, S. Y. Choi, M. Drees, John R. Ellis, and C. E. M. Wagner, "CPsuperH: A Computational tool for Higgs phenomenology in the minimal supersymmetric standard model with explicit CP violation," Comput. Phys. Commun. **156**, 283–317 (2004), arXiv:hep-ph/0307377 [hep-ph] (24, 32, 34, 35, 76, 103, 104, 141 and 143)

[55] R. Hempfling, "Yukawa coupling unification with supersymmetric threshold corrections," Phys. Rev. D **49**, 6168–6172 (Jun 1994) (27)

[56] Lawrence J. Hall, Riccardo Rattazzi, and Uri Sarid, "The Top quark mass in supersymmetric SO(10) unification," Phys. Rev. **D50**, 7048–7065 (1994), arXiv:hep-ph/9306309 [hep-ph] (27)

[57] Marcela Carena, M. Olechowski, S. Pokorski, and C. E. M. Wagner, "Electroweak symmetry breaking and bottom - top Yukawa unification," Nucl. Phys. **B426**, 269–300 (1994), arXiv:hep-ph/9402253 [hep-ph] (27)

[58] Damien M. Pierce, Jonathan A. Bagger, Konstantin T. Matchev, and Ren-jie Zhang, "Precision corrections in the minimal supersymmetric standard model," Nucl. Phys. **B491**, 3–67 (1997), arXiv:hep-ph/9606211 [hep-ph] (27)

[59] Jose Antonio Coarasa Perez, Ricardo A. Jimenez, and Joan Sola, "Strong effects on the hadronic widths of the neutral Higgs bosons in the MSSM," Phys. Lett. **B389**, 312–320 (1996), arXiv:hep-ph/9511402 [hep-ph] (27)

[60] Ricardo A. Jimenez and Joan Sola, "Supersymmetric QCD corrections to the top quark decay of a heavy charged Higgs boson," Phys. Lett. **B389**, 53–61 (1996), arXiv:hep-ph/9511292 [hep-ph] (27)

[61] Konstantin T. Matchev and Damien M. Pierce, "New limits on the SUSY Higgs boson mass," Phys. Lett. **B445**, 331–336 (1999), arXiv:hep-ph/9805275 [hep-ph] (27)

[62] Piotr H. Chankowski, John R. Ellis, Marek Olechowski, and Stefan Pokorski, "Haggling over the fine tuning price of LEP," Nucl. Phys. **B544**, 39–63 (1999), arXiv:hep-ph/9808275 [hep-ph] (27)

[63] K. S. Babu and Christopher F. Kolda, "Signatures of supersymmetry and Yukawa unification in Higgs decays," Phys. Lett. **B451**, 77–85 (1999), arXiv:hep-ph/9811308 [hep-ph] (27)

[64] John R. Ellis, Jae Sik Lee, and Apostolos Pilaftsis, "B-Meson Observables in the Maximally CP-Violating MSSM with Minimal Flavour Violation," Phys. Rev. **D76**, 115011 (2007), arXiv:0708.2079 [hep-ph] (27, 32, 46, 49, 52 and 144)

[65] K. S. Babu, Christopher F. Kolda, John March-Russell, and Frank Wilczek, "CP violation, Higgs couplings, and supersymmetry," Phys. Rev. **D59**, 016004 (1999), arXiv:hep-ph/9804355 [hep-ph] (30)

[66] E. Braaten and J. P. Leveille, "Higgs-boson decay and the running mass," Phys. Rev. D **22**, 715–721 (Aug 1980) (33)

[67] Manuel Drees and Ken ichi Hikasa, "Note on qcd corrections to hadronic higgs decay," Physics Letters B **240**, 455 – 464 (1990) (33)

[68] S. Y. Choi and Jae Sik Lee, "MSSM Higgs boson production at hadron colliders with explicit CP violation," Phys. Rev. **D61**, 115002 (2000), arXiv:hep-ph/9910557 [hep-ph] (34 and 39)

[69] S. Y. Choi, Kaoru Hagiwara, and Jae Sik Lee, "Higgs boson decays in the minimal supersymmetric standard model with radiative higgs sector CP violation," Phys. Rev. D **64**, 032004 (Jul 2001) (34)

[70] S.Y. Choi, M. Drees, J.S. Lee, and J. Song, "Supersymmetric higgs boson decays in the mssm with explicit cp violation," The European Physical Journal C - Particles and Fields **25**, 307–313 (2002) (34)

[71] M. Spira, A. Djouadi, D. Graudenz, and P. M. Zerwas, "Higgs boson production at the LHC," Nucl. Phys. **B453**, 17–82 (1995), arXiv:hep-ph/9504378 [hep-ph] (36 and 37)

[72] Michael Spira, "QCD effects in Higgs physics," Fortsch. Phys. **46**, 203–284 (1998), arXiv:hep-ph/9705337 [hep-ph] (36, 37 and 39)

[73] Abdelhak Djouadi, "The Anatomy of electro-weak symmetry breaking. I: The Higgs boson in the standard model," Phys. Rept. **457**, 1–216 (2008), arXiv:hep-ph/0503172 [hep-ph] (37)

[74] CERN (38)

[75] Abdelhak Djouadi and Jeremie Quevillon, "The MSSM Higgs sector at a high M_{SUSY}: reopening the low tanβ regime and heavy Higgs searches," JHEP **10**, 028 (2013), arXiv:1304.1787 [hep-ph] (38)

[76] Duane A. Dicus and Scott Willenbrock, Phys. Rev. **D39**, 751 (1989) (38 and 40)

[77] A. D. Martin, W. J. Stirling, R. S. Thorne, and G. Watt, "Parton distributions for the LHC," Eur. Phys. J. **C63**, 189–285 (2009), arXiv:0901.0002 [hep-ph] (39, 89 and 92)

[78] D. Graudenz, M. Spira, and P. M. Zerwas, "QCD corrections to Higgs boson production at proton proton colliders," Phys. Rev. Lett. **70**, 1372–1375 (1993) (39)

[79] S. Dawson, A. Djouadi, and M. Spira, "QCD corrections to SUSY Higgs production: The Role of squark loops," Phys. Rev. Lett. **77**, 16–19 (1996), arXiv:hep-ph/9603423 [hep-ph] (39)

[80] Abdelhak Djouadi and Michael Spira, "SUSY - QCD corrections to Higgs boson production at hadron colliders," Phys. Rev. **D62**, 014004 (2000), arXiv:hep-ph/9912476 [hep-ph] (39)

[81] Julien Baglio and Abdelhak Djouadi, "Higgs production at the lHC," JHEP **03**, 055 (2011), arXiv:1012.0530 [hep-ph] (39, 40 and 75)

[82] John M. Campbell, R. Keith Ellis, F. Maltoni, and S. Willenbrock, "Higgs-Boson production in association with a single bottom quark," Phys. Rev. **D67**, 095002 (2003), arXiv:hep-ph/0204093 [hep-ph] (40, 41 and 92)

[83] F. Maltoni, Z. Sullivan, and S. Willenbrock, "Higgs-boson production via bottom-quark fusion," Phys. Rev. **D67**, 093005 (2003), arXiv:hep-ph/0301033 [hep-ph] (40)

[84] Robert V. Harlander and William B. Kilgore, "Higgs boson production in bottom quark fusion at next-to-next-to leading order," Phys. Rev. **D68**, 013001 (2003), arXiv:hep-ph/0304035 [hep-ph] (40)

[85] Stefan Dittmaier, Michael Kramer, 1, and Michael Spira, "Higgs radiation off bottom quarks at the Tevatron and the CERN LHC," Phys. Rev. **D70**, 074010 (2004), arXiv:hep-ph/0309204 [hep-ph] (40)

[86] S. Dawson, C. B. Jackson, L. Reina, and D. Wackeroth, "Exclusive Higgs boson production with bottom quarks at hadron colliders," Phys. Rev. **D69**, 074027 (2004), arXiv:hep-ph/0311067 [hep-ph] (40)

[87] D. Dicus, T. Stelzer, Z. Sullivan, and S. Willenbrock, "Higgs boson production in association with bottom quarks at next-to-leading order," Phys. Rev. **D59**, 094016 (1999), arXiv:hep-ph/9811492 [hep-ph] (40)

[88] Takeshi Fukuyama, "Searching for New Physics beyond the Standard Model in Electric Dipole Moment," Int. J. Mod. Phys. **A27**, 1230015 (2012), arXiv:1201.4252 [hep-ph] (44)

[89] EP Shabalin, "Electric dipole moment of the quark in a gauge theory with left-handed currents," Sov. J. Nucl. Phys.(Engl. Transl.);(United States) **28** (1978) (44)

[90] Andrzej Czarnecki and Bernd Krause, "Neutron electric dipole moment in the standard model: Valence quark contributions," Phys. Rev. Lett. **78**, 4339–4342 (1997), arXiv:hep-ph/9704355 [hep-ph] (44)

[91] C. A. Baker *et al.*, "Reply to comment on 'An Improved experimental limit on the electric dipole moment of the neutron'," Phys. Rev. Lett. **98**, 149102 (2007), arXiv:0704.1354 [hep-ex] (44)

[92] I.B. Khriplovich and A.R. Zhitnitsky, "What is the value of the neutron electric dipole moment in the kobayashi-maskawa model?." Physics Letters B **109**, 490 – 492 (1982) (44)

[93] Michael J. Booth, "The Electric dipole moment of the W and electron in the Standard Model," (1993), arXiv:hep-ph/9301293 [hep-ph] (44)

[94] Tomoko Kadoyoshi and Noriyuki Oshimo, "Neutron electric dipole moment from supersymmetric anomalous W boson coupling," Phys. Rev. **D55**, 1481–1486 (1997), arXiv:hep-ph/9607301 [hep-ph] (45)

[95] Darwin Chang, Wai-Yee Keung, and Jiang Liu, "The electric dipole moment of W boson," Nucl. Phys. **B355**, 295–304 (1991) (45)

[96] Todd H. West, "Fermion electric dipole moments induced by T and P odd W W gamma interactions in the multi - Higgs and supersymmetry models," Phys. Rev. **D50**, 7025–7034 (1994) (45)

[97] Stephen M. Barr and A. Zee, "Electric Dipole Moment of the Electron and of the Neutron," Phys. Rev. Lett. **65**, 21–24 (1990), [Erratum: Phys. Rev. Lett.65,2920(1990)] (45)

[98] Maxim Pospelov and Adam Ritz, "Electric dipole moments as probes of new physics," Annals Phys. **318**, 119–169 (2005), arXiv:hep-ph/0504231 [hep-ph] (45 and 62)

[99] Alexander L. Kagan and Matthias Neubert, "QCD anatomy of B —> X(s gamma) decays," Eur. Phys. J. **C7**, 5–27 (1999), arXiv:hep-ph/9805303 [hep-ph] (46 and 47)

[100] Alexander L. Kagan and Matthias Neubert, "Direct CP violation in $B \to X_s\gamma$ decays as a signature of new physics," Phys. Rev. **D58**, 094012 (1998), arXiv:hep-ph/9803368 [hep-ph] (46 and 47)

[101] E. Lunghi and J. Matias, "Huge right-handed current effects in B->K*(K pi)l+l- in supersymmetry," JHEP **04**, 058 (2007), arXiv:hep-ph/0612166 [hep-ph] (47)

[102] G. Degrassi, P. Gambino, and G. F. Giudice, "B —> X(s gamma) in supersymmetry: Large contributions beyond the leading order," JHEP **12**, 009 (2000), arXiv:hep-ph/0009337 [hep-ph] (47)

[103] Mario E. Gomez, Tarek Ibrahim, Pran Nath, and Solveig Skadhauge, "An Improved analysis of b –> s gamma in supersymmetry," Phys. Rev. **D74**, 015015 (2006), arXiv:hep-ph/0601163 [hep-ph] (49)

[104] Alexander Lenz and Ulrich Nierste, "Numerical Updates of Lifetimes and Mixing Parameters of B Mesons," in *CKM unitarity triangle. Proceedings, 6th International Workshop, CKM 2010, Warwick, UK, September 6-10, 2010* (2011) arXiv:1102.4274 [hep-ph] (52)

[105] Andrzej J. Buras, Piotr H. Chankowski, Janusz Rosiek, and Lucja Slawianowska, "Δ M(s) / Δ M(d), sin 2 Beta and the angle γ in the presence of new $\Delta F = 2$ operators," Nucl. Phys. **B619**, 434–466 (2001), arXiv:hep-ph/0107048 [hep-ph] (53)

[106] *Combined coupling measurements of the Higgs-like boson with the ATLAS detector using up to 25 fb^{-1} of proton-proton collision data*, Tech. Rep. ATLAS-CONF-2013-034 (CERN, Geneva, 2013) `http://cds.cern.ch/record/1528170` (55 and 65)

[107] *Combination of standard model Higgs boson searches and measurements of the properties of the new boson with a mass near 125 GeV*, Tech. Rep. CMS-PAS-HIG-13-005 (CERN, Geneva, 2013) `https://cds.cern.ch/record/1542387` (55, 56 and 65)

[108] Georges Aad *et al.* (ATLAS), "Measurements of Higgs boson production and couplings in diboson final states with the ATLAS detector at the LHC," Phys. Lett. **B726**, 88–119 (2013), [Erratum: Phys. Lett.B734,406(2014)], arXiv:1307.1427 [hep-ex] (55, 56, 65 and 70)

[109] *Observation and study of the Higgs boson candidate in the two photon decay channel with the ATLAS detector at the LHC*, Tech. Rep. ATLAS-CONF-2012-168 (CERN, Geneva, 2012) `http://cds.cern.ch/record/1499625` (56)

[110] *Updated measurements of the Higgs boson at 125 GeV in the two photon decay channel*, Tech. Rep. CMS-PAS-HIG-13-001 (CERN, Geneva, 2013) `https://cds.cern.ch/record/1530524` (56)

[111] "Search for the Standard Model Higgs boson in H-> tau tau decays in proton-proton collisions with the ATLAS detector," (2012) (57)

[112] "Search for the Standard-Model Higgs boson decaying to tau pairs in proton-proton collisions at sqrt(s) = 7 and 8 TeV," (2013) (57, 83 and 84)

[113] *Properties of the Higgs-like boson in the decay H to ZZ to 4l in pp collisions at sqrt s =7 and 8 TeV*, Tech. Rep. CMS-PAS-HIG-13-002 (CERN, Geneva, 2013) `https://cds.cern.ch/record/1523767` (56)

[114] Georges Aad *et al.* (ATLAS), "Search for charged Higgs bosons decaying via $H^+ \to \tau\nu$ in top quark pair events using pp collision data at $\sqrt{s} = 7$ TeV with the ATLAS detector," JHEP **06**, 039 (2012), arXiv:1204.2760 [hep-ex] (56)

[115] *Updated search for a light charged Higgs boson in top quark decays in pp collisions at sqrt(s) = 7 TeV*, Tech. Rep. CMS-PAS-HIG-12-052 (CERN, Geneva, 2012) `https://cds.cern.ch/record/1502246` (56)

[116] Georges Aad *et al.* (ATLAS), "Search for the neutral Higgs bosons of the Minimal Supersymmetric Standard Model in pp collisions at $\sqrt{s} = 7$ TeV with the ATLAS detector," JHEP **02**, 095 (2013), arXiv:1211.6956 [hep-ex] (57, 58, 82, 83, 84, 91 and 93)

[117] Georges Aad *et al.* (ATLAS), "Search for neutral Higgs bosons of the minimal supersymmetric standard model in pp collisions at $\sqrt{s} = 8$ TeV with the ATLAS detector," JHEP **11**, 056 (2014), arXiv:1409.6064 [hep-ex] (58 and 59)

[118] *Higgs to tau tau (MSSM)*, Tech. Rep. CMS-PAS-HIG-13-021 (CERN, Geneva, 2013) `https://cds.cern.ch/record/1623367` (58, 59, 91 and 93)

[119] *Search for new phenomena using large jet multiplicities and missing transverse momentum with ATLAS in 5.8 fb^{-1} of $\sqrt{s} = 8$ TeV proton-proton collisions*, Tech. Rep. ATLAS-CONF-2012-103 (CERN, Geneva, 2012) `http://cds.cern.ch/record/1472672` (58)

[120] *Search for gluino pair production in final states with missing transverse momentum and at least three b-jets using 12.8 fb-1 of pp collisions at sqrt(s) = 8 TeV with the ATLAS Detector.*, Tech. Rep. ATLAS-CONF-2012-145 (CERN, Geneva, 2012) `http://cds.cern.ch/record/1493484` (58)

[121] *Search for supersymmetry using events with three leptons, multiple jets, and missing transverse momentum in 13.0 fb^{-1} of pp collisions with the ATLAS detector at $\sqrt{s} = 8$ TeV*, Tech. Rep. ATLAS-CONF-2012-151 (CERN, Geneva, 2012) `http://cds.cern.ch/record/1493490` (58)

[122] *Search for strongly produced superpartners in final states with two same sign leptons with the ATLAS detector using 21 fb-1 of proton-proton collisions at sqrt(s)=8 TeV.*, Tech. Rep. ATLAS-CONF-2013-007 (CERN, Geneva, 2013) `https://cds.cern.ch/record/1522430` (58)

[123] Serguei Chatrchyan *et al.* (CMS), "Search for gluino mediated bottom- and top-squark production in multijet final states in pp collisions at 8 TeV," Phys. Lett. **B725**, 243–270 (2013), arXiv:1305.2390 [hep-ex] (58)

[124] *Search for Supersymmetry in pp collisions at 8 TeV in events with a single lepton, multiple jets and b-tags*, Tech. Rep. CMS-PAS-SUS-13-007 (CERN, Geneva, 2013) `https://cds.cern.ch/record/1523786` (58)

[125] Serguei Chatrchyan *et al.* (CMS), "Search for new physics in events with same-sign dileptons and b jets in pp collisions at $\sqrt{s} = 8$ TeV," JHEP **03**, 037 (2013), [Erratum: JHEP07,041(2013)], arXiv:1212.6194 [hep-ex] (58)

[126] Serguei Chatrchyan *et al.* (CMS), "Search for supersymmetry in hadronic final states with missing transverse energy using the variables α_T and b-quark multiplicity in pp collisions at $\sqrt{s} = 8$ TeV," Eur. Phys. J. **C73**, 2568 (2013), arXiv:1303.2985 [hep-ex] (59 and 60)

[127] *Search for direct production of the top squark in the all-hadronic ttbar + etmiss final state in 21 fb-1 of p-pcollisions at sqrt(s)=8 TeV with the ATLAS detector*, Tech. Rep. ATLAS-CONF-2013-024 (CERN, Geneva, 2013) `http://cds.cern.ch/record/1525880` (59 and 72)

[128] *Search for direct top squark pair production in final states with one isolated lepton, jets, and missing transverse momentum in sqrts* $= 8, TeV$ *pp collisions using 21* fb^{-1} *of ATLAS data*, Tech. Rep. ATLAS-CONF-2013-037 (CERN, Geneva, 2013) `https://cds.cern.ch/record/1532431` (59 and 72)

[129] *Search for direct third generation squark pair production in final states with missing transverse momentum and two b-jets in* $\sqrt{s} = 8$ *TeV pp collisions with the ATLAS detector.*, Tech. Rep. ATLAS-CONF-2013-053 (CERN, Geneva, 2013) `http://cds.cern.ch/record/1547570` (59, 60 and 72)

[130] *Search for top-squark pair production in the single lepton final state in pp collisions at 8 TeV*, Tech. Rep. CMS-PAS-SUS-13-011 (CERN, Geneva, 2013) `http://cds.cern.ch/record/1547550` (59 and 72)

[131] *Search for supersymmetry in pp collisions at sqrt(s) = 8 TeV in events with three leptons and at least one b-tagged jet*, Tech. Rep. CMS-PAS-SUS-13-008 (CERN, Geneva, 2013) `https://cds.cern.ch/record/1547560` (60)

[132] *Search for direct production of charginos and neutralinos in events with three leptons and missing transverse momentum in 21 fb^{-1} of pp collisions at $\sqrt{s}$ = 8 TeV with the ATLAS detector*, Tech. Rep. ATLAS-CONF-2013-035 (CERN, Geneva, 2013) `https://cds.cern.ch/record/1532426` (61 and 73)

[133] *Search for direct EWK production of SUSY particles in multilepton modes with 8TeV data*, Tech. Rep. CMS-PAS-SUS-12-022 (CERN, Geneva, 2013) `https://cds.cern.ch/record/1546777` (61 and 73)

[134] A. Bharucha, S. Heinemeyer, and F. von der Pahlen, "Direct Chargino-Neutralino Production at the LHC: Interpreting the Exclusion Limits in the Complex MSSM," Eur. Phys. J. **C73**, 2629 (2013), arXiv:1307.4237 [hep-ph] (61)

[135] Antonio Masiero and Oscar Vives, "New physics in CP violation experiments," Ann. Rev. Nucl. Part. Sci. **51**, 161–187 (2001), arXiv:hep-ph/0104027 [hep-ph] (61)

[136] M. Raidal *et al.*, "Flavour physics of leptons and dipole moments," *Flavor in the era of the LHC. Proceedings, CERN Workshop, Geneva, Switzerland, November 2005-March 2007*, Eur. Phys. J. **C57**, 13–182 (2008), arXiv:0801.1826 [hep-ph] (61)

[137] L. Calibbi, R. N. Hodgkinson, J. Jones Perez, A. Masiero, and O. Vives, "Flavour and Collider Interplay for SUSY at LHC7," Eur. Phys. J. **C72**, 1863 (2012), arXiv:1111.0176 [hep-ph] (61)

[138] B. C. Regan, Eugene D. Commins, Christian J. Schmidt, and David DeMille, "New limit on the electron electric dipole moment," Phys. Rev. Lett. **88**, 071805 (Feb 2002) (62)

[139] C. A. Baker *et al.*, "An Improved experimental limit on the electric dipole moment of the neutron," Phys. Rev. Lett. **97**, 131801 (2006), arXiv:hep-ex/0602020 [hep-ex] (62)

[140] W. C. Griffith, M. D. Swallows, T. H. Loftus, M. V. Romalis, B. R. Heckel, and E. N. Fortson, "Improved limit on the permanent electric dipole moment of 199hg," Phys. Rev. Lett. **102**, 101601 (Mar 2009) (62)

[141] John R. Ellis, Jae Sik Lee, and Apostolos Pilaftsis, "Electric Dipole Moments in the MSSM Reloaded," JHEP **10**, 049 (2008), arXiv:0808.1819 [hep-ph] (62)

[142] Darwin Chang, Wai-Yee Keung, and Apostolos Pilaftsis, "New two loop contribution to electric dipole moment in supersymmetric theories," Phys. Rev. Lett. **82**, 900–903 (1999), [Erratum: Phys. Rev. Lett.83,3972(1999)], arXiv:hep-ph/9811202 [hep-ph] (62)

[143] Mayumi Aoki, Tomoko Kadoyoshi, Akio Sugamoto, and Noriyuki Oshimo, "Electric dipole moments of neutron and electron in supersymmetric model," in *CP violation and its origin. Proceedings, 5th KEK Meeting, Tsukuba, Japan, March 6-7, 1997* (1997) pp. 52–67, arXiv:hep-ph/9706500 [hep-ph] (62)

[144] R. Aaij *et al.* (LHCb), "Measurement of the $B_s^0 \to \mu^+\mu^-$ branching fraction and search for $B^0 \to \mu^+\mu^-$ decays at the LHCb experiment," Phys. Rev. Lett. **111**, 101805 (2013), arXiv:1307.5024 [hep-ex] (62)

[145] Serguei Chatrchyan *et al.* (CMS), "Measurement of the B(s) to mu+ mu- branching fraction and search for B0 to mu+ mu- with the CMS Experiment," Phys. Rev. Lett. **111**, 101804 (2013), arXiv:1307.5025 [hep-ex] (62)

[146] S. Chen *et al.* (CLEO), "Branching fraction and photon energy spectrum for $b \to s\gamma$," Phys. Rev. Lett. **87**, 251807 (2001), arXiv:hep-ex/0108032 [hep-ex] (62)

[147] Kazuo Abe *et al.* (Belle), "A Measurement of the branching fraction for the inclusive B —> X(s) gamma decays with BELLE," Phys. Lett. **B511**, 151–158 (2001), arXiv:hep-ex/0103042 [hep-ex] (62)

[148] A. Limosani *et al.* (Belle), "Measurement of Inclusive Radiative B-meson Decays with a Photon Energy Threshold of 1.7-GeV," Phys. Rev. Lett. **103**, 241801 (2009), arXiv:0907.1384 [hep-ex] (62)

[149] J. P. Lees *et al.* (BaBar), "Exclusive Measurements of $b \to s\gamma$ Transition Rate and Photon Energy Spectrum," Phys. Rev. **D86**, 052012 (2012), arXiv:1207.2520 [hep-ex] (62)

[150] J. P. Lees *et al.* (BaBar), "Measurement of B($B \to X_s\gamma$), the $B \to X_s\gamma$ photon energy spectrum, and the direct CP asymmetry in $B \to X_{s+d}\gamma$ decays," Phys. Rev. **D86**, 112008 (2012), arXiv:1207.5772 [hep-ex] (62)

[151] Bernard Aubert *et al.* (BaBar), "Measurement of the $B \to X_s\gamma$ branching fraction and photon energy spectrum using the recoil method," Phys. Rev. **D77**, 051103 (2008), arXiv:0711.4889 [hep-ex] (62)

[152] Y. Amhis *et al.* (Heavy Flavor Averaging Group), "Averages of B-Hadron, C-Hadron, and tau-lepton properties as of early 2012," (2012), arXiv:1207.1158 [hep-ex] (62)

[153] HFAG, "Hfag: Rare b decay parameters," `http://www.slac.stanford.edu/xorg/hfag/rare/` (62)

[154] Y. Amhis *et al.* (Heavy Flavor Averaging Group (HFAG)), "Averages of b-hadron, c-hadron, and tau-lepton properties as of summer 2014," (2014), arXiv:1412.7515 [hep-ex] (63)

[155] Sinya Aoki *et al.*, "Review of lattice results concerning low-energy particle physics," Eur. Phys. J. **C74**, 2890 (2014), arXiv:1310.8555 [hep-lat] (63)

[156] Georges Aad *et al.* (ATLAS), "Observation of a new particle in the search for the Standard Model Higgs boson with the ATLAS detector at the LHC," Phys. Lett. **B716**, 1–29 (2012), arXiv:1207.7214 [hep-ex] (65)

[157] Serguei Chatrchyan *et al.* (CMS), "Observation of a new boson at a mass of 125 GeV with the CMS experiment at the LHC," Phys. Lett. **B716**, 30–61 (2012), arXiv:1207.7235 [hep-ex] (65)

[158] *Measurements of the properties of the Higgs-like boson in the WW to l nu+l nu decay channel with the ATLAS detector using 25 fb-1 of proton-proton collision data*, Tech. Rep. ATLAS-CONF-2013-030 (CERN, Geneva, 2013) `http://cds.cern.ch/record/1527126` (65)

[159] *Measurements of the properties of the Higgs-like boson in the four lepton decay channel with the ATLAS detector using 25 fb-1 of proton-proton collision data*, Tech. Rep. ATLAS-CONF-2013-013 (CERN, Geneva, 2013) `http://cds.cern.ch/record/1523699` (65)

[160] *Measurements of the properties of the Higgs-like boson in the two photon decay channel with the ATLAS detector using 25 fb-1 of proton-proton collision data*, Tech. Rep. ATLAS-CONF-2013-012 (CERN, Geneva, 2013) `http://cds.cern.ch/record/1523698` (65)

[161] *Properties of the observed Higgs-like resonance using the diphoton channel*, Tech. Rep. CMS-PAS-HIG-13-016 (CERN, Geneva, 2013) `https://cds.cern.ch/record/1558930` (65 and 82)

[162] *Search for the standard model Higgs boson produced in association with top quarks in multilepton final states*, Tech. Rep. CMS-PAS-HIG-13-020 (CERN, Geneva, 2013) `https://cds.cern.ch/record/1604480` (65)

[163] *Update of the search for the Standard Model Higgs boson decaying into WW in the vector boson fusion production channel*, Tech. Rep. CMS-PAS-HIG-13-022 (CERN, Geneva, 2013) `https://cds.cern.ch/record/1590404` (65)

[164] *Search for Higgs Boson Production in Association with a Top-Quark Pair and Decaying to Bottom Quarks or Tau Leptons*, Tech. Rep. CMS-PAS-HIG-13-019 (CERN, Geneva, 2013) `https://cds.cern.ch/record/1564682` (65)

[165] CMS Collaboration (CMS), "Search for a standard model like Higgs boson in the decay channel H to ZZ to l+l- q qbar at CMS," (2013) (65)

[166] G. Barenboim, C. Bosch, M. L. López-Ibañez, and O. Vives, "Eviction of a 125 GeV "heavy"-Higgs from the MSSM," JHEP **11**, 051 (2013), arXiv:1307.5973 [hep-ph] (65, 66 and 89)

[167] G. Barenboim, C. Bosch, M. L. López-Ibáñez, and O. Vives, "Improved τ-weapons for Higgs boson hunting," Phys. Rev. **D90**, 015003 (2014), arXiv:1311.7321 [hep-ph] (65 and 85)

[168] G. Barenboim, C. Bosch, J. S. Lee, M. L. López-Ibáñez, and O. Vives, "Flavor-changing Higgs boson decays into bottom and strange quarks in supersymmetric models," Phys. Rev. **D92**, 095017 (2015), arXiv:1507.08304 [hep-ph] (65 and 97)

[169] Marcela Carena, J. R. Espinosa, M. Quiros, and C. E. M. Wagner, "Analytical expressions for radiatively corrected Higgs masses and couplings in the MSSM," Phys. Lett. **B355**, 209–221 (1995), arXiv:hep-ph/9504316 [hep-ph] (67)

[170] Marcela Carena, Stefania Gori, Nausheen R. Shah, and Carlos E. M. Wagner, "A 125 GeV SM-like Higgs in the MSSM and the $\gamma\gamma$ rate," JHEP **03**, 014 (2012), arXiv:1112.3336 [hep-ph] (74 and 86)

[171] Marcela Carena, Stefania Gori, Nausheen R. Shah, Carlos E. M. Wagner, and Lian-Tao Wang, "Light Stau Phenomenology and the Higgs $\gamma\gamma$ Rate," JHEP **07**, 175 (2012), arXiv:1205.5842 [hep-ph] (74 and 86)

[172] Georges Aad *et al.* (ATLAS), "Search for the Standard Model Higgs boson in the H to $\tau^+\tau^-$ decay mode in $\sqrt{s} = 7$ TeV pp collisions with ATLAS," JHEP **09**, 070 (2012), arXiv:1206.5971 [hep-ex] (83 and 84)

[173] Philip Bechtle, Oliver Brein, Sven Heinemeyer, Georg Weiglein, and Karina E. Williams, "HiggsBounds: Confronting Arbitrary Higgs Sectors with Exclusion Bounds from LEP and the Tevatron," Comput. Phys. Commun. **181**, 138–167 (2010), arXiv:0811.4169 [hep-ph] (85)

[174] Philip Bechtle, Oliver Brein, Sven Heinemeyer, Oscar Stal, Tim Stefaniak, Georg Weiglein, and Karina E. Williams, "HiggsBounds-4: Improved Tests of Extended Higgs Sectors against Exclusion Bounds from LEP, the Tevatron and the LHC," Eur. Phys. J. **C74**, 2693 (2014), arXiv:1311.0055 [hep-ph] (85)

[175] M. Misiak *et al.*, "Estimate of $\mathcal{B}(\bar{B} \to X_s\gamma)$ at $O(\alpha_s^2)$," Phys. Rev. Lett. **98**, 022002 (2007), arXiv:hep-ph/0609232 [hep-ph] (85)

[176] Antonio Delgado, Gian F. Giudice, Gino Isidori, Maurizio Pierini, and Alessandro Strumia, "The light stop window," Eur. Phys. J. **C73**, 2370 (2013), arXiv:1212.6847 [hep-ph] (86)

[177] *Search for pair-produced top squarks decaying into a charm quark and the lightest neutralinos with 20.3 fb^{-1} of pp collisions at $\sqrt{s} = 8$ TeV with the ATLAS detector at the LHC*, Tech. Rep. ATLAS-CONF-2013-068 (CERN, Geneva, 2013) `http://cds.cern.ch/record/1562880` (86)

[178] Marcela Carena, Stefania Gori, Nausheen R. Shah, Carlos E. M. Wagner, and Lian-Tao Wang, "Light Stops, Light Staus and the 125 GeV Higgs," JHEP **08**, 087 (2013), arXiv:1303.4414 [hep-ph] (86)

[179] *Search for charged Higgs bosons in the τ+jets final state with pp collision data recorded at $\sqrt{s} = 8$ TeV with the ATLAS experiment*, Tech. Rep. ATLAS-CONF-2013-090 (CERN, Geneva, 2013) (92 and 93)

[180] G. C. Branco, P. M. Ferreira, L. Lavoura, M. N. Rebelo, Marc Sher, and Joao P. Silva, "Theory and phenomenology of two-Higgs-doublet models," Phys. Rept. **516**, 1–102 (2012), arXiv:1106.0034 [hep-ph] (97)

[181] Walter D. Goldberger, Benjamin Grinstein, and Witold Skiba, "Distinguishing the Higgs boson from the dilaton at the Large Hadron Collider," Phys. Rev. Lett. **100**, 111802 (2008), arXiv:0708.1463 [hep-ph] (97)

[182] JiJi Fan, Walter D. Goldberger, Andreas Ross, and Witold Skiba, "Standard Model couplings and collider signatures of a light scalar," Phys. Rev. **D79**, 035017 (2009), arXiv:0803.2040 [hep-ph] (97)

[183] S. Casagrande, F. Goertz, U. Haisch, M. Neubert, and T. Pfoh, "Flavor Physics in the Randall-Sundrum Model: I. Theoretical Setup and Electroweak Precision Tests," JHEP **10**, 094 (2008), arXiv:0807.4937 [hep-ph] (97)

[184] Aleksandr Azatov, Manuel Toharia, and Lijun Zhu, "Higgs Mediated FCNC's in Warped Extra Dimensions," Phys. Rev. **D80**, 035016 (2009), arXiv:0906.1990 [hep-ph] (97)

[185] Kaustubh Agashe and Roberto Contino, "Composite Higgs-Mediated FCNC," Phys. Rev. **D80**, 075016 (2009), arXiv:0906.1542 [hep-ph] (97)

[186] *Updated coupling measurements of the Higgs boson with the ATLAS detector using up to 25 fb^{-1} of proton-proton collision data*, Tech. Rep. ATLAS-CONF-2014-009 (CERN, Geneva, 2014) `http://cds.cern.ch/record/1670012` (98)

[187] J. S. Lee, M. Carena, J. Ellis, A. Pilaftsis, and C. E. M. Wagner, "CPsuperH2.0: an Improved Computational Tool for Higgs Phenomenology in the MSSM with Explicit CP Violation," Comput. Phys. Commun. **180**, 312–331 (2009), arXiv:0712.2360 [hep-ph] (103)

[188] J. S. Lee, M. Carena, J. Ellis, A. Pilaftsis, and C. E. M. Wagner, "CPsuperH2.3: an Updated Tool for Phenomenology in the MSSM with Explicit CP Violation," Comput. Phys. Commun. **184**, 1220–1233 (2013), arXiv:1208.2212 [hep-ph] (103)

[189] C.D. Froggatt and H.B. Nielsen, "Hierarchy of quark masses, cabibbo angles and cp violation," Nuclear Physics B **147**, 277 – 298 (1979) (113)

[190] Georges Aad and others, "Search for new phenomena in final states with large jet multiplicities and missing transverse momentum with ATLAS using 13 TeV proton-proton collisions," Phys. Lett. **B757**, 334–355 (2016) (113 and 133)

[191] Georges Aad and others, "Search for gluinos in events with an isolated lepton, jets and missing transverse momentum at 13 tev with the ATLAS detector," Eur. Phys. J. **C76**, 565 (2016) (113 and 133)

[192] ATLAS Collaboration, "Search for supersymmetry at 13 tev in final states with jets and two same-sign leptons or three leptons with the ATLAS detector," The European Physical Journal C **76** (May 2016), arXiv: 1602.09058, http://arxiv.org/abs/1602.09058 (113)

[193] Georges Aad and others, "Search for pair production of gluinos decaying via stop and sbottom in events with b-jets and large missing transverse momentum in pp collisions at 13 TeV with the ATLAS detector," Phys. Rev. **D94**, 032003 (2016) (113 and 133)

[194] Morad Aaboud and others, "Search for new phenomena in final states with an energetic jet and large missing transverse momentum in pp collisions at 13 TeV using the ATLAS detector," Phys. Rev. **D94**, 032005 (2016) (113 and 133)

[195] ATLAS Collaboration, "Search for squarks and gluinos in final states with jets and missing transverse momentum at 13 TeV with the ATLAS detector," The European Physical Journal C **76** (Jul. 2016), arXiv: 1605.03814, http://arxiv.org/abs/1605.03814 (113 and 133)

[196] ATLAS Collaboration, "Search for top squarks in final states with one isolated lepton, jets, and missing transverse momentum in 13 tev in pp collisions with the ATLAS detector," Physical Review D **94** (Sep. 2016), doi:\bibinfo{doi}{10.1103/PhysRevD.94.052009}, arXiv: 1606.03903, http://arxiv.org/abs/1606.03903 (113)

[197] CMS Collaboration, "Search for supersymmetry in the multijet and missing transverse momentum final state in pp collisions at 13 TeV," Physics Letters B **758**, 152–180 (Jul. 2016), http://arxiv.org/abs/1602.06581 (113 and 133)

[198] CMS Collaboration, "Search for new physics with the MT2 variable in all-jets final states produced in pp collisions at 13 tev," Journal of High Energy Physics **2016** (Oct. 2016), http://arxiv.org/abs/1603.04053 (113)

[199] CMS Collaboration, "Search for new physics in same-sign dilepton events in proton-proton collisions at 13 TeV," The European Physical Journal C **76** (Aug. 2016), http://arxiv.org/abs/1605.03171 (113)

[200] CMS Collaboration, "Search for supersymmetry in pp collisions at 13 tev in the single-lepton final state using the sum of masses of large-radius jets," Journal of High Energy Physics **2016** (Aug. 2016), doi:\bibinfo{doi}{10.1007/JHEP08(2016)122}, http://arxiv.org/abs/1605.04608 (113)

[201] CMS Collaboration, "Search for new physics in final states with two opposite-sign, same-flavor leptons, jets, and missing transverse momentum in pp collisions at 13 tev," arXiv:1607.00915 [hep-ex](Jul. 2016), `http://arxiv.org/abs/1607.00915` (113)

[202] D. J. H. Chung, L. L. Everett, G. L. Kane, S. F. King, Joseph D. Lykken, and Lian-Tao Wang, "The Soft supersymmetry breaking Lagrangian: Theory and applications," Phys. Rept. **407**, 1–203 (2005), arXiv:hep-ph/0312378 [hep-ph] (114)

[203] F. J. Botella, M. Nebot, and O. Vives, "Invariant approach to flavor-dependent CP-violating phases in the MSSM," JHEP **01**, 106 (2006), arXiv:hep-ph/0407349 [hep-ph] (114 and 133)

[204] M.T. Grisaru, W. Siegel, and M. Roček, "Improved methods for supergraphs," Nuclear Physics B **159**, 429 – 450 (1979) (117)

[205] S. J. Gates, Marcus T. Grisaru, M. Rocek, and W. Siegel, "Superspace Or One Thousand and One Lessons in Supersymmetry," Front. Phys. **58**, 1–548 (1983), arXiv:hep-th/0108200 [hep-th] (117)

[206] Manuel Drees, Rohini Godbole, and Probir Roy, *Theory and phenomenology of Sparticles: an account of four-dimensional N=1 supersymmetry in high-energy physics* (World Scientific, Singapore, 2004) `http://cds.cern.ch/record/873465` (117)

[207] Graham G. Ross and O. Vives, "Yukawa structure, flavor and CP violation in supergravity," Phys. Rev. **D67**, 095013 (2003), arXiv:hep-ph/0211279 [hep-ph] (119)

[208] L. Calibbi, J. Jones-Perez, and O. Vives, "Electric dipole moments from flavoured CP violation in SUSY," Phys. Rev. **D78**, 075007 (2008), arXiv:0804.4620 [hep-ph] (119 and 133)

[209] L. Calibbi, J. Jones-Perez, A. Masiero, Jae-hyeon Park, W. Porod, and O. Vives, "FCNC and CP Violation Observables in a SU(3)-flavoured MSSM," Nucl. Phys. **B831**, 26–71 (2010), arXiv:0907.4069 [hep-ph] (119 and 133)

[210] Steve F. King, Iain N. R. Peddie, Graham G. Ross, Liliana Velasco-Sevilla, and Oscar Vives, "Kahler corrections and softly broken family symmetries," JHEP **07**, 049 (2005), arXiv:hep-ph/0407012 [hep-ph] (119, 124 and 126)

[211] Graham G. Ross, Liliana Velasco-Sevilla, and Oscar Vives, "Spontaneous CP violation and nonAbelian family symmetry in SUSY," Nucl. Phys. **B692**, 50–82 (2004), arXiv:hep-ph/0401064 [hep-ph] (122 and 133)

[212] K. S. Babu, Ilia Gogoladze, Shabbar Raza, and Qaisar Shafi, "Flavor Symmetry Based MSSM (sMSSM): Theoretical Models and Phenomenological Analysis," Phys. Rev. **D90**, 056001 (2014), arXiv:1406.6078 [hep-ph] (122)

[213] Hajime Ishimori, Tatsuo Kobayashi, Hiroshi Ohki, Yusuke Shimizu, Hiroshi Okada, and Morimitsu Tanimoto, "Non-Abelian Discrete Symmetries in Particle Physics," Prog. Theor. Phys. Suppl. **183**, 1–163 (2010), arXiv:1003.3552 [hep-th] (122)

[214] Guido Altarelli and Ferruccio Feruglio, "Discrete Flavor Symmetries and Models of Neutrino Mixing," Rev. Mod. Phys. **82**, 2701–2729 (2010), arXiv:1002.0211 [hep-ph] (122)

[215] Stephen F. King and Christoph Luhn, "Neutrino Mass and Mixing with Discrete Symmetry," Rept. Prog. Phys. **76**, 056201 (2013), arXiv:1301.1340 [hep-ph] (122)

[216] Ivo de Medeiros Varzielas and Graham G. Ross, "SU(3) family symmetry and neutrino bi-tri-maximal mixing," Nucl. Phys. **B733**, 31–47 (2006), arXiv:hep-ph/0507176 [hep-ph] (126)

[217] Norbert K. Falck, "Renormalization Group Equations for Softly Broken Supersymmetry: The Most General Case," Z. Phys. **C30**, 247 (1986) (132)

[218] S. Bertolini, Francesca Borzumati, A. Masiero, and G. Ridolfi, "Effects of supergravity induced electroweak breaking on rare B decays and mixings," Nucl. Phys. **B353**, 591–649 (1991) (132)

[219] Stephen P. Martin and Michael T. Vaughn, "Two loop renormalization group equations for soft supersymmetry breaking couplings," Phys. Rev. **D50**, 2282 (1994), [Erratum: Phys. Rev.D78,039903(2008)], arXiv:hep-ph/9311340 [hep-ph] (132)

[220] Youichi Yamada, "Two loop renormalization group equations for soft SUSY breaking scalar interactions: Supergraph method," Phys. Rev. **D50**, 3537–3545 (1994), arXiv:hep-ph/9401241 [hep-ph] (132)

[221] F. Gabbiani and A. Masiero, "Fcnc in generalized supersymmetric theories," Nuclear Physics B **322**, 235 – 254 (1989) (132)

[222] John S. Hagelin, S. Kelley, and Toshiaki Tanaka, "Supersymmetric flavor-changing neutral currents: exact amplitudes and phenomenological analysis," Nuclear Physics B **415**, 293 – 331 (1994) (132)

[223] F. Gabbiani, E. Gabrielli, A. Masiero, and L. Silvestrini, "A Complete analysis of FCNC and CP constraints in general SUSY extensions of the standard model," Nucl. Phys. **B477**, 321–352 (1996), arXiv:hep-ph/9604387 [hep-ph] (132)

[224] Marco Ciuchini *et al.*, "Delta M(K) and epsilon(K) in SUSY at the next-to-leading order," JHEP **10**, 008 (1998), arXiv:hep-ph/9808328 [hep-ph] (132)

[225] A. Masiero and O. Vives, "CP violation and flavor changing effects in K and B mesons from nonuniversal soft breaking terms," Phys. Rev. Lett. **86**, 26–29 (2001), arXiv:hep-ph/0007320 [hep-ph] (132)

[226] M. Jay Péres D. Das, M.L. López-Ibáñez and O. Vives, "Work in progress," (2017) (132 and 135)

[227] F. J. Botella and Joao P. Silva, "Jarlskog - like invariants for theories with scalars and fermions," Phys. Rev. **D51**, 3870–3875 (1995), arXiv:hep-ph/9411288 [hep-ph] (133)

[228] Arcadi Santamaria, "Masses, mixings, Yukawa couplings and their symmetries," Phys. Lett. **B305**, 90–97 (1993), arXiv:hep-ph/9302301 [hep-ph] (133)

[229] John Ellis, Robert N. Hodgkinson, Jae Sik Lee, and Apostolos Pilaftsis, "Flavour Geometry and Effective Yukawa Couplings in the MSSM," JHEP **02**, 016 (2010), arXiv:0911.3611 [hep-ph] (144)

[230] Athanasios Dedes and Apostolos Pilaftsis, "Resummed effective Lagrangian for Higgs mediated FCNC interactions in the CP violating MSSM," Phys. Rev. **D67**, 015012 (2003), arXiv:hep-ph/0209306 [hep-ph] (144)

[231] Andrzej J. Buras, Andrea Romanino, and Luca Silvestrini, "K —> pi neutrino anti-neutrino: A Model independent analysis and supersymmetry," Nucl. Phys. **B520**, 3–30 (1998), arXiv:hep-ph/9712398 [hep-ph] (149)

[232] A. Masiero, S. K. Vempati, and O. Vives, "Flavour physics and grand unification," in *Particle physics beyond the standard model. Proceedings, Summer*

School on Theoretical Physics, 84th Session, Les Houches, France, August 1-26, 2005 (2005) pp. 1–78, arXiv:0711.2903 [hep-ph] (149)

[233] L. Clavelli, T. Gajdosik, and W. Majerotto, "Gaugino mass dependence of electron and neutron electric dipole moments," Phys. Lett. **B494**, 287–296 (2000), arXiv:hep-ph/0007342 [hep-ph] (150)